frontiers | Research Topics

Molecular targets in oncological and hematological disease management: innovations in precision medicine

Edited by
Adrian Bogdan Tigu, Stefan Eugen Szedlacsek and Gregory Wiedman

Published in
Frontiers in Pharmacology

ISSN 1664-8714
ISBN 978-2-8325-5516-3
DOI 10.3389/978-2-8325-5516-3

About Frontiers

Frontiers is more than just an open access publisher of scholarly articles: it is a pioneering approach to the world of academia, radically improving the way scholarly research is managed. The grand vision of Frontiers is a world where all people have an equal opportunity to seek, share and generate knowledge. Frontiers provides immediate and permanent online open access to all its publications, but this alone is not enough to realize our grand goals.

Frontiers journal series

The Frontiers journal series is a multi-tier and interdisciplinary set of open-access, online journals, promising a paradigm shift from the current review, selection and dissemination processes in academic publishing. All Frontiers journals are driven by researchers for researchers; therefore, they constitute a service to the scholarly community. At the same time, the *Frontiers journal series* operates on a revolutionary invention, the tiered publishing system, initially addressing specific communities of scholars, and gradually climbing up to broader public understanding, thus serving the interests of the lay society, too.

Dedication to quality

Each Frontiers article is a landmark of the highest quality, thanks to genuinely collaborative interactions between authors and review editors, who include some of the world's best academicians. Research must be certified by peers before entering a stream of knowledge that may eventually reach the public - and shape society; therefore, Frontiers only applies the most rigorous and unbiased reviews. Frontiers revolutionizes research publishing by freely delivering the most outstanding research, evaluated with no bias from both the academic and social point of view. By applying the most advanced information technologies, Frontiers is catapulting scholarly publishing into a new generation.

What are Frontiers Research Topics?

Frontiers Research Topics are very popular trademarks of the *Frontiers journals series*: they are collections of at least ten articles, all centered on a particular subject. With their unique mix of varied contributions from Original Research to Review Articles, Frontiers Research Topics unify the most influential researchers, the latest key findings and historical advances in a hot research area.

Find out more on how to host your own Frontiers Research Topic or contribute to one as an author by contacting the Frontiers editorial office: frontiersin.org/about/contact

Molecular targets in oncological and hematological disease management: innovations in precision medicine

Topic editors

Adrian Bogdan Tigu — University of Medicine and Pharmacy Iuliu Hatieganu, Romania

Stefan Eugen Szedlacsek — Institute of Biochemistry of the Romanian Academy, Romania

Gregory Wiedman — Seton Hall University, United States

Citation

Tigu, A. B., Szedlacsek, S. E., Wiedman, G., eds. (2024). *Molecular targets in oncological and hematological disease management: innovations in precision medicine*. Lausanne: Frontiers Media SA. doi: 10.3389/978-2-8325-5516-3

Table of contents

frontiers | Frontiers in Pharmacology

TYPE Editorial
PUBLISHED 20 September 2024
DOI 10.3389/fphar.2024.1494396

OPEN ACCESS

EDITED AND REVIEWED BY
Alastair George Stewart,
The University of Melbourne, Australia

*CORRESPONDENCE
Adrian Bogdan Tigu,
tiguadrianbogdan@yahoo.com
Gregory Wiedman,
gregory.wiedman@shu.edu
Stefan Eugen Szedlacsek,
szedlacs@yahoo.co.uk

RECEIVED 10 September 2024
ACCEPTED 16 September 2024
PUBLISHED 20 September 2024

CITATION
Tigu AB, Wiedman G and Szedlacsek SE (2024) Editorial: Molecular targets in oncological and hematological disease management: innovations in precision medicine.
Front. Pharmacol. 15:1494396.
doi: 10.3389/fphar.2024.1494396

Editorial: Molecular targets in oncological and hematological disease management: innovations in precision medicine

Adrian Bogdan Tigu[1]*, Gregory Wiedman[2]* and Stefan Eugen Szedlacsek[3]*

[1]Department of Translational Medicine, Institute of Medical Research and Life Sciences - MedFuture, "Iuliu Haţieganu" University of Medicine and Pharmacy, Cluj-Napoca, Romania, [2]Department of Chemistry and Biochemistry, Seton Hall University, South Orange, NJ, United States, [3]Department of Enzymology, Institute of Biochemistry of the Romanian Academy, Bucharest, Romania

KEYWORDS

targeted therapy, precision medicine, molecular diagnosis, innovations, nanomedicine

Editorial on the Research Topic
Molecular targets in oncological and hematological disease management: innovations in precision medicine

Targeted therapies represent a significant advancement in medicine, particularly in treating complex diseases such as cancer. These therapies, designed to specifically target biological mechanisms driving disease, can alter pathways that exacerbate disease progression, effectively slowing or halting tumor growth. Unlike traditional therapies that broadly affect both healthy and cancerous cells, targeted therapies minimize collateral damage by focusing on specific molecular triggers. This precision leads to superior outcomes while reducing adverse effects and toxicity (Buongervino et al., 2021; Fu et al., 2022; Zatovicova et al., 2022).

By providing a more specific and focused intervention, targeted therapies lead to improved treatment outcomes while reducing the risks of adverse effects and morbidity. Traditional medicines tend to affect a broader range of systems, often leading to more negative side effects (Canova et al., 2023; Disselhorst and Baas, 2020; Lohiya et al., 2023; Pralea et al., 2024). In contrast, targeted therapies focus on disease-related molecules, keeping healthy cells unexposed and minimizing patient toxicity.

Recent advances in precision medicine have accelerated the development of therapies targeting key genetic mutations or molecular abnormalities driving tumor growth (Zafar et al., 2024; Zhang et al., 2024). Personalized treatments designed according to each tumor's unique DNA profile offer improved efficacy and reduced toxicity (Dailah et al., 2024; Guo et al., 2024; Liu et al., 2024; Tomuleasa et al., 2024). This Research Topic explores therapeutic agents that target disease-associated molecules, investigating strategies to alter molecular pathways responsible for disease progression and resistance to treatment.

Shafiei et al. investigated silibinin-loaded magnetic niosomal nanoparticles (MNNPs) for colorectal cancer treatment. Their findings demonstrated a significant increase in the cytotoxic effects of silibinin on cancer cells while sparing healthy cells. This study illustrates the growing importance of nanoparticle-based drug delivery systems in precision oncology, improving drug bioavailability and reducing side effects. The innovation presented in this study opens the door for broader applications of nanotechnology in cancer treatment.

Liu et al. reviewed diverse experimental models used in colorectal cancer (CRC) research, offering an in-depth overview of *in vitro* and *in vivo* models. Their work emphasizes the need to refine models to better replicate human CRC, providing a framework for testing targeted therapies like Shafiei's MNNPs in ways that closely mimic human disease.

In hematological diseases, Li et al. examined the role of hemopexin (HPX) in mitigating heme toxicity during hemolysis, which commonly occurs in diseases such as sickle cell anemia and transfusion-induced hemolysis. While HPX protects against free heme, under certain conditions, it may exacerbate disease progression. This dual role emphasizes the need for more nuanced therapeutic approaches in hematology, similar to the precision seen in CRC treatments. Both studies demonstrate the complex dynamics of molecular precision in reducing harm and mitigating disease.

Zhang et al. presented a case study of a patient with severe combined immunodeficiency (SCID) who developed colon lymphoma due to a novel DCLRE1C mutation. It illustrates the intersection of immune system failure and cancer, highlighting the need for precision in both diagnostics and treatment. Early genetic diagnosis, as underscored by Li's research on biomarkers, is critical for timely intervention, further emphasizing the importance of molecular precision in preventing and managing complex disease profiles.

Iacobescu et al. explored proteomics-based biomarkers for predicting and managing graft-versus-host disease (GVHD) in patients undergoing allogeneic hematopoietic stem cell transplantation (allo-HSCT). Their review delves into both single protein markers and protein panels, offering a comprehensive look at how these biomarkers can be used to stratify risk and diagnose GVHD. The authors emphasize how non-invasive biospecimens, such as blood or saliva, could be harnessed to enhance the precision of GVHD management.

Mocan et al. performed a proteomic exploration to identify novel serum biomarkers for intrahepatic cholangiocarcinoma (iCCA). Using high-throughput mass spectrometry, they identified several potential biomarkers, including S100A9, haptoglobin (HP), and serum amyloid A (SAA), which could distinguish iCCA from other liver conditions, such as cirrhosis and hepatocellular carcinoma. Their findings underscore the importance of proteomics in early cancer diagnosis and open the door to developing non-invasive diagnostic tools that could improve survival rates by enabling earlier detection and treatment.

Zhang et al. conducted a pan-cancer analysis of the TET family genes, particularly TET3, uncovering its role in tumor progression and drug sensitivity. Their bioinformatics analysis revealed that TET3 is involved in several cancer-related pathways, including cell cycle regulation, DNA damage response, and immune modulation. Targeting TET3 could inhibit tumor growth and increase chemotherapy sensitivity, positioning TET3 as a potential therapeutic target in a variety of cancers.

Chomczyk et al. provided an in-depth analysis of TP53 mutations in acute myeloid leukemia (AML) and their implications for disease progression. The review discussed the metabolic rewiring and immune evasion mechanisms driven by TP53 mutations, which are present in a subset of AML cases and associated with poor prognosis. Despite advances in targeted therapies, TP53-mutated AML remains a challenge due to its resistance to chemotherapy. This review called for further research into therapies targeting the metabolic vulnerabilities of TP53-mutated AML.

Munteanu et al. advanced the conversation around targeted therapies with their *in vivo* imaging system (IVIS) therapeutic assessment of tyrosine kinase inhibitor (TKI)-loaded gold nanoparticles for treating acute myeloid leukemia (AML). By using IVIS, the authors were able to track and assess the therapeutic effects of FLT3 inhibitors loaded into gold nanoparticles. Their preclinical study demonstrated that these nanocarriers improved drug delivery and bioavailability, offering enhanced tumor inhibition in FLT3-mutated AML models. This work reinforces the potential of nanomedicine in boosting the efficacy of precision therapies while minimizing systemic toxicity.

In conclusion, the studies featured in this Research Topic provide a comprehensive view of the current landscape of molecular targets in oncology and hematology. From novel drug delivery systems to biomarker identification, these contributions highlight the critical role of precision medicine in advancing treatment by targeting disease mechanisms, improving patient outcomes, and reducing the burden of traditional therapies.

Author contributions

AT: Writing–review and editing, Writing–original draft. GW: Writing–review and editing, Writing–original draft. SS: Writing–review and editing, Writing–original draft.

Funding

The author(s) declare that no financial support was received for the research, authorship, and/or publication of this article.

Acknowledgments

We would like to express our gratitude to all the authors who contributed to this Research Topic, as well as to the reviewers and invited editors who have played a significant role in enhancing its quality.

Conflict of interest

The authors declare that the research was conducted in the absence of any commercial or financial relationships that could be construed as a potential conflict of interest.

Publisher's note

References

Buongervino, S., Lane, M. V., Garrigan, E., Zhelev, D. V., Dimitrov, D. S., and Bosse, K. R. (2021). Antibody-drug conjugate efficacy in neuroblastoma: role of payload, resistance mechanisms, target density, and antibody internalization. *Mol. Cancer Ther.* 20 (11), 2228–2239. doi:10.1158/1535-7163.MCT-20-1034

Canova, S., Trevisan, B., Abbate, M. I., Colonese, F., Sala, L., Baggi, A., et al. (2023). Novel therapeutic options for small cell lung cancer. *Curr. Oncol. Rep.* 25 (11), 1277–1294. doi:10.1007/s11912-023-01465-7

Dailah, H. G., Hommdi, A. A., Koriri, M. D., Algathlan, E. M., and Mohan, S. (2024). Potential role of immunotherapy and targeted therapy in the treatment of cancer: a contemporary nursing practice. *Heliyon* 10 (2), e24559. doi:10.1016/j.heliyon.2024.e24559

Disselhorst, M. J., and Baas, P. (2020). Chemotherapy options versus "novel" therapies: how should we treat patients with malignant pleural mesothelioma. *Transl. Lung Cancer Res.* 9 (Suppl. 1), S77-S85–S85. doi:10.21037/tlcr.2020.01.16

Fu, Z., Li, S., Han, S., Shi, C., and Zhang, Y. (2022). Antibody drug conjugate: the "biological missile" for targeted cancer therapy. *Signal Transduct. Target Ther.* 7 (1), 93. doi:10.1038/s41392-022-00947-7

Guo, M., Sun, Y., Wei, Y., Xu, J., and Zhang, C. (2024). Advances in targeted therapy and biomarker research in thyroid cancer. *Front. Endocrinol. (Lausanne)* 15, 1372553. doi:10.3389/fendo.2024.1372553

Liu, B., Zhou, H., Tan, L., Siu, K. T. H., and Guan, X. Y. (2024). Exploring treatment options in cancer: tumor treatment strategies. *Signal Transduct. Target Ther.* 9 (1), 175. doi:10.1038/s41392-024-01856-7

Lohiya, D. V., Mehendale, A. M., Lohiya, D. V., Lahoti, H. S., and Agrawal, V. N. (2023). Novel chemotherapy modalities for different cancers. *Cureus* 15 (9), e45474. doi:10.7759/cureus.45474

Pralea, I. E., Moldovan, R. C., Tigu, A. B., Moldovan, C. S., Fischer-Fodor, E., and Iuga, C. A. (2024). Cellular responses induced by NCT-503 treatment on triple-negativebreast cancer cell lines: a proteomics approach. *Biomedicines* 12 (5), 1087. doi:10.3390/biomedicines12051087

Tomuleasa, C., Tigu, A. B., Munteanu, R., Moldovan, C. S., Kegyes, D., Onaciu, A., et al. (2024). Therapeutic advances of targeting receptor tyrosine kinases in cancer. *Signal Transduct. Target Ther.* 9 (1), 201. doi:10.1038/s41392-024-01899-w

Zafar, A., Khan, M. J., Abu, J., and Naeem, A. (2024). Revolutionizing cancer care strategies: immunotherapy, gene therapy, and molecular targeted therapy. *Mol. Biol. Rep.* 51 (1), 219. doi:10.1007/s11033-023-09096-8

Zatovicova, M., Kajanova, I., Barathova, M., Takacova, M., Labudova, M., Csaderova, L., et al. (2022). Novel humanized monoclonal antibodies for targeting hypoxic human tumors via two distinct extracellular domains of carbonic anhydrase IX. *Cancer Metab.* 10 (1), 3. doi:10.1186/s40170-022-00279-8

Zhang, S., Xiao, X., Yi, Y., Wang, X., Zhu, L., Shen, Y., et al. (2024). Tumor initiation and early tumorigenesis: molecular mechanisms and interventional targets. *Signal Transduct. Target Ther.* 9 (1), 149. doi:10.1038/s41392-024-01848-7

frontiers | Frontiers in Pharmacology

TYPE Original Research
PUBLISHED 27 June 2023
DOI 10.3389/fphar.2023.1174120

OPEN ACCESS

EDITED BY
William Raoul,
Croissance et Cancer, France

REVIEWED BY
Miguel Pereira-Silva,
University of Coimbra, Portugal
Jean-Michel Escoffre,
INSERM U1253 Imagerie et Cerveau (iBrain), France

*CORRESPONDENCE
Nosratollah Zarghami,
zarghami@tbzmed.ac.ir

†These authors have contributed equally to this work

RECEIVED 25 February 2023
ACCEPTED 23 May 2023
PUBLISHED 27 June 2023

CITATION
Shafiei G, Jafari-Gharabaghlou D, Farhoudi-Sefidan-Jadid M, Alizadeh E, Fathi M and Zarghami N (2023), Targeted delivery of silibinin via magnetic niosomal nanoparticles: potential application in treatment of colon cancer cells. *Front. Pharmacol.* 14:1174120. doi: 10.3389/fphar.2023.1174120

Targeted delivery of silibinin via magnetic niosomal nanoparticles: potential application in treatment of colon cancer cells

Golchin Shafiei[1,2†], Davoud Jafari-Gharabaghlou[3†], Mahdi Farhoudi-Sefidan-Jadid[3], Effat Alizadeh[1], Marziyeh Fathi[2] and Nosratollah Zarghami[3,4*]

[1]Department of Medical Biotechnology, Faculty of Advanced Medical Sciences, Tabriz University of Medical Sciences, Tabriz, Iran, [2]Research Center for Pharmaceutical Nanotechnology, Biomedicine Institute, Tabriz University of Medical Sciences, Tabriz, Iran, [3]Department of Clinical Biochemistry and Laboratory Medicine, Faculty of Medicine, Tabriz University of Medical Sciences, Tabriz, Iran, [4]Department of Medical Biochemistry, Faculty of Medicine, Istanbul Aydin University, Istanbul, Turkey

Introduction: In recent years, various nanoparticles (NPs) have been discovered and synthesized for the targeted therapy of cancer cells. Targeted delivery increases the local concentration of therapeutics and minimizes side effects. Therefore, NPs-mediated targeted drug delivery systems have become a promising approach for the treatment of various cancers. As a result, in the current study, we aimed to design silibinin-loaded magnetic niosomes nanoparticles (MNNPs) and investigate their cytotoxicity property in colorectal cancer cell treatment.

Methods: MNPs ferrofluids were prepared and encapsulated into niosomes (NIOs) by the thin film hydration method. Afterward, the morphology, size, and chemical structure of the synthesized MNNPs were evaluated using the TEM, DLS, and FT-IR techniques, respectively.

Results and Discussion: The distribution number of MNNPs was obtained at about 50 nm and 70 nm with a surface charge of −19.0 mV by TEM and DLS analysis, respectively. Silibinin loading efficiency in NIOs was about 90%, and the drug release pattern showed a controlled release with a maximum amount of about 49% and 70%, within 4 h in pH = 7.4 and pH = 5.8, respectively. To investigate the cytotoxicity effect, HT-29 cells were treated with the various concentration of the drugs for 24 and 48 h and evaluated by the MTT as well as flow cytometry assays. Obtained results demonstrated promoted cell cytotoxicity of silibinin-loaded MNNPs (5-fold decrease in cell viability) compared to pure silibinin (3-fold decrease in cell viability) while had no significant cytotoxic effect on HEK-293 (normal cell line) cells, and the cellular uptake level of MNNPs by the HT-29 cell line was enhanced compared to the control group. In conclusion, silibinin-loaded MNNPs complex can be considered as an efficient treatment approach for colorectal cancer cells.

KEYWORDS

silibinin, niosome, targeted therapy, magnetic nanoparticle, drug delivery, colon cancer

Introduction

Generally, cancer is a disorder in which abnormal cells are reinforced by escaping the conventional regulations of cellular division (Soltanian and Matin, 2011). Millions of people are being suffered from cancer, and the mortality caused by different kinds of cancer is dramatically growing in the world. Only in the United States, 1.7 million new cases of cancer were reported and over half a million people died of cancer in 2019, according to the Center for Disease Control (CDC) report (Hulvat, 2020). By 2029, it is estimated that there will be 16.8 million cancer deaths and 25.5 million new cancer cases annually (Thun et al., 2010). Colorectal cancer (CRC) is one of the most common malignancies in the digestive system, and it has been reported as the third most common malignant tumor worldwide (OLeary et al., 2018). The occurrence of CRC is expanding in metropolitan regions and industrialized nations, as well as nations encountering financial change, like Eastern Europe, most Asian nations, and a few South American nations (Bray et al., 2018). According to a recent study in Iran, the prevalence of CRC caused by adenomatous polyps (the most common cause) is about 34%, which is almost equal to the rate reported in developed countries. Targeted drug delivery for the pathogenesis factors of CRC has become an advance, and the recruitment of nanotechnology approaches has opened new horizons in this area (Tiwari et al., 2020).

Each cancer treatment method has benefits and disadvantages, and combined treatment is vital to get the best results (Mohammadian et al., 2016a; Mokhtari et al., 2017; Hassani et al., 2022). Since more than 85% of human cancers are solid tumors, current cancer therapy techniques usually contain invasive procedures, like chemotherapy, to shrink tumors before surgical removal (Rolston, 2017). Chemotherapy drugs target rapidly dividing cells, which are property of most types of cancer cells and some normal tissues. Although cytotoxic cancer drugs are highly effective, they exhibit significant adverse effects that limit the dose of chemotherapy drugs (Pérez-Herrero and Fernández-Medarde, 2015; Alagheband et al., 2022). Problems associated with chemotherapy are drug non-specificity caused by poor drug delivery systems. These problems are being solved using nanoparticles (NPs) as drug delivery systems (DDSs) or nanocarriers like protein cages, liposomes, micelles, niosomes (NIOs), metal, polymer, and protein NPs (Jadid et al., 2023; Jafari-Gharabaghlou et al., 2023). NIOs are a type of NPs used in drug delivery and consist of layered structures of vesicles made from non-ionic surfactants. NIOs are carriers of a hydrophobic and hydrophilic anticancer drug because they have an amphiphilic property, and can increase the half-life of the drugs conjugated with NPs in cancer cells (Coviello et al., 2015; Eatemadi et al., 2016). Owing to their lower toxicity, they improve the therapeutic index by limiting the drug action to the target cells. The non-ionic surfactant in NIOs is biodegradable and biocompatible, thus does not stimulate the body's immune system (Liu et al., 2017). Moreover, there is no need to manage and store surfactants in a specific condition. To boost the DDS function, a localized magnetic field is applied to direct the aggregation of NIOs in the target (Liu et al., 2017). Recently, magnetic NIOs NPs (MNNPs) conjugated with anticancer drugs are investigated. Promising results are reported about stimulus-responsive drug release at the target cancer site by applying an external magnetic field (Jamshidifar et al., 2021; Maurer et al., 2021; Momekova et al., 2021; Salmani Javan et al., 2022). The role of MNPs in bio-medicine, especially in the field of drug delivery, is important because their inherent magnetism facilitates many tasks, including targeting, which is very important and necessary in drug delivery (Mou et al., 2015). The combination of NIOs and MNPs provides both carrier targeting as well as drug protection properties that can be used as an efficient system for drug delivery (Pardakhty1 and Moazeni, 2013). Metal NPs can be enclosed inside NIOs with the desired drug to form MNNPs. Within the last decades, studies have focused on magnetic delivery approaches for vesicular DDSs, however, MNNPs have not been investigated widely. Plant-based drugs are usually the extract of medicinal herbs with different therapeutic applications (Solowey et al., 2014). Within the past decades, researchers have focused on herbal extracts, because of their anticancer and anti-neoplastic properties. Silibinin is an extract obtained from the medicinal plant *Silybum marianum* (Valková et al., 2021). Silibinin is the most active component of silymarin flavonoids that induces apoptosis and in the last 2 decades has been evaluated for the treatment of many tumors (alone or in combination with other chemotherapeutic agents) (Davis-Searles et al., 2005; Kaur et al., 2009). Previously, silibinin was administrated as a supplement in foods for liver diseases remedy (Carrier et al., 2003). Today, the anticancer property of silibinin is known to be related to the presence of flavonoid factors and some strategies to fight cancer cells, including interfering with the cell cycle, inhibiting angiogenesis, invasion, and metastasis through the effect of many molecular events (Denev et al., 2020). This plant extract is an inducer of cancer cell apoptosis and has been investigated for treatment of many tumors (alone or in combination with other chemotherapeutic agents) in the last 2 decades (Ghasemali et al., 2013; Badrzadeh et al., 2014; Jahanafrooz et al., 2018). Nonetheless, hydrophobicity is the most challenging obstacle regarding the application of silibinin in the body (Figure 1) (Iyengar and Devaraj, 2020). Therefore, targeted delivery systems for silibinin are essential to minimize side effects due to systemic drug distribution and achieve a maximum therapeutic effect. This research aimed to study the role of silibinin loaded in MNNPs compared with free drugs in targeting the HT-29 colorectal cancer cell line. To this end, MNNPs and silibinin-loaded MNNPs were synthesized and their physicochemical and morphological properties were evaluated. The MTT assay was done to investigate cell viability. Furthermore, cell cytotoxicity effects, apoptosis, and the cellular uptake rate of MNNPs were examined *in vitro*.

Materials and methods

Materials

Fetal bovine serum (FBS) and trypsin-EDTA were purchased from Gibco (Invitrogen, United Kingdom). Silibinin, DMEM (Dulbecco's Modified Eagle Medium), tween 80, cholesterol, sorbitan monostearate (Span 60), 3– (4,5 dimethylthiazol-2-yl)-2,5-diphenyltetrazolium bromide (MTT), trypsin, dimethyl sulfoxide (DMSO), phosphoric acid, and phosphate-buffered saline (PBS) were obtained from Sigma-Aldrich (St Louis, MO).

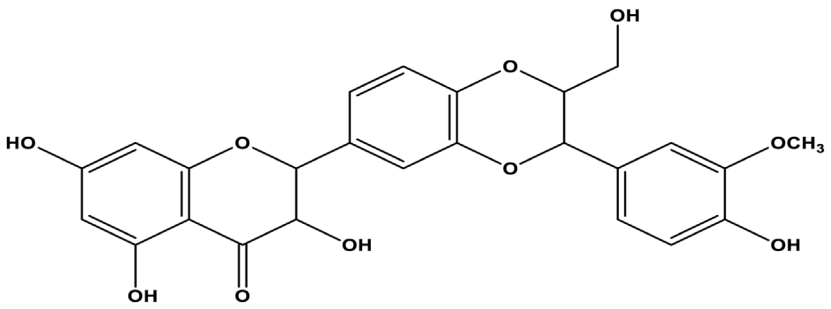

FIGURE 1
Molecular structure of silibinin.

Methanol, chloroform, ethanol, penicillin G, streptomycin, iron (III) chloride, and iron (II) chloride tetrahydrate were purchased from Merck, Germany. Annexin V-FITC apoptosis detection kit [including binding buffer, annexin V, and propidium iodide (PI)] was prepared from eBiosciences (MA, United States).

Cell culture

The HT-29 (colorectal cancer cell line) and HEK-293 (normal cell line) were purchased from the Pasteur Institute cell bank of Iran. The cells were grown in DMEM medium supplemented with FBS (10%), 0.05 mg/mL penicillin G, and 0.08 mg/mL streptomycin. HT-29 colon cancer cells were placed in sterile flasks and incubated at 37°C in a humidified atmosphere containing 5% CO2.

Synthesis and coating of MNPs

Generally, the co-precipitation method was applied to synthesize MNPs (Kedar et al., 1997). The amount of 6.5 g of $FeCL_3$ and 4 g of $FeCL_2$. $4H_2O$ were blended in 100 mL of deionized water in a three-neck flask, and then 200 mL of 2 M NaOH was added dropwise into the flask and stirred for 2 h at a speed rate of 1,000 rpm under N_2 at room temperature. The resulting MNPs were washed twice with distilled water and ethanol (96%) and the final precipitate was placed in a 50°C oven to dry. In the next step, the MNPs were coated with a succinate starch. To synthesis succinate starch, 25 mL of distilled water was added to 4 g of starch, and then 12.5 mL of 2 M NaOH was added to obtain a clear, yellowish solution. Subsequently, 3.7 g of succinic acid (SA) was added to the solution, and the mixture was stirred (1,200 rpm) for 4 h at 100°C. After cooling, 50 mL of cold ethanol (96%) was added to form a white precipitate. Afterward, the sediment was washed several times with ethanol (96%) and dried in an oven at 60°C. To prepare MNPs Ferro fluid, 100 mg of MNPs and 100 mg of succinate starch were mixed in 10 mL of distilled water and stirred (1,000 rpm) for 24 h at room temperature. Finally, the supernatant solution was separated and in order to deposit the iron nanoparticles attached with starch it was placed on a magnet, then the supernatant solution was discarded and the precipitate was collected and dried at room temperature (Fathi et al., 2014; Shahbazi et al., 2023).

Synthesis of NIOs by thin film hydration method

Thin-film hydration method was used to synthesize NIOs. Briefly, 20 mg of Span 60, 15 mg of Tween 80, and 7 mg of cholesterol were dissolved in 6 mL of chloroform and 6 mL of methanol solvents (with a 1:1 ratio). Next, the Solvents were evaporated from the mixture by rotary evaporator (120 rpm, 60°C, 1 h). Finally, a thin layer film of milky surfactant was formed on the wall of the flask. In the next step, 10 mL PBS was added and placed in the rotary for 10 min until the transformation of pro-niosomes to NIOs (Shahbazi et al., 2023). Then, the NIOs suspension was placed in ice bath and exposed to sonication with a probe sonicator (Amplitude of 25%, 200 w) (Fisher Scientific Co., US), to reduce the size of NIOs and to break NIOs aggregates. Silibinin was added in the first step of synthesis due to its lipophilic nature while ferrofluid MNPs were added along with PBS.

MNNPs size, surface charge, and structural characteristics

The dynamic light scattering (DLS) method was used to assess the size and surface charge of synthesized NPs. Furthermore, a transmission electron microscope (TEM) (LEO906E, Carl Zeiss, Oberkochen, Germany), operating at 80 kV was used to determine the size and morphology of the prepared MNNPs. For TEM and FT-IR analysis, the samples were freeze-dried by a freeze-dryer (Dena Vacuum, FD-5005-BT, Iran). Also, Fourier transforms infrared (FT-IR Tensor 27 spectrometer) spectrum (500–4,000 cm-1) was used to evaluate the structural analysis of synthesized NPs, and a vibrating sample magnetometer (VSM) (MDK, Iran) was used to evaluate the magnetization value of MNNPs.

Assessment of drug loading (DL) and encapsulation efficiency (EE) of MNNPs

To determine the amount of loaded silibinin and also to remove the unloaded drug, a dialysis membrane method was performed. Briefly, 5 mL of the silibinin loaded MNNPs were added into a container with 50 mL PBS and magnetically stirred at 120 rpm. To

protect the stability of MNNPs, the container was exposed to the ice. The encapsulation efficiency (EE) and drug loading capacity (DL) were determined by the measurement of unloaded drug via UV-Vis spectroscopy at 288 nm considering the calibration curve by the following formula:

$$\text{EE (\%)} = \frac{\text{Mass of drug in NPs}}{\text{Total drug mass}} \times 100$$

$$\text{DL (\%)} = \frac{\text{Mass of drug in NPs}}{\text{Total NPs mass}} \times 100$$

Assessment of drug release rate of MNNPs

First, the MNNPs containing silibinin were transferred to two clamped dialysis bags that were inserted in distilled water for 24 h. For the simulation of normal and abnormal (cancer) conditions, PBS (pH = 7.4) and composed of methanol and 0.02 M phosphoric acid (50: 50, v/v) (pH = 5.8) were used, respectively. Buffer solutions (50 mL of each) were added into two lidded containers, and the dialysis bags were exposed to buffers. Bags were shaken (100 rpm) at 37°C. At different time intervals, 2 mL of the sample was replaced with 2 mL of fresh solution. The release pattern was calculated using UV-Vis spectrophotometer at 288 nm. Also, the release curves were evaluated by various kinetic models (Fathi et al., 2018).

MTT assay

The cytotoxicity of drugs was evaluated by MTT assay, briefly, 6.5×10^3 HT-29 and HEK-293 cells/well were seeded in a 96-well plate and incubator at 37°C with 5% CO_2 for 24 h. Afterward, cells were exposed to various doses of free and encapsulated silibinin and incubated for 24 and 48 h. After the required incubation time, 50 µL of the MTT solution (2 mg/mL) was added to each well, and plates were covered with an aluminum foil and incubated for 4 h. After this time, the supernatant was removed, and 100 µL of DMSO was added and shaken for 10 min. Finally, the plates were transferred to the ELISA reader (Biotech Co., United States), and the optical densities (ODs) were read at a reference wavelength of 570 nm in comparison to untreated control cells.

Cell apoptosis assessment

Flow cytometry technique was used to analyze cell apoptosis, in summary, 70,000 HT-29 cells were seeded to each well in 6-well plates. For cell treatment, silibinin and NIOs complex (40 µg/mL) were used and treated for 48 h. After separating, the cells were washed twice with PBS and centrifuged at 190 g for 5 min. Then, 100 µL of binding buffer, 5 µL of FITC (0.25 µg/mL), and 5 µL of propidium iodide (20 µg/mL) were added to each sample and left for 20 min in the dark at room temperature. Finally, 100 µL of binding buffer (0.1 M Hepes (pH 7.4), 1.4 M NaCl, and 25 mM CaCl2) was added, and reading was performed using a flow cytometry device (Thermo Fisher Scientific Co., United States) in the darkness.

Assessment of cellular uptake of NIOs

For this purpose, 5 mg of FITC was dissolved in 1 mL of methanol, and 250 µL was added to each falcon and mixed with 1 mL of niosomal complexes. Covered falcons were placed in a shaker with ice at a speed of 100 rpm overnight, and then the contents of the falcons were washed in two steps under dark conditions using PBS. Subsequently, 70,000 HT-29 cells were seeded in each well of 6-well plates and exposed to niosomal complex for 4 h in the darkness in a humidified atmosphere containing 5% CO2. After the treatment, the cells were transferred to falcons and centrifuged for 5 min at 190 g, after discarding the supernatant, washed with PBS and centrifuged, and this process was repeated and finally, the reading was done with a flow cytometry device.

Statistical analysis

Statistical analysis was performed using the non-parametric paired Wilcoxon test and statistical significance was described when the *p*-value was less than 0.05. All statistical analyzes were performed by Flowjo-V10 and Prism software version 9.3. The results were expressed as the mean ± standard deviation (SD) of three independent experiments.

Results and discussion

Measurement and characterization of synthesized MNNPs

Generally, MNNPs size is one of the principal characteristics regarding the release of the drug from the MNNPs, physical stability, cellular absorption, and biological distribution (Barani et al., 2019). The size and surface charge of the synthesized MNNPs were checked using the DLS method. The distribution intensity of MNNPs was obtained at 70 nm with DLS (Figure 2A). According to the TEM image, shapes and distributions of MNNPs were homogeneous spherical with a size of 50 nm (Figure 2B). Typically, the size of MNNPs in the TEM images was smaller than in DLS as DLS, the hydrodynamic diameter of the MNNPs was measured. The larger MNNPs in the images are associated with the overlapping/agglomeration of some smaller MNNPs during the preparation (Liu et al., 2021). Lately, researchers have focused on the surfactants coating the MNNPs, because they can act as a steric barrier and intercept agglomeration caused by magnetic dipole–dipole attractions between MNNPs (Ramimoghadam et al., 2015). The different sizes have been reported by previous research, and it seems that other physical attributes of MNNPs like surface charge as well as different structures of chemical compounds and synthesis methods are responsible for the size of MNNPs (Barani et al., 2020; Ag Seleci et al., 2021). Considering that NPs in the range of 70–200 nm are stable in the bloodstream and are considered long-circulating agents, synthesized MNNPs with the above size can be used for smart drug delivery in pharmaceutical purposes, according to previous published studies (Barar and Omidi, 2014).

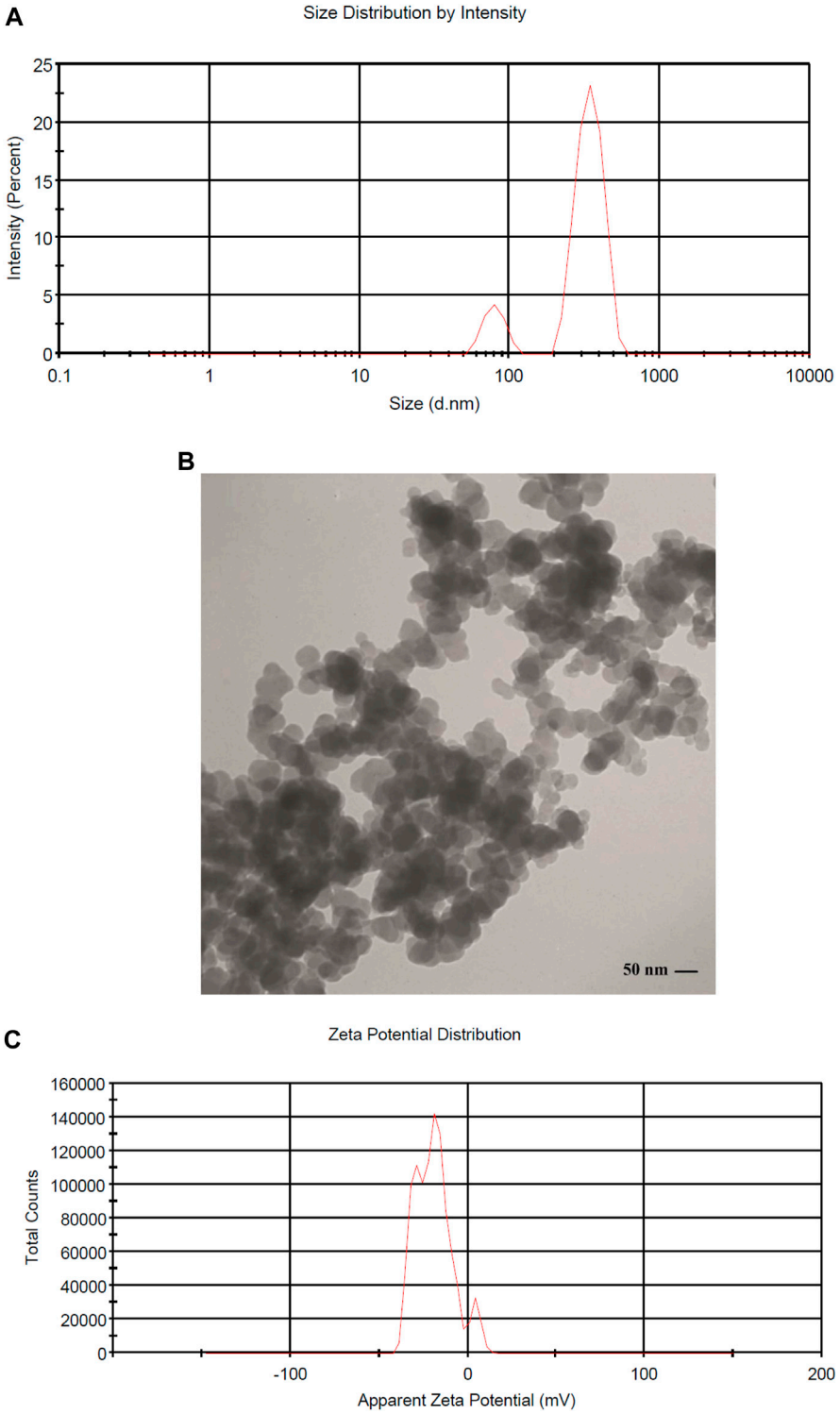

FIGURE 2
(A) DLS histogram showing the size distribution intensity of magnetic niosome NPs MNNPs, **(B)** Characterization of MNNPs size and morphology using Transmission Electron Microscopy (TEM), and **(C)** zeta potential distribution of MNNPs.

In addition, it was demonstrated that NPs less than 200 nm can be escaped of the immunes system, while NPs with size less than 70 nm can be accumulated by the liver (Barar and Omidi, 2014). MNNPs charge is another important feature that has a considerable impact in entering and capturing the drug into the cell and size distribution of MNNPs.

It is established that making a targeted surface charge of synthesized NPs is a practical strategy to control their

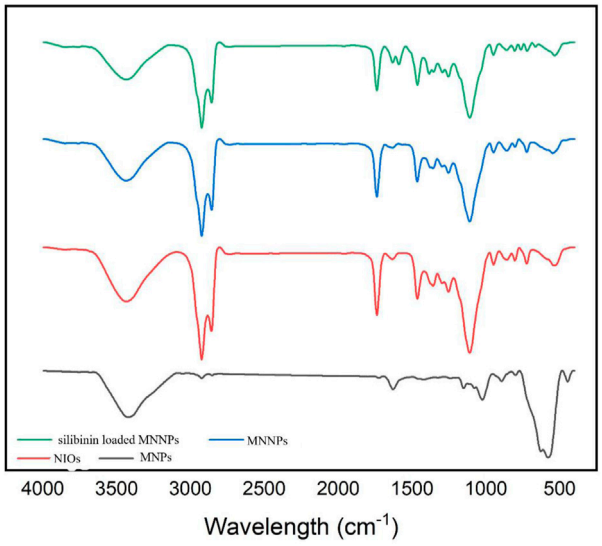

FIGURE 3
FTIR spectrum for magnetic nanoparticles (MNPs), niosomes (NIOs), magnetic niosomes nanoparticles (MNNPs), and silibinin loaded MNNPs. The results demonstrated that the silibinin was effectively encapsulated in MNNPs.

assimilation into the particular destination (Osaka et al., 2009; Stiufiuc et al., 2013). Usually, a positive charge of NPs surface through coating leads to convenient and fast cellular uptake when NPs are encountered with the negative charge on the cell membrane (Su et al., 2012). In this research, the surface charge of the synthesized MNNPs was determined using the DLS method as the zeta potential was −19.0 mV (Figure 2C) and polydispersity index (PDI) was 0.52. The zeta potential result reveals that the surface charges of synthesized MNNPs are negative. This negative charge reduces the toxicity of the system and improves its performance by preventing the accumulation and deposition of NPs. FT-IR technique was used to study the chemical structure of the prepared MNNPs, and to measure the non-interaction of the synthesized niosomal system with silibinin and MNPs. Expected peaks related to MNPs, modified NIOs, MNNPs, and silibinin loaded MNNPs were monitored, which indicated that silibinin and MNPs were loaded in NIOs (Figure 3). In examining the FT-IR spectrum of drug-free NIOs (Figure 3), the peak at 3,433 cm^{-1} is characteristic of the–OH group and the peak at 1738 cm^{-1} is related to C=O stretching vibrations. Finally, the peaks at 2,923 cm^{-1} and 1,109 cm^{-1} are related to the C-H bond and vibrations of C-O bond stretching, respectively (Mehta and Jindal, 2013; Samed et al., 2018). For NIOs containing silibinin and MNPs, the peak at 1,631 cm^{-1} corresponds to C=O stretching vibrations, and the peak at 3,435 cm^{-1} is associated with the -CH bond. Furthermore, the absorption peaks at 2,923 cm^{-1}, 1,108 cm^{-1}, and 720 cm^{-1} belong to the C-H bond, stretching vibrations of the C-O bond, and Fe-O bond in Fe_3O_4, respectively (Ebrahimnezhad et al., 2013). By comparing the peaks in the FT-IR spectrum related to NIOs, MNNPs, and silibinin loaded MNNPs, it was observed that slight changes occurred in the peaks related to NIOs containing silibinin compared to NIOs without drug, and this confirmed that

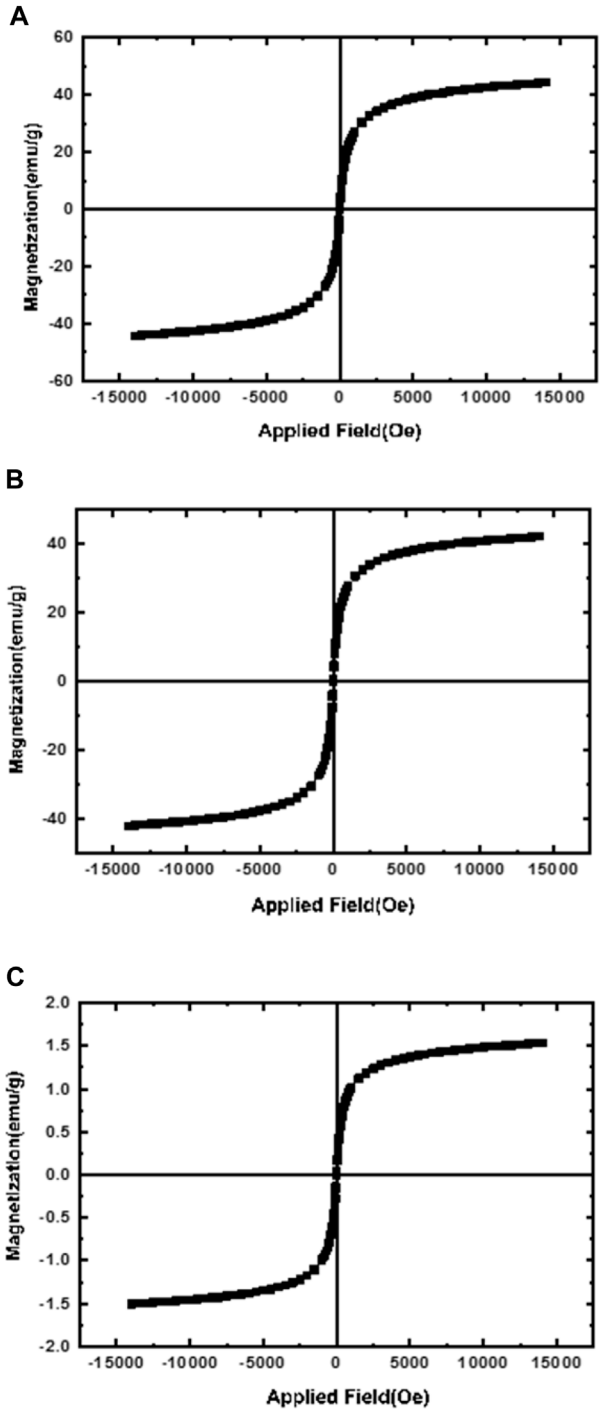

FIGURE 4
Magnetization curves of **(A)** magnetic nanoparticles (MNPs); **(B)** Starch-modified MNPs, and **(C)** magnetic niosomes nanoparticles (MNNPs). The results confirmed the loading of MNPs and silibinin in NIOs is done properly.

silibinin drug is placed in the NIOs nisome. Also, considering that no new peak was added and disappeared in the FT-IR spectrum of NIOs containing the drug, it can be assumed that no chemical interaction occurred between the NIOs and the drug as both kept their nature and remained away from change.

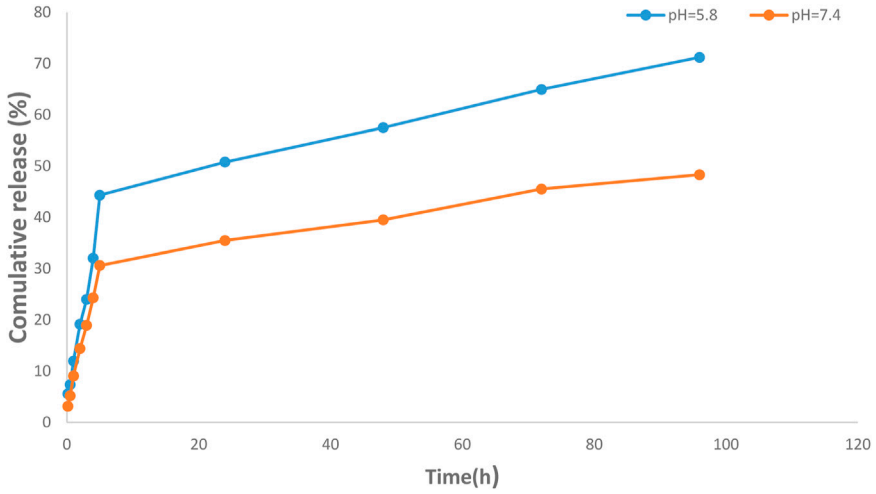

FIGURE 5
Investigation of drug release efficiency from magnetic nisome nanoparticles (MNNPs) at pH = 5.8 and 7.4 at 37°C. The pores of the dialysis membrane are large enough to allow the free movement of silibinin, but small enough to prevent the diffusion of nanoparticles. The results demonstrated a sustained release pattern from the nanoparticle with a partially burst-release at the initial stage and followed sustained during the 96 h study period. Data are presented as mean ± SD of three independent experiments.

Vibrating sample magnetometer (VSM) was used to evaluate the superparamagnetism of NPs. Since the reason for using magnetic NPs is the targeted delivery of the carrier by applying an external magnetic field, it is very important and necessary to determine the magnetic properties of these NPs. the magnetic activities of MNNPs, starch modified MNPs, and MNPs were demonstrated using vibrating sample magnetometry (VSM) at room temperature. The hysteresis curve in Figure 4A; Figure 4B showed that the saturation magnetization of MNPs was 42 emu/g. Compared to the saturation magnetization of MNNPs in Figure 4C, which is 1.5 emu/g, this value is higher. This difference confirms that the loading of MNPs and silibinin in NIOs is done properly, according to previous studies published in this area. The Figure 4 does not show any hysteresis curve indicating the superparamagnetic behavior of the synthesized particles (Yang et al., 2006).

Encapsulation efficiency, drug release rate of MNNPs and kinetics models

Encapsulation efficiency (EE) is defined as the ratio of the amount of drug in the MNNPs to the total amount of drug applied in NPs formulation. Currently, a large number of NPs systems have relatively low EE, thus developing strategies to increase EE remains a challenge (Liu et al., 2019). EE has been increased while there is a drug concentration increase thanks to polymers and MNNPs, based on the previously published studies (Prabha and Raj, 2016; Ghadiri et al., 2017; Erdagi and Yildiz, 2019). Jin et al. (2018) argued lowering the pH is a promising way to boost the EE efficiency up to approximately 70% in the MNNPs formation while this efficiency without pH change is between 10% and 15% at maximum. In the present study, the EE in NIOs was more than 90%, which indicates the high potential of MNNPs in EE. Span 60 and also cholesterol which are used in the NIOs structure increase the amount of the hydrophobic drug loading into NIOs (Jadon et al., 2009). The results indicated the release of the silibinin with a gentle and slow gradient from MNNPs. Evaluating the drug release pattern shows that the designed NIOs, while indicating a controlled release, have a burst release within 4 h, then in the conditions of normal cells (pH 7.4) and cancer cells (pH 5.8) released about 49% and 70%, respectively during 100 h (Figure 5). These findings reveal that MNNPs are sensitive to different pH. The high acidity of tumor cells is attributed to hypoxia, or lack of oxygen owing to the inadequate blood supply (Justus et al., 2013). It was demonstrated that the MNNPs indicated better performance in tumor microenvironment (pH 5.0–6.8) compared to the physiological condition which make them the suitable candidate for DDS (Mohammadian et al., 2016b; Myat et al., 2022). Considering that tumor cells have a significantly acidic cytoplasmic pHs compared to normal cells, therefore MNNPs are more efficient with more DR at acidic pH compared to pH = 7.4 (AlSawaftah et al., 2022). This makes NIOs a good candidate for drug delivery in cancer. The results indicated the release of the silibinin with a gentle and slow gradient from MNNPs. Our findings are in agreement with previous studies that confirmed the promising role of MNNPs in the drug release process. Barani et al. reported, the drug's release profile from MNNPs showed a first rapid release (about 50% of the drug was released within 10 h), followed by a slower and longer-lasting release (65% of the drug was released within 30 h) in acidic conditions (Barani et al., 2019). Similar outcomes were obtained by Zheng et al. (2009) Preparation and definition of magnetic cationic liposomes for gene transfer research. Tavano et al. (2013) synthesized MNNPs loading doxorubicin (an anticancer drug) for smart drug delivery and argued that the utilization

TABLE 1 The kinetics models used to fit the silibinin release data from MNNPs at different pHs. The bold values indicated the best fitted models.

Kinetics model	Equation	Coefficient of determination (R^2)	
		pH = 5.8	pH = 7.4
Zero order	$F = k_0\, t$	0.7542	0.7274
First order	$\ln(1 - F) = -k_f\, t$	0.8673	0.7959
Higuchi	$F = k_H \sqrt{t}$	0.9030	0.8896
Power law	$\ln F = \ln k_P + P \ln t$	**0.9506**	**0.9627**
Square root of mass	$1 - \sqrt{1 - F} = k_{1/2}\, t$	0.8131	0.7622
Hixson-Crowell	$1 - \sqrt[3]{1 - F} = k_{1/3}\, t$	0.8319	0.7736
Three seconds' root of mass	$1 - \sqrt[3]{(1 - F)^2} = k_{2/3}\, t$	0.7937	0.7507
Weibull	$\ln(-\ln(1 - F)) = -\beta \ln t_d + \beta \ln t$	0.9462	0.9208
Reciprocal powered time	$(\frac{1}{F} - 1) = \frac{m}{t^b}$	**0.9610**	**0.9365**

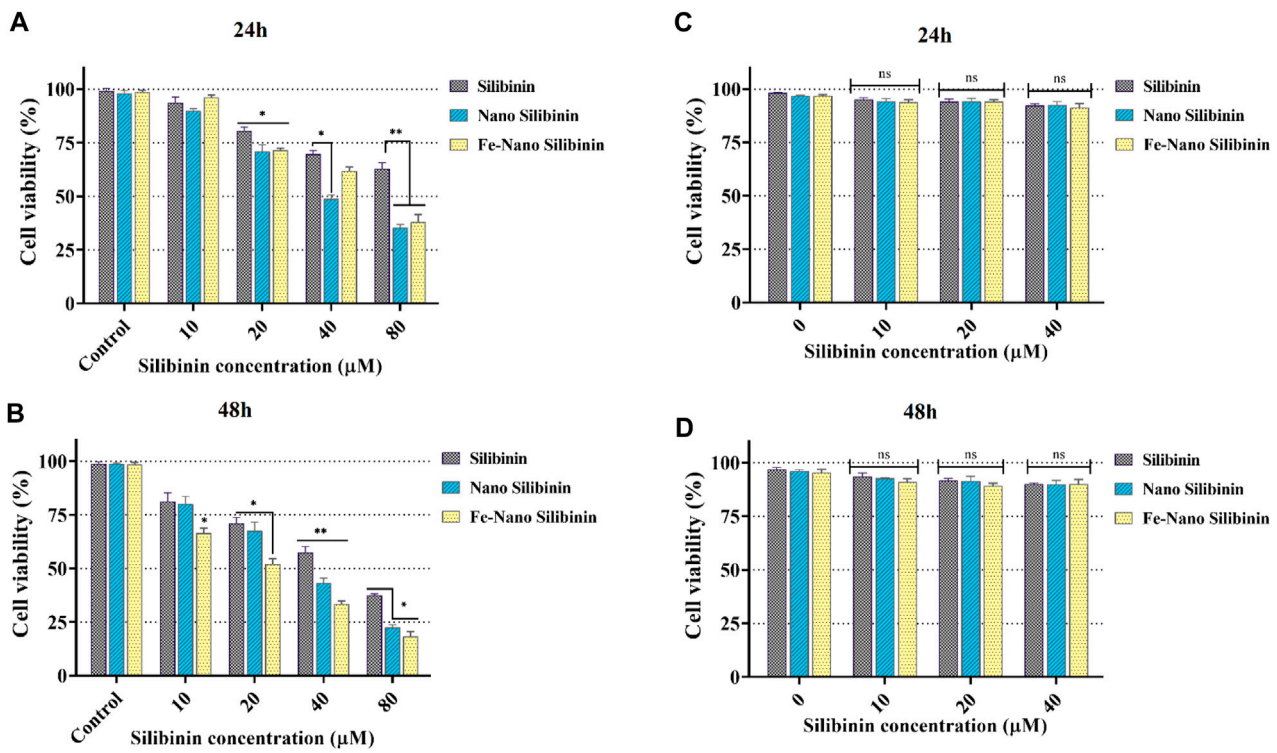

FIGURE 6
MTT assay results revealed *in vitro* cytotoxicity of blank NIOs (control), Silibinin, Silibinin loaded NIOs, Silibinin loaded magnetic NIOs NPs on HT-29 colon cancer cells [**(A)** and **(B)**], and HEK-293 normal cell line [**(C)** and **(D)**] after 24 h and 48 h incubation time. Encapsulation of silibinin in MNNPs improved its cytotoxic effect on HT-29 colon cancer cells, while it had no significant cytotoxic effect on HEK-293 cells. Data are presented as mean ± SD of three independent experiments. Error bars show standard variations and significance is indicated by *$p < 0.05$, **$p < 0.01$ and ***$p < 0.001$ compared to the control group.

of MNNPs can improve the release rate of formulations. Table 1 shows various kinetic models that were used to fit the silibinin release curves at different pHs. According to Table 1, the fitted model for release curves were Pawer law and Reciprocal powered time at pH = 7.4 and 5.8.

Cell cytotoxicity of MNNPs

Through receptor-mediated endocytosis, targeted NPs can enter the target cells, increasing the concentration of drug molecules within the cell. P-glycoprotein does not recognize drug molecules

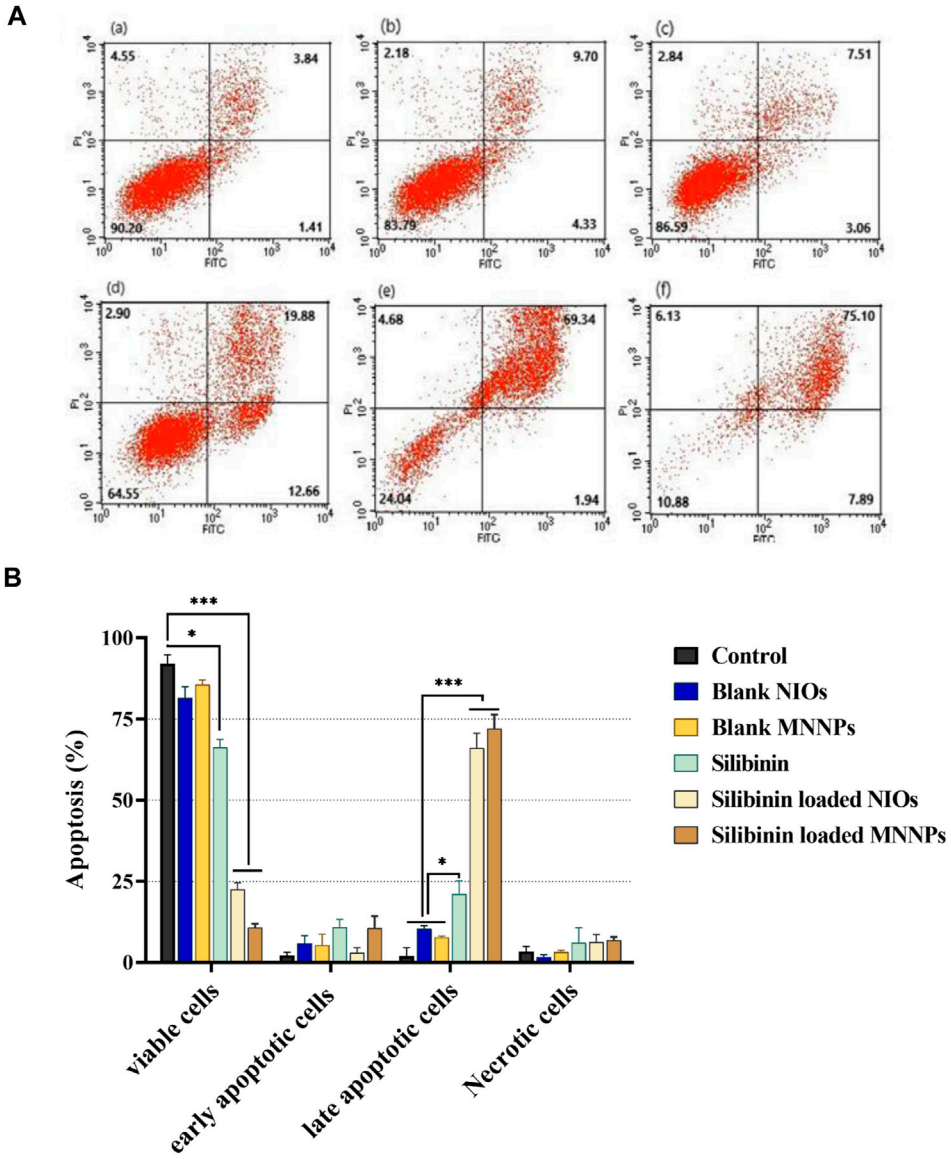

FIGURE 7
(A). Apoptosis analysis on HT-29 cell line under treatment (a) control, (b) blank NIOs, (c) blank MNNPs, (d) Silibinin, (e) Silibinin loaded NIOs, (f) Silibinin loaded MNNPs. **(B)**. HT-29 cells treated with pure silibinin and niosomal complexes were evaluated after 48 h by FITC-labeled annexin V/PI flow cytometry. The obtained results confirmed that NIOs loaded with the silibinin significantly increase the apoptosis of HT-29 cells, which emphasizes the increase in the absorption of drugs from NIOs by the cells. This result is consistent with the MTT results. Data were analyzed using Flowjo-V10 analysis software and shown as mean ± SD of three independent experiments. Significance is indicated by $*p < 0.05$, $**p < 0.01$ and $***p < 0.001$ compared to the control group.

during this process, and membrane efflux transporters pump free drug molecules out of the cell (Wang et al., 2016). In the cell cytotoxicity assessment by the MTT method, HT-29 and HEK-293 cells were treated with free-drug and silibinin MNNPs for 24 and 48 h at various concentrations (10, 20, 40, and 80 μg/mL) (Figure 6). The results showed that NIOs containing silibinin caused more cell death in the studied times compared to pure silibinin in the HT-29 colon cancer cells and had no significant cytotoxic effect on HEK-293 cells. Thus, nanocarriers can increase the cell cytotoxicity of the drug against HT-29 cells, and there is a dose-dependent and relatively time-dependent manner regarding using complex. These results confirm the previous studies reported that the cytotoxicity of the drug-loaded MNNPs follows dose-dependent and time-dependent trends (Huang et al., 2015; Dhavale et al., 2021). The IC50 of the MNNPs complex was observed at 40 μg/mL within 48 h, therefore this concentration was considered for the following tests. The survival of over 90% of cells under drug-free NIOs treatment revealed that MNNPs have a very tiny lethal effect on the cells. This biocompatibility makes these MNNPs excellent candidates for therapeutic purposes. Additionally, the MTT test revealed that there was no significant correlation between the control group and silibinin-free NIOs.

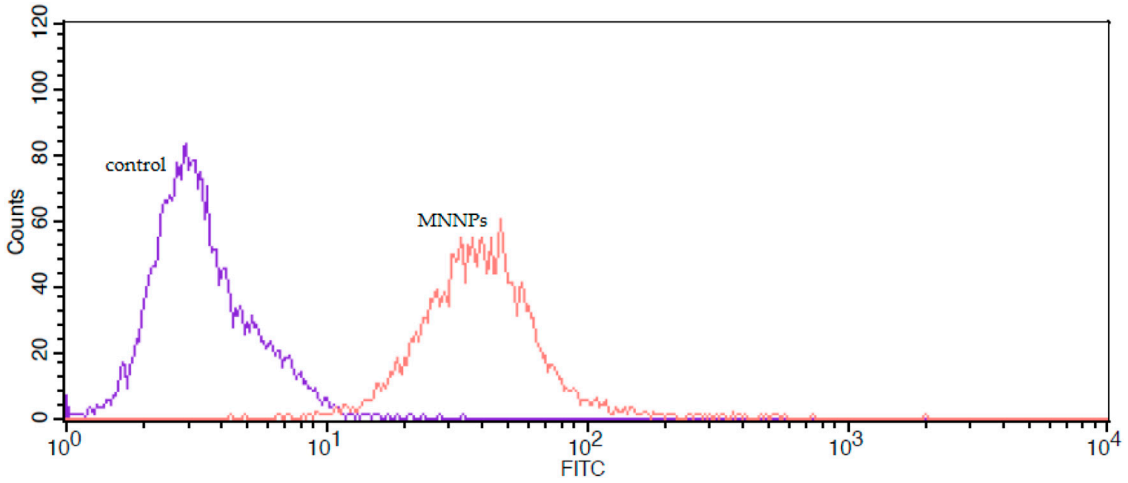

FIGURE 8
The flow cytometry analysis of uptake of FITC-labeled magnetic nisome nanoparticles (MNNPs) by HT-29 cells.

Apoptosis and cellular uptake analysis on HT-29 cell line

HT-29 cells that treated with pure silibinin and silibinin loaded MNNPs were evaluated after 48 h' incubation by FITC-labeled Annexin V/PI flow cytometry technique. As shown in Figure 7, silibinin-loaded MNNPs significantly induce apoptosis of HT-29 cells more than other forms, furthermore, silibinin-loaded MNNPs exhibited a greater cytotoxic effect compared to the free silibinin, which demonstrates the increase in the uptake of silibinin from MNNPs by the cells. These findings are consistent with earlier research, which indicated that the internalization and subsequent intracellular release of the anticancer drug from NPs is responsible for the cytotoxic effect of NPs (Zaki, 2014). It is proposed that this formulation (niosome and magnetic niosome) can increase the drug bioavailability which can induce cancer cell apoptosis by causing DNA damage or the oxidation of proteins, lipids, and enzymes, resulting in cell death and also helping to destroy and inhibit the mitochondrial respiratory complex (Rodrigues Pereira da Silva et al., 2016; Van Houten et al., 2016; Juan et al., 2021). El-Far and co. argued that the cytotoxicity percentage by IC50 value between paclitaxel–metal NPs–NIOs and oxaliplatin–metal NPs–NIOs at the same concentrations did not differ significantly (pH 0.5). Therefore, they recommended that MNNPs are considered a suitable targeting nanocarrier system for drug delivery in colorectal cancer, target tumor cells and prolong circulation for both drugs (El-Far et al., 2022).

Also, cellular uptake was studied by FITC labeled NPs and via flow cytometry. Figure 8 illustrates the cellular uptake level of MNNPs by the HT-29 cell line was 99% compared to the control group. These findings indicated that the MNNPs could enhance cellular uptake significantly and induce apoptosis in the HT-29 cell line after treatment, and are consistent with previous studies that used flow cytometry to examine apoptosis and MNP uptake in cells (Depan and Misra, 2012; Li et al., 2018; Lu et al., 2018).

Conclusion

In the current study, silibinin was loaded into NIOs containing MNPs (MNNPs) as a novel formulation to evaluate its apoptosis effect in colorectal cancer cells treatment. The size distribution, surface charge, and chemical structure of synthesized MNNPs were suitable for immune escape and confirmed that silibinin was entrapped in NIOs. According to the obtained cytotoxicity evaluations, silibinin loaded in MNNPs has more cytotoxic effects on HT-29 colon cancer cells in a dose- and time-dependent manner, and the cellular uptake of MNNPs by the HT-29 cell line was higher than controls. Drug loading evaluation exhibited a high efficiency and drug-loaded MNNPs showed an accelerated release rate in acidic pH in cancer cells compared to the neutral condition. To sum up, the MNNPs as nanocarriers are excellent candidates for the treatment of cancer cells, especially colorectal cancer. However, further *in vivo* experiments are required to prove the potential of the developed formulation as a suitable vehicle for the various cancerous cells treatment.

Data availability statement

The original contributions presented in the study are included in the article/supplementary materials, further inquiries can be directed to the corresponding author.

Author contributions

GS: Methodology, Investigation, Data curation, Original draft preparation. DJ and MF: Methodology, Investigation, Data curation, Original draft preparation. MF: Methodology, Investigation, Original draft preparation. EA: Reviewing and Editing. NZ: Supervision, Conceptualization, Writing- Reviewing and Editing. All authors contributed to the article and approved the submitted version.

Funding

This study is a part of an MSc thesis (Grant no: 68129) and the authors acknowledge the financial support provided by the Research Vice-Chancellor of Tabriz University of Medical Sciences.

Acknowledgments

The authors want to thank the Research Center for Pharmaceutical Nanotechnology and Department of Medical Biotechnology, Faculty of Advanced Medical Sciences at Tabriz University of Medical Sciences for technical supports.

Conflict of interest

The authors declare that the research was conducted in the absence of any commercial or financial relationships that could be construed as a potential conflict of interest.

Publisher's note

All claims expressed in this article are solely those of the authors and do not necessarily represent those of their affiliated organizations, or those of the publisher, the editors and the reviewers. Any product that may be evaluated in this article, or claim that may be made by its manufacturer, is not guaranteed or endorsed by the publisher.

References

Ag Seleci, D., Maurer, V., Barlas, F. B., Porsiel, J. C., Temel, B., Ceylan, E., et al. (2021). Transferrin-decorated niosomes with integrated InP/ZnS quantum dots and magnetic iron oxide nanoparticles: Dual targeting and imaging of glioma. *Int. J. Mol. Sci.* 22 (9), 4556. doi:10.3390/ijms22094556

Alagheband, Y., Jafari-gharabaghlou, D., Imani, M., Mousazadeh, H., Dadashpour, M., Firouzi-Amandi, A., et al. (2022). Design and fabrication of a dual-drug loaded nano-platform for synergistic anticancer and cytotoxicity effects on the expression of leptin in lung cancer treatment. *J. Drug Deliv. Sci. Technol.* 73, 103389. doi:10.1016/j.jddst.2022.103389

AlSawaftah, N. M., Awad, N. S., Pitt, W. G., and Husseini, G. A. (2022). pH-responsive nanocarriers in cancer therapy. *Polymers* 14 (5), 936. doi:10.3390/polym14050936

Badrzadeh, F., Akbarzadeh, A., Zarghami, N., Yamchi, M. R., Zeighamian, V., Tabatabae, F. S., et al. (2014). Comparison between effects of free curcumin and curcumin loaded NIPAAm-MAA nanoparticles on telomerase and PinX1 gene expression in lung cancer cells. *Asian Pac. J. Cancer Prev.* 15 (20), 8931–8936. doi:10.7314/apjcp.2014.15.20.8931

Barani, M., Nematollahi, M. H., Zaboli, M., Mirzaei, M., Torkzadeh-Mahani, M., Pardakhty, A., et al. (2019). *In silico* and *in vitro* study of magnetic niosomes for gene delivery: The effect of ergosterol and cholesterol. *Mater. Sci. Eng. C* 94, 234–246. doi:10.1016/j.msec.2018.09.026

Barani, M., Torkzadeh-Mahani, M., Mirzaei, M., and Nematollahi, M. H. (2020). Comprehensive evaluation of gene expression in negative and positive trigger-based targeting niosomes in HEK-293 cell line. *Iran. J. Pharm. Res. IJPR.* 19 (1), 166–180. doi:10.22037/ijpr.2019.112058.13507

Barar, J., and Omidi, Y. (2014). Surface modified multifunctional nanomedicines for simultaneous imaging and therapy of cancer. *BioImpacts BI* 4 (1), 3–14. doi:10.5681/bi.2014.011

Bray, F., Ferlay, J., Soerjomataram, I., Siegel, R. L., Torre, L. A., and Jemal, A. (2018). Global cancer statistics 2018: GLOBOCAN estimates of incidence and mortality worldwide for 36 cancers in 185 countries. *CA a cancer J. Clin.* 68 (6), 394–424. doi:10.3322/caac.21492

Carrier, D. J., Crowe, T., Sokhansanj, S., Wahab, J., and Barl, B. (2003). Milk thistle, Silybum marianum (L) Gaertn, flower head development and associated marker compound profile. *J. herbs, spices Med. plants* 10 (1), 65–74. doi:10.1300/j044v10n01_08

Coviello, T., Trotta, A., Marianecci, C., Carafa, M., Di Marzio, L., Rinaldi, F., et al. (2015). Gel-embedded niosomes: Preparation, characterization and release studies of a new system for topical drug delivery. *Colloids surfaces B biointerfaces* 125, 291–299. doi:10.1016/j.colsurfb.2014.10.060

Davis-Searles, P. R., Nakanishi, Y., Kim, N. C., Graf, T. N., Oberlies, N. H., Wani, M. C., et al. (2005). Milk thistle and prostate cancer: Differential effects of pure flavonolignans from Silybum marianum on antiproliferative end points in human prostate carcinoma cells. *Cancer Res.* 65 (10), 4448–4457. doi:10.1158/0008-5472.CAN-04-4662

Denev, P., Ognyanov, M., Georgiev, Y., Teneva, D., Klisurova, D., and Yanakieva, I. Z. (2020). Chemical composition and antioxidant activity of partially defatted milk thistle (Silybum marianum L) seeds. *Bulg. Chem. Commun.* 52, 182–187.

Depan, D., and Misra, R. (2012). Hybrid nanoparticle architecture for cellular uptake and bioimaging: Direct crystallization of a polymer immobilized with magnetic nanoparticles on carbon nanotubes. *Nanoscale* 4 (20), 6325–6335. doi:10.1039/c2nr31345f

Dhavale, R. P., Dhavale, R., Sahoo, S., Kollu, P., Jadhav, S., Patil, P., et al. (2021). Chitosan coated magnetic nanoparticles as carriers of anticancer drug telmisartan: pH-responsive controlled drug release and cytotoxicity studies. *J. Phys. Chem. Solids* 148, 109749. doi:10.1016/j.jpcs.2020.109749

Eatemadi, A., Daraee, H., Aiyelabegan, H. T., Negahdari, B., Rajeian, B., and Zarghami, N. (2016). Synthesis and characterization of chrysin-loaded PCL-PEG-PCL nanoparticle and its effect on breast cancer cell line. *Biomed. Pharmacother.* 84, 1915–1922. doi:10.1016/j.biopha.2016.10.095

Ebrahimnezhad, Z., Zarghami, N., Keyhani, M., Amirsaadat, S., Akbarzadeh, A., Rahmati, M., et al. (2013). Inhibition of hTERT gene expression by silibinin-loaded PLGA-PEG-Fe3O4 in T47D breast cancer cell line. *BioImpacts BI* 3 (2), 67–74. doi:10.5681/bi.2013.005

El-Far, S. W., Abo El-Enin, H. A., Abdou, E. M., Nafea, O. E., and Abdelmonem, R. (2022). Targeting colorectal cancer cells with niosomes systems loaded with two anticancer drugs models; comparative *in vitro* and anticancer studies. *Pharmaceuticals* 15 (7), 816. doi:10.3390/ph15070816

Erdagi, S. I., and Yildiz, U. (2019). Diosgenin-conjugated PCL–MPEG polymeric nanoparticles for the co-delivery of anticancer drugs: Design, optimization, *in vitro* drug release and evaluation of anticancer activity. *New J. Chem.* 43 (17), 6622–6635. doi:10.1039/c9nj00659a

Fathi, M., Entezami, A. A. J. S., and Analysis, I. (2014). Stable aqueous dispersion of magnetic iron oxide core–shell nanoparticles prepared by biocompatible maleate polymers. *Surf. Interface Anal.* 46 (3), 145–151. doi:10.1002/sia.5362

Fathi, M., Zangabad, P. S., Barar, J., Aghanejad, A., Erfan-Niya, H., and Yjijobm, O. (2018). Thermo-sensitive chitosan copolymer-gold hybrid nanoparticles as a nanocarrier for delivery of erlotinib. *Int. J. Biol. Macromol.* 106, 266–276. doi:10.1016/j.ijbiomac.2017.08.020

Ghadiri, M., Vasheghani-Farahani, E., Atyabi, F., Kobarfard, F., Mohamadyar-Toupkanlou, F., and Hosseinkhani, H. (2017). Transferrin-conjugated magnetic dextran-spermine nanoparticles for targeted drug transport across blood-brain barrier. *J. Biomed. Mater. Res. Part A* 105 (10), 2851–2864. doi:10.1002/jbm.a.36145

Ghasemali, S., Nejati-Koshki, K., Akbarzadeh, A., Tafsiri, E., Zarghami, N., Rahmati-Yamchi, M., et al. (2013). Inhibitory effects of β-cyclodextrin-helenalin complexes on H-TERT gene expression in the T47D breast cancer cell line-results of real time quantitative PCR. *Asian Pac. J. Cancer Prev.* 14 (11), 6949–6953. doi:10.7314/apjcp.2013.14.11.6949

Hassani, N., Jafari-Gharabaghlou, D., Dadashpour, M., and Zarghami, N. (2022). The effect of dual bioactive compounds artemisinin and metformin co-loaded in PLGA-PEG nanoparticles on breast cancer cell lines: Potential apoptotic and anti-proliferative action. *Appl. Biochem. Biotechnol.* 194 (10), 4930–4945. doi:10.1007/s12010-022-04000-9

Huang, Y., Zhou, Z., Liang, J., Ding, P., Cao, L., Chen, Z., et al. (2015). Preparation, characterisation and *in vitro* cytotoxicity studies of chelerythrine-loaded magnetic Fe3O4@ O-carboxymethylchitosan nanoparticles. *J. Exp. Nanosci.* 10 (7), 483–498. doi:10.1080/17458080.2013.843209

Hulvat, M. C. (2020). Cancer incidence and trends. *Surg. Clin.* 100 (3), 469–481. doi:10.1016/j.suc.2020.01.002

Iyengar, R. M., and Devaraj, E. (2020). Silibinin triggers the mitochondrial pathway of apoptosis in human Oral squamous carcinoma cells. *Asian Pac. J. Cancer Prev. APJCP.* 21 (7), 1877–1882. doi:10.31557/APJCP.2020.21.7.1877

Jadid, M. F. S., Jafari-Gharabaghlou, D., Bahrami, M. K., Bonabi, E., and Zarghami, N. (2023). Enhanced anti-cancer effect of curcumin loaded-niosomal nanoparticles in combination with heat-killed *Saccharomyces cerevisiae* against human colon cancer cells. *J. Drug Deliv. Sci. Technol.* 80, 104167. doi:10.1016/j.jddst.2023.104167

Jadon, P. S., Gajbhiye, V., Jadon, R. S., Gajbhiye, K. R., and Ganesh, N. (2009). Enhanced oral bioavailability of griseofulvin via niosomes. *AAPS pharmscitech* 10, 1186–1192. doi:10.1208/s12249-009-9325-z

Jafari-Gharabaghlou, D., Dadashpour, M., Khanghah, O. J., Salmani-Javan, E., and Zarghami, N. (2023). Potentiation of folate-functionalized PLGA-PEG nanoparticles

loaded with metformin for the treatment of breast cancer: Possible clinical application. *Mol. Biol. Rep.* 50, 3023–3033. doi:10.1007/s11033-022-08171-w

Jahanafrooz, Z., Motamed, N., Rinner, B., Mokhtarzadeh, A., and Baradaran, B. (2018). Silibinin to improve cancer therapeutic, as an apoptotic inducer, autophagy modulator, cell cycle inhibitor, and microRNAs regulator. *Life Sci.* 213, 236–247. doi:10.1016/j.lfs.2018.10.009

Jamshidifar, E., Eshrati Yeganeh, F., Shayan, M., Tavakkoli Yaraki, M., Bourbour, M., Moammeri, A., et al. (2021). Super magnetic niosomal nanocarrier as a new approach for treatment of breast cancer: A case study on SK-BR-3 and MDA-MB-231 cell lines. *Int. J. Mol. Sci.* 22 (15), 7948. doi:10.3390/ijms22157948

Jin, M., Jin, G., Kang, L., Chen, L., Gao, Z., and Huang, W. (2018). Smart polymeric nanoparticles with pH-responsive and PEG-detachable properties for co-delivering paclitaxel and survivin siRNA to enhance antitumor outcomes. *Int. J. nanomedicine* 13, 2405–2426. doi:10.2147/IJN.S161426

Juan, C. A., Pérez de la Lastra, J. M., Plou, F. J., and Pérez-Lebeña, E. (2021). The chemistry of reactive oxygen species (ROS) revisited: Outlining their role in biological macromolecules (DNA, lipids and proteins) and induced pathologies. *Int. J. Mol. Sci.* 22 (9), 4642. doi:10.3390/ijms22094642

Justus, C. R., Dong, L., and Yang, L. V. (2013). Acidic tumor microenvironment and pH-sensing G protein-coupled receptors. *Front. physiology* 4, 354. doi:10.3389/fphys.2013.00354

Kaur, M., Velmurugan, B., Tyagi, A., Deep, G., Katiyar, S., Agarwal, C., et al. (2009). Silibinin suppresses growth and induces apoptotic death of human colorectal carcinoma LoVo cells in culture and tumor xenograft. *Mol. Cancer Ther.* 8 (8), 2366–2374. doi:10.1158/1535-7163.MCT-09-0304

Kedar, E., Palgi, O., Golod, G., Babai, I., and Barenholz, Y. (1997). Delivery of cytokines by liposomes. III. Liposome-encapsulated GM-CSF and TNF-alpha show improved pharmacokinetics and biological activity and reduced toxicity in mice. *J. Immunother.* 20 (3), 180–193. doi:10.1097/00002371-199705000-00003

Li, J., Wang, X., Zheng, D., Lin, X., Wei, Z., Zhang, D., et al. (2018). Cancer cell membrane-coated magnetic nanoparticles for MR/NIR fluorescence dual-modal imaging and photodynamic therapy. *Biomaterials Sci.* 6 (7), 1834–1845. doi:10.1039/c8bm00343b

Liu, F., Jin, H., Wang, Y., Chen, C., Li, M., Mao, S., et al. (2017). Anti-CD123 antibody-modified niosomes for targeted delivery of daunorubicin against acute myeloid leukemia. *Drug Deliv.* 24 (1), 882–890. doi:10.1080/10717544.2017.1333170

Liu, J. F., Jang, B., Issadore, D., and Tsourkas, A. (2019). Use of magnetic fields and nanoparticles to trigger drug release and improve tumor targeting. *Wiley Interdiscip. Rev. Nanomedicine Nanobiotechnology.* 11 (6), e1571. doi:10.1002/wnan.1571

Liu, Y., Li, S., Li, H., Hossen, M. A., Sameen, D. E., Dai, J., et al. (2021). Synthesis and properties of core-shell thymol-loaded zein/shellac nanoparticles by coaxial electrospray as edible coatings. *Mater. Des.* 212, 110214. doi:10.1016/j.matdes.2021.110214

Lu, Q., Dai, X., Zhang, P., Tan, X., Zhong, Y., Yao, C., et al. (2018). Fe3O4@ Au composite magnetic nanoparticles modified with cetuximab for targeted magneto-photothermal therapy of glioma cells. *Int. J. nanomedicine* 13, 2491–2505. doi:10.2147/IJN.S157935

Maurer, V., Altin, S., Ag Seleci, D., Zarinwall, A., Temel, B., Vogt, P. M., et al. (2021). *In-vitro* application of magnetic hybrid niosomes: Targeted sirna-delivery for enhanced breast cancer therapy. *Pharmaceutics* 13 (3), 394. doi:10.3390/pharmaceutics13030394

Mehta, S., and Jindal, N. (2013). Formulation of Tyloxapol niosomes for encapsulation, stabilization and dissolution of anti-tubercular drugs. *Colloids Surfaces B Biointerfaces.* 101, 434–441. doi:10.1016/j.colsurfb.2012.07.006

Mohammadian, F., Abhari, A., Dariushnejad, H., Nikanfar, A., Pilehvar-Soltanahmadi, Y., and Zarghami, N. (2016). Effects of chrysin-PLGA-PEG nanoparticles on proliferation and gene expression of miRNAs in gastric cancer cell line. *Iran. J. cancer Prev.* 9 (4), e4190. doi:10.17795/ijcp-4190

Mohammadian, F., Abhari, A., Dariushnejad, H., Zarghami, F., Nikanfar, A., Pilehvar-Soltanahmadi, Y., et al. (2016). Upregulation of Mir-34a in AGS gastric cancer cells by a PLGA-PEG-PLGA chrysin nano formulation. *Asian Pac. J. Cancer Prev.* 16 (18), 8259–8263. doi:10.7314/apjcp.2015.16.18.8259

Mokhtari, R. B., Homayouni, T. S., Baluch, N., Morgatskaya, E., Kumar, S., Das, B., et al. (2017). Combination therapy in combating cancer. *Oncotarget* 8 (23), 38022–38043. doi:10.18632/oncotarget.16723

Momekova, D. B., Gugleva, V. E., and Petrov, P. D. (2021). Nanoarchitectonics of multifunctional niosomes for advanced drug delivery. *ACS omega* 6 (49), 33265–33273. doi:10.1021/acsomega.1c05083

Mou, X., Ali, Z., Li, S., and He, N. (2015). Applications of magnetic nanoparticles in targeted drug delivery system. *J. Nanosci. Nanotechnol.* 15 (1), 54–62. doi:10.1166/jnn.2015.9585

Myat, Y. Y., Ngawhirunpat, T., Rojanarata, T., Opanasopit, P., Bradley, M., Patrojanasophon, P., et al. (2022). Synthesis of polyethylene glycol diacrylate/acrylic acid nanoparticles as nanocarriers for the controlled delivery of doxorubicin to colorectal cancer cells. *Pharmaceutics* 14 (3), 479. doi:10.3390/pharmaceutics14030479

OLeary, M. P., Warner, S. G., Kim, S-I., Chaurasiya, S., Lu, J., Choi, A. H., et al. (2018). A novel oncolytic chimeric orthopoxvirus encoding luciferase enables real-time view of colorectal cancer cell infection. *Mol. Therapy-Oncolytics.* 9, 13–21. doi:10.1016/j.omto.2018.03.001

Osaka, T., Nakanishi, T., Shanmugam, S., Takahama, S., and Zhang, H. (2009). Effect of surface charge of magnetite nanoparticles on their internalization into breast cancer and umbilical vein endothelial cells. *Colloids Surfaces B Biointerfaces.* 71 (2), 325–330. doi:10.1016/j.colsurfb.2009.03.004

Pardakhty1, A., and Moazeni, E. (2013). Nano-niosomes in drug, vaccine and gene delivery: A rapid overview. *Nanomedicine J.* 1.

Pérez-Herrero, E., and Fernández-Medarde, A. (2015). Advanced targeted therapies in cancer: Drug nanocarriers, the future of chemotherapy. *Eur. J. Pharm. Biopharm.* 93, 52–79. doi:10.1016/j.ejpb.2015.03.018

Prabha, G., and Raj, V. (2016). Preparation and characterization of polymer nanocomposites coated magnetic nanoparticles for drug delivery applications. *J. Magnetism Magnetic Mater.* 408, 26–34. doi:10.1016/j.jmmm.2016.01.070

Ramimoghadam, D., Bagheri, S., and Abd Hamid, S. B. (2015). Stable monodisperse nanomagnetic colloidal suspensions: An overview. *Colloids Surfaces B Biointerfaces.* 133, 388–411. doi:10.1016/j.colsurfb.2015.02.003

Rodrigues Pereira da Silva, L. C., do Carmoa, F. A., Eurico Nasciutti, L., Zancan, P., Cunha Sathler, P., and Mendes Cabral, L. (2016). Targeted nanosystems to prostate cancer. *Curr. Pharm. Des.* 22 (39), 5962–5975. doi:10.2174/1381612822666160715131359

Rolston, K. V. (2017). Infections in cancer patients with solid tumors: A review. *Infect. Dis. Ther.* 6 (1), 69–83. doi:10.1007/s40121-017-0146-1

Salmani Javan, E., Lotfi, F., Jafari-Gharabaghlou, D., Mousazadeh, H., Dadashpour, M., and Zarghami, N. (2022). Development of a magnetic nanostructure for co-delivery of metformin and silibinin on growth of lung cancer cells: Possible action through leptin gene and its receptor regulation. *Asian Pac. J. Cancer Prev.* 23 (2), 519–527. doi:10.31557/APJCP.2022.23.2.519

Samed, N., Sharma, V., and Sundaramurthy, A. (2018). Hydrogen bonded niosomes for encapsulation and release of hydrophilic and hydrophobic anti-diabetic drugs: An efficient system for oral anti-diabetic formulation. *Appl. Surf. Sci.* 449, 567–573. doi:10.1016/j.apsusc.2017.11.055

Shahbazi, R., Jafari-Gharabaghlou, D., Mirjafary, Z., Saeidian, H., and Zarghami, N. (2023). Design and optimization various formulations of PEGylated niosomal nanoparticles loaded with phytochemical agents: Potential anti-cancer effects against human lung cancer cells. *Pharmacol. Rep.* 75, 442–455. doi:10.1007/s43440-023-00462-8

Solowey, E., Lichtenstein, M., Sallon, S., Paavilainen, H., Solowey, E., and Lorberboum-Galski, H. (2014). Evaluating medicinal plants for anticancer activity. *Sci. World J.* 2014, 721402. doi:10.1155/2014/721402

Soltanian, S., and Matin, M. M. (2011). Cancer stem cells and cancer therapy. *Tumor Biol.* 32, 425–440. doi:10.1007/s13277-011-0155-8

Stiufiuc, R., Iacovita, C., Nicoara, R., Stiufiuc, G., Florea, A., Achim, M., et al. (2013). One-step synthesis of PEGylated gold nanoparticles with tunable surface charge. *J. Nanomater.* 2013, 1–7. doi:10.1155/2013/146031

Su, G., Zhou, H., Mu, Q., Zhang, Y., Li, L., Jiao, P., et al. (2012). Effective surface charge density determines the electrostatic attraction between nanoparticles and cells. *J. Phys. Chem. C* 116 (8), 4993–4998. doi:10.1021/jp211041m

Tavano, L., Vivacqua, M., Carito, V., Muzzalupo, R., Caroleo, M. C., and Nicoletta, F. (2013). Doxorubicin loaded magneto-niosomes for targeted drug delivery. *Colloids Surfaces B Biointerfaces* 102, 803–807. doi:10.1016/j.colsurfb.2012.09.019

Thun, M. J., DeLancey, J. O., Center, M. M., Jemal, A., and Ward, E. M. (2010). The global burden of cancer: Priorities for prevention. *Carcinogenesis* 31 (1), 100–110. doi:10.1093/carcin/bgp263

Tiwari, A., Saraf, S., Jain, A., Panda, P. K., Verma, A., and Jain, S. K. (2020). Basics to advances in nanotherapy of colorectal cancer. *Drug Deliv. Transl. Res.* 10 (2), 319–338. doi:10.1007/s13346-019-00680-9

Valková, V., Ďúranová, H., Bilčíková, J., and Habán, M. (2021). Milk thistle (Silybum marianum): A valuable medicinal plant with several therapeutic purposes. *J. Microbiol. Biotechnol. Food Sci.* 2021, 836–843. doi:10.15414/jmbfs.2020.9.4.836-843

Van Houten, B., Hunter, S. E., and Meyer, J. N. (2016). Mitochondrial DNA damage induced autophagy, cell death, and disease. *Front. Biosci. (Landmark Ed.* 21, 42–54. doi:10.2741/4375

Wang, J., Wang, F., Li, F., Zhang, W., Shen, Y., Zhou, D., et al. (2016). A multifunctional poly (curcumin) nanomedicine for dual-modal targeted delivery, intracellular responsive release, dual-drug treatment and imaging of multidrug resistant cancer cells. *J. Mater. Chem. B* 4 (17), 2954–2962. doi:10.1039/c5tb02450a

Yang, J., Lee, H., Hyung, W., Park, S-B., and Sjjom, H. (2006). Magnetic PECA nanoparticles as drug carriers for targeted delivery: Synthesis and release characteristics. *J. Microencapsul.* 23 (2), 203–212. doi:10.1080/02652040500435444

Zaki, N. M. (2014). Augmented cytotoxicity of hydroxycamptothecin-loaded nanoparticles in lung and colon cancer cells by chemosensitizing pharmaceutical excipients. *Drug Deliv.* 21 (4), 265–275. doi:10.3109/10717544.2013.838808

Zheng, X., Lu, J., Deng, L., Xiong, Y., and Chen, J. (2009). Preparation and characterization of magnetic cationic liposome in gene delivery. *Int. J. Pharm.* 366 (1-2), 211–217. doi:10.1016/j.ijpharm.2008.09.019

frontiers | Frontiers in Pharmacology

TYPE Review
PUBLISHED 04 July 2023
DOI 10.3389/fphar.2023.1193213

OPEN ACCESS

EDITED BY
Li Li,
The University of Queensland, Australia

REVIEWED BY
Haibo Xu,
Chengdu University of Traditional Chinese Medicine, China
Lihong Zhou,
Shanghai University of Traditional Chinese Medicine, China

*CORRESPONDENCE
Haibo Cheng,
hbcheng_njucm@163.com
Dongdong Sun,
sundd@njucm.edu.cn

†These authors have contributed equally to this work

RECEIVED 18 April 2023
ACCEPTED 05 June 2023
PUBLISHED 04 July 2023

CITATION
Liu L, Yan Q, Chen Z, Wei X, Li L, Tang D, Tan J, Xu C, Yu C, Lai Y, Fan M, Tao L, Shen W, Li L, Wu M, Cheng H and Sun D (2023), Overview of research progress and application of experimental models of colorectal cancer.
Front. Pharmacol. 14:1193213.
doi: 10.3389/fphar.2023.1193213

Overview of research progress and application of experimental models of colorectal cancer

Li Liu[1,2,3†], Qiuying Yan[2,3†], Zihan Chen[1†], Xiaoman Wei[2], Lin Li[1], Dongxin Tang[4], Jiani Tan[2,3], Changliang Xu[2,3], Chengtao Yu[2,3], Yueyang Lai[2,3], Minmin Fan[2,3], Lihuiping Tao[2,3], Weixing Shen[2,3], Liu Li[2,3], Mianhua Wu[2], Haibo Cheng[2,3]* and Dongdong Sun[1,2,3]*

[1]School of Integrated Chinese and Western Medicine, Nanjing University of Chinese Medicine, Nanjing, China, [2]Collaborative Innovation Center of Jiangsu Province of Cancer Prevention and Treatment of Chinese Medicine, Nanjing University of Chinese Medicine, Nanjing, China, [3]Research Center for Pathogenesis Theory of Cancerous Toxin and Application, Nanjing University of Chinese Medicine, Nanjing, China, [4]The First Clinical Medical College, Guizhou University of Traditional Chinese Medicine, Guiyang, China

Colorectal cancer (CRC) is the third most common malignancy in terms of global tumor incidence, and the rates of morbidity and mortality due to CRC are rising. Experimental models of CRC play a vital role in CRC research. Clinical studies aimed at investigating the evolution and mechanism underlying the formation of CRC are based on cellular and animal models with broad applications. The present review classifies the different experimental models used in CRC research, and describes the characteristics and limitations of these models by comparing the research models with the clinical symptoms. The review also discusses the future prospects of developing new experimental models of CRC.

KEYWORDS

colorectal cancer, cellular models, animal models, preclinical studies, drug development

1 Introduction

Colorectal cancer (CRC) is the most common malignancy worldwide, in terms of both morbidity and mortality (Sung et al., 2021). The understanding of the origin of CRC has increased dramatically over the past few decades. However, despite breakthroughs in diagnosis and treatment, CRC continues to be a major health concern worldwide. The morbidity and mortality due to CRC are on the rise owing to the overall low screening rates and changes in lifestyle, including poor diets, irregular lifestyles, smoking, and other factors (Minami et al., 2022). Strategies for the early screening and intervention of precancerous CRC lesions in developed countries have reduced the rates of incidence and mortality due to CRC (Zorzi and Urso, 2022). Similar to studies on other illnesses, research studies on CRC critically depend on experimental models with reliable and distinct characteristics. Although CRC tumors have heterogeneous characteristics, experimental models of CRC are established in such a manner that they represent the characteristics of CRC tumors. Selection of the appropriate model that reflects the tumor system is a crucial challenge in cancer screening. Therefore, experimental models of CRC have been extensively studied for determining the optimum model for studying the invasion, progression, and early detection of CRC. This review discusses the significance of CRC models as a platform for screening drugs and developing novel therapeutic approaches for CRC. The application of cellular and animal models of CRC were also summarized and discussed to aid further preclinical studies on CRC.

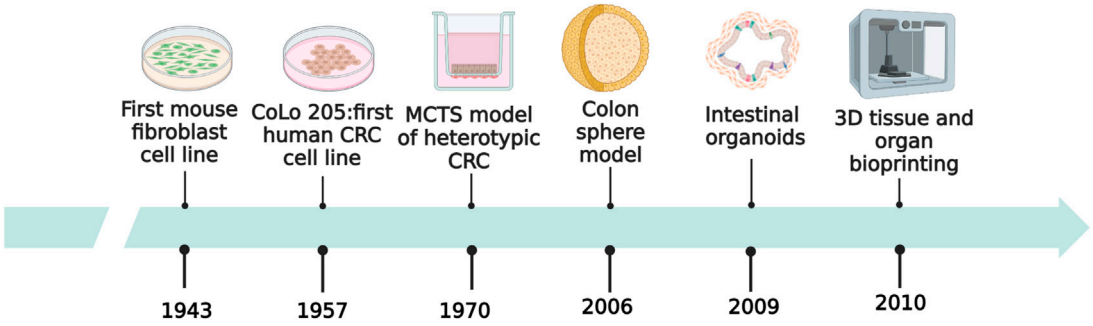

FIGURE 1
History of development of *in vitro* models of CRC.

2 Cellular models based on intestinal cells and CRC cells

In vitro models of CRC established using intestinal cells and CRC cells are frequently employed for obtaining rapidly growing cellular models of CRC and for facilitating experimental control. *In vitro* models of CRC can simultaneously generate several populations of homogeneous cells. Specific cellular targets of macroscopic systems can be conveniently studied using these models by analyzing the experimental results (Saeidnia et al., 2015).

The first mammalian cell line was established in 1943, which served as a prelude to *in vitro* cell culture. The CoLo 205 CRC cell line was established in 1957, which promoted *in vitro* studies on CRC. Figure 1 depicts the history of development of *in vitro* models of CRC (Sanford et al., 1948; Ricci et al., 2007; Sharma et al., 2010; Jedrzejczak, 2017).

2.1 Two-dimensional (2D) cellular models of CRC

CRC cell lines are *in vitro* tumor models with different origins and types, and serve as fundamental tools for investigating the biomarkers of drug sensitivity, resistance, and toxicity. CRC cell lines are established by isolating CRC cells from patients or animals with CRC followed by culture on artificial media. The appropriate cell lines are selected based on the type of cancer or gene expression levels, according to the aims of the study. SW620, Caco-2, RKO, SW480, HT8, HT29, HT116, LoVo, and LS174 T cell lines are currently widely used in basic research studies on CRC (Akashi et al., 2000; Vécsey et al., 2002; Lind et al., 2004; Barretina et al., 2012; Ahmed et al., 2013; Gemei et al., 2013; Mouradov et al., 2014; Maletzki et al., 2015; Boot et al., 2016; Berg et al., 2017; Mooi et al., 2018; Kim et al., 2020; Bian et al., 2021).

Although the characteristics of CRC cell lines are highly consistent with those of human cancer models, they have certain limitations. CRC cell lines facilitate the investigation of the molecular and phenotypic characteristics of CRC. However, as only one side of the cells is in contact with the medium during culture, the majority of cells gradually flatten, undergo abnormal division, and lose their differentiation phenotype following isolation from tissues and plate culture. Additionally, CRC cells continue to proliferate *in vitro*, which may cause the cell lines to lose the characteristics of the original tumor. Another limitation of CRC cell lines is the scarcity of matrix ingredients in the tumor microenvironment (TME), including the cells and acellular components constituting the structural complexity of the *in vivo* environment. Altogether, these indicate that CRC cell lines fail to accurately mimic the *in vivo* growth characteristics of tumor cells.

2.2 Three-dimensional (3D) cellular models of CRC

Owing to the limitations of 2D cellular models of CRC, researchers are committed towards exploiting novel and physiologically representative models of CRC. *In vitro* 3D culture models, including spheroids and organoids, are therefore used for overcoming the limitations of 2D cellular models. Spheroids comprise a mixture of single-cell or multicellular systems, while organoids are generally formed of specific stem cells or ancestral cells from organs (Kimlin et al., 2013; Boucherit et al., 2020). Spheroids and organoids are superior at mimicking tumor cell heterogeneity and the complex interactions among different cells (Thoma et al., 2014).

2.2.1 Spheroids

Spheroids are one of the most commonly used models in CRC research. They are constructed by suspending cancer cell lines or isolated tumor tissues from patients in CRC. They have a convenient mode of production and application, and are particularly effective for studying micrometastases or avascular tumors. Spheroid models can be categorized into four types according to the origin and morphology of the cancer cells from which they are derived. These categories include multicellular tumor spheroids (MCTS), tumorospheres, tissue-derived tumor spheres (TDTS), and organotypic multicellular spheroids (OMS; Figure 2) (Weiswald et al., 2015).

MCTS models, first constructed by Bauleth-Ramos, consist of colonic epithelia, human intestinal fiber cells, and human mononuclear cells, and are inoculated into hydrogel microwells to form the spheroid model (Inch et al., 1970; Bauleth-Ramos, T

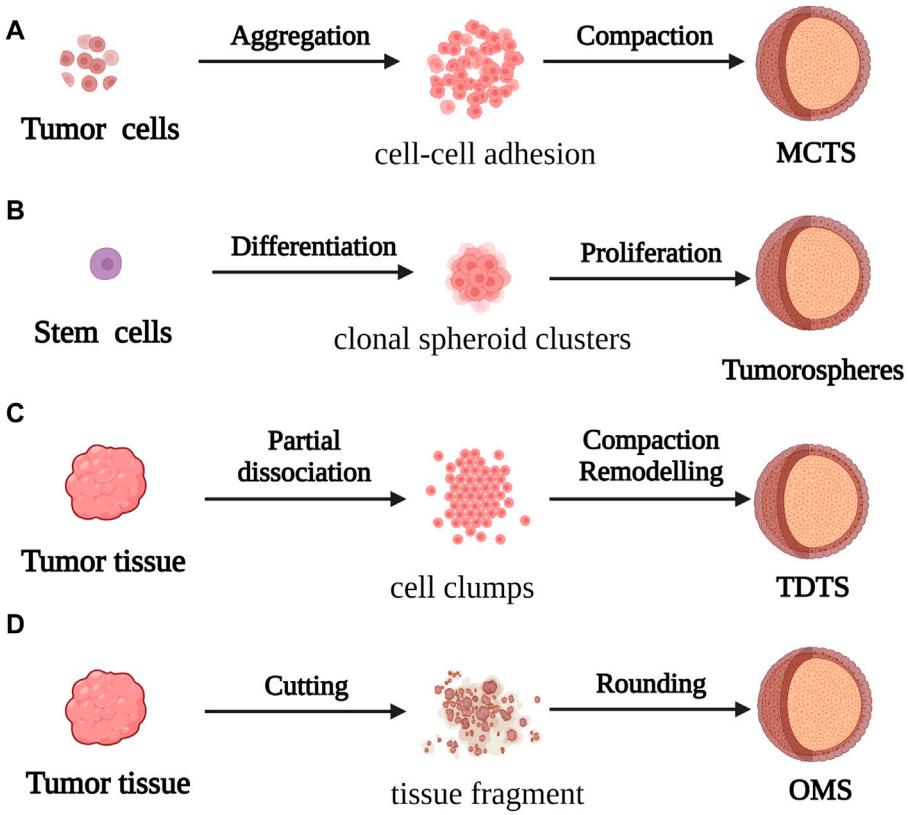

FIGURE 2
For the formation process of spherical cancer models **(A)** MCTS: Cell suspensions cultured under non-adherent conditions were aggregated and compacted to obtain MCTS; **(B)** Tumorospheres: Stem cells cultured under low-adherent conditions formed Tumorospheres by clonal proliferation **(C)** TDTS: Partial dissociation of tumor tissue and compaction/remodeling produced TDTS; **(D)** OMS: Cut tumor tissue aggregates formed OMS during culture under non-adherent conditions.

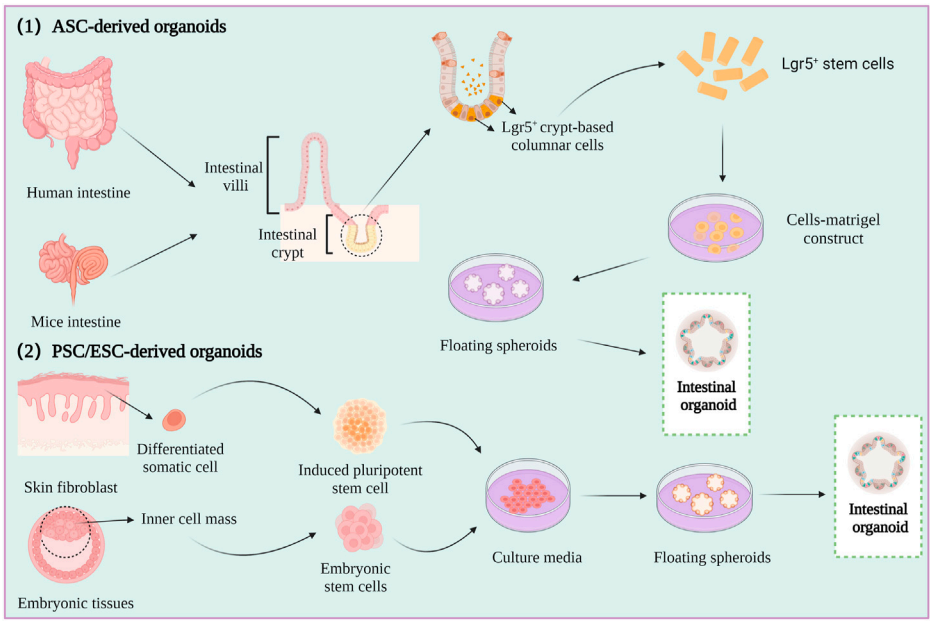

FIGURE 3
Intestine organoid cultures.

TABLE 1 Applications of cellular models of CRC.

Mechanism being investigated	Research model	Cell lines	References
Apoptosis	Induction of apoptosis via the overexpression of neurofibromin (*NF2*), heterogeneous nuclear ribonucleoprotein L (*HNRNPL*), and other genes	HCT116 and SW620	Wu et al. (2020)
		HIEC, Caco2, HCT116, LoVo, and SW480	Zhao et al. (2021)
	Induction of apoptosis via the knockdown of ribosomal protein lateral stalk subunit P0 pseudogene 2 (*RPLP0P2*), Cadherin 17 (*CDH17*), and other genes	HCT116, HT29, SW480, and RKO	Yuan et al. (2021)
		KM12SM, KM12C, Colo320, HT29, RKO, and SW480	Tian et al. (2018)
	Inhibition of apoptosis via the knockdown of receptor interacting protein kinase 3 (*RIP3*)	SW480, HCT-116, $RIP3^{+/+-MEF}$, and $RIP3^{-/-MEF}$	Han et al. (2018)
	Inhibition of glycolysis and promotion of apoptosis via the knockdown of hypoxia-inducible factor-1α (*HIF-1*α)	FHC, CCD841 CoN, HT29, SW480, LoVo, HCT116, and SW620	Liu et al. (2019)
	Cu nanoparticles (CuNPs)-induced apoptosis of CRC cells	SW480	Ghasemi et al. (2020)
Autophagy	Inhibition of autophagy with chloroquine	HCT116 and SW480	Ma et al. (2020)
	Rapamycin-induced model of autophagy	KM12SM, KM12C, Colo320, HT29, RKO, and SW480	Tian et al. (2018)
Angiogenesis	Inhibition of angiogenesis via the knockdown of cellular-myelocytomatosis viral oncogene (*c-Myc*), vascular endothelial growth factor (*VEGF*), and other genes	HCT116	Yin et al. (2010)
	Co-culture of patient-derived cancer-associated fibroblasts (CAFs) and HUVECs	Patient-derived CAFs	Unterleuthner et al. (2020)
Invasion and metastasis	Promotion of invasion and metastasis via the overexpression of zinc-finger protein 326 (*ZNF326*), metastasis associated 1 family member 3 (*MTA3*), and other genes	SW480, SW620, CL187, and RKO	Yang et al. (2021)
		LoVo and HCT15	Jiao et al. (2017)
	Inhibition of invasion and metastasis via the overexpression of t-box transcription factor 5 (*TBX5*)	HT29, SW620, SW480, LoVo, and HCT116	Dong et al. (2020)
	Inhibition of invasive metastasis via the knockdown of sphingosine phosphate lyase 1 (*SGPL1*), forkhead Box O6 (*FOXO6*), and other genes	DLD-1, Caco-2, and CCD 841 CoN	Faqar et al. (2021)
		HCT116-CSC	Zou et al. (2022)
		NCM460, Caco2, HT29, HCT116, and SW480	Li et al. (2019)
	Co-culture of EMT-CRC cells and HUVECs	NCM460, LoVo, HCT-116, DLD-1, SW620, and SW480	Dou et al. (2021)
Metabolic reprogramming	Reprogramming of energy metabolism via the overexpression of mitochondrial citrate carrier solute carrier family 25 member 1 (*SLC25A1*), human kallikrein 2 (*HK2*), and other genes	NCM460, SW480, HCT116, SW620, LoVo, LS174T, and HT29	Yang et al. (2021a)
	Inhibition of metabolic reprogramming via *HIF-1*α knockout	HCT8, HCT15, HCT116, LoVo, SW480, SW1116, HT29, Caco-2, DLD-1, and T84	Dong et al. (2022)
Immune escape	Promotion of immune escape *via* lipopolysaccharide (LPS)-induced macrophage infiltration	HCT-8, HCT-116, SW620, SW480, DLD-1, CaCo-2, CT26, and HT-29	Liu et al. (2020a)
	Induction of immune escape via the overexpression of antigen-presenting-cell, B7 homolog x (*B7x*), and other genes	HCA-7, HT-29, 293T, and TALL-104	Cen et al. (2021)
		LoVo, Colo-205, SW480, SW620, HCT-116, CT-26, and MC-38	Li et al. (2020c)
Inflammation	LPS-induced model of inflammation	HCT116 and SW480	Zhu et al. (2019)
		—	Schafer and Werner (2008)
		Colon 26	Choo et al. (2005)
		—	Schottelius and Baldwin (1999)
	Induction of tumor necrosis factor-α (*TNF*-α), nuclear factor-kappa B (*NF-kB*), and other pro-inflammatory factors	Caco-2, HT29, SW480, SW48, and DLD1	Li et al. (2012)
		Volo	Tai et al. (2012)

(Continued on following page)

TABLE 1 (*Continued*) Applications of cellular models of CRC.

Mechanism being investigated	Research model	Cell lines	References
EMT	Suppression of EMT via the knockdown of Pleckstrin homology-like domain family A member 2 (*PHLDA2*), SRY-Box transcription Factor 2 (*SOX2*), and other genes	HCT116 and SW480	Ma et al. (2020)
		SW480 and SW620	Zhu et al. (2021)
		HCT116 and LoVo	Qi et al. (2021)
		HCT116 and DLD-1	Ju et al. (2020)
		HCT116, SW480, HT29, and SW620	Hua et al. (2020)
	Induction of EMT via interleukin-6 (*IL-6*), *TNF*-α, and other inflammatory factors	SW480, SW620, and Caco-2	Rokavec et al. (2014)
		HCT116 and Caco-2	Wang et al. (2013)
	Induction of EMT via the overexpression of cryopyrin-associated periodic syndromes 1 (*CAPS1*), nuclear factor of activated T-cells (*NFATc1*), and other genes	FHC, HT29, SW480, SW620, and DLD1	Zhao et al. (2019)
		SW620, LoVo, Caco-2, SW480, HT29, HCT116, and DLD-1	Shen et al. (2021)
		HCT116	Li et al. (2021)
	Induction of EMT by X-ray irradiation	SW480	Lin et al. (2017)
Genomic instability/ mutation (CIN)	—	CRC PDOs	Bolhaqueiro et al. (2019)
	Induction of CIN by DNA damage caused by the overexpression of iroquois homeobox gene 5 (*IRX5*), integrin-linked kinase (*ILK*), and other genes	SW480 and DLD-1	Sun et al. (2020)
		HCT116	Chadla et al. (2021)
Senescent cells	Induction of cellular senescence via the overexpression of lamin B1 (*LMNB1*), tribbles homolog 2 (*TRIB2*), and other genes	SW480, HT29, and IEC-6	Liu et al. (2013)
		HEK 293 T, SW48, and LoVo	Hou et al. (2018)
	Drug-induced senescence of CRC cells using oxaliplatin, adriamycin, aspirin, and other drugs	SW620 and HCT116	Jung et al. (2015)
		SW837, HCT116, and SW48	Tato-Costa et al. (2016)
		PROb and CT26	Seignez et al. (2014)
		HCT116	Vétillard et al. (2015)
		HCT116 and SW480	Zhang et al. (2011)
		C85	Dabrowska et al. (2011)
			Dabrowska et al. (2019)

et al., 2020). MCTS models are similar to solid tumors in terms of the growth kinetics, metabolic rate, and resistance to chemotherapy and radiotherapy *in vivo* (Ivascu and Kubbies, 2006), and have been employed for screening and evaluating the efficacy of drugs. However, the variability of MCTS models makes it difficult to obtain repeatable and stable experimental data, which affects the use of these models in tumor research.

The tumorosphere model of CRC stem cells (CSCs) was used in the early 2000s for evaluating the differentiation capacity of tumors. However, because there are no morphological phenotypes associated with the phenotypic instability of CSCs, the tumorosphere model is unable to faithfully simulate the *in vivo* 3D framework and physiological condition of tumors (Valent et al., 2012).

The TDTS models consist of cancer and stromal cells, and are commonly used in studies on CRC. TDTS models of CRC tumors have a unique histological feature similar to the poorly differentiated globules produced by permanent cancer cell lines, and can fully simulate the characteristics of *in vitro* 3D cell culture models of CRC (Santini and Rainaldi, 1999; Weiswald et al., 2009).

OMS models are enriched in stem cells which can represent the complexity of parental tumor cells similar to *in vivo* tissues by forming an extracellular layer of epithelioid cells and an intracellular layer of mesenchymal cells, and thus maintaining the multicellular nature of CRC (Rajcevic et al., 2014). However, the difficulty of producing homogeneous spheres in a reproducible manner combined with the insufficiency of stable experimental data can prove to be a challenge during the application of the OMS model in CRC research and drug development.

2.2.2 Organoids

Spheroids are a simple experimental model that only partly represent the *in vivo* characteristics of tumor tissues. However, organoids are relatively complex three-dimensional (3D) culture models that are frequently used in CRC research. Organoids are self-

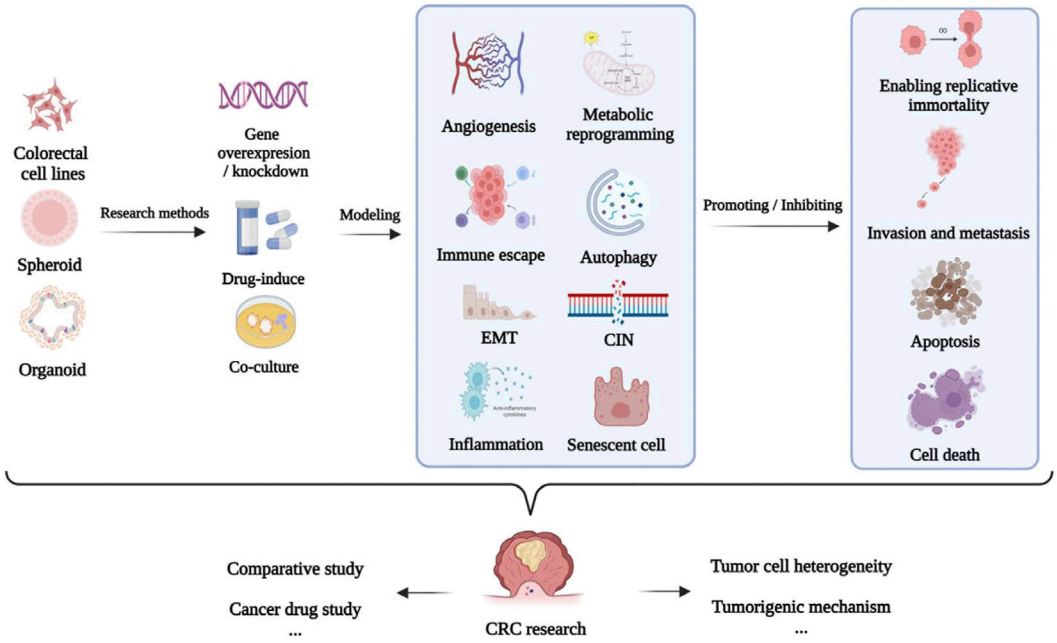

FIGURE 4
Application of CRC cellular models.

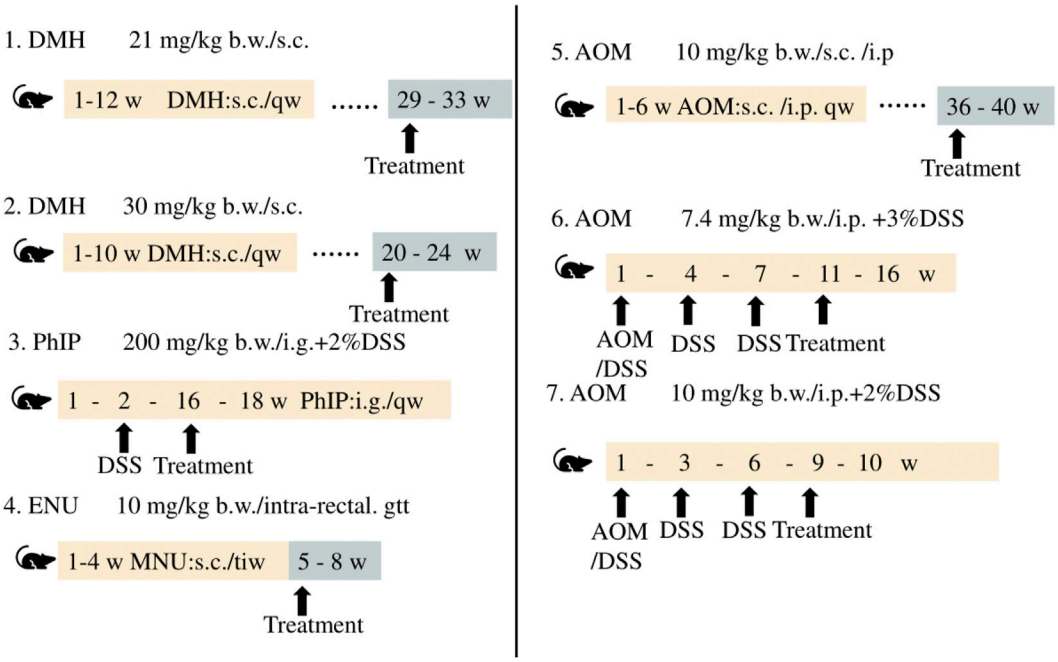

FIGURE 5
Chemically induced CRC animal models.

organizing organotypic cultures that are produced from various stem cells, including tissue specific adult stem cells (ASCs), embryonic stem cells (ESCs), or induced pluripotent stem cells (iPSCs) (Fujii et al., 2018; Fujii and Sato, 2021). The stem cells are grown in matrigel 3D culture conditions to mimic the *in vivo* growth environment, and to produce stable, near-physiological epithelial structures (Figure 3) (Lancaster and knoblich, 2014; Huch and Koo, 2015).

TABLE 2 Murine models of CRC.

Model	Strategy for model generation	Pathological mechanism	Detailed methodology	Range of application	Limitations	References
Spontaneous animal model of CRC	Mutant animal models of CRC	Proliferation	Mutation in *APC*	FAP model for studying hereditary CRC	Survival time < 4 months, tumor formation in small intestine, difficulty in metastasis	Moser et al. (1990)
						Shoemaker et al. (1997)
						Shoemaker et al. (1998)
						Barker et al. (2007)
			Mutation in *APC/Cre*	Induction of colorectal adenoma	Difficulty in metastasis	Robanus-Maandag et al. (2010)
						Chen et al. (2020)
			Mutations in *Mlh1, Msh2, Msh3, Msh6,* and *Pms2*	Hereditary nonpolyposis CRC (HNPCC)	Multi-tissue tumors, difficulty in metastasis	Lynch et al. (1997)
						Papadopoulos and Lindblom (1997)
						Manceau et al. (2011)
			Mutation in *SMAD4*	Familial juvenile polyposis model, acceleration of tumor development	Difficulty in metastasis	Takaku et al. (1998)
						Lu et al. (1998)
			Mutation in *KRAS*	Induction of colonic hyperplasia and generation of aberrant crypt foci (ACF) carcinogenesis model	CRC cannot be induced by mutations in single genes, but is induced in combination with other gene mutations that induce carcinogenesis and enhance the incidence of CRC.	Bos et al. (1987)
						Campbell et al. (1998)
						Jen et al. (1994)
						Janssen et al. (2002)
						Janssen et al. (2006)
						Calcagno et al. (2008)
			Mutation in *PIK3CA*	Induction of colon adenoma	Single mutations generally do not induce CRC.	Juric et al. (2018)
		Invasion and metastasis	Mutation in *FBXW7*	Model of highly invasive colorectal cancer	Single mutations generally do not induce CRC.	Mao et al. (2004)
			Mutation in *p53*	Induction of distal intestinal tumor	Single mutations generally do not induce CRC.	Nakayama et al. (2017)
						Kadosh et al. (2020)
Diet- and chemical-induced models of CRC	Diet-induced models of CRC	Inflammation	High-fat diet (HFD)/ western diet (NMD)	Colorectal barrier dysfunction and inflammation, invasive adenocarcinoma	Requires a long duration and has a low carcinogenic efficiency	Itano et al. (2012)
						Yu et al. (2022)
	Chemical-induced models of CRC		2,4,6-Trinitro-benzenesulfonic acid (TNBS)	Induction of colitis-driven CRC	Cannot be used alone, necessary to break the intestinal mucosal screen before use, mortality rate of modeling is high	Scheiffele and Fuss (2002)
			Anaerobic oxidation of methane (AOM) + dextran sodium sulfate (DSS)	Tumors driven by colitis, induced distal CRC	The modeling rate is low and molding time is uncertain	Neufert et al. (2007)
						De-Robertis et al. (2011)
						Liang et al. (2017)
						Sun et al. (2022)

(Continued on following page)

TABLE 2 (*Continued*) Murine models of CRC.

Model	Strategy for model generation	Pathological mechanism	Detailed methodology	Range of application	Limitations	References
		Proliferation	AOM	ACF and CRC epithelial tumor model	The period of modeling is long and time-consuming, cannot be used for studying CRC metastases	Femia and Caderni (2008)
						Izzo et al. (2008)
						Orlando et al. (2008)
			1,2 Dimethyl hydrazine (DMH)	Human sporadic CRC research model, tumorigenicity specificity	Requires a long time and has a low carcinogenic efficiency	Ma et al. (1996)
						Kissow et al. (2012)
						Aranganathan and Nalini (2013)
			Parahydrogen-induced polarization (PhIP)	ACF-induced rat model	Low incidence, long study cycle	Ito et al. (1991)
						Tanaka et al. (2005)
			3,2′-Dimethyl-4-Aminobiphenyl (DMAB)	Induced colon and small intestinal carcinogenesis	Requires multiple administration, low specificity	Reddy and Mori (1981)
						Reddy (1998)
		CIN	N-ethyl-N-nitrosourea (ENU)/N- methyl -N-nitrosourea (MNU)/ N-methyl-N-nitrosoguanidine (MNNG)	Induced distal CRC model	Induced mutations are random and drug volume quantification is difficult	Huang et al. (2020)
Animal model of transplanted CRC	Animal model of orthotopic tumor transplantation	Invasion and metastasis	Cecal transplantation	Induction of primary CRC that can metastasize to local lymphatic vessels, lungs, and liver	Risk of laparotomy is high in this model. CRC originates from the mucosa, and whether tumor metastasis results from the overflow of intraperitoneal cells cannot be excluded	Talmadge et al. (2007)
						Martin et al. (2013)
						Lee et al. (2014)
						O'Rourke et al. (2017)
	Animal model of ectopic tumor transplantation		Spleen planting	Study of advanced CRC	The operation is complex and requires highly advanced technical skills	Kasuya et al. (2005)
						Bai et al. (2015)
						Yang et al. (2021c)
			Tail vein injection	Lung metastasis model of CRC	Differs from human CRC metastasis, multiple metastases are prone to occur	Wang et al. (2020)
			Liver implantation	Liver metastasis model of CRC	Only the late metastatic process of CRC is simulated; tumor forms only at the site of implantation	Panis and Nordlinger (1991)
						Kopetz et al. (2009)
						Roque et al. (2019)
			Intraperitoneal injection of CRC cell for inducing metastasis	Peritoneal metastasis model of CRC	Unsuitable for studying early metastasis of lymph nodes in CRC.	Li et al. (2016)
		Proliferation	Hypodermic implantation	Real-time monitoring of CRC growth	Cannot simulate the *in situ* growth of CRC, not easy to study tumor invasion and metastasis	Rygaard and poulsen (1969)
						Lehmann et al. (2017)

The first intestinal epithelial 3D organoids were constructed by growing leucine-rich repeat-containing G-protein-coupled receptor 5 ($LGR5^+$) intestinal stem cells in a medium containing stem cell niche restatement factors and tissue-specific growth factors (Sato et al., 2011). An increasing number of studies have described the formation of patient-derived organoids (PDOs) by culturing minced

TABLE 3 Other animal models of CRC.

Classification	Animal	Advantages	Disadvantages	References
Invertebrate	*Drosophila melanogaster* (fruit fly)	The model can represent the composition of mammalian intestinal cells, aids in avoiding cancer heterogeneity	The model has no acquired immune function and has a short life cycle. It is impossible to simulate the complexity of tumor development	Bhandari and Shashidhara, 2001 Martorell et al., 2014
Vertebrate	*Danio rerio* (zebrafish)	Histopathological features of intestinal tumors are similar to those of human tumors. High transparency of seedlings, small size, short developmental cycle, *in vitro* fertilization, and large number of eggs. Requires small experimental dosage and is less time-consuming	The culture temperature is inconsistent with the growth temperature of tumor cells. Long-term tumor transplantation experiments cannot be performed	Amatruda et al. (2002) Trede et al. (2004) Haldi et al. (2006) Brugman et al. (2009) Paquette et al. (2013)
	Canis lupus familiaris (Dog)	The model has a similar physiological structure to humans, and the mechanism of pathogenesis is similar to sporadic CRC in humans. Gentle character, good experimental coordination, and repeatability	Long duration of modeling, observational inconveniences, not suitable for acute experiments	Kamano et al. (1981) Kamano et al. (1983) Youmans et al. (2012)
	Felis catus (Domestic cat)	The histological subtype of the model is similar to that of advanced CRC in humans. Model can be used for studying the germination of intestinal tumor in CRC.	Low incidence, tumors mostly occur in the small intestine	Uneyama et al. (2021) Groll et al. (2021)
	Sus scrofa (Pig)	The anatomical structure of the small intestine is similar to that of humans. Model has a moderate size and long life. The progression and accumulation of mutations in CRC can be monitored by colonoscopy screening	The model cannot be used to study acute CRC as the process of cancer formation is slow	Llanos et al. (2006) Sangild et al. (2006) Flisikowska et al. (2012) Dean (2013) Flisikowska et al. (2017) Gonzalez et al. (2019)
	Ovis aries (Sheep)	Cellular differentiation in the model is similar to that of colon adenocarcinoma in humans. Model can be used to study advanced CRC.	Adenocarcinoma develops in the small intestine	Munday et al. (2006)
	Macaca mulatta (Rhesus monkey)	Shares high genomic homology with humans; anatomical and physiological similarities. Shares same clinicopathological features as human Lynch syndrome	Research cycle or modeling time-consuming	Bakken et al. (2016) Dray et al. (2018) Ozirmak et al. (2022)

human CRC tumors in human intestinal stem cell medium (HISC), and the phenotype and genotype of the PDOs have been reported to be highly similar to those of the original tumor (Van et al., 2015; Vlachogiannis et al., 2018).

Organoids are typically used for investigating the mechanism underlying the development of CRC, screening anti-CRC drugs, and determining the efficacy and mechanism of action of drugs. However, there are various limitations to the application of organoids in studies on CRC, which are described hereafter. First, the current methods for organoid culture lack the technological means for maintaining the blood vessels, immune system, and peripheral nervous system of tumor cells, and organoids lacking these characteristics cannot be used in CRC research (Bredenoord et al., 2017). Second, as PDO models lack the cellular and acellular components of the TME of the original tumor, they cannot equivalently represent the *in vivo* environment of the tumor (Li X. et al., 2020). Third, there are no specific media for culturing organoids to date. Furthermore, it is unclear whether organoids can represent the overall heterogeneity of the tumor and all cell types in the tumor. Organoids can be applied to relevant studies by optimizing the culture conditions for maintaining the expression of genes related to microsatellite instability, B-Raf proto-oncogene, serine/threonine kinase (*BRAF*) mutations, poor differentiation, or mucinous phenotypes related to CRC. The application of organoids to CRC research can be improved by employing the co-culture model of organoids in which immune cells and mesenchymal cells are co-cultured for simulating the *in vivo* TME.

2.3 Application of cellular models of CRC

The establishment of models using the corresponding tumor cells is crucial for investigating the mechanism underlying the development of CRC and discovery of anti-CRC drugs (Senga and Grose, 2021). The applications of different cellular models of CRC according to the different molecular mechanisms underlying tumor formation, including epithelial–mesenchymal transition (EMT), apoptosis, invasion, metastasis, chromosome instability (CIN), and immune escape, are summarized in Table 1 and Figure 4.

TABLE 4 Applications of animal models of CRC.

Purpose of study	Research methods/models	References
Studying apoptosis in CRC	Investigation of apoptosis in CRC with CRC xenograft models	Han et al. (2018)
		Li et al. (2020a)
Investigation of angiogenesis in CRC	Studying the effect of AOM/DSS-induced expression of severe acute respiratory infection (*SARI*) gene on angiogenesis in CRC	Dai et al. (2016)
	DMH/DSS-induced expression of CRC angiogenesis factor in rat model	Liu et al. (2015a)
	Induction of tumor angiogenesis *in vivo via* the expression of *VEGF* and interleukin-8 (*IL-8*)	Liu et al. (2015b)
	Studying angiogenesis in CRC xenografts following induction with drugs, C-X-C motif chemokine ligand 12 (*CXCL12*), and *CXCL11*	Rupertus et al. (2014)
		Yu et al. (2005)
		Jakopovic et al. (2020)
	Drug-induced *in vivo* inhibition of angiogenesis	Petrović et al. (2020)
	Dickkopf associated protein 2 (*DKK2*)-induced angiogenesis in CRC xenografts	Ding et al. (2016)
		Deng et al. (2019)
	Inhibition of angiogenesis by potentially inappropriate medication (PIM) kinase in orthotopically transplanted CRC tumors	Casillas et al. (2018)
	Induction of angiogenesis by hepatectomy in CRC xenografts	Lo et al. (2018)
	EG-VEGF induced angiogenesis in orthotopically transplanted CRC tumors	Goi et al. (2004)
Investigation of metabolic reprogramming in CRC	Induction of metabolic reprogramming in CRC xenograft model using hexokinase, free fatty acid (FFA), acetyl coenzyme A, citrate, and other agents	Bu et al. (2018)
		Wang et al. (2018)
		Dong et al. (2022)
		Zhang et al. (2022)
	AOM/DSS-induced CRC model of metabolic reprogramming	Wu et al. (2020)
		Yin et al. (2021)
	Initiation of metabolic reprogramming by DSS-induced inflammation	Qu et al. (2017)
Study of invasion and metastasis in CRC	CRC xenograft model for studying invasion and metastasis in CRC	Rokavec et al. (2014)
		Erreni et al. (2016)
		Li et al. (2019b)
Study of immune escape in CRC	Gene mutation-induced model of immune escape	Xing et al. (2021)
		Wei et al. (2022)
	Generation of immune escape model by ablation of zebrafish macrophages using chlorophosphonate liposomes	Póvoa et al. (2021)
Study of inflammation in CRC	TNBS/oxazolone/DSS-induced inflammatory CRC	Wirtz et al. (2007)
	LPS/DSS-induced inflammation	Garlanda et al. (2004)
	DSS-induced inflammation of intestinal epithelium and mucosa	Mashimo et al. (1996)
		Van et al. (2006)
	DSS/AOM-induced inflammation in sporadic CRC	De et al. (2019)
		Liang et al. (2017)
	TNBS-induced inflammation	Scheiffele and Fuss (2002)
	DMH-induced inflammation	Kumar et al. (2019)
	Radiofrequency ablation (RFA)-induced inflammation	Shi et al. (2019)
	HFD-induced inflammation	Hu et al. (2021)

(Continued on following page)

TABLE 4 (*Continued*) Applications of animal models of CRC.

Purpose of study	Research methods/models	References
	Gene mutation-induced inflammatory CRC	Puppa et al. (2011)
		De et al. (2020)
	High-iron diet-induced inflammatory CRC	Seril et al. (2006)
Investigation of the mechanism of EMT in CRC	Induction of EMT models via mutations/overexpression/knockdown *p* rostate transmembrane protein androgen induced 1 (*PMEPA1*), SOX2, histone deacetylase 1 (*HDAC1*), and other genes	Wang et al. (2014)
		Matsuda et al. (2016)
		Li et al. (2017a)
		Zhuang et al. (2018)
		Yang et al. (2019)
		Zhang et al. (2019)
		Liu et al. (2020b)
		Shen et al. (2021)
		Qi et al. (2021)
		Zhu et al. (2021)
		Liu et al. (2020)
	Transforming growth factor-β (*TGF*-β)-induced model of EMT	Li et al. (2021)
	Tumor EMT-induced metastatic model of CRC	Adams et al., 2021
Epigenetic reprogramming	CRC xenograft model for studying epigenetic reprogramming in CRC	Kodach et al. (2021)
	Induction of gene mutation for studying epigenetic reprogramming in CRC	Hashimoto et al. (2017)
Study of cell aging in CRC	Xenotransplantation model for studying cellular aging in CRC	Gao et al. (2010)
		Liu et al. (2013)
		Mikuła et al. (2015)
		Hou et al. (2018)
	DMH/DSS-induced model of cellular aging	Liu et al. (2013)
	AOM/DSS-induced model of cellular aging	Foersch et al. (2015)
Polymorphic microbiota	AOM/DSS-induced model for studying composition of intestinal microbiota	Wu et al. (2016)

TABLE 5 Applications of animal models of CRC.

TCM syndrome	Research methods/models	References
CRC with spleen qi deficiency syndromeHou et al., 2018 (SDS)	Restricted feeding/fatigue/purging + hypodermic implantation of C26 tumor cells to establish a spleen deficiency with cachexia model	Zhang et al. (2020)
CRC with damp-heat syndrome (DHS)	HFD/AOM/DSS-induced malignant tumor (stasis-toxin) model	Cao and Zhou (2020)
		Huang et al. (2022)
CRC with internal retention of toxin stagnation syndrome (IRTSS)	LPS tail vein and peritoneal injection + hypodermic implantation of C26 tumor cells to establish colorectal tumor-bearing with syndrome of heat-toxicity and blood stasis model	Li et al. (2017b)

3 CRC animal models based on experimental animals

The occurrence of diseases such as cancer that occur spontaneously in animals is largely attributed to genetic diversity and immune functions. Therefore, studying the methods for generating animal models of CRC can aid in elucidating the mechanisms underlying the development of cancer (Marian, 2004). Animal models can compensate for the limitations of cellular models that are incapable of simulating the mechanism underlying the development of CRC. Rat and murine models are the most frequently used animal models of CRC, and other animal

models of CRC, including fruit fly, zebrafish, and pigs, are also commonly used as sentinels and preclinical models in CRC research.

3.1 Rodent models

Rodent models are conducive tools for conducting cancer research, and are extensively used for elucidating the etiopathogenesis and molecular mechanisms underlying the development of CRC. Previous studies have demonstrated that the protein-coding genes of mice and humans share high homogeneity (Mouse Genome Sequencing Consortium, 2002). Additionally, the use of murine models is advantageous owing to the fact that mice have a short intergenerational interval, high reproducibility, and similar genetic background and formula as humans, compared to other animal models. Murine models of CRC can therefore be used as effective tools for studying the mechanism underlying the pathogenesis of CRC and determining novel strategies for the prevention and treatment of CRC (Doyle et al., 2012).

Transgenic mice models can serve as effective tools for preclinical evaluation and screening during the optimization and development of anticancer drugs. Mutations in *APC* (adenomatous polyposis coli) are commonly inherited in adenoma-carcinoma transitions observed during the development of CRC (Van et al., 2000). Additionally, the absence of mutations in DNA mismatch repair (MMR) genes increases deletion mutations in *APC*, which accelerates the formation of adenomas (Huang et al., 2004). It has been reported that mutations in tumor protein 53 (*p53*), Kirsten rats arcomaviral oncogene homolog (*KRAS*), phosphatidylinositol-4,5-bisphosphate 3-kinase catalytic subunit alpha (*PIK3CA*), F-box and WD repeat domain containing 7 (*FBXW7*), SMAD family member 4 (*SMAD4*), transcription factor 7-like 2 (*TCF7L2*), NRAS proto-oncogene (*NRAS*), AT-rich interaction domain 1 A (*ARID1A*), SRY-box transcription factor 9 (*SOX9*), and APC membrane recruitment protein 1 (*FAM123B*) can also increase the risk of CRC (Cancer Genome Atlas Network, 2012). Transgenic murine models are extensively used for studying the occurrence and elimination of tumors, underlying molecular pathways, and genomic regulation via gain-of-function or loss-of-function mutations in oncogenes and cancer suppressor genes.

CRC is caused by various risk factors, including poor dietary habits, environment, exposure to carcinogenic chemicals, and other factors (Hecht, 2003; Mehta et al., 2017). Animal models of CRC generated by treatment with chemicals serve as effective models in studies aimed at determining novel therapeutic approaches and investigating the diagnosis, prognosis, and identification of predictive markers. The differences among the methods and duration of treatment for inducing CRC with different chemical agents are depicted in Figure 5.

The use of chemical agents for generating models of CRC requires a long duration and these models have longer experimental cycles. Mofikawa et al. established the first orthotopic transplantation model of CRC in 1986 by transplanting human CRC cells under the cecal wall of nude mice. This shortened the period of study using animal models of CRC, and initiated the establishment of tumor transplantation models. Table 2 summarizes the different murine models of CRC, and describes their scope of application and limitations in tumor research.

3.2 Other animal models of CRC

In addition to rodents, invertebrates such as fruit fly can be used for personalized diagnosis and developing potential therapeutic strategies for CRC. Vertebrates such as zebrafish, dogs, cats, pigs, and non-human primates are also used in studies on CRC. The advantages and disadvantages of the different animal models used in CRC research are summarized in Table 3.

3.3 Application of animal models of CRC

The carcinogenesis of CRC is affected by several contributing factors. The selection of the animal model of CRC depends on the purpose of the study, as summarized in Table 4.

Traditional Chinese medicine (TCM) and western medicine are two different medical theoretical systems. The research model based on the etiological mechanism theory of TCM is applied to animal studies with TCM syndrome, as shown in Table 5.

4 Conclusions and future directions

Understanding the inherent advantages and limitations of the different models of CRC, and the appropriate application of these models in drug development and studies on the mechanism of tumor occurrence and development are important in CRC research.

Human cell lines and xenograft models have been extensively employed over the past few decades owing to their low cost and ease of application. However, these models are incapable of reproducing the heterogeneity of CRC tumors (Harma et al., 2010). The cell co-culture technique can overcome the limitations of monolayer cell culture, and enables the construction of *in vitro* physiological or pathological models that closely represent the *in vivo* condition, and can be used for studying the interactions between cells, and between cells and the culture environment. It has been reported that 3D models can mimic the physiological characteristics of parental tumors, including tumor heterogeneity (Li et al., 2019). However, the shape, size, and activity of organoids are different under the same culture conditions, and the matrix limits the penetration of drugs and hinders drug screening (Zhao et al., 2020). It is therefore imperative to construct a model that closely represents the characteristics of CRC *in vivo*.

The intestinal microarray platforms used in CRC research, which consist of intestinal organoids and organic chips, can summarize the important structural features and functions of the natural duodenum. This platform can be applied for studying drug conveyance, metabolism, and drug-drug interactions (Kasendra et al., 2018). Multi-locus transfer chips consist of multiple 3D organoids that connect the CRC-like organs, liver, lungs, and endothelial flow via recirculating fluid systems, and enables cell tracking by fluorescence imaging technology. The transfer sites of CRC cells are also included in multi-locus transfer chips (Aleman and Skardal, 2019).

Animal models of CRC have been widely used for studying the complexity of CRC. There are primarily two types of animal models, namely, *in situ* models and the cell and tissue transplantation models of CRC. Owing to the relatively simple modeling approach of human tumor xenotransplantation, this model is presently widely used for studying the efficacy of anti-CRC drugs. The effects of CRC xenotransplantation can be closely related to clinical activity via the rational application of these models. For instance, genetically engineered murine models have been used for studying the progression of tissue-specific molecular changes in CRC by determining the effect of specific molecular targets. Chemical induced-CRC animal model is one of the most commonly CRC models, in which CAC model is usually induced by AOM/DSS to study the mechanism of inflammation related-tumorigenesis and development (Zeng et al., 2022). The CRC model with TCM syndrome is an artificial disease and syndrome experimental animal model created by simulating and replicating characteristics of human disease prototype according to TCM theory. An animal model combining with CRC and TCM syndromes might be useful to mimic the clinical characteristics of CRC patients with TCM syndrome (Zhang et al., 2020). Mouse is the commonly used to the models mentioned above, however, it is increasingly accepted that the use of larger animal models, especially dogs and pigs, can provide deeper insights in cancer research (Croker et al., 2009).

The application of molecular tools and genetic strategies has aided the advancement of cancer research, and the cellular and animal models of CRC are being continually improved. Further understanding of the genetic and epigenetic events in CRC, including the alterations in molecular networks associated with the initial stages of development, are facilitated by high-resolution approaches.

Although CRC research has advanced immensely in recent years, several clinical issues remain to be resolved to date, which is partly attributed to the absence of suitable preclinical research models. The application of *in vivo* and *in vitro* models in CRC research, combined with advanced scientific techniques for simulating a more realistic tumor environment *in vivo* and *in vitro*, can help replicate the complex scenarios of tumor occurrence and development, identify novel therapeutic approaches for inhibiting tumor growth, and elucidate the molecular mechanisms underlying tumor formation.

Author contributions

All authors listed have made a substantial, direct, and intellectual contribution to the work and approved it for publication.

Funding

This work was supported by the National Natural Science Foundation of China (82074318, 81930117 and 82004310), Natural Science Foundation Youth Project of Jiangsu Province (BK 20200846), Natural Science Research of Jiangsu Higher Education Institutions of China (19KJA310007), Qinglan Project of Jiangsu Province, College Students' Innovative Entrepreneurial Training Plan Program (202010315023Z and 202010315025), a project funded by the Priority Academic Program Development of Jiangsu Higher Education Institutions.

Acknowledgments

The authors must be grateful to the BioRender (www.biorender.com), as the figures in this review were drawn by using the BioRender platform.

Conflict of interest

The authors declare that the research was conducted in the absence of any commercial or financial relationships that could be construed as a potential conflict of interest.

Publisher's note

References

Ahmed, D., Eide, P. W., Eilertsen, I. A., Danielsen, S. A., Eknæs, M., Hektoen, M., et al. (2013). Epigenetic and genetic features of 24 colon cancer cell lines. *Oncogenesis* 2 (9), e71. doi:10.1038/oncsis.2013.35

Akashi, H., Han, H. J., Iizaka, M., and Nakamura, Y. (2000). Growth-suppressive effect of non-steroidal anti-inflammatory drugs on 11 colon-cancer cell lines and fluorescence differential display of genes whose expression is influenced by sulindac. *Int. J. Cancer* 88 (6), 873–880. doi:10.1002/1097-0215(20001215)88:6<873:aid-ijc6>3.0.co;2-b

Aleman, J., and Skardal, A. (2019). A multi-site metastasis-on-a-chip microphysiological system for assessing metastatic preference of cancer cells. *Biotechnol. Bioeng.* 116 (4), 936–944. doi:10.1002/bit.26871

Amatruda, J. F., Shepard, J. L., Stern, H. M., and Zon, L. I. (2002). Zebrafish as a cancer model system. *Cancer Cell.* 1 (3), 229–231. doi:10.1016/s1535-6108(02)00052-1

Aranganathan, S., and Nalini, N. (2013). Antiproliferative efficacy of hesperetin (citrus flavanoid) in 1,2-dimethylhydrazine-induced colon cancer. *Phytotherapy Res. PTR* 27 (7), 999–1005. doi:10.1002/ptr.4826

Bai, J. S., Wang, J., and Zhao, X. F. (2015). Nude mice hemispleen method in hepatic metastases of colon cancer model. 37, 447–450. doi:10.11724/jdmu.2015.05.08

Bakken, T. E., Miller, J. A., Ding, S. L., Sunkin, S. M., Smith, K. A., Ng, L., et al. (2016). A comprehensive transcriptional map of primate brain development. *Nature* 535 (7612), 367–375. doi:10.1038/nature18637

Barker, N., Van Es, J. H., Kuipers, J., Kujala, P., Van den Born, M., Cozijnsen, M., et al. (2007). Identification of stem cells in small intestine and colon by marker gene Lgr5. *Nature* 449 (7165), 1003–1007. doi:10.1038/nature06196

Barretina, J., Caponigro, G., Stransky, N., Venkatesan, K., Margolin, A. A., Kim, S., et al. (2012). The cancer cell line encyclopedia enables predictive modelling of anticancer drug sensitivity. *Nature* 483 (7391), 603–607. doi:10.1038/nature11003

Berg, K. C. G., Eide, P. W., Eilertsen, I. A., Johannessen, B., Bruun, J., Danielsen, S. A., et al. (2017). Multi-omics of 34 colorectal cancer cell lines - a resource for biomedical studies. *Mol. Cancer* 16 (1), 116. doi:10.1186/s12943-017-0691-y

Bhandari, P., and Shashidhara, L. S. (2001). Studies on human colon cancer gene APC by targeted expression in Drosophila. *Oncogene* 20 (47), 6871–6880. doi:10.1038/sj.onc.1204849

Bian, X., Cao, F., Wang, X., Hou, Y., Zhao, H., and Liu, Y. (2021). Establishment and characterization of a new human colon cancer cell line, PUMC-CRC1. *Sci. Rep.* 11 (1), 13122. doi:10.1038/s41598-021-92491-7

Bolhaqueiro, A. C. F., Ponsioen, B., Bakker, B., Klaasen, S. J., Kucukkose, E., Van Jaarsveld, R. H., et al. (2019). Ongoing chromosomal instability and karyotype evolution in human colorectal cancer organoids. *Nat. Genet.* 51 (5), 824–834. doi:10.1038/s41588-019-0399-6

Boot, A., Van Eendenburg, J., Crobach, S., Ruano, D., Speetjens, F., Calame, J., et al. (2016). Characterization of novel low passage primary and metastatic colorectal cancer cell lines. *Oncotarget* 7 (12), 14499–14509. doi:10.18632/oncotarget.7391

Bos, J. L., Fearon, E. R., Hamilton, S. R., Verlaan-de Vries, M., van Boom, J. H., van der Eb, A. J., et al. (1987). Prevalence of Ras gene mutations in human colorectal cancers. *Nature* 327 (6120), 293–297. doi:10.1038/327293a0

Boucherit, N., Gorvel, L., and Olive, D. (2020). 3D tumor models and their use for the testing of immunotherapies. *Front. Immunol.* 11, 603640–640. doi:10.3389/fimmu.2020.603640

Bredenoord, A. L., Clevers, H., and Knoblich, J. A. (2017). Human tissues in a dish: The research and ethical implications of organoid technology. *Science* 355 (6322), eaaf9414. doi:10.1126/science.aaf9414

Brugman, S., Liu, K. Y., Lindenbergh-Kortleve, D., Samsom, J. N., Furuta, G. T., Renshaw, S. A., et al. (2009). Oxazolone-induced enterocolitis in zebrafish depends on the composition of the intestinal microbiota. *Gastroenterology* 137 (5), 1757–1767. doi:10.1053/j.gastro.2009.07.069

Bu, P., Chen, K. Y., Xiang, K., Johnson, C., Crown, S. B., Rakhilin, N., et al. (2018). Aldolase B mediated fructose metabolism drives metabolic reprogramming of colon cancer liver metastasis. *Cell. Metab.* 27 (6), 1249–1262. doi:10.1016/j.cmet.2018.04.003

Calcagno, S. R., Li, S., Colon, M., Kreinest, P. A., Thompson, E. A., Fields, A. P., et al. (2008). Oncogenic K-ras promotes early carcinogenesis in the mouse proximal colon. *Int. J. Cancer* 122, 2462–2470. doi:10.1002/ijc.23383

Campbell, S. L., Khosravi-Far, R., Rossman, K. L., Clark, G. J., and Der, C. J. (1998). Increasing complexity of Ras signaling. *Oncogene* 17 (11), 1395–1413. doi:10.1038/sj.onc.1202174

Cancer Genome Atlas Network (2012). Comprehensive molecular characterization of human colon and rectal cancer. *Nature* 487 (7407), 330–337. doi:10.1038/nature11252

Cao, W., and Zhou, X. (2020). Establishment of intestinal cancer model in mice with damp-heat, phlegm-stagnation and stasis-toxin. *J. Hunan Univ. Chin. Med.* 40 (01), 38–41. doi:10.3969/j.issn.1674-070X.2020.01.009

Casali, A., and Batlle, E. (2009). Intestinal stem cells in mammals and drosophila. *Cell. Stem Cell.* 4 (2), 124–127. doi:10.1016/j.stem.2009.01.009

Casillas, A. L., Toth, R. K., Sainz, A. G., Singh, N., Desai, A. A., Kraft, A. S., et al. (2018). Hypoxia-inducible PIM kinase expression promotes resistance to antiangiogenic agents. *Clin. Cancer Res.* 24 (1), 169–180. doi:10.1158/1078-0432.CCR-17-1318

Cen, B., Wei, J., Wang, D., Xiong, Y., Shay, J. W., and DuBois, R. N. (2021). Mutant APC promotes tumor immune evasion via PD-L1 in colorectal cancer. *Oncogene* 40 (41), 5984–5992. doi:10.1038/s41388-021-01972-6

Chadla, P., Arbi, M., Nikou, S., Kalliakoudas, T., Papadaki, H., Taraviras, S., et al. (2021). Integrin-linked-kinase overexpression is implicated in mechanisms of genomic instability in human colorectal cancer. *Dig. Dis. Sci.* 66 (5), 1510–1523. doi:10.1007/s10620-020-06364-6

Chen, L., Vasoya, R. P., Toke, N. H., Parthasarathy, A., Luo, S., Chiles, E., et al. (2020). HNF4 regulates fatty acid oxidation and is required for renewal of intestinal stem cells in mice. *Gastroenterology* 158 (4), 985–999. doi:10.1053/j.gastro.2019.11.031

Choo, M. K., Sakurai, H., Koizumi, K., and Saiki, I. (2005). Stimulation of cultured colon 26 cells with TNF-alpha promotes lung metastasis through the extracellular signal-regulated kinase pathway. *Cancer Lett.* 230 (1), 47–56. doi:10.1016/j.canlet.2004.12.027

Croker, A. K., Goodale, D., Chu, J., Postenka, C., Hedley, B. D., Hess, D. A., et al. (2009). High aldehyde dehydrogenase and expression of cancer stem cell markers selects for breast cancer cells with enhanced malignant and metastatic ability. *J. Cell. Mol. Med.* 13 (8B), 2236–2252. doi:10.1111/j.1582-4934.2008.00455.x

Dabrowska, M., Skoneczny, M., and Rode, W. (2011). Functional gene expression profile underlying methotrexate-induced senescence in human colon cancer cells. *Tumour Biol.* 32 (5), 965–976. doi:10.1007/s13277-011-0198-x

Dabrowska, M., Skoneczny, M., Uram, L., and Rode, W. (2019). Methotrexate-induced senescence of human colon cancer cells depends on p53 acetylation, but not genomic aberrations. *Anticancer Drugs* 30 (4), 374–382. doi:10.1097/CAD.0000000000000731

Dai, L., Cui, X., Zhang, X., Cheng, L., Liu, Y., Yang, Y., et al. (2016). SARI inhibits angiogenesis and tumour growth of human colon cancer through directly targeting ceruloplasmin. *Nat. Commun.* 7, 11996. doi:10.1038/ncomms11996

De Oliveira, T., Ramakrishnan, M., Diamanti, M. A., Ziegler, P. K., Brombacher, F., and Greten, F. R. (2019). Loss of Stat6 affects chromatin condensation in intestinal epithelial cells causing diverse outcome in murine models of inflammation-associated and sporadic colon carcinogenesis. *Oncogene* 38 (11), 1787–1801. doi:10.1038/s41388-018-0551-2

De Robertis, M., Massi, E., Poeta, M. L., Carotti, S., Morini, S., Cecchetelli, L., et al. (2011). The AOM/DSS murine model for the study of colon carcinogenesis: From pathways to diagnosis and therapy studies. *J. Carcinog.* 10, 9. doi:10.4103/1477-3163.78279

De Santis, S., Verna, G., Serino, G., Armentano, R., Cavalcanti, E., Liso, M., et al. (2020). Winnie-APC$^{Min/+}$ mice: A spontaneous model of colitis-associated colorectal cancer combining genetics and inflammation. *Int. J. Mol. Sci.* 21 (8), 2972. doi:10.3390/ijms21082972

Dean, P. G. (2013). Commentary on "The pig as a preclinical model for intestinal ischemia-reperfusion and transplantation studies. *J. Surg. Res.* 185 (2), 541–542. doi:10.1016/j.jss.2012.10.014

Deng, F., Zhou, R., Lin, C., Yang, S., Wang, H., Li, W., et al. (2019). Tumor-secreted dickkopf-2 accelerates aerobic glycolysis and promotes angiogenesis in colorectal cancer. *Theranostics* 9 (4), 1001–1014. doi:10.7150/thno.30056

Ding, C., Li, L., Yang, T., Fan, X., and Wu, G. (2016). Combined application of anti-VEGF and anti-EGFR attenuates the growth and angiogenesis of colorectal cancer mainly through suppressing AKT and ERK signaling in mice model. *BMC Cancer* 16 (1), 791. doi:10.1186/s12885-016-2834-8

Dolara, P., Luceri, C., De Filippo, C., Femia, A. P., Giovannelli, L., Caderni, G., et al. (2005). Red wine polyphenols influence carcinogenesis, intestinal microflora, oxidative damage and gene expression profiles of colonic mucosa in F344 rats. *Mutat. Res.* 591 (1-2), 237–246. doi:10.1016/j.mrfmmm.2005.04.022

Dong, M. J., Zhou, Y., Duan, M., Gao, Q. M., and Zhao, J. H. (2020). Clinical significance and mechanism of TBX5 gene in colorectal cancer. *Zhonghua Zhong Liu Za Zhi* 42 (5), 383–390. doi:10.3760/cma.j.cn112152-112152-20190829-00560

Dong, S., Liang, S., Cheng, Z., Zhang, X., Luo, L., Li, L., et al. (2022). ROS/PI3K/AKT and Wnt/β-catenin signalings activate HIF-1α-induced metabolic reprogramming to impart 5-fluorouracil resistance in colorectal cancer. *J. Exp. Clin. Cancer Res.* 41 (1), 15. doi:10.1186/s13046-021-02229-6

Dou, R., Liu, K., Yang, C., Zheng, J., Shi, D., Lin, X., et al. (2021). EMT-cancer cells-derived exosomal miR-27b-3p promotes circulating tumour cells-mediated metastasis by modulating vascular permeability in colorectal cancer. *Clin. Transl. Med.* 11 (12), 595. doi:10.1002/ctm2.595

Doyle, A., McGarry, M. P., Lee, N. A., and Lee, J. J. (2012). The construction of transgenic and gene knockout/knockin mouse models of human disease. *Transgenic Res.* 21 (2), 327–349. doi:10.1007/s11248-011-9537-3

Dray, B. K., Raveendran, M., Harris, R. A., Benavides, F., Gray, S. B., Perez, C. J., et al. (2018). Mismatch repair gene mutations lead to lynch syndrome colorectal cancer in rhesus macaques. *Genes. Cancer* 9 (3-4), 142–152. doi:10.18632/genesandcancer.170

Erreni, M., Siddiqui, I., Marelli, G., Grizzi, F., Bianchi, P., Morone, D., et al. (2016). The fractalkine-receptor Axis improves human colorectal cancer prognosis by limiting tumor metastatic dissemination. *J. Immunol.* 196 (2), 902–914. doi:10.4049/jimmunol.1501335

Faqar-Uz-Zaman, W. F., Schmidt, K. G., Thomas, D., Pfeilschifter, J. M., Radeke, H. H., and Schwiebs, A. (2021). S1P lyase siRNA dampens malignancy of DLD-1 colorectal cancer Cells. *Lipids* 56 (2), 155–166. doi:10.1002/lipd.12282

Femia, A. P., and Caderni, G. (2008). Rodent models of colon carcinogenesis for the study of chemopreventive activity of natural products. *Planta Med.* 74 (13), 1602–1607. doi:10.1055/s-2008-1074577

Flisikowska, T., Merkl, C., Landmann, M., Eser, S., Rezaei, N., Cui, X., et al. (2012). A porcine model of familial adenomatous polyposis. *Gastroenterology* 143 (5), 1173–1175. doi:10.1053/j.gastro.2012.07.110

Flisikowska, T., Stachowiak, M., Xu, H., Wagner, A., Hernandez-Caceres, A., Wurmser, C., et al. (2017). Porcine familial adenomatous polyposis model enables systematic analysis of early events in adenoma progression. *Sci. Rep.* 7 (1), 6613. doi:10.1038/s41598-017-06741-8

Foersch, S., Sperka, T., Lindner, C., Taut, A., Rudolph, K. L., Breier, G., et al. (2015). VEGFR2 signaling prevents colorectal cancer cell senescence to promote tumorigenesis in mice with colitis. *Gastroenterology* 149 (1), 177–189. doi:10.1053/j.gastro.2015.03.016

Fujii, M., Matano, M., Toshimitsu, K., Takano, A., Mikami, Y., Nishikori, S., et al. (2018). Human intestinal organoids maintain self-renewal capacity and cellular diversity in niche-inspired culture condition. *Cell. Stem Cell.* 23 (6), 787–793. doi:10.1016/j.stem.2018.11.016

Fujii, M., and Sato, T. (2021). Somatic cell-derived organoids as prototypes of human epithelial tissues and diseases. *Nat. Mat.* 20, 20156–20169. doi:10.1038/s41563-020-0754-0

Gao, F. H., Hu, X. H., Li, W., Liu, H., Zhang, Y. J., Guo, Z. Y., et al. (2010). Oridonin induces apoptosis and senescence in colorectal cancer cells by increasing histone hyperacetylation and regulation of p16, p21, p27 and c-Myc. *BMC Cancer* 10, 610. doi:10.1186/1471-2407-10-610

Garlanda, C., Riva, F., Polentarutti, N., Buracchi, C., Sironi, M., De Bortoli, M., et al. (2004). Intestinal inflammation in mice deficient in Tir8, an inhibitory member of the IL-1 receptor family. *Proc. Natl. Acad. Sci. U. S. A.* 101 (10), 3522–3526. doi:10.1073/pnas.0308680101

Ghasemi, P., Shafiee, G., Ziamajidi, N., and Abbasalipourkabir, R. (2020). Copper nanoparticles induce apoptosis and oxidative stress in SW480 human colon cancer cell line. *Biol. Trace Elem. Res.* doi:10.1007/s12011-022-03458-2

Goi, T., Fujioka, M., Satoh, Y., Tabata, S., Koneri, K., Nagano, H., et al. (2004). Angiogenesis and tumor proliferation/metastasis of human colorectal cancer cell line SW620 transfected with endocrine glands-derived-vascular endothelial growth factor, as a new angiogenic factor. *Cancer Res.* 64 (6), 1906–1910. doi:10.1158/0008-5472.can-3696-2

Gonzalez, L. M., Stewart, A. S., Freund, J., Kucera, C. R., Dekaney, C. M., Magness, S. T., et al. (2019). Preservation of reserve intestinal epithelial stem cells following severe ischemic injury. *Am. J. Physiol. Gastrointest. Liver Physiol.* 316 (4), G482-G494–G494. doi:10.1152/ajpgi.00262.2018

Gregorieff, A., Liu, Y., Inanlou, M. R., Khomchuk, Y., and Wrana, J. L. (2015). Yap-dependent reprogramming of Lgr5(+) stem cells drives intestinal regeneration and cancer. *Nature* 526 (7575), 715–718. doi:10.1038/nature15382

Groll, T., Schopf, F., Denk, D., Mogler, C., Schwittlick, U., Aupperle-Lellbach, H., et al. (2021). Bridging the species gap: Morphological and molecular comparison of feline and human intestinal carcinomas. *Cancers (Basel).* 13 (23), 5941. doi:10.3390/cancers13235941

Haldi, M., Ton, C., Seng, W. L., and McGrath, P. (2006). Human melanoma cells transplanted into zebrafish proliferate, migrate, produce melanin, form masses and stimulate angiogenesis in zebrafish. *Angiogenesis* 9, 9139–9151. doi:10.1007/s10456-006-9040-2

Han, Q., Ma, Y., Wang, H., Dai, Y., Chen, C., Liu, Y., et al. (2018). Resibufogenin suppresses colorectal cancer growth and metastasis through RIP3-mediated necroptosis. *J. Transl. Med.* 16 (1), 201. doi:10.1186/s12967-018-1580-x

Harma, S., Haber, D., and Settleman, J. (2010). Cell line-based platforms to evaluate the therapeutic efficacy of candidate anticancer agents. *Nat. Rev. Cancer* 10 (4), 241–253. doi:10.1038/nrc2820

Hashimoto, K., Yamada, Y., Semi, K., Yagi, M., Tanaka, A., Itakura, F., et al. (2017). Cellular context-dependent consequences of APC mutations on gene regulation and cellular behavior. *Proc. Natl. Acad. Sci. U. S. A.* 114 (4), 758–763. doi:10.1073/pnas.1614197114

Hason, M., and Bartůněk, P. (2019). Zebrafish models of cancer-new insights on modeling human cancer in a non-mammalian vertebrate. *Genes. (Basel).* 10 (11), 935. doi:10.3390/genes10110935

Hecht, S. S. (2003). Tobacco carcinogens, their biomarkers and tobacco-induced cancer. *Nat. Rev. Cancer* 3 (10), 733–744. doi:10.1038/nrc1190

Hou, Z., Guo, K., Sun, X., Hu, F., Chen, Q., Luo, X., et al. (2018). TRIB2 functions as novel oncogene in colorectal cancer by blocking cellular senescence through AP4/p21 signaling. *Mol. Cancer* 17 (1), 172. doi:10.1186/s12943-018-0922-x

Hu, X., Fatima, S., Chen, M., Xu, K., Huang, C., Gong, R. H., et al. (2021). Toll-like receptor 4 is a master regulator for colorectal cancer growth under high-fat diet by programming cancer metabolism. *Cell. Death Dis.* 12 (8), 791. doi:10.1038/s41419-021-04076-x

Hua, R., Yu, J., Yan, X., Ni, Q., Zhi, X., Li, X., et al. (2020). Syndecan-2 in colorectal cancer plays oncogenic role via epithelial-mesenchymal transition and MAPK pathway. *Biomed. Pharmacother.* 121, 109630. doi:10.1016/j.biopha.2019.109630

Huang, J., Jiang, T., Kang, J., Xu, J., Dengzhang, Y., Zhao, Z., et al. (2022). Synergistic effect of Huangqin decoction combined treatment with Radix *Actinidiae chinensis* on DSS and AOM-induced colorectal cancer. *Front. Pharmacol.* 13, 933070. doi:10.3389/fphar.2022.933070

Huang, J., Zheng, S., Jin, S. H., and Zhang, S. Z. (2004). Somatic mutations of APC gene in carcinomas from hereditary non-polyposis colorectal cancer patients. *World J. Gastroenterol.* 10 (6), 834–836. doi:10.3748/wjg.v10.i6.834

Huang, Z., Liu, C. A., Cai, P. Z., Xu, F. P., Zhu, W. J., Wang, W. W., et al. (2020). Omega-3PUFA Attenuates MNU-induced colorectal cancer in rats by blocking PI3K/AKT/Bcl-2 signaling. *Onco Targets Ther.* 13, 1953–1965. doi:10.2147/OTT.S241298

Huch, M., and Koo, B. K. (2015). Modeling mouse and human development using organoid cultures. *Development* 142 (18), 3113–3125. doi:10.1242/dev.118570

Inch, W. R., McCredie, J. A., and Sutherland, R. M. (1970). Growth of nodular carcinomas in rodents compared with multi-cell spheroids in tissue culture. *Growth* 34 (3), 271–282.

Itano, O., Fan, K., Yang, K., Suzuki, K., Quimby, F., Dong, Z., et al. (2012). Effect of caloric intake on Western-style diet-induced intestinal tumors in a mouse model for hereditary colon cancer. *Nutr. Cancer* 64 (3), 401–408. doi:10.1080/01635581.2012.660672

Ito, N., Hasegawa, R., Sano, M., Tamano, S., Esumi, H., Takayama, S., et al. (1991). A new colon and mammary carcinogen in cooked food, 2-amino-1-methyl-6-phenylimidazo[4,5-b] pyridine (PhIP). *Carcinogenesis* 12 (8), 1503–1506. doi:10.1093/carcin/12.8.1503

Ivascu, A., and Kubbies, M. (2006). Rapid generation of single-tumor spheroids for high-throughput cell function and toxicity analysis. *J. Biomol. Screen* 11 (8), 922–932. doi:10.1177/1087057106292763

Izzo, A. A., Aviello, G., Petrosino, S., Orlando, P., Marsicano, G., Lutz, B., et al. (2008). Increased endocannabinoid levels reduce the development of precancerous lesions in the mouse colon. *J. Mol. Med. Berl.* 86 (1), 89–98. doi:10.1007/s00109-007-0248-4

Jakopovic, B., Oršolić, N., and Kraljević, P. S. (2020). Antitumor, immunomodulatory and antiangiogenic efficacy of medicinal mushroom extract mixtures in advanced colorectal cancer animal model. *Molecules* 25 (21), 5005. doi:10.3390/molecules25215005

Janssen, K. P., Alberici, P., Fsihi, H., Gaspar, C., Breukel, C., Franken, P., et al. (2006). APC and oncogenic KRAS are synergistic in enhancing Wnt signaling in intestinal tumor formation and progression. *Gastroenterology* 131 (4), 1096–1109. doi:10.1053/j.gastro.2006.08.011

Janssen, K. P., El-Marjou, F., Pinto, D., Sastre, X., Rouillard, D., Fouquet, C., et al. (2002). Targeted expression of oncogenic KRAS in intestinal epithelium causes spontaneous tumorigenesis in mice. *Gastroenterology* 123 (2), 492–504. doi:10.1053/gast.2002.34786

Jedrzejczak, S. M. (2017). "History of cell culture," in *In new insights into cell culture technology* (Rijeka, Croatia: InTech). doi:10.5772/66905

Jen, J., Powell, S. M., Papadopoulos, N., Smith, K. J., Hamilton, S. R., Vogelstein, B., et al. (1994). Molecular determinants of dysplasia in colorectal lesions. *Cancer Res.* 54 (21), 5523–5526.

Jiao, T., Li, Y., Gao, T., Zhang, Y., Feng, M., Liu, M., et al. (2017). MTA3 regulates malignant progression of colorectal cancer through Wnt signaling pathway. *Tumour Biol.* 39 (3), 1010428317695027. doi:10.1177/1010428317695027

Ju, S., Wang, F., Wang, Y., and Ju, S. (2020). CSN8 is a key regulator in hypoxia-induced epithelial-mesenchymal transition and dormancy of colorectal cancer cells. *Mol. Cancer* 19 (1), 168. doi:10.1186/s12943-020-01285-4

Jung, Y. R., Kim, E. J., Choi, H. J., Park, J. J., Kim, H. S., Lee, Y. J., et al. (2015). Aspirin targets SIRT1 and AMPK to induce senescence of colorectal carcinoma cells. *Mol. Pharmacol.* 88 (4), 708–719. doi:10.1124/mol.115.098616

Juric, D., Rodon, J., Tabernero, J., Janku, F., Burris, H. A., Schellens, J. H. M., et al. (2018). Phosphatidylinositol 3-kinase α-selective inhibition with alpelisib (BYL719) in PIK3CA-altered solid tumors: Results from the first-in-human study. *J. Clin. Oncol.* 36 (13), 1291–1299. doi:10.1200/JCO.2017.72.7107

Kadosh, E., Snir-Alkalay, I., Venkatachalam, A., May, S., Lasry, A., Elyada, E., et al. (2020). The gut microbiome switches mutant p53 from tumour-suppressive to oncogenic. *Nature* 586 (7827), 133–138. doi:10.1038/s41586-020-2541-0

Kamano, T., Kishino, H., Mizukami, K., Azuma, N., Tamura, J., Katami, A., et al. (1983). Histopathological study on N-ethyl-N'-nitro-N-nitrosoguanidine-induced colon cancer in dogs. *Int. J. Cancer* 32 (2), 255–258. doi:10.1002/ijc.2910320219

Kamano, T., Kurihara, M., Kishino, H., Mizukami, K., Kidokoro, T., Wakabayashi, K., et al. (1981). Experimental colonic cancer in a dog. *Jpn. J. Surg.* 11 (3), 214–218. doi:10.1007/BF02468841

Kasendra, M., Tovaglieri, A., Sontheimer-Phelps, A., Jalili-Firoozinezhad, S., Bein, A., Chalkiadaki, A., et al. (2018). Development of a primary human small intestine-on-a-chip using biopsy-derived organoids. *Sci. Rep.* 8 (1), 2871. doi:10.1038/s41598-018-21201-7

Kasuya, H., Kuruppu, D. K., Donahue, J. M., Choi, E. W., Kawasaki, H., Tanabe, K. K., et al. (2020). Establishment and characterization of 18 human colorectal cancer cell lines. *Sci. Rep.* 10 (1), 6801. doi:10.1038/s41598-020-63812-z

Kasuya, H., Kuruppu, D. K., Donahue, J. M., Choi, E. W., Kawasaki, H., and Tanabe, K. K. (2005). Mouse models of subcutaneous spleen reservoir for multiple portal venous injections to treat liver malignancies. *Cancer Res.* 65 (9), 3823–3827. doi:10.1158/0008-5472.CAN-04-2631

Kim, S. C., Kim, H. S., Kim, J. H., Jeong, N., Shin, Y. K., Kim, M. J., et al. (2020). Establishment and characterization of 18 human colorectal cancer cell lines. *Sci. Rep.* 10 (1), 6801. doi:10.1038/s41598-020-63812-z

Kimlin, L. C., Casagrande, G., and Virador, V. M. (2013). *In vitro* three-dimensional (3D) models in cancer research: An update. *Mol. Carcinog.* 52 (3), 167–182. doi:10.1002/mc.21844

Kissow, H., Hartmann, B., Holst, J. J., Viby, N. E., Hansen, L. S., Rosenkilde, M. M., et al. (2012). Glucagon-like peptide-1 (GLP-1) receptor agonism or DPP-4 inhibition does not accelerate neoplasia in carcinogen treated mice. *Regul. Pept.* 179 (1-3), 91–100. doi:10.1016/j.regpep.2012.08.016

Kodach, L. L., Jacobs, R. J., Voorneveld, P. W., Wildenberg, M. E., Verspaget, H. W., Van Wezel, T., et al. (2011). Statins augment the chemosensitivity of colorectal cancer cells inducing epigenetic reprogramming and reducing colorectal cancer cell 'stemness' via the bone morphogenetic protein pathway. *Gut* 60 (11), 1544–1553. doi:10.1136/gut.2011.237495

Kopetz, S., Lesslie, D. P., Dallas, N. A., Park, S. I., Johnson, M., Parikh, N. U., et al. (2009). Synergistic activity of the SRC family kinase inhibitor dasatinib and oxaliplatin in colon carcinoma cells is mediated by oxidative stress. *Cancer Res.* 69 (9), 3842–3849. doi:10.1158/0008-5472.CAN-08-2246

Kumar, V. L., Verma, S., and Das, P. (2019). Artesunate suppresses inflammation and oxidative stress in a rat model of colorectal cancer. *Drug Dev. Res.* 80 (8), 1089–1097. doi:10.1002/ddr.21590

Lancaster, M. A., and Knoblich, J. A. (2014). Organogenesis in a dish: Modeling development and disease using organoid technologies. *Science* 345 (6194), 1247125. doi:10.1126/science.1247125

Lee, W. Y., Hong, H. K., Ham, S. K., Kim, C. I., and Cho, Y. B. (2014). Comparison of colorectal cancer in differentially established liver metastasis models. *Anticancer Res.* 34 (7), 3321–3328.

Lehmann, B., Biburger, M., Brückner, C., Ipsen-Escobedo, A., Gordan, S., Lehmann, C., et al. (2017). Tumor location determines tissue-specific recruitment of tumor-associated macrophages and antibody-dependent immunotherapy response. *Sci. Immunol.* 2 (7), 6413. doi:10.1126/sciimmunol.aah6413

Li, M., and Izpisua Belmonte, J. C. (2019a). Organoids-preclinical models of human disease. *N. Engl. J. Med.* 380 (6), 569–579. doi:10.1056/NEJMra1806175

Li, Q., Tang, H., Hu, F., and Qin, C. (2019b). Silencing of FOXO6 inhibits the proliferation, invasion, and glycolysis in colorectal cancer cells. *J. Cell. Biochem.* 120 (3), 3853–3860. doi:10.1002/jcb.27667

Li, Q., Zhang, S., Hu, M., Xu, M., and Jiang, X. (2020a). Silencing of synaptotagmin 13 inhibits tumor growth through suppressing proliferation and promoting apoptosis of colorectal cancer cells. *Int. J. Mol. Med.* 45 (1), 234–244. doi:10.3892/ijmm.2019.4412

Li, S., Shi, X., Chen, M., Xu, N., Sun, D., Bai, R., et al. (2019c). Angiogenin promotes colorectal cancer metastasis via tiRNA production. *Int. J. Cancer* 145 (5), 1395–1407. doi:10.1002/ijc.32245

Li, S., Zhang, J., Qian, S., Wu, X., Sun, L., Ling, T., et al. (2021). S100A8 promotes epithelial-mesenchymal transition and metastasis under TGF-β/USF2 axis in colorectal cancer. *Cancer Commun.* 41 (2), 154–170. doi:10.1002/cac2.12130

Li, X., Larsson, P., Ljuslinder, I., Öhlund, D., Myte, R., Löfgren-Burström, A., et al. (2020b). *Ex vivo* organoid cultures reveal the importance of the tumor microenvironment for maintenance of colorectal cancer stem cells. *Cancers (Basel)* 12 (4), 923. doi:10.3390/cancers12040923

Li, Y., Deuring, J., Peppelenbosch, M. P., Kuipers, E. J., De Haar, C., and Van der Woude, C. J. (2012). IL-6-induced DNMT1 activity mediates SOCS3 promoter hypermethylation in ulcerative colitis-related colorectal cancer. *Carcinogenesis* 33 (10), 1889–1896. doi:10.1093/carcin/bgs214

Li, Y., Liu, Y., Zhao, N., Yang, X., Li, Y., Zhai, F., et al. (2020c). Checkpoint regulator B7x is epigenetically regulated by HDAC3 and mediates resistance to HDAC inhibitors by reprogramming the tumor immune environment in colorectal cancer. *Cell. Death Dis.* 11 (9), 753. doi:10.1038/s41419-020-02968-y

Li, Y., Qian, L. Y., Tang, P. L., Guo, Y., Men, C., Cui, Y., et al. (2017b). Cathelicidin LL37 promotes epithelial and smooth-muscle-like differentiation of adipose-derived stem cells through the wnt/β-catenin and NF-κB pathways. *Chin. J. Traditional Chin. Med.* 82 (03), 1336–1345. doi:10.1134/S0006297917110116

Li, Y., Yang, Y., Li, J., Liu, H., Chen, F., Li, B., et al. (2017a). USP22 drives colorectal cancer invasion and metastasis via epithelial-mesenchymal transition by activating AP4. *Oncotarget* 8 (20), 32683–32695. doi:10.18632/oncotarget.15950

Li, Z., Wang, J., Zhou, T., and Ye, X. (2016). Establishment of a colorectal cancer nude mouse visualization model of HIF-1α overexpression. *Oncol. Lett.* 11 (4), 2725–2732. doi:10.3892/ol.2016.4287

Liang, X., Xie, R., Su, J., Ye, B., Wei, S., Liang, Z., et al. (2017). Inhibition of RNA polymerase III transcription by triptolide attenuates colorectal tumorigenesis. *J. Exp. Clin. Cancer Res.* 38 (1), 217. doi:10.1186/s13046-019-1232-x

Lin, S., Chen, S., Chen, Z., Dai, Q., and Ke, C. (2017). X-ray-induced epithelial-mesenchymal transition in SW480 colorectal cancer cells and its potential mechanisms. *J. BUON* 22 (6), 1457–1462.

Lind, G. E., Thorstensen, L., Løvig, T., Meling, G. I., Hamelin, R., Rognum, T. O., et al. (2004). A CpG island hypermethylation profile of primary colorectal carcinomas and colon cancer cell lines. *Mol. Cancer* 3, 28. doi:10.1186/1476-4598-3-28

Liu, C., Yao, Z., Wang, J., Zhang, W., Yang, Y., Zhang, Y., et al. (2020a). Macrophage-derived CCL5 facilitates immune escape of colorectal cancer cells via the p65/STAT3-CSN5-PD-L1 pathway. *Cell. Death Differ.* 27 (6), 1765–1781. doi:10.1038/s41418-019-0460-0

Liu, J., Deng, G. H., Zhang, J., Wang, Y., Xia, X. Y., Luo, X. M., et al. (2015a). The effect of chronic stress on anti-angiogenesis of sunitinib in colorectal cancer models. *Psychoneuroendocrinology* 52, 130–142. doi:10.1016/j.psyneuen.2014.11.008

Liu, L., Wang, J., Shi, L., Zhang, W., Du, X., Wang, Z., et al. (2013). β-Asarone induces senescence in colorectal cancer cells by inducing lamin B1 expression. *Phytomedicine* 20 (6), 512–520. doi:10.1016/j.phymed.2012.12.008

Liu, M., Xiao, Y., Tang, W., Li, J., Hong, L., Dai, W., et al. (2020b). HOXD9 promote epithelial-mesenchymal transition and metastasis in colorectal carcinoma. *Cancer Med.* 9 (11), 3932–3943. doi:10.1002/cam4.2967

Liu, W., Li, W., Liu, H., and Yu, X. (2019). Xanthohumol inhibits colorectal cancer cells via downregulation of Hexokinases II-mediated glycolysis. *Int. J. Biol. Sci.* 15 (11), 2497–2508. doi:10.7150/ijbs.37481

Liu, W. X., Gu, S. Z., Zhang, S., Ren, Y., Sang, L. X., and Dai, C. (2015b). Angiopoietin and vascular endothelial growth factor expression in colorectal disease models. *World J. Gastroenterol.* 21 (9), 2645–2650. doi:10.3748/wjgv21i9.2645

Llanos, J. C., Bakonyi Neto, A., Lerco, M. M., Clark, R. M., Polachini do Valle, A., and Sousa, M. M. (2006). Induction of short gut syndrome and transplantation in a porcine model. *Transpl. Proc.* 38 (6), 1855–1856. doi:10.1016/j.transproceed.2006.06.085

Lo Dico, R., Tijeras-Raballand, A., Bonnin, P., Launay, J. M., Kaci, R., Pimpie, C., et al. (2018). Hepatectomy increases metastatic graft and growth in an immunocompetent murine model of peritoneal metastases. *Eur. J. Surg. Oncol.* 44 (6), 784–791. doi:10.1016/j.ejso.2018.01.096

Lu, S. L., Kawabata, M., Imamura, T., Akiyama, Y., Nomizu, T., Miyazono, K., et al. (1998). HNPCC associated with germline mutation in the TGF-beta type II receptor gene. *Nat. Genet.* 19 (1), 17–18. doi:10.1038/ng0598-17

Lynch, H. T., Smyrk, T., and Lynch, J. (1997). An update of HNPCC (Lynch syndrome). *Cancer Genet. Cytogenet* 93 (1), 84–99. doi:10.1016/s0165-4608(96)00290-7

Ma, Q., Hoper, M., Anderson, N., and Rowlands, B. J. (1996). Effect of supplemental L-arginine in a chemical-induced model of colorectal cancer. *World J. Surg.* 20 (8), 1087–1091. doi:10.1007/s002689900165

Ma, Z., Lou, S., and Jiang, Z. (2020). PHLDA2 regulates EMT and autophagy in colorectal cancer via the PI3K/AKT signaling pathway. *Aging (Albany NY)* 12 (9), 7985–8000. doi:10.18632/aging.103117

Maletzki, C., Gock, M., Randow, M., Klar, E., Huehns, M., Prall, F., et al. (2015). Establishment and characterization of cell lines from chromosomal instable colorectal cancer. *World J. Gastroenterol.* 21 (1), 164–176. doi:10.3748/wjgv21.i1.164

Manceau, G., Karoui, M., Charachon, A., Delchier, J. C., and Sobhani, I. (2011). HNPCC (hereditary non-polyposis colorectal cancer) or lynch syndrome: A syndrome related to a failure of DNA repair system. *Bull. Cancer* 98 (3), 323–336. doi:10.1684/bdc.2011.1328

Mao, J. H., Perez-Losada, J., Wu, D., Delrosario, R., Tsunematsu, R., Nakayama, K. I., et al. (2004). Fbxw7/Cdc4 is a p53-dependent, haploinsufficient tumour suppressor gene. *Nature* 432, 775–779. doi:10.1038/nature03155

Marian, B. (2004). Colorectal cancer: Modeling causes, prevention and therapy. *Drug Discov. Today Dis. Models* 1 (1), 11–17. doi:10.1016/jddmod.2004.07.006

Martin, E. S., Belmont, P. J., Sinnamon, M. J., Richard, L. G., Yuan, J., Coffee, E. M., et al. (2013). Development of a colon cancer GEMM-derived orthotopic transplant model for drug discovery and validation. *Clin. Cancer Res.* 19 (11), 2929–2940. doi:10.1158/1078-0432.CCR-12-2307

Martorell, Ò., Merlos-Suárez, A., Campbell, K., Barriga, F. M., Christov, C. P., Miguel-Aliaga, I., et al. (2014). Conserved mechanisms of tumorigenesis in the Drosophila adult midgut. *PLoS ONE* 9, 88413. doi:10.1371/journal.pone.0088413

Mashimo, H., Wu, D. C., Podolsky, D. K., and Fishman, M. C. (1996). Impaired defense of intestinal mucosa in mice lacking intestinal trefoil factor. *Science* 274 (5285), 262–265. doi:10.1126/science.274.5285.262

Matsuda, Y., Miura, K., Yamane, J., Shima, H., Fujibuchi, W., Ishida, K., et al. (2016). SERPINI1 regulates epithelial-mesenchymal transition in an orthotopic implantation model of colorectal cancer. *Cancer Sci.* 07 (5), 619–628. doi:10.1111/cas.12909

Mehta, G., Hsiao, A. Y., Ingram, M., Luker, G. D., and Takayama, S. (2012). Opportunities and challenges for use of tumor spheroids as models to test drug delivery and efficacy. *J. Control Release* 164 (2), 192–204. doi:10.1016/j.jconrel.2012.04.045

Mehta, R. S., Song, M., Nishihara, R., Drew, D. A., Wu, K., Qian, Z. R., et al. (2017). Dietary patterns and risk of colorectal cancer: Analysis by tumor location and molecular subtypes. *Gastroenterology* 152 (8), 1944–1953.e1. doi:10.1053/j.gastro.2017.02.015

Mikuła-Pietrasik, J., Sosińska, P., Maksin, K., Kucińska, M. G., Piotrowska, H., Murias, M., et al. (2015). Colorectal cancer-promoting activity of the senescent peritoneal mesothelium. *Oncotarget* 6 (30), 29178–29195. doi:10.18632/oncotarget.4932

Minami, Y., Kanemura, S., Kusaka, J., Kinouchi, M., Suzuki, S., Nishino, Y., et al. (2022). Associations of cigarette smoking, alcohol drinking and body mass index with survival after colorectal cancer diagnosis by anatomic subsite: A prospective patient cohort study in Japan. *Jpn. J. Clin. Oncol.* 52 (12), 1375–1388. doi:10.1093/jjco/hyac140

Mooi, J. K., Luk, I. Y., and Mariadason, J. M. (2018). Cell line models of molecular subtypes of colorectal cancer. *Methods Mol. Biol.* 1765, 3–26. doi:10.1007/978-1-4939-7765-9_1

Moser, A. R., Pitot, H. C., and Dove, W. F. (1990). A dominant mutation that predisposes to multiple intestinal neoplasia in the mouse. *Science* 247 (4940), 322–324. doi:10.1126/science.2296722

Mouradov, D., Sloggett, C., Jorissen, R. N., Love, C. G., Li, S., Burgess, A. W., et al. (2014). Colorectal cancer cell lines are representative models of the main molecular subtypes of primary cancer. *Cancer Res.* 74 (12), 3238–3247. doi:10.1158/0008-5472.CAN-14-0013

Mouse Genome Sequencing Consortium, Waterston, R. H., Lindblad-Toh, K., Birney, E., Rogers, J., Abril, J. F., Agarwal, P., et al. (2002). Initial sequencing and comparative analysis of the mouse genome. *Nature* 420 (6915), 520–562. doi:10.1038/nature01262

Munday, J. S., Brennan, M. M., Jaber, A. M., and Kiupel, M. (2006). Ovine intestinal adenocarcinomas: Histologic and phenotypic comparison with human colon cancer. *Comp. Med.* 56 (2), 136–141.

Nakayama, M., Sakai, E., Echizen, K., Yamada, Y., Oshima, H., Han, T. S., et al. (2017). Intestinal cancer progression by mutant p53 through the acquisition of invasiveness associated with complex glandular formation. *Oncogene* 36 (42), 5885–5896. doi:10.1038/onc.2017.194

Neufert, C., Becker, C., and Neurath, M. F. (2007). An inducible mouse model of colon carcinogenesis for the analysis of sporadic and inflammation-driven tumor progression. *Nat. Protoc.* 2, 1998–2004. doi:10.1038/nprot.2007.279

O'Rourke, K. P., Loizou, E., Livshits, G., Schatoff, E. M., Baslan, T., Manchado, E., et al. (2017). Transplantation of engineered organoids enables rapid generation of metastatic mouse models of colorectal cancer. *Nat. Biotechnol.* 35 (6), 577–582. doi:10.1038/nbt.3837

Orlando, F. A., Tan, D., Baltodano, J. D., Khoury, T., Gibbs, J. F., Hassid, V. J., et al. (2008). Aberrant crypt foci as precursors in colorectal cancer progression. *J. Surg. Oncol.* 98 (3), 207–213. doi:10.1002/jso.21106

Ozirmak Lermi, N., Gray, S. B., Bowen, C. M., Reyes-Uribe, L., Dray, B. K., Deng, N., et al. (2022). Comparative molecular genomic analyses of a spontaneous rhesus macaque model of mismatch repair-deficient colorectal cancer. *PLoS Genet.* 18 (4), 1010163. doi:10.1371/journal.pgen.1010163

Panis, Y., and Nordlinger, B. (1991). Experimental models for hepatic metastases from colorectal tumors. *Ann. Chir.* 45 (3), 222–228.

Papadopoulos, N., and Lindblom, A. (1997). Molecular basis of HNPCC: Mutations of MMR genes. *Hum. Mutat.* 10 (2), 89–99. doi:10.1002/(SICI)1098-1004(1997)10:2<89:AID-HUMU1>3.0.CO;2-H

Paquette, C. E., Kent, M. L., Buchner, C., Tanguay, R. L., Guillemin, K., Mason, T. J., et al. (2013). A retrospective study of the prevalence and classification of intestinal neoplasia in zebrafish (*Danio rerio*). *Zebrafish* 10 (2), 228–236. doi:10.1089/zeb.2012.0828

Petrović, J., Glamočlija, J., Ilić-Tomić, T., Soković, M., Robajac, D., Nedić, O., et al. (2020). Lectin from Laetiporus sulphureus effectively inhibits angiogenesis and tumor development in the zebrafish xenograft models of colorectal carcinoma and melanoma. *Int. J. Biol. Macromol.* 148, 129–139. doi:10.1016/j.ijbiomac.2020.01.033

Póvoa, V., Rebelo de Almeida, C., Maia-Gil, M., Sobral, D., Domingues, M., Martinez-Lopez, M., et al. (2021). Innate immune evasion revealed in a colorectal zebrafish xenograft model. *Nat. Commun.* 12 (1), 1156. doi:10.1038/s41467-021-21421-y

Puppa, M. J., White, J. P., Sato, S., Cairns, M., Baynes, J. W., and Carson, J. A. (2011). Gut barrier dysfunction in the $APC^{(Min/+)}$ mouse model of colon cancer cachexia. *Biochim. Biophys. Acta* 1812 (12), 1601–1606. doi:10.1016/j.bbadis.2011.08.010

Qi, Z. P., Yalikong, A., Zhang, J. W., Cai, S. L., Li, B., Di, S., et al. (2021). HDAC2 promotes the EMT of colorectal cancer cells and via the modular scaffold function of ENSG00000274093.1. *J. Cell. Mol. Med.* 25 (2), 1190–1197. doi:10.1111/jcmm.16186

Qu, D., Shen, L., Liu, S., Li, H., Ma, Y., Zhang, R., et al. (2017). Chronic inflammation confers to the metabolic reprogramming associated with tumorigenesis of colorectal cancer. *Cancer Biol. Ther.* 18 (4), 237–244. doi:10.1080/15384047.2017.1294292

Rajcevic, U., Knol, J. C., Piersma, S., Bougnaud, S., Fack, F., Sundlisaeter, E., et al. (2014). Colorectal cancer derived organotypic spheroids maintain essential tissue characteristics but adapt their metabolism in culture. *Proteome Sci.* 12, 39. doi:10.1186/1477-5956-12-39

Reddy, B. S. (1998). Colon carcinogenesis models for chemoprevention studies. *Hematol. Oncol. Clin. North Am.* 12 (5), 963–973. doi:10.1016/s0889-8588(05)70036-8

Reddy, B. S., and Mori, H. (1981). Effect of dietary wheat bran and dehydrated citrus fiber on 3,2'-dimethyl-4-aminobiphenyl-induced intestinal carcinogenesis in F344 rats. *Carcinogenesis* 2 (1), 21–25. doi:10.1093/carcin/2.1.21

Ricci-Vitiani, L., Lombardi, D. G., Pilozzi, E., Biffoni, M., Todaro, M., Peschle, C., et al. (2007). Identification and expansion of human colon-cancer-initiating cells. *Nature* 445 (7123), 111–115. doi:10.1038/nature05384

Robanus-Maandag, E. C., Koelink, P. J., Breukel, C., Salvatori, D. C., Jagmohan-Changur, S. C., Bosch, C. A., et al. (2010). A new conditional APC-mutant mouse model for colorectal cancer. *Carcinogenesis* 31 (5), 946–952. doi:10.1093/carcin/bgq046

Rokavec, M., Öner, M. G., Li, H., Jackstadt, R., Jiang, L., Lodygin, D., et al. (2014). IL-6R/STAT3/miR-34a feedback loop promotes EMT-mediated colorectal cancer invasion and metastasis. *J. Clin. Investig.* 124 (4), 1853–1867. doi:10.1172/JCI73531

Roque-Lima, B., Roque, C. C. T. A., Begnami, M. D., Peresi, P., Lima, E. N. P., Mello, C. A. L., et al. (2019). Development of patient-derived orthotopic xenografts from metastatic colorectal cancer in nude mice. *J. Drug Target* 27 (9), 943–949. doi:10.1080/1061186X.2018.1509983

Rupertus, K., Sinistra, J., Scheuer, C., Nickels, R. M., Schilling, M. K., Menger, M. D., et al. (2014). Interaction of the chemokines I-TAC (CXCL11) and SDF-1 (CXCL12) in the regulation of tumor angiogenesis of colorectal cancer. *Clin. Exp. Metastasis* 31 (4), 447–459. doi:10.1007/s10585-014-9639-4

Rygaard, J., and Poulsen, C. O. (1969). Heterotransplantation of a human malignant tumour to "nude"mice. *Acta Pathol. Microbiol. Scand.* 77, 758–760. doi:10.1111/j.1699-0463.1969.tb04520.x

Saeidnia, S., Manayi, A., and Abdollahi, M. (2015). From *in vitro* experiments to *in vivo* and clinical studies; pros and cons. *Curr. Drug Discov. Technol.* 12 (4), 218–224. doi:10.2174/1570163813666160114093140

Sanford, K. K., Earle, W. R., and Likely, G. D. (1948). The growth *in vitro* of single isolated tissue cells. J. Natl. Cancer Inst. 9 (3), 229–246.

Sangild, P. T., Siggers, R. H., Schmidt, M., Elnif, J., Bjornvad, C. R., Thymann, T., et al. (2006). Diet and colonization-dependent intestinal dysfunction predisposes to necrotizing enterocolitis in preterm pigs. *Gastroenterology* 130 (6), 1776–1792. doi:10.1053/j.gastro.2006.02.026

Santini, M. T., and Rainaldi, G. (1999). Three-dimensional spheroid model in tumor biology. *Pathobiology* 67 (3), 148–157. doi:10.1159/000028065

Sato, T., Stange, D. E., Ferrante, M., Vries, R. G., Van Es, J. H., Van den Brink, S., et al. (2011). Long-term expansion of epithelial organoids from human colon, adenoma, adenocarcinoma, and Barrett's epithelium. *Gastroenterology* 141 (5), 1762–1772. doi:10.1053/j.gastro.2011.07.050

Schafer, M., and Werner, S. (2008). Cancer as an overhealing wound: An old hypothesis revisited. *Nat. Rev. Mol. Cell. Biol.* 9 (8), 628–638. doi:10.1038/nrm2455

Scheiffele, F., and Fuss, I. J. (2002). Induction of TNBS colitis in mice. *Curr. Protoc. Immunol.* 15, 15.19. doi:10.1002/0471142735.im1519s49

Schottelius, A., and Baldwin, A., Jr (1999). A role for transcription factor NF-κB in intestinal inflammation. *Int. J. Color. Dis.* 14, 18–28. doi:10.1007/s003840050178

Seignez, C., Martin, A., Rollet, C. E., Racoeur, C., Scagliarini, A., Jeannin, J. F., et al. (2014). Senescence of tumor cells induced by oxaliplatin increases the efficiency of a lipid A immunotherapy via the recruitment of neutrophils. *Oncotarget* 5 (22), 11442–11451. doi:10.18632/oncotarget.2556

Senga, S. S., and Grose, R. P. (2021). Hallmarks of cancer-the new testament. *Open Biol.* 11 (1), 200358. doi:10.1098/rsob.200358

Seril, D. N., Liao, J., West, A. B., and Yang, G. Y. (2006). High-iron diet: Foe or feat in ulcerative colitis and ulcerative colitis-associated carcinogenesis. *J. Clin. Gastroenterol.* 40 (5), 391–397. doi:10.1097/00004836-200605000-00006

Sharma, S. V., Haber, D. A., and Settleman, J. (2010). Cell line-based platforms to evaluate the therapeutic efficacy of candidate anticancer agents. *Nat. Rev. Cancer* 10 (4), 241–253. doi:10.1038/nrc2820

Shen, T., Yue, C., Wang, X., Wang, Z., Wu, Y., Zhao, C., et al. (2021). NFATc1 promotes epithelial-mesenchymal transition and facilitates colorectal cancer metastasis by targeting SNAI1. *Exp. Cell. Res.* 408 (1), 112854. doi:10.1016/j.yexcr.2021.112854

Shi, L., Wang, J., Ding, N., Zhang, Y., Zhu, Y., Dong, S., et al. (2019). Inflammation induced by incomplete radiofrequency ablation accelerates tumor progression and hinders PD-1 immunotherapy. *Nat. Commun.* 10 (1), 5421. doi:10.1038/s41467-019-13204-3

Shoemaker, A. R., Gould, K. A., Luongo, C., Moser, A. R., and Dove, W. F. (1997). Studies of neoplasia in the Min mouse. *Biochim. Biophys. Acta* 1332 (2), 25–48. doi:10.1016/s0304-419x(96)00041-8

Shoemaker, A. R., Moser, A. R., Midgley, C. A., Clipson, L., Newton, M. A., and Dove, W. F. (1998). A resistant genetic background leading to incomplete penetrance of intestinal neoplasia and reduced loss of heterozygosity in $APC^{Min/+}$ mice. *Proc. Natl. Acad. Sci. U. S. A.* 95 (18), 10826–10831. doi:10.1073/pnas.95.18.10826

Smits, R., Kartheuser, A., Jagmohan-Changur, S., Leblanc, V., Breukel, C., De Vries, A., et al. (1997). Loss of APC and the entire chromosome 18 but absence of mutations at the Ras and Tp53 genes in intestinal tumors from APC1638N, a mouse model for APC-driven carcinogenesis. *Carcinogenesis* 18, 321–327. doi:10.1093/carcin/18.2.321

Sun, Q., Yang, H., Liu, M., Ren, S., Zhao, H., Ming, T., et al. (2022). Berberine suppresses colorectal cancer by regulation of Hedgehog signaling pathway activity and gut microbiota. *Phytomedicine* 103, 154227. doi:10.1016/j.phymed.2022.154227

Sun, X., Jiang, X., Wu, J., Ma, R., Wu, Y., Cao, H., et al. (2020). IRX5 prompts genomic instability in colorectal cancer cells. *J. Cell. Biochem.* 121 (11), 4680–4689. doi:10.1002/jcb.29693

Sung, H., Ferlay, J., Siegel, R. L., Laversanne, M., Soerjomataram, I., Jemal, A., et al. (2021). Global cancer statistics 2020: GLOBOCAN estimates of incidence and mortality worldwide for 36 cancers in 185 countries. *CA Cancer J. Clin.* 71 (3), 209–249. doi:10.3322/caac.21660

Tai, J., Wang, G., Liu, T., Wang, L., Lin, C., and Li, F. (2012). Effects of siRNA targeting c-Myc and VEGF on human colorectal cancer Volo cells. *J. Biochem. Mol. Toxicol.* 26 (12), 499–505. doi:10.1002/jbt.21455

Takaku, K., Oshima, M., Miyoshi, H., Matsui, M., Seldin, M. F., and Taketo, M. M. (1998). Intestinal tumorigenesis in compound mutant mice of both Dpc4 (SMAD4) and APC genes. *Cell.* 92, 645–656. doi:10.1016/s0092-8674(00)81132-0

Talmadge, J. E., Singh, R. K., Fidler, I. J., and Raz, A. (2007). Murine models to evaluate novel and conventional therapeutic strategies for cancer. *Am. J. Pathol.* 170 (3), 793–804. doi:10.2353/ajpath.2007.060929

Tanaka, T., Suzuki, R., Kohno, H., Sugie, S., Takahashi, M., and Wakabayashi, K. (2005). Colonic adenocarcinomas rapidly induced by the combined treatment with 2-amino-1-methyl-6-phenylimidazo [4,5-b] pyridine and dextran sodium sulfate in male ICR mice possess β-catenin gene mutations and increases immunoreactivity for β-catenin, cyclooxygenase-2 and inducible nitric oxide synthase. *Carcinogenesis* 26, 229–238. doi:10.1093/carcin/bgh292

Tato-Costa, J., Casimiro, S., Pacheco, T., Pires, R., Fernandes, A., Alho, I., et al. (2016). Therapy-induced cellular senescence induces epithelial-to-mesenchymal transition and increases invasiveness in rectal cancer. *Clin. Colorectal Cancer* 15 (2), 170–178. doi:10.1016/j.clcc.2015.09.003

Thoma, C. R., Zimmermann, M., Agarkova, I., Kelm, J. M., and Krek, W. (2014). 3D cell culture systems modeling tumor growth determinants in cancer target discovery. *Adv. Drug Deliv. Rev.* 69-70, 29–41. doi:10.1016/j.addr.2014.03.001

Tian, X., Han, Z., Zhu, Q., Tan, J., Liu, W., Wang, Y., et al. (2018). Silencing of cadherin-17 enhances apoptosis and inhibits autophagy in colorectal cancer cells. *Biomed. Pharmacother.* 108, 331–337. doi:10.1016/j.biopha.2018.09.020

Trede, N. S., Langenau, D. M., Traver, D., Look, A. T., and Zon, L. I. (2004). The use of zebrafish to understand immunity. *Immunity* 20 (4), 367–379. doi:10.1016/s1074-7613(04)00084-6

Uneyama, M., Chambers, J. K., Nakashima, K., Uchida, K., and Nakayama, H. (2021). Histological classification and immunohistochemical study of feline colorectal epithelial tumors. *Vet. Pathol.* 58 (2), 305–314. doi:10.1177/0300985820974279

Unterleuthner, D., Neuhold, P., Schwarz, K., Janker, L., Neuditschko, B., Nivarthi, H., et al. (2020). Cancer-associated fibroblast-derived WNT2 increases tumor angiogenesis in colon cancer. *Angiogenesis* 23 (2), 159–177. doi:10.1007/s10456-019-09688-8

Valent, P., Bonnet, D., De Maria, R., Lapidot, T., Copland, M., Melo, J. V., et al. (2012). Cancer stem cell definitions and terminology: The devil is in the details. *Nat. Rev. Cancer* 12 (11), 767–775. doi:10.1038/nrc3368

Van de Wetering, M., Francies, H. E., Francis, J. M., Bounova, G., Iorio, F., Pronk, A., et al. (2015). Prospective derivation of a living organoid biobank of colorectal cancer patients. *Cell.* 161 (4), 933–945. doi:10.1016/j.cell.2015.03.053

Van der Sluis, M., De Koning, B. A., De Bruijn, A. C., Velcich, A., Meijerink, J. P., Van Goudoever, J. B., et al. (2006). MUC2-deficient mice spontaneously develop colitis, indicating that MUC2 is critical for colonic protection. *Gastroenterology* 131 (1), 117–129. doi:10.1053/j.gastro.2006.04.020

Van, R. B., Tops, C. M., and Vasen, H. F. (2000). From gene to disease; the APC gene and familial adenomatous polyposis coli. *Ned. Tijdschr. Geneeskd.* 144 (42), 2007–2009.

Vécsey-Semjén, B., Becker, K. F., Sinski, A., Blennow, E., Vietor, I., Zatloukal, K., et al. (2002). Novel colon cancer cell lines leading to better understanding of the diversity of respective primary cancers. *Oncogene* 21 (30), 4646–4662. doi:10.1038/sj.onc.1205577

Vétillard, A., Jonchère, B., Moreau, M., Toutain, B., Henry, C., Fontanel, S., et al. (2015). Akt inhibition improves irinotecan treatment and prevents cell emergence by switching the senescence response to apoptosis. Oncotarget 6 (41), 43342–43362. doi:10.18632/oncotarget.6126

Vlachogiannis, G., Hedayat, S., Vatsiou, A., Jamin, Y., Fernández-Mateos, J., Khan, K., et al. (2018). Patient-derived organoids model treatment response of metastatic gastrointestinal cancers. *Science* 359 (6378), 920–926. doi:10.1126/scienceaao2774

Wang, G., Yang, X., Li, C., Cao, X., Luo, X., and Hu, J. (2014). PIK3R3 induces epithelial-to-mesenchymal transition and promotes metastasis in colorectal cancer. *Mol. Cancer Ther.* 13 (7), 1837–1847. doi:10.1158/1535-7163.MCT-14-0049

Wang, H., Wang, H. S., Zhou, B. H., Li, C. L., Zhang, F., Wang, X. F., et al. (2013). Epithelial-mesenchymal transition (EMT) induced by TNF-α requires AKT/GSK-3β-mediated stabilization of snail in colorectal cancer. *PLoS One* 8 (2), e56664. doi:10.1371/journal.pone.0056664

Wang, J., Chen, D., Song, W., Liu, Z., Ma, W., Li, X., et al. (2020). ATP6L promotes metastasis of colorectal cancer by inducing epithelial-mesenchymal transition. *Cancer Sci.* 111 (2), 477–488. doi:10.1111/cas.14283

Wang, L., Zuo, X., Xie, K., and Wei, D. (2018). The role of CD44 and cancer stem cells. *Methods Mol. Biol.* 1692, 31–42. doi:10.1007/978-1-4939-7401-6_3

Wei, J., Zhang, J., Wang, D., Cen, B., Lang, J. D., and DuBois, R. N. (2022). The COX-2-PGE2 pathway promotes tumor evasion in colorectal adenomas. *Cancer Prev. Res. (Phila).* 15 (5), 285–296. doi:10.1158/1940-6207.CAPR-21-0572

Weiswald, L. B., Bellet, D., and Dangles, M. V. (2015). Spherical cancer models in tumor biology. *Neoplasia* 17 (1), 1–15. doi:10.1016/j.neo.2014.12.004

Weiswald, L. B., Richon, S., Validire, P., Briffod, M., Lai-Kuen, R., Cordelières, F. P., et al. (2009). Newly characterised *ex vivo* colospheres as a three-dimensional colon cancer cell model of tumour aggressiveness. *Br. J. Cancer* 101 (3), 473–482. doi:10.1038/sj.bjc.6605173

Wirtz, S., Neufert, C., Weigmann, B., and Neurath, M. F. (2007). Chemically induced mouse models of intestinal inflammation. *Nat. Protoc.* 2 (3), 541–546. doi:10.1038/nprot.2007.41

Wu, M., Wu, Y., Deng, B., Li, J., Cao, H., Qu, Y., et al. (2016). Isoliquiritigenin decreases the incidence of colitis-associated colorectal cancer by modulating the intestinal microbiota. *Oncotarget* 7 (51), 85318–85331. doi:10.18632/oncotarget.13347

Wu, X., Mao, F., Li, N., Li, W., Luo, Y., Shi, W., et al. (2020). NF2/Merlin suppresses proliferation and induces apoptosis in colorectal cancer cells. *Front. Biosci. (Landmark Ed.* 25 (3), 513–525. doi:10.2741/4817

Wu, Z., Zuo, M., Zeng, L., Cui, K., Liu, B., Yan, C., et al. (2021). OMA1 reprograms metabolism under hypoxia to promote colorectal cancer development. *EMBO Rep.* 22 (1), 50827. doi:10.15252/embr.202050827

Xing, C., Wang, M., Ajibade, A. A., Tan, P., Fu, C., Chen, L., et al. (2021). Microbiota regulate innate immune signaling and protective immunity against cancer. *Cell. Host Microbe* 29 (6), 959–974.e7. doi:10.1016/j.chom.2021.03.016

Yang, Y., He, J., Zhang, B., Zhang, Z., Jia, G., Liu, S., et al. (2021a). SLC25A1 promotes tumor growth and survival by reprogramming energy metabolism in colorectal cancer. *Cell. Death Dis.* 12 (12), 1108. doi:10.1038/s41419-021-04411-2

Yang, Y. S., Wen, D., and Zhao, X. F. (2021c). Sophocarpine can enhance the inhibiting effect of oxaliplatin on colon cancer liver metastasis-*in vitro* and *in vivo*. *Naunyn Schmiedeb. Arch. Pharmacol.* 394 (6), 1263–1274. doi:10.1007/s00210-020-02032-8

Yang, Y., Yan, T., Han, Q., Zhang, M., Zhang, Y., Luo, Y., et al. (2021b). ZNF326 promotes colorectal cancer epithelial-mesenchymal transition. *Pathol. Res. Pract.* 225, 153554. doi:10.1016/j.prp.2021.153554

Yang, Z., Wu, D., Chen, Y., Min, Z., and Quan, Y. (2019). GRHL2 inhibits colorectal cancer progression and metastasis via oppressing epithelial-mesenchymal transition. *Cancer Biol. Ther.* 20 (9), 1195–1205. doi:10.1080/15384047.2019.1599664

Yin, K., Lee, J., Liu, Z., Kim, H., Martin, D. R., Wu, D., et al. (2021). Mitophagy protein PINK1 suppresses colon tumor growth by metabolic reprogramming via p53 activation and reducing acetyl-CoA production. *Cell. Death Differ.* 28 (8), 2421–2435. doi:10.1038/s41418-021-00760-9

Yin, Y., Cao, L. Y., Wu, W. Q., Li, H., Jiang, Y., and Zhang, H. F ((2010). Blocking effects of siRNA on VEGF expression in human colorectal cancer cells. *World J. Gastroenterol.* 16 (9), 1086–1092. doi:10.3748/wjg.v16.i9.1086

Youmans, L., Taylor, C., Shin, E., Harrell, A., Ellis, A. E., Séguin, B., et al. (2012). Frequent alteration of the tumor suppressor gene APC in sporadic canine colorectal tumors. *PLoS One* 7 (12), 50813. doi:10.1371/journal.pone.0050813

Yu, H. K., Ahn, J. H., Lee, H. J., Lee, S. K., Hong, S. W., Yoon, Y., et al. (2005). Expression of human apolipoprotein(a) kringles in colon cancer cells suppresses angiogenesis-dependent tumor growth and peritoneal dissemination. *J. Gene Med.* 7 (1), 39–49. doi:10.1002/jgm.638

Yu, Y., Cai, Y., Yang, B., Xie, S., Shen, W., Wu, Y., et al. (2022). High-fat diet enhances the liver metastasis potential of colorectal cancer through microbiota dysbiosis. *Cancers (Basel).* 14 (11), 2573. doi:10.3390/cancers14112573

Yuan, H., Tu, S., Ma, Y., and Sun, Y. (2021). Downregulation of lncRNA RPLP0P2 inhibits cell proliferation, invasion and migration, and promotes apoptosis in colorectal cancer. *Mol. Med. Rep.* 23 (5), 309. doi:10.3892/mmr.2021.11948

Zeng, S., Tan, L., Sun, Q., Chen, L., Zhao, H., Liu, M., et al. (2022). Suppression of colitis-associated colorectal cancer by scutellarin through inhibiting Hedgehog signaling pathway activity. *Phytomedicine* 98, 153972. doi:10.1016/j.phymed.2022.153972

Zhang, C., Wang, X. Y., Zhang, P., He, T. C., Han, J. H., Zhang, R., et al. (2022). Cancer-derived exosomal HSPC111 promotes colorectal cancer liver metastasis by reprogramming lipid metabolism in cancer-associated fibroblasts. *Cell. Death Dis.* 13 (1), 57. doi:10.1038/s41419-022-04506-4

Zhang, L., Wang, X., Lai, C., Zhang, H., and Lai, M. (2019). PMEPA1 induces EMT via a non-canonical TGF-β signalling in colorectal cancer. *J. Cell. Mol. Med.* 23 (5), 3603–3615. doi:10.1111/jcmm.14261

Zhang, W. L., Li, N., Shen, Q., Fan, M., Guo, X. D., Zhang, X. W., et al. (2020). Establishment of a mouse model of cancer cachexia with spleen deficiency syndrome and the effects of atractylenolide I. *Acta Pharmacol. Sin.* 41 (2), 237–248. doi:10.1038/s41401-019-0275-z

Zhang, Y., Gao, Y., Zhang, G., Huang, S., Dong, Z., Kong, C., et al. (2011). DNMT3a plays a role in switches between doxorubicin-induced senescence and apoptosis of colorectal cancer cells. *Int. J. Cancer* 128 (3), 551–561. doi:10.1002/ijc.25365

Zhao, G. X., Xu, Y. Y., Weng, S. Q., Zhang, S., Chen, Y., Shen, X. Z., et al. (2019). CAPS1 promotes colorectal cancer metastasis via Snail mediated epithelial mesenchymal transformation. *Oncogene* 38 (23), 4574–4589. doi:10.1038/s41388-019-0740-7

Zhao, Q., Guan, J., and Wang, X. (2020). Intestinal stem cells and intestinal organoids. *J. Genet. Genomics* 47 (6), 289–299. doi:10.1016/j.jgg.2020.06.005

Zhao, Y., Wang, Y., and Wang, Q. (2021). HNRNPL affects the proliferation and apoptosis of colorectal cancer cells by regulating PD-L1. *Pathol. Res. Pract.* 218, 153320. doi:10.1016/j.prp.2020.153320

Zhao, Y., Zhang, B., Ma, Y., Zhao, F., Chen, J., Wang, B., et al. (2022). Colorectal cancer patient-derived 2d and 3d models efficiently recapitulate inter- and intratumoral heterogeneity. *Adv. Sci. (Weinheim, Baden-Wurttemberg, Ger.* 9 (22), e2201539. doi:10.1002/advs.202201539

Zhu, G., Cheng, Z., Lin, C., Hoffman, R. M., Huang, Y., Singh, S. R., et al. (2019). MyD88 regulates LPS-induced NF-κB/MAPK cytokines and promotes inflammation and malignancy in colorectal cancer cells. *Cancer Genomics Proteomics* 16 (6), 409–419. doi:10.21873/cgp.20145

Zhu, Y., Huang, S., Chen, S., Chen, J., Wang, Z., Wang, Y., et al. (2021). SOX2 promotes chemoresistance, cancer stem cells properties, and epithelial-mesenchymal transition by β-catenin and Beclin1/autophagy signaling in colorectal cancer. *Cell. Death Dis.* 12 (5), 449. doi:10.1038/s41419-021-03733-5

Zhuang, Y. W., Wu, C. E., Zhou, J. Y., Zhao, Z. M., Liu, C. L., Shen, J. Y., et al. (2018). Solasodine reverses stemness and epithelial-mesenchymal transition in human colorectal cancer. Biochem. Biophys. R*es. Commun.* 505 (2), 485–491. doi:10.1016/j.bbrc.2018.09.094

Zorzi, M., and Urso, E. D. L. (2022). Impact of colorectal cancer screening on incidence, mortality and surgery rates: Evidences from programs based on the fecal immunochemical test in Italy. *Dig. Liver Dis.* S1590-8658 (22), 336–341. doi:10.1016/j.dld.2022.08.013

Zou, W., Zhang, Y., Bai, G., Zhuang, J., Wei, L., Wang, Z., et al. (2022). siRNA-induced CD44 knockdown suppresses the proliferation and invasion of colorectal cancer stem cells through inhibiting epithelial-mesenchymal transition. *J. Cell. Mol. Med.* 26 (7), 1969–1978. doi:10.1111/jcmm.17221

Glossary

ACF	Aberrant crypt foci
AOM	Anaerobic oxidation of methane
APC	Adenomatous polyposis coli
ARID1A	AT-rich interaction domain 1A
ASCs	Adult stem cells
B7x	B7 homolog x
BRAF	B-Raf proto-oncogene, serine/threonine kinase
CAFs	Cancer-associated fibroblasts
CAPS1	Cryopyrin-associated periodic syndromes 1
CDH17	Cadherin 17
CIN	Chromosome instability
C-Myc	Cellular-myelocytomatosis viral oncogene
CRC	Colorectal cancer
CSCs	Colorectal cancer stem cells
CXCL12	C-X-C motif chemokine ligand 12
DHS	Damp-heat syndrome
DKK2	Dickkopf associated protein 2
DMH	1,2 Dimethyl hydrazine
DMAB	3,2′-Dimethyl-4-Aminobiphenyl
DSS	Dextran sodium sulfate
EMT	Epithelial-mesenchymal transition
ENU	N-ethyl-N-nitrosourea
ESCs	Embryonic stem cells
FAM123B	APC membrane recruitment protein 1
FBXW7	F-box and WD repeat domain containing 7
FFA	Free fatty acids
FOXO6	Forkhead Box O6
HDAC1	Histone deacetylase 1
HFD	High-fat diet
HIF-1α	Hypoxia-inducible factor-1α
HISC	Human intestinal stem cell
HK2	Human kallikrein 2
HNRNPL	Heterogeneous nuclear ribonucleoprotein L
HNPCC	Hereditary nonpolyposis colorectal cancer
ILK	Integrin-linked kinase
iPSCs	Induced pluripotent stem cells
IL-6	Interleukin-6
IL-8	Interleukin-8
IRTSS	Internal retention of toxin stagnation syndrome
IRX5	Iroquois homeobox gene 5
KRAS	Kirsten rats arcomaviral oncogene homolog
LGR5$^+$	Leucine-rich repeat-containing G-protein-coupled receptor 5
LMNB1	Lamin B1
LPS	Lipopolysaccharide
MCTS	Multicellular tumor spheroids
MNU	N-methyl-N-nitrosourea
MNNG	N-methyl-N-nitrosoguanidine
MTA3	Metastasis associated 1 family member 3
NFATc1	Nuclear factor of activated T-cells
NF2	Neurofibromin 2
NF-kB	Nuclear factor-kappa B
NRAS	NRAS proto-oncogene, GTPase
OMS	Organotypic multicellular spheroids
p53	Tumor protein 53
PDOs	Patient-derived organoids
PhIP	Parahydrogen-induced polarization
PHLDA2	Pleckstrin homology-like domain family A member 2
PIM	Potentially inappropriate medication
PIK3CA	Phosphatidylinositol-4,5-bisphosphate 3-kinase catalytic subunit alpha
PMEPA1	Prostate transmembrane protein androgen induced 1
RIP3	Receptor interacting protein kinase 3
RPLP0P2	Ribosomal protein lateral stalk subunit P0 pseudogene 2
SARI	Severe acute respiratory infection
SDS	Spleen qi deficiency syndrome
SGPL1	Sphingosine phosphate lyase 1
SLC25A1	Solute carrier family 25 member 1
SMAD4	SMAD family member 4
SOX2	SRY-box transcription Factor 2
SOX9	SRY-box transcription factor 9
TBX5	T-box transcription factor 5
TCF7L2	Transcription factor 7-like 2
TCM	Traditional Chinese medicine
TDTS	Tissue-derived tumor spheres
TGF-β	Transforming growth factor β
TME	Tumor microenvironment
TNBS	2,4,6-Trinitro-benzenesulfonic acid
TNF-α	Tumor necrosis factor-α
TRIB2	Tribbles homolog 2
VEGF	Vascular endothelial growth factor
ZNF326	Zinc-finger protein 326

frontiers | Frontiers in Oncology

TYPE Case Report
PUBLISHED 12 October 2023
DOI 10.3389/fonc.2023.1282678

OPEN ACCESS

EDITED BY
Adrian Bogdan Tigu,
University of Medicine and Pharmacy Iuliu Hatieganu, Romania

REVIEWED BY
Alun Wang,
Tulane University, United States
Diana Cenariu,
University of Medicine and Pharmacy Iuliu Hatieganu, Romania

*CORRESPONDENCE
Huigang Lu
lugszdx@163.com

†These authors have contributed equally to this work

RECEIVED 24 August 2023
ACCEPTED 25 September 2023
PUBLISHED 12 October 2023

CITATION
Zhang X, Jiang W, Jin Z, Wang X, Song X, Huang S, Zhang M and Lu H (2023) A novel splice donor mutation in *DCLRE1C* caused atypical severe combined immunodeficiency in a patient with colon lymphoma: case report and literature review. *Front. Oncol.* 13:1282678. doi: 10.3389/fonc.2023.1282678

A novel splice donor mutation in *DCLRE1C* caused atypical severe combined immunodeficiency in a patient with colon lymphoma: case report and literature review

Xiaoqing Zhang[1†], Wujun Jiang[1†], Zhongqin Jin[1], Xueqian Wang[2], Xiaoxiang Song[3], Shan Huang[4], Min Zhang[5] and Huigang Lu[1*]

[1]Department of Medicine, Children's Hospital of Soochow University, Suzhou, China, [2]Department of Prenatal Screening and Diagnosis Center, Affiliated Maternity and Child Health Care Hospital of Nantong University, Nantong, China, [3]Department of Clinical Immunology, Children's Hospital of Soochow University, Suzhou, China, [4]Department of Pathology, First Affiliated Hospital of Soochow University, Suzhou, China, [5]Department of Pathology, Children's Hospital of Soochow University, Suzhou, China

Introduction: Hypomorphic mutations of *DCLRE1C* cause an atypical severe combined immunodeficiency (SCID), and Epstein-Barr virus (EBV)-related colon lymphoma is a rare complication.

Case presentation: A teenage boy presented with colon EBV-related colon lymphoma, plantar warts, and a history of recurrent pneumonia. His peripheral blood lymphocyte count and serum level of immunoglobulin (Ig) G were normal, but he exhibited a $T^+B^-NK^+$ immunophenotype. Genetic analysis by whole exome sequencing revealed compound heterozygous mutations of *DCLRE1C* (NM_001033855.3), including a novel paternal splicing donor mutation (c.109 + 2T>C) in intron 1, and a maternal c.1147C>T (p.R383X) nonsense mutation in exon 13. Based on his clinical features and genetic results, the diagnosis of atypical SCID with colon lymphoma was established. Our review shows that seven patients, including our patient, have been reported to develop lymphoma, all with hypomorphic *DCLRE1C* mutations. Among these cases, six had EBV-related B-cell lineage lymphoma, and one had Hodgkin lymphoma with EBV reactivation. Unfortunately, all of the patients died.

Conclusion: Recognizing the radiosensitivity of the disease is critical for the prognosis. Hematopoietic stem cell transplantation before being infected with EBV is an optimal treatment.

KEYWORDS

***DCLRE1C*, ARTEMIS, hypomorphic mutation, severe combined immunodeficiency, radiosensitive immunodeficiency**

Introduction

The nuclease ARTEMIS, encoded by the DNA cross-link repair enzyme 1C (*DCLRE1C*), is involved in double-stranded DNA repair and V(D)J recombination via non-homologous end joining (NHEJ). Null mutations of *DCLRE1C* lead to complete ARTEMIS deficiency and cause $T^-B^-NK^+$ severe combined immunodeficiency (SCID) with sensitivity to ionizing radiation and usually present in the first year of life (1). Hypomorphic mutations of *DCLRE1C* cause reduced ARTEMIS function and 'leaky' SCID, resulting in severe and progressive consequences with an initially indolent and late-onset clinical course. Mutations in *DCLRE1C* occur more frequently in Western countries (2). In China, only several cases with *DCLRE1C* mutations associated with SCID were recently reported (3–6). Here, we described a male Chinese adolescent with a novel hypomorphic mutation who displayed a milder immunodeficiency but progressed to malignant colon lymphoma. This study was approved by the institutional ethics committee of Children's Hospital of Soochow University (No.2022CS053).

Case presentation

A 13.5-year-old male patient with nonconsanguineous parents was admitted to our hospital with a complaint of abdominal pain for one month. The abdominal pain was paroxysmal, located around the periumbilical and right lower quadrants. Three days before being admitted to the hospital, he had loose stools with mucus and blood in a row. His peripheral blood showed a normal level of lymphocytes, neutrophils, erythrocytes, and platelets. Both abdominal ultrasound and computerized tomography (CT) revealed ileocecitis and a small volume of ascites (Figure 1A). He had recurrent pneumonia since the first year of life and had no history of transfusions. His sister had oral ulcers and died of severe pneumonia at four months old. Both his father and grandfather had histories of tuberculosis. Physical examination revealed a normal nutritional status, tenderness around the umbilicus and right lower abdomen on palpation, and skin lesions on the soles of the left foot (Figure 1B). There were no palpable enlarged lymph nodes or rales of bilateral lungs on auscultation. The number of lymphocytes was 2.63×10^3/μl. The percentage of $CD3^+$ T lymphocytes was 83.48% (reference range: 55-83%), of which $CD3^+CD4^+$ T lymphocytes was 22.69% (reference range: 28-57%), $CD3^+CD8^+$ T lymphocytes was 51.50% (reference range: 10-39%), and $CD4^+/CD8^+$ ratio was 0.44 (reference range: 0.98-1.94). The percentage of B cells was only 0.17%, dramatically lower than the reference range (6-19%), while that of NK cells was normal. Serum levels of immunoglobulin (Ig)M and IgA were low (IgA 0.01 g/L, reference 0.63-3.04 g/L; IgM 0.29 g/L, reference 0.50-2.48 g/L). However, the serum levels of IgG and IgE were normal. The DNA copy number of EBV in blood was determined by quantitative PCR (qPCR) at 3.83×10^3 copies/ml. Other tests were negative, including cytomegalovirus (CMV) DNA PCR, T-spot, human immunodeficiency virus (HIV) antibody, antinuclear antibodies, antineutrophil cytoplasmic autoantibodies, anti-dsDNA antibody, anti-Sm antibody, anti-SSA/SSB antibody, anti-Ro-52 antibody, anti-ribonucleoprotein (RNP) antibody, anti-Jo-1 antibody, anti-SCL-70 antibody, tumor markers, fecal culture, and fecal Clostridium difficile gene Xpert assay. Chest CT showed bronchiectasis in both lungs (Figure 1C), and echocardiography revealed mild aortic valve regurgitation. He received a colonoscopy, during which a massive ulcer with yellow pus moss in the ascending colon was observed (Figure 1D). Diffuse proliferation of medium-sized lymphocytes was found in the biopsy from the ulcer (Figures 2A, B), the nuclei exhibit clear heterogeneity, appearing basophilic, with the presence of prominent large nucleoli. Immunohistochemical analysis showed the cells were positive for $CD20^+$ (Figure 2C), CD79a, MUM1, very weakly positive for CD138 and CD68, sporadically positive for CD2, CD3, and Kappa-light chain (Figure 2D), and negative for Lambda-light chain (Figure 2E). Ki-67 revealed a proliferative fraction of 60% of the cells. EBV-encoded mRNA (EBER) *in situ* hybridization was tested positive (Figure 2F), and acid-fast staining was negative. Transplacental maternal lymphocytes were excluded by short tandem repeat analysis. Combined with his past history of recurrent respiratory tract infections, nearly deficient B cells, and positive family history, a clinical diagnosis of primary immunodeficiency, colon lymphoma, and plantar warts was determined.

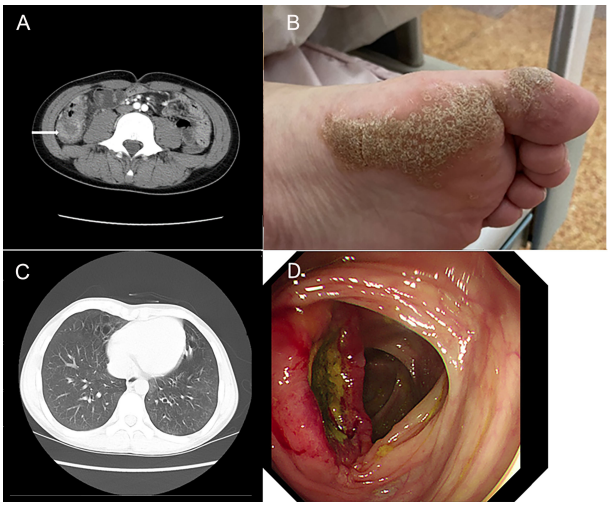

FIGURE 1
Clinical images show the clinical manifestation of the patient. **(A)** Computerized abdomen tomography (CT) revealed the thickened intestinal wall of ileocecum and patchy blurred shadows around it. **(B)** Skin lesions on the soles of the patient's left foot. **(C)** Chest CT showed bronchiectasis in both lungs. **(D)** A huge ulcer with yellow pus moss on it of ascending colon on colonoscopy.

After a consent form was signed, trio-whole exome sequences (WES) were performed. We prioritized variants that were previously reported, considered loss-of-function (nonsense, frameshift, or splice sites mutations) or absent in gnomAD. The genetic analysis demonstrated compound heterozygous mutations of *DCLRE1C*, including a paternally inherited splicing donor mutation (c.109 + 2T>C) in intron 1 and a maternally inherited c.1147C>T (p.R383X) nonsense mutation in exon 13 (NM_001033855.3). Sanger sequencing confirmed the carrying status of variants (Figure 3). There are only two carriers in gnomAD of c.1147C>T (PM2_Surpporting).

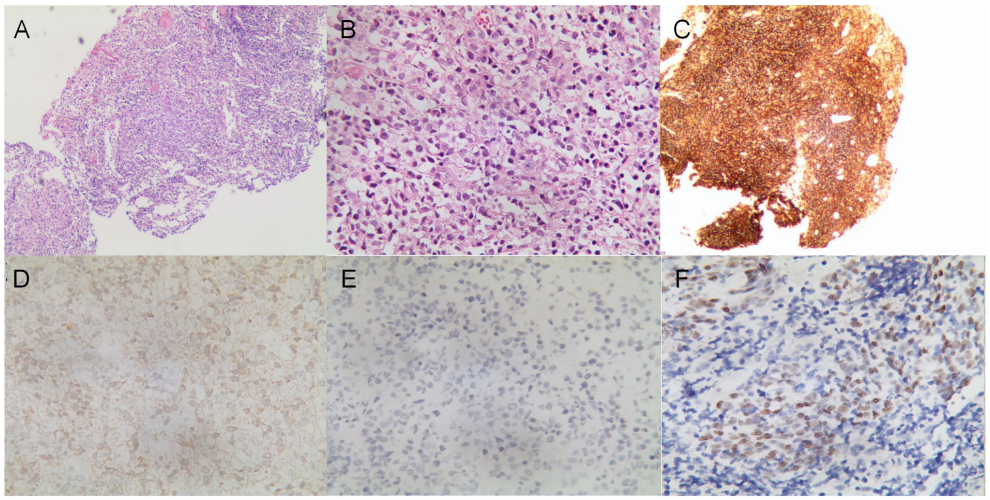

FIGURE 2
Histological analysis of the mucous membrane of the colonic ulcer. **(A, B)** Diffuse lymphoid proliferation of medium-sized lymphocytes stained with hematoxylin–eosin **(A)** (×40), and **(B)** (×400). **(C–E)** Diffuse CD20 positive lymphoid infiltration **(C)** (×40), sporadically positive for Kappa-light chain **(D)** and negative for Lambda-light chain **(E)** on immunohistochemistry (×400). **(F)** *In situ* hybridization showed EBER positive for lymphoma tumor cells (×400).

Since c.1147C>T is located at the 3'-most 50bp of the penultimate exon, nonsense-mediated RNA decay may not occur (7, 8). But the truncated protein loses part of the β-CASP domain (156-385) and the entire C-terminal domain (386-692), which account for 44.7% of the whole protein (PVS1-Strong) (7). Four typical SCID patients with homozygosity for c.1147C>T were identified (9–11) (PM3). Functional study *in vitro* revealed that the recombination and DNA repair activity of p.R383X were decreased (12) (PS3_Surpporting). The patients of the previous and our study carrying c.1147C>T exhibit immunodeficiency which matched the disease phenotype (PP4). In all, c.1147 C>T was classified as likely pathogenic by PM2_Supporting, PVS1-Strong, PM3, PS3_Surpporting, and PP4. c.109 + 2T>C is absent in gnomAD (PM2_ Supporting) and the canonical splicing donor of intron 1 (PVS1_Moderate). It is in trans with c.1147C>T in our case with confirmed paternity and maternity (PM3). The immunodeficient nature of our patient matched the disease characteristics (PP4). In all, c.109 + 2T>C is classified as likely pathogenic by PM2_Supporting, PVS1- Moderate, PM3, and PP4.

The patient was transferred to a different hospital, where further examination confirmed the colon lymphoma to be of the B-cell non-Hodgkin lymphoma variety. He underwent chemotherapy and, tragically, succumbed on the very day he received hematopoietic stem cell transplantation, when it was 1.5 years since the diagnosis of colon lymphoma.

Discussion

DCLRE1C, located on chromosome 10p13, consists of 14 exons. ARTEMIS comprises 692 amino acids, including the highly conserved β-lactamase and β-CASP domains in the N-terminal part (amino acid 1-385) that serves as the enzymatically active

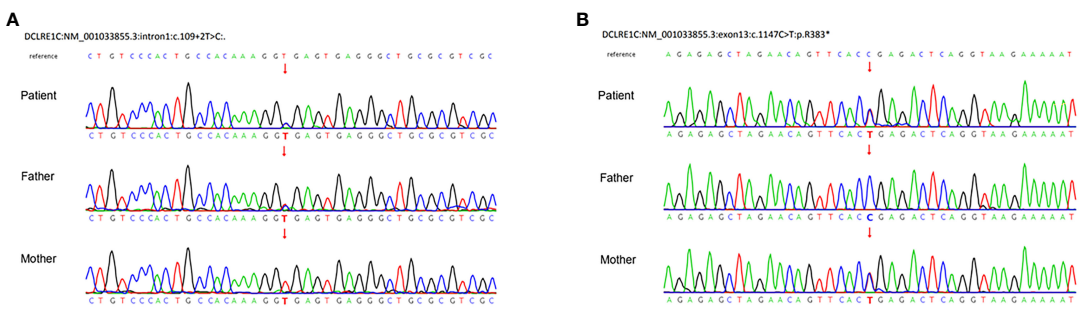

FIGURE 3
Sanger sequences demonstrated compound heterozygous mutations of the *DCLRE1C* gene. **(A)** A paternal splicing donor mutation (c.109 + 2T>C) in intron1. **(B)** A maternal c.1147C>T (p.R383X) nonsense mutation in exon13 (NM_001033855.3).

10.3389/fonc.2023.1282678

motif, and the C-terminal domain that modulates the nuclease activities. Nevertheless, nonsense-mediated RNA decay is not predicted to occur for the c.1147C>T mutation. The truncated protein p.R383X loses part of the β-CASP domain (156-385) and whole C-terminal part domain (386-692). According to recent studies, this nonsense variant encodes function-null variants, as in typical SCID patients with homozygous c.1147C>T mutations, whose *DCLRE1C* mRNA is intact but lacks V(D)J recombination and double-strand breaks (DSB) DNA repair (9). The novel paternal variant c.109 + 2T>C is a canonical splice-site mutation in intron 1. The splice-site mutation at the adjacent nucleotide position (c.109 + 1G>T) was reported to generate some canonical wild-type transcripts, implying that it is associated with a late-onset and less severe phenotype (13). Therefore, it is reasonable to deduce that the novel splice site mutation c.109 + 2T>C is a hypomorphic variant, leading to the leaky phenotype in the patient.

In our case, the counts of absolute lymphocyte number (ALN) and $CD3^+$ lymphocytes were within the reference range, and maternal engraftment was ruled out. He had a B-cell deficiency with surprisingly normal IgG and IgE serum levels. Similar laboratory findings were found in other patients with hypomorphic *DCLRE1C* mutations (14), whose naïve T cells decreased, indicating that T cell development was affected by the hypomorphic mutations; compensatory proliferation might have caused the normal peripheral T cells due to residual V(D)J recombination. The central compartment of B cell progenitors was thought to be more prone to depletion than the T cell compartment (14), despite the fact that ARTEMIS was proposed to play equal roles in recombination for T and B cells. Since ARTEMIS participates in NHEJ, which is involved in the Ig class switch, normal serum levels of his IgG and IgE support the presence of a residual functional B cell compartment and V(D)J recombination.

We searched on PubMed using the keywords 'severe combined immunodeficiency,' 'lymphoma,' and '*DCLRE1C*' or 'ARTEMIS' for articles published from 2001 to 2023. We reviewed the genetic and clinical features of patients with ARTEMIS deficiency complicated by lymphoma (Table 1). Seven patients, including our patient, have been reported to develop lymphoma, all with hypomorphic *DCLRE1C* mutations (15–18). Six patients had EBV-related B-cell lineage lymphoma, and one had Hodgkin lymphoma with EBV reactivation. The average age of lymphoma onset was 11.75 years old (ranging from 9 months to 23 years old), with a male-to-female ratio of 4:3. Our patient is approximately at the average age of tumorigenesis. The mechanisms of lymphoma in these patients remain unclear. Since most of them were EBV-related B-cell lineage lymphomas, no lymphoma has been found in null mutation patients. One explanation for this is that EBV mainly infects B cells, and patients with non-functional *DCLRE1C* mutations cannot establish infection. Additionally, most patients may have died before getting infected with EBV (19). Besides, patients with reduced functional mutations lack sufficient $CD8^+$ cytotoxicity against EBV infection, resulting in EBV-driven B cell colony proliferation (19). Lastly, the partial activity of ARTEMIS results in impaired NHEJ, which plays a vital role in DNA DSBs and is associated with profound genomic instability. This has been documented in cells from two of these patients (P1 has a clonal trisomy of chromosome 9, and P2 has a translocation of

TABLE 1 Genetic and clinical characteristics of patients with ARTEMIS deficiency complicated with lymphoma.

Patient	gender	origin	Age of diagnosis of lymphoma	mutations	Lymphocyte counts and subpopulations	PHA responses	Immunoglobulins	Cytogenetic analysis	Sites of involvement	EBV-associated	Treatment	Outcome	Ref.
P1	*M*	*France*	*9m*	*Compound heterozygous del. Exon1-3*, del. T1384–A1390*	*ALN:66/ul↓↓ CD^{3+}:8/ul↓↓ CD^{19+}:8/ul↓↓ $CD^{16+}CD^{56+}$:18/ul↓↓*	35.8±22cpm× 10^{-3} (normally >40)	*IgG:14.4 g/L↑(9months) IgA:0.18 g/L↓ IgM:6.11 g/L↑*	*Trisomy, Chr. 9*	*Cervical lymph node, liver, lung, striated muscle*	*Yes*	anti–B cell-specific mAb	Died (5 days after diagnosis)	(15)
P2 (sister of P1)	*F*	*France*	*5y*	*Same as* P1	*ALN:500-1100/ul↓ CD^{3+}: 280-580/ul↓ CD^{19+}: 8-110/ul↓ $CD^{16+}CD^{56+}$::227/ul*	26.6 ± *18* cpm× 10^{-3}(normally >40)	*IgG:1.33 g/L↓(10months) IgA:<0.07 g/L↓ IgM:0.56 g/L*	*Translocation, Chr. 7:14*	*liver*	*Yes*	HSCT and anti–B cell-specific mAb	Died(diagnosed 38days after HSCT,12days later died despite treatment with anti–B cell-specific mAb)	(15)
P3	*M*	*Turkey*	*23y*	*Homozygous c.632G>T*	*ALN:800/ul↓ CD^{4+}:177/ul↓*	*Nr*	*IgG:6.1 g/L↓ IgA:0.4 g/L IgM:0.1 g/L↓*	Nr.	*Neck, masseter muscle, lung spleen,*	*Yes*	*Chemotherapy, radiation, HSCT*	Died (of multiple infections)	(16)

(Continued)

TABLE 1 Continued

Patient	gender	origin	Age of diagnosis of lymphoma	mutations	Lymphocyte counts and subpopulations	PHA responses	Immunoglobulins	Cytogenetic analysis	Sites of involvement	EBV-associated	Treatment	Outcome	Ref.
					CD^{8+}:277/ul CD^{19+}: <5/ul↓↓				*gastroventricular mucosa, adrenal gland,*				
P4	*F*	*Israel*	*13y*	*Homozygous c.1299_1306dup*	*CD^{3+}:2200/ul CD^{4+}:600/ul CD^{8+}:1300/ul↑ CD^{19+}:350/ul $CD^{16+}CD^{56+}$:1600/ul↑*	*<20%*↓(stimulation index % of control)	*IgG:1950mg/ml↑ IgA: <17 mg/ml↓ IgM:504 mg/ml↑*	Nr.	*Retroperitoneal lymph nodes*	Yes	*rituximab*	Died (several hours after using rituximab)	(17)
P5	*M*	*Israel*	*15y*	*Same as P5*	*CD^{3+}:410/ul↓ CD^{4+}:210/ul CD^{8+}:180/ul CD^{19+}:<10/ul↓↓* $CD^{16+}CD^{56+}$:30/ *ul↓*	*73%*(stimulation index % of control)	*IgG:1660 mg/ml↑ IgA: <22 mg/ml↓ IgM:192 mg/ml↑*	Nr.	Mediastinum, *liver*	*Yes*	Nr.	Died (of respiratory failure before chemotherapy or HSCT)	(17)
P6	*F*	*Turkey*	*12y*	*Homozygous c.194C*>T	*ALN: Normal CD^{19+}:0.4%↓↓ CD^{20+}:0.7%↓↓ CD^{4+}: 14.7%↓*	Nr.	*IgG:1070mg/dl IgA: <8.2mg/dl↓ IgM:163 mg/dl*	Nr.	Lymph nodes in the right cervical and infraclavicular regions	Hodgkin lymphoma with EBV reactivation	*Chemotherapy, radiotherapy*	Died (of delayed radiation myelopathy)	(18)
P7	M	China	13.5y	Compound heterozygousc.109 +2T>C, c.1147C>T*	ALN:2630/ul CD3+:2195/ul CD4+:597/ul CD8+:1354/ul↑ CD19+:4/ul↓↓ CD16+CD56 +:420/ul	Not done	IgG:7.75 g/L IgA:0.01 g/L↓ IgM:0.29 g/L↓ IgE:2.50IU/ml	Not done	colon	Yes	Chemotherapy, *HSCT*	Died (on the very first day of HSCT)	

*null mutations; PHA, Proliferations of phytohemagglutinin; ALN, absolute lymphocyte number; mAb, monoclonal antibody; HSCT, hematopoietic stem cell transplantation; Nr, Not report.

10.3389/fonc.2023.1282678

Chromosome 7 and 14). And genomic instability is known to be susceptible to malignancy (20).

The outcome of these lymphomas is poor. None of these patients were alive despite multiple managements. Three patients succumbed before hematopoietic stem cell transplantation (HSCT). Three patients underwent HSCT, but died afterward. One patient died of delayed radiation myelopathy as an adverse effect of radiotherapy. Three patients died after anti–B-cell-specific monoclonal antibody treatment. Patient P5 surrendered to respiratory failure before further treatment, while patient P3 succumbed to multiple infections (Pneumocystis jirovecii pneumonia, Herpes simplex virus, Staphylococcus aureus, and Candida albicans) 5 months after HSCT (16). Pavel et al. reported a 14-year-old boy with a radiosensitive defect, normal lymphocyte subpopulations, abnormal lymphocyte phytohemagglutinin A, hypogammaglobulinemia, and a heterozygous loss of exon 11 in *DCLRE1C* was diagnosed with B-cell non-Hodgkin lymphoma. He survived after receiving HSCT with reduced-intensity conditioning regimens, and no EBV infection was mentioned (21). Thus, EBV infection could be fatal in this group of patients. The high mortality of this disease calls for an early diagnosis before patients being EBV infected. Patients with radiosensitive CID have a higher priority to receive a curative therapy, HSCT. However, the survival rate has been reported to be lower than other types of CID (22). Recognizing the radiosensitive nature of the disease is quite essential. Radiomimetic drugs, such as alkylating-containing regiments, and radiation therapy should be tailored in pre-and post-transplant treatment to reduce related toxicity and optimize the prognosis (21). The most recent findings on lentiviral gene therapy offer a promising avenue for treating this illness (23). Nevertheless, the impact on a greater quantity of cases and the safety of its application to patients with EBV infection remain uncertain.

In conclusion, we reported a leaky SCID with heterozygous *DCLRE1C* mutations, including a novel splice mutation. This is the first reported case of atypical SCID associated with a hypomorphic *DCLRE1C* mutation in Chinese, presenting an uncommon complication of colon lymphoma. Leaky SCID should be considered in patients with a late-onset of the disease and a lack of immune cells or immunoglobulins. The combination of leaky SCID and a history of malignancy indicates potentially radiosensitive immunodeficiency. Genetic detection and radiosensitivity testing are crucial for diagnosis. HSCT before being infected with EBV should be considered as an optimal option in clinics.

Data availability statement

The original contributions presented in the study are included in the article/supplementary material. Further inquiries can be directed to the corresponding author.

Ethics statement

Written informed consent was obtained from the individual(s), and minor(s)' legal guardian/next of kin, for the publication of any potentially identifiable images or data included in this article.

Author contributions

XZ: Conceptualization, Data curation, Investigation, Methodology, Resources, Writing – original draft, Writing – review & editing, Validation, Visualization. ZJ: Conceptualization, Data curation, Investigation, Methodology, Visualization, Writing – original draft. XW: Data curation, Investigation, Methodology, Writing – original draft. XS: Data curation, Investigation, Methodology, Project administration, Resources, Writing – review & editing. SH: Data curation, Investigation, Resources, Writing – review & editing, Supervision. WJ: Data curation, Investigation, Writing – review & editing, Software, Visualization. MZ: Investigation, Writing – review & editing, Conceptualization, Methodology, Resources. HL: Conceptualization, Investigation, Methodology, Resources, Writing – review & editing, Data curation, Project administration, Supervision, Writing – original draft.

Funding

The author(s) declare financial support was received for the research, authorship, and/or publication of this article. This work was supported by a grant from Science and Technology Program of Jiangsu (SBK2021042695).

Conflict of interest

The authors declare that the research was conducted in the absence of any commercial or financial relationships that could be construed as a potential conflict of interest.

Publisher's note

All claims expressed in this article are solely those of the authors and do not necessarily represent those of their affiliated organizations, or those of the publisher, the editors and the reviewers. Any product that may be evaluated in this article, or claim that may be made by its manufacturer, is not guaranteed or endorsed by the publisher.

References

1. Moshous D, Callebaut I, De Chasseval R, Corneo B, Cavazzana-Calvo M, Le Deist F, et al. Artemis, a novel DNA double-strand break repair/V(D)J recombination protein, is mutated in human severe combined immune deficiency. *Cell* (2001) 105 (2):177–86. doi: 10.1016/S0092-8674(01)00309-9

2. Li L, Moshous D, Zhou Y, Wang J, Xie G, Salido E, et al. A founder mutation in Artemis, an SNM1-like protein, causes SCID in Athabascan-speaking Native Americans. *J Immunol* (2002) 168(12):6323–9. doi: 10.4049/jimmunol.168.12.6323

3. Mou W, Gao L, He J, Yin J, Xu B, Gui J. Compound heterozygous DCLRE1C mutations lead to clinically typical Severe Combined Immunodeficiency presenting with graft versus host disease. *Immunogenetics* (2021) 73(6):425–34. doi: 10.1007/s00251-021-01219-4

4. Xu X, Yan D, Yin J, Zheng J, Wang X, Shu J. Analysis of a child with severe combined immunodeficiency due to variants of DCLRE1C gene. *Zhonghua Yi Xue Yi Chuan Xue Za Zhi* (2022) 39(7):743–8. doi: 10.3760/cma.j.cn511374-20210317-00236

5. Xiao F, Lu Y, Wu B, Liu B, Li G, Zhang P, et al. High-frequency exon deletion of DNA cross-link repair 1C accounting for severe combined immunodeficiency may be missed by whole-exome sequencing. *Front Genet* (2021) 12:677748. doi: 10.3389/fgene.2021.677748

6. Deng S, Rao S, Wang AR, Shi W. Case report: Rubella virus-induced cutaneous granulomas in a girl with atypical SCID caused by DCLRE1C gene mutations. *Front Genet* (2023) 14:1115027. doi: 10.3389/fgene.2023.1115027

7. Abou Tayoun AN, Pesaran T, Distefano MT, Oza A, Rehm HL, Biesecker LG, et al. Recommendations for interpreting the loss of function PVS1 ACMG/AMP variant criterion. *Hum Mutat* (2018) 39(11):1517–24. doi: 10.1002/humu.23626

8. Lewis BP, Green RE, Brenner SE. Evidence for the widespread coupling of alternative splicing and nonsense-mediated mRNA decay in humans. *Proc Natl Acad Sci* (2003) 100(1):189–92. doi: 10.1073/pnas.0136770100

9. Pannicke U, Honig M, Schulze I, Rohr J, Heinz GA, Braun S, et al. The most frequent DCLRE1C (ARTEMIS) mutations are based on homologous recombination events. *Hum Mutat* (2010) 31(2):197–207. doi: 10.1002/humu.21168

10. El Hawary RE, Meshaal SS, Abd Elaziz DS, Alkady R, Lotfy S, Eldash A, et al. Genetic testing in Egyptian patients with inborn errors of immunity: a single-center experience. *J Clin Immunol* (2022) 42(5):1051–70. doi: 10.1007/s10875-022-01272-y

11. Wu Z, Subramanian N, Jacobsen EM, Laib Sampaio K, van der Merwe J, Honig M, et al. NK cells from RAG- or DCLRE1C-deficient patients inhibit HCMV. *Microorganisms* (2019) 7(11):546. doi: 10.3390/microorganisms7110546

12. Mousallem T, Urban TJ, McSweeney KM, Kleinstein SE, Zhu M, Adeli M, et al. Clinical application of whole-genome sequencing in patients with primary immunodeficiency. *J Allergy Clin Immunol* (2015) 136(2):476–9.e6. doi: 10.1016/j.jaci.2015.02.040

13. Felgentreff K, Lee YN, Frugoni F, Du L, van der Burg M, Giliani S, et al. Functional analysis of naturally occurring DCLRE1C mutations and correlation with the clinical phenotype of ARTEMIS deficiency. *J Allergy Clin Immunol* (2015) 136(1):140–50.e7. doi: 10.1016/j.jaci.2015.03.005

14. Volk T, Pannicke U, Reisli I, Bulashevska A, Ritter J, Bjorkman A, et al. DCLRE1C (ARTEMIS) mutations causing phenotypes ranging from atypical severe combined immunodeficiency to mere antibody deficiency. *Hum Mol Genet* (2015) 24(25):7361–72. doi: 10.1093/hmg/ddv437

15. Moshous D, Pannetier C, Rd C, Fl D, Cavazzana-Calvo M, Romana S, et al. Partial T and B lymphocyte immunodeficiency and predisposition to lymphoma in patients with hypomorphic mutations in Artemis. *J Clin Invest* (2003) 111(3):381–7. doi: 10.1172/JCI16774

16. Fevang B, Fagerli UM, Sorte H, Aarset H, Hov H, Langmyr M, et al. Runaway train: a leaky radiosensitive SCID with skin lesions and multiple lymphomas. *Case Rep Immunol* (2018) 2018:2053716. doi: 10.1155/2018/2053716

17. Nahum A, Somech R, Shubinsky G, Levy J, Broides A. Unusual phenotype in patients with a hypomorphic mutation in the DCLRE1C gene: IgG hypergammaglobulinemia with IgA and IgE deficiency. *Clin Immunol* (2020) 213:108366. doi: 10.1016/j.clim.2020.108366

18. Kara B, Seher N, Ucaryilmaz H, Yavas G, Paksoy Y, Artac H, et al. Delayed radiation myelopathy in a child with Hodgkin lymphoma and ARTEMIS mutation. *J Pediatr Hematol Oncol* (2021) 43(3):e404–e7. doi: 10.1097/MPH.0000000000001815

19. Latour S, Winter S. Inherited immunodeficiencies with high predisposition to epstein-barr virus-driven lymphoproliferative diseases. *Front Immunol* (2018) 9:1103. doi: 10.3389/fimmu.2018.01103

20. Huang Y, Giblin W, Kubec M, Westfield G, St Charles J, Chadde L, et al. Impact of a hypomorphic Artemis disease allele on lymphocyte development, DNA end processing, and genome stability. *J Exp Med* (2009) 206(4):893–908. doi: 10.1084/jem.20082396

21. Lobachevsky P, Woodbine L, Hsiao KC, Choo S, Fraser C, Gray P, et al. Evaluation of severe combined immunodeficiency and combined immunodeficiency pediatric patients on the basis of cellular radiosensitivity. *J Mol Diagn* (2015) 17(5):560–75. doi: 10.1016/j.jmoldx.2015.05.004

22. Buckley RH. Transplantation of hematopoietic stem cells in human severe combined immunodeficiency: longterm outcomes. *Immunologic Res* (2011) 49(1-3):25–43. doi: 10.1007/s12026-010-8191-9

23. Cowan MJ, Yu J, Facchino J, Fraser-Browne C, Sanford U, Kawahara M, et al. Lentiviral gene therapy for artemis-deficient SCID. *N Engl J Med* (2022) 387(25):2344–55. doi: 10.1056/NEJMoa2206575

frontiers | Frontiers in Immunology

TYPE Review
PUBLISHED 01 November 2023
DOI 10.3389/fimmu.2023.1274333

OPEN ACCESS

EDITED BY
Adrian Bogdan Tigu,
University of Medicine and Pharmacy Iuliu Hatieganu, Romania

REVIEWED BY
Bancos Anamaria,
University of Medicine and Pharmacy Iuliu Hatieganu, Romania
Maria-Elena Santa,
University of Medicine and Pharmacy Iuliu Hatieganu, Romania
Nicola Conran,
State University of Campinas, Brazil

*CORRESPONDENCE
Shanshan Luo
2018XH0258@hust.edu.cn
Jun Deng
dengjun09@sina.com

†These authors have contributed equally to this work and share first authorship

RECEIVED 08 August 2023
ACCEPTED 19 October 2023
PUBLISHED 01 November 2023

CITATION
Li Y, Chen R, Wang C, Deng J and Luo S (2023) Double-edged functions of hemopexin in hematological related diseases: from basic mechanisms to clinical application.
Front. Immunol. 14:1274333.
doi: 10.3389/fimmu.2023.1274333

Double-edged functions of hemopexin in hematological related diseases: from basic mechanisms to clinical application

Yijin Li†, Renyu Chen†, Chaofan Wang, Jun Deng* and Shanshan Luo*

Institute of Hematology, Union Hospital, Tongji Medical College, Huazhong University of Science and Technology, Wuhan, China

It is now understood that hemolysis and the subsequent release of heme into circulation play a critical role in driving the progression of various diseases. Hemopexin (HPX), a heme-binding protein with the highest affinity for heme in plasma, serves as an effective antagonist against heme toxicity resulting from severe acute or chronic hemolysis. In the present study, changes in HPX concentration were characterized at different stages of hemolytic diseases, underscoring its potential as a biomarker for assessing disease progression and prognosis. In many heme overload-driven conditions, such as sickle cell disease, transfusion-induced hemolysis, and sepsis, endogenous HPX levels are often insufficient to provide protection. Consequently, there is growing interest in developing HPX therapeutics to mitigate toxic heme exposure. Strategies include HPX supplementation when endogenous levels are depleted and enhancing HPX's functionality through modifications, offering a potent defense against heme toxicity. It is worth noting that HPX may also exert deleterious effects under certain circumstances. This review aims to provide a comprehensive overview of HPX's roles in the progression and prognosis of hematological diseases. It highlights HPX-based clinical therapies for different hematological disorders, discusses advancements in HPX production and modification technologies, and offers a theoretical basis for the clinical application of HPX.

KEYWORDS

hemopexin, hematological diseases, systemic infections, heme, clinical

Introduction

Numerous hemolytic and thrombotic-related diseases are characterized by the excessive turnover of red blood cells (RBCs) resulting from genetic defects or acquired pathologies linked to factors such as blood transfusions, infections, and mechanical stresses. The rupture of RBC membranes leads to the release of harmful contents, including hemoglobin (Hb), heme, and

arginase, among others. Hemopexin (HPX) is pivotal in the immune defense against hemolytic stress. It is a plasma glycoprotein composed of a single 60-kDa peptide chain, known for its exceptional binding affinity to heme. HPX exhibits a 1:1 binding ratio with heme at low concentrations and at least a 2:1 ratio (heme: hemopexin) at higher heme concentrations. While primarily expressed by the liver, HPX is also found in tissues such as the nervous system, skeletal muscle, retina, and kidney. It typically circulates in human plasma within a concentration range of 0.5–1.5 mg/ml (1). HPX plays a multifaceted role by sequestering free heme released from haptoglobin, participating in heme transport, and preventing peroxidation damage by induction of heme oxygenase 1 (HO-1) and metalloproteinase 1 genes (2). And it was found that HO-1 activity affects skeletal muscle aerobic capacity through heme metabolism (3).

The heme detoxification process is primarily driven by HPX through CD91/LRP1-mediated endocytosis in the liver, leading to heme degradation, reutilization, and iron metabolism. Some HPX molecules are recycled back into the plasma (4). Impaired heme clearance occurs when CD91 is saturated with its ligands or when HPX levels are depleted. Overloaded heme can bind to human serum albumin (HSA), but this complex is unstable and prone to dissociation. Free heme can penetrate plasma membranes and interact with low-density lipoproteins (LDL) (5). Heme exerts deleterious effects on endothelial function, systemic infections, and various end-organ tissues, including the lungs, kidneys, and brain. In addition to its protective role against heme toxicity, HPX mitigates methemoglobin (metHb) toxicity (6). Given its protective function against heme toxicity in hemolysis and concurrent inflammation, HPX has been investigated as a potential biomarker and therapeutic agent in heme-related pathologies and atherosclerosis. In many hemolytic diseases, HPX levels significantly decrease with disease progression, although much controversy remains regarding its classification as an acute phase reactant in humans (5, 7). Furthermore, HPX responds to certain forms of "systemic stress". In this respect, HPX mRNA levels were notably increased in rodents subjected to sham abdominal surgery, which served as a control for partial hepatectomy (8).

Consistent with the findings of previous reviews regarding HPX's protective role in heme-mediated pathophysiological processes, recent studies in conditions such as sickle cell disease, transfusion-induced hemolysis, sepsis, atherosclerosis, and thrombosis have validated and elaborated on the positive effects of HPX on these pathological conditions (5). However, it is important to note that this conclusion is not universally applicable, especially for systemic infections caused by certain pathogens, intracerebral hemorrhage, and Hemolytic-Uremic Syndrome (HUS), where HPX concentrations are negatively correlated with disease severity. Additionally, due to its well-established role as a heme-toxicity antagonist, significant efforts have been directed toward developing HPX-based therapies for heme-related pathologies. This review aims to provide an overview of the multifaceted roles of HPX in the pathophysiological processes of hematological-related diseases and offer an update on the latest developments in pre-clinical HPX research.

Abbreviations: HPX, Hemopexin; RBC, Red blood cell; Hb, Hemoglobin; HO-1, Heme oxygenase 1; HAS, Human serum albumin; LRP1, Low-density lipoprotein receptor related protein 1; LDL, Low-density lipoprotein cholesterol; MetHb, Methemoglobin; CFH, Cell-free Hb; Hp, Haptoglobin; ROS, Reactive oxygen species; SCD, Sickle cell disease; AKI, Acute kidney injury; eNOS, Endothelial nitric oxide synthase; PH, Pulmonary hypertension; C3, Complement factor 3; SRBCs, Stored red blood cells; CFU, Colony-forming unit; DIC, Disseminated intravascular coagulation; DHF, Dengue Hemorrhagic Fever; DF, Dengue Fever; HUS, hemolytic-uremic syndrome; WT, Wild type; ICH, Intracerebral hemorrhage; CSF, Cerebrospinal fluid; CNS, Central nervous system; BBB, Blood-brain barrier; SAH, Subarachnoid hemorrhage; ApoE, Apolipoprotein E; OCS, Open canalicular system; ER, Endoplasmic reticulum; IVCL, Inferior vena cava; CHD, Coronary heart disease; SAH, Subarachnoid hemorrhage; rhHPX, Recombinant human HPX; PBS, Phosphate buffer saline; SS, Human Hb βS; AA, Human Hb βA.

HPX's role in combating heme toxicity

HPX plays a pivotal role as part of the second-line defense following hemolysis. Cell-free hemoglobin (CFH) released during hemolysis is rapidly scavenged and removed from circulation primarily through the plasma protein haptoglobin (Hp) (9, 10). In various pathological conditions, such as sickle cell disease, malaria, and hemorrhage, CFH is disassociated into dimers, oxidized into methemoglobin, and quickly degraded into toxic heme (11). Structurally, heme consists of four pyrrole rings, forming an iron-protoporphyrin complex. When the iron atom is in the ferrous state, it is referred to as heme, while in the ferric state, it is known as hemin. Indeed, heme is indispensable to all living organisms but can also be a lethal molecule. Initially, heme binds to lipoproteins in the plasma before gradually transitioning to albumin and HPX (12, 13). HPX's role in scavenging heme is a crucial step in the battle against oxidative and inflammatory disorders caused by free heme (Figure 1) (14). Mechanistically, the heme-HPX complex is phagocytosed by macrophages through CD91 and subsequently broken down inside the cells. Heme undergoes metabolism, forming bilirubin, carbon monoxide, and iron, facilitated by heme/Bach1/Nrf2-induced heme oxygenase-1 (HO-1). Iron is either bound to ferritin for storage or exported from macrophages to hematopoietic tissues via the iron-transporter ferroportin, where it is reused to support erythropoiesis. Free heme can activate inflammatory systems, including the complement system through the alternative pathway. Moreover, heme's autoxidation generates reactive oxygen species (ROS) and redox-active iron, rendering it toxic to cells, tissues, and organs. As such, the clearance of heme is of utmost importance in certain hematologic disorders, especially when hemolysis depletes plasma Hp, leaving HPX as a critical second-line defense following hemolysis (2, 11, 15).

Hemopexin's role in hemolytic diseases

Hemopexin's role in sickle cell disease

Sickle cell disease is a hereditary condition resulting from a genetic mutation in HBB, which encodes the β-subunit of

10.3389/fimmu.2023.1274333

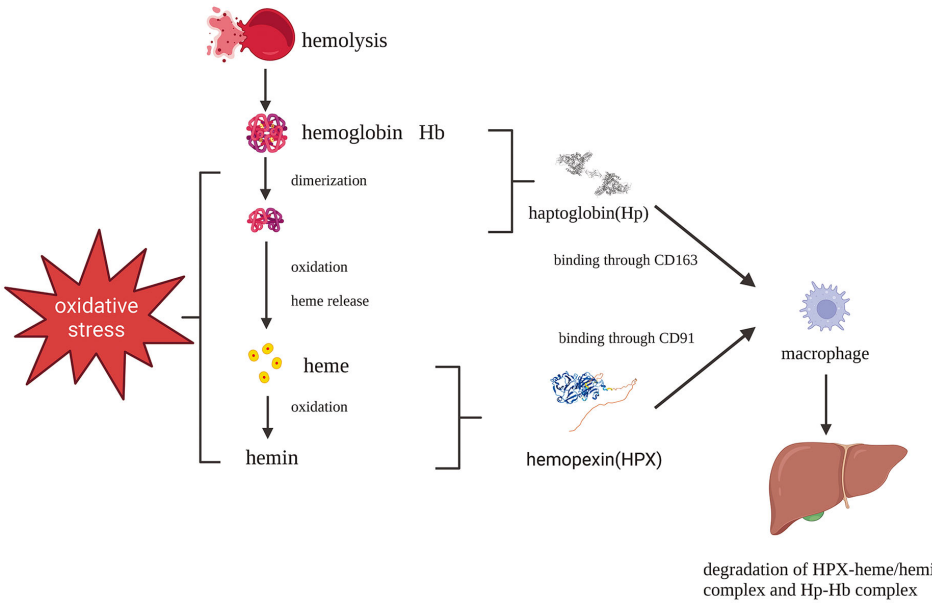

FIGURE 1
Protective pathways after hemolysis: Hb-Hp complex and heme-HPX complex fend against Hb and heme toxicity which are phagocytosed by macrophages mediated by CD163 and CD91, respectively. Created with Biorender.com.

hemoglobin. It affects approximately 300,000 to 400,000 neonates worldwide each year (16). Current evidence suggests that hemoglobin containing mutant β-globin subunits tends to polymerize, leading to the sickling of erythrocytes, rendering them susceptible to hemolysis. The severity of SCD varies significantly and is often reflected in serum HPX levels. HPX has been identified as a mitigating factor in the pathophysiological processes contributing to the SCD phenotype, including microvascular stasis, NO scavenging, vaso-occlusion, increased levels of proinflammatory cytokines/chemokines, proinflammatory macrophages, acute kidney injury (AKI), silent cerebral infarction, immune system activation, and more. Recent studies have provided compelling evidence of HPX's beneficial effects on SCD, as outlined in Table 1. For example, Vinchi F et al. discovered that HPX plays a role in preventing heme-iron accumulation in the cardiovascular system, thereby limiting the production of reactive oxygen species (ROS), increasing endothelial nitric oxide synthase (eNOS), promoting heme detoxification, and more (22). These molecular-level changes were associated with increased blood pressure and ventricular remodeling. Exogenous administration of HPX was found to nearly normalize blood pressure and improve cardiac function (22). Pulmonary hypertension (PH) is a common complication in SCD, occurring in 6-10% of the SCD population and often resulting in right ventricular dysfunction (17). Buehler et al. used an SCD murine model to simulate PH and right ventricular dysfunction, characterized by oxidation and fibrosis in SCD patients (18). They confirmed that HPX could alleviate cardiopulmonary disease in SCD mice by preventing heme-driven oxidative protein modification in the vasculature and ventricle (18). Another study revealed that chlorine inhalation triggered acute hemolysis and induced Acute Chest Syndrome in SCD mice, while post-exposure HPX administration reduced mortality and mitigated lung injury (23). In a clinical study, lower HPX levels were observed in SCD patients experiencing vaso-occlusive crises compared to patients in a steady state, further supporting the potential benefits of HPX administration in SCD (19). An additional preclinical study found that intravenously injected HPX effectively alleviated vascular stasis induced by either Hb injection or hypoxia-reoxygenation in a dose-dependent manner (20). Notably, pre-complexed HPX with heme also resolved stasis, suggesting inherent protective effects of the HPX-heme complex beyond reducing free heme levels (20). Researchers have disclosed that HPX deficiency promoted AKI in SCD, whereas HPX supplementation protected SCD mice from AKI (24, 25). Increased free heme and depletion of HPX led to the deposition of complement factor 3 (C3) and membrane attack complex in the glomeruli of patients with SCD (21). Furthermore, Poillerat V et al. found that HPX prevented heme-mediated complement activation in both plasma and the kidneys (26). In line with previous research, a recent study revealed that hemopexin could protect factor I activity *in vitro*, facilitating the degradation of soluble and surface-bound C3b, thus inhibiting complement activation and subsequent vascular and organ injury (27). Notably, Gotardo et al. developed a chronic hemolysis model in 2023, which demonstrated a decrease in Hp and HPX in accordance with chronic hemolytic anemia, thus enhancing our understanding of animal models in this field (28).

Hemopexin in transfusion-induced hemolysis

During transfusions, a portion of RBCs may undergo hemolysis within macrophages. Stored RBCs for transfusion undergoing

TABLE 1 Pre-clinical research on HPX and SCD.

Model	Age, Species	Treatment	Conclusions	Reference
Berkeley sickle cell mice	8-week-old; C57Bl/6 and Berk-SS mice	Subcutaneous injection of (1) saline vehicle control (n=14) (VC) (2); low dose hemopexin (LD-HPX; 100 mg/kg) (n=12); and (3) high dose hemopexin (HD-HPX, 300 mg/kg) (n=12) three times per week for 3 months.	HPX attenuates cardiopulmonary disease by preventing oxidative stress and fibrosis in the peripheral lung vasculature and oxidation in the right ventricle	(17)
SCD mice	8–16 weeks; Humanized SCD mice (SS) and humanized normal hemoglobin control mice (AA)	Cl_2 exposure at 500 ppm for 30 min followed by either purified human hemopexin intraperitoneal injection at 10 mg/kg or vehicle with the same volume of PBS 30 min after the Cl_2 exposure.	Post-exposure administration of hemopexin reduced mortality, plasma heme level, and RBC fragility after Cl_2 exposure	(18)
SCD mice	12-16 weeks; Townes-SS sickle mice on a 129/B6 mixed genetic background	Injection of different doses of equimolar heme-hemopexin (5, 15, 60, and 160 mg/kg) or saline 40 min post intravenous hemoglobin injection (1 μmol/kg)	HPX dose-dependently reduces vascular stasis induced by Hb injection or hypoxia reoxygenation.	(19)
SCD mice	4-6 months; Townes expressing human Hb βS (SS) and human Hb βA (AA) mice, hemopexin-knockout mice	SS mice received oral gavage of vehicle (DMSO) or D3T 3 times per week for 3-5 months since 1 month old. Hemopexin-knockout mice were transplanted with whole bone marrow cells from SS mice (SS $HPX^{-/-}$ and SS $HPX^{+/+}$)	The plasma A1M to HPX ratio is associated with AKI biomarkers in SCD. HPX replacement therapy can potentially treat AKI in SCD	(20)
Phenylhydrazine-induced hemolysis	8-week-old; C56BL/6 male mice	Intravenous injection of 100 mg/kg or 500mg/kg HPX	Alleviated heme-mediated complement activation in the plasma and in the kidney.	(21)

"storage lesion" may compromise the quality of the blood bag, causing Hb and heme release, and adverse vascular effects including hypoperfusion and impaired endothelial function (29, 30). Transfusing RBCs stored for over 14 days has been associated with adverse outcomes in hospitalized patients (31). Despite the clear need for blood transfusions, several clinical trials and pre-clinical studies have shown that RBC administration can have detrimental effects (32, 33). Exposure to toxic substances resulting from hemolysis, including Hb, heme, and iron, is the primary cause of transfusion reactions. This results in the saturation of transferrin and reduced plasma levels of HPX and Hp, leading to the accumulation of labile plasma iron, heme, and Hb (15, 34). Brant M. Wagener et al. highlighted the crucial role of heme in the adverse effects associated with transfusions of stored RBCs (33). Restoring sequestration proteins has been suggested as a potential method to protect against tissue injury post-transfusion. A preclinical study investigated the effects of exogenous HPX on disease pathology in mice with hemorrhagic shock after transfusing stored red blood cells (SRBCs). The findings supported the protective effect of HPX in improving the survival rate and dampening the inflammatory response, although HPX did not prevent SRBC-induced hemoglobinuria and kidney injury (35). The study by Brant M. Wagener et al. demonstrated that HPX improved the survival rate of mice subjected to massive resuscitation with stored RBCs and infected with P. aeruginosa K-strain, offering evidence for HPX administration as a potential therapy to enhance the safety of SRBC transfusions. While Hp prevented hemoglobinuria, HPX showed no substantial effect (33). It is worth noting that the administration of HPX pre- or post-transfusion has been minimally investigated in clinical trials.

Hemopexin's role in systemic infection

Hemopexin's role in heme appropriation by bacteria and fungi

Iron is a crucial element for redox chemistry and represents a fundamental requirement for pathogens (36, 37). Transfusions of RBCs can result in increased concentrations of non-transferrin-bound iron, which can enhance pathogen proliferation and exacerbate existing infections, thus complicating the condition (33, 38). Pathogens such as *Staphylococcus aureus*, *Haemophilus influenzae*, and *Candida albicans* have developed mechanisms to release hemolytic factors that enable them to assimilate iron from hemoproteins or free heme (39, 40). They have also evolved other means to acquire iron from the host, including the expression of siderophores, hemophores, and heme uptake systems (41). For instance, *Haemophilus influenzae* can dislodge heme from hemopexin, a process facilitated by the *Hxu* operon, which encodes genes responsible for the expression of HxuA/HxuB/HxuC and is essential for extracting heme from hemopexin (42–45). *Porphyromonas gingivalis* employs HmuY as a hemophore with a distinct structure that resists proteolysis by proteases secreted for heme utilization (46). In contrast to extracting heme from host hemoproteins, *Porphyromonas gingivalis* secretes proteases to degrade hemoglobin, haptoglobin, and hemopexin, releasing heme for binding to HmuY (47). In this case, hemopexin promotes pathogen proliferation (Figure 2).

However, for pathogens that are unable to utilize hemopexin, it hinders iron acquisition. For example, the HasA/HasR system, which directly binds to heme, has been identified in pathogens like *Serratia* marcescens, *Pseudomonas aeruginosa*, *and Yersinia* species, potentially competing with hemopexin for free heme. A recent study found that

10.3389/fimmu.2023.1274333

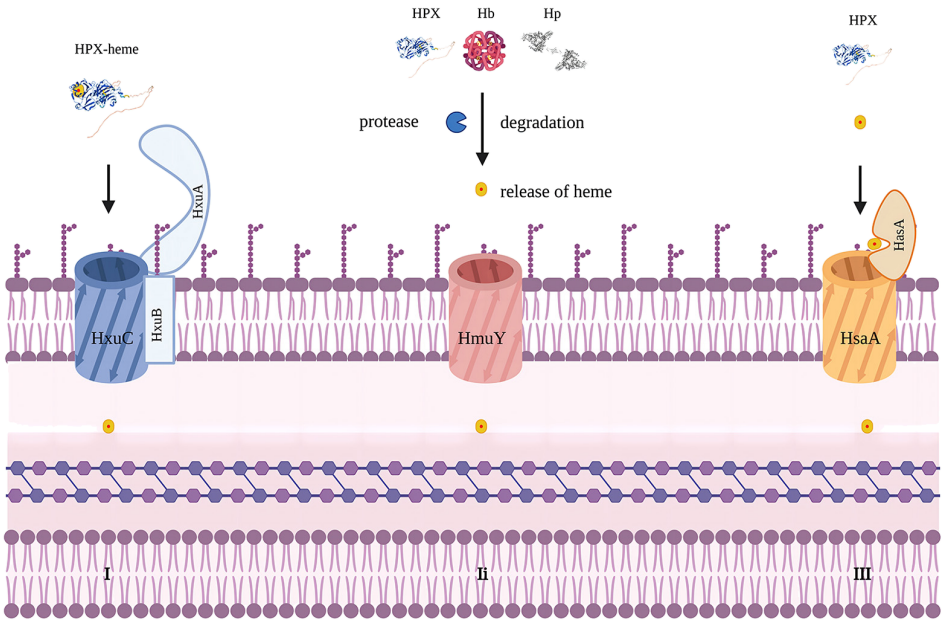

FIGURE 2
Mechanisms to acquire heme in bacteria. Modified from figure 2 in Diverse structural approaches to heme appropriation by pathogenic bacteria. This figure mainly represents HxuA/HxuB/HxuC system for heme acquirement in Haemophilus influaenzae. I. HxuA binds hemopexin and mediates heme release for import by HxuC. HxuB forms the secrete channel. II. representing HmuY system in Porphyromonas gingivalis which secretes proteases that degrade Hb, Hp and HPX and release heme for HmuY scavenging. III. representing HsaA/HsaR system in Serratia Marcescens. HsaA competes with HPX for free heme. Created with Biorender.com.

IL-22-induced hemopexin contributes to nutritional immunity against *Citrobacter rodentium* by limiting iron acquisition by pathogens (Table 2) (50). In a study by Brant M. Wagener, hemopexin improved *P. aeruginosa*-induced pulmonary edema formation, post-pneumonia survival in mice undergoing massive resuscitation with stored RBCs, and reduced lung bacterial colony-forming units (CFUs) (33). HPX is also suspected of participating in the nutritional defense against *Yersinia pestis*. Higher levels of HPX induced by EV67 have been reported to prolong survival and reduce pathogen proliferation in mice challenged with a virulent strain of *Y.pestis*, making HPX a promising adjuvant therapy. The utilization of hemoglobin iron depends on a relay network of extracellular hemophores, namely, Csa2, Rbt5, and Pgt7. Specifically, Csa2 binds to hemin, while Rbt5 and Pgt7 bind to heme, facilitating heme extraction from hemoglobin and its transfer across the cell envelope (48, 49, 51). Mariel Pinsky et al. revealed that hemopexin could inhibit hemin utilization by *Candida albicans* only when the hemin concentration was lower than an equimolar concentration (52). The inhibitory effect of hemopexin was mitigated by the presence of human serum albumin (HSA), and hemin was gradually transferred to hemopexin from HSA rather than initially binding to hemopexin when released in a 1:50 HPX-HSA mixture.

Hemopexin's role in sepsis

Sepsis arises from the dysregulation of the host's immune responses to infection, leading to life-threatening organ dysfunction. Recent estimates indicate that nearly 50 million cases of sepsis were recorded worldwide, with 11.0 million sepsis-related deaths reported, accounting for 19.7% of all global deaths in 2017 (53). Although age-standardized incidents and mortality rates have decreased significantly from 1990 to 2017, sepsis remains a significant global health burden (53).

It is now understood that sepsis exposes red blood cells to various physiological stressors, increasing the risk of hemolysis and the release of cell-free hemoglobin into circulation. One of the most recognized causes of hemolysis during sepsis is disseminated intravascular coagulation (DIC), a common complication of sepsis (54). During sepsis, red blood cells also undergo deformation, driven by cytokines and pathogen-specific factors such as hemolysins produced by *Staphylococcus aureus*, *Enterococcus spp*, and *Escherichia coli* (55–57). Consistent with the process of sepsis-induced hemolysis, the plasma level of cell-free hemoglobin significantly increases in sepsis patients, positively correlated with mortality (58, 59). Accordingly, septic patients with lower hemopexin levels tend to experience death earlier than those with higher hemopexin levels. It has been found that the concentrations of hemopexin in the plasma of non-survivors are significantly lower than those in survivors with sepsis (60, 61). In pre-clinical studies (62). Larsen et al. investigated the role of heme and HPX in a polymicrobial sepsis murine model. They administered exogenous heme to low-grade polymicrobial infection mice, which markedly increased markers of organ dysfunction and sepsis severity. In cases of fatal severe sepsis after high-grade infection, reduced serum concentrations of HPX have been reported. However, when HPX was administered to mice after high-grade infection, it prevented tissue damage and lethality (62).

TABLE 2 Pre-clinical research on HPX and infection.

Pathogens	Age, species	Treatment	Result	Reference
Citrobacter rodentium	6-8 weeks old, C57BL6 mice	IL22$^{-/-}$, Hp$^{-/-}$, HPX$^{-/-}$, and Hp$^{-/-}$HPX$^{-/-}$ mice	IL-22-induced HPX contributes to nutritional immunity against *Citrobacter rodentium*	(46)
Pseudomonas aeruginosa	NA, C57BL/6 mice	Resuscitate trauma-hemorrhage mice with stored RBCs, followed by HPX administration and airway instillation of *Pseudomonas aeruginosa*	Reduced lung bacterial CFUs	(31)
Candida albicans	NA, *C. albicans* ccc2–/– cells	*C. albicans* ccc2-/- cells were grown for 2 days, in increasing human hemopexin concentrations in the presence of 5 μM heme, with or without 100 μM HSA	Hemopexin can inhibit hemin utilization by *Candida albicans*. This inhibitory effect of hemopexin is mitigated by the presence of HSA	(48)
Yersinia pestis	8-12weeks old, C57BL/6	Mice was injected with lethal dose of *Y.pestis* strain or together with EV67.	Post-exposure EV76 induced a rapid expression of HPX and Hp, restrained the proliferation and dissemination of *Y.pestis*, and extended survival time	(49)

NA, not applicable.

The protective role of HPX is attributed to its ability to neutralize the oxidative and cytotoxic effects caused by heme. To carry out this beneficial process, the expression of OH-1 is required to catabolize HPX-bound heme (62). Moreover, HPX can suppress the systemic growth of *E.coli* in *C. rodentium*, shedding light on its therapeutic potential in sepsis (50). Therefore, HPX can be regarded as a potential therapeutic strategy for preventing fatal consequences in individuals with severe sepsis (63). However, there has been a scarcity of pertinent pre-clinical and clinical trials conducted to elucidate the impact of HPX replenishment in sepsis.

Hemopexin's role in malaria, hemolytic-uremic syndrome, and dengue hemorrhagic fever

There were 247 million malaria cases in 2021, resulting in the loss of 61,900 lives in 2021, according to the World Health Organization (WHO). Malaria is characterized by hemolysis, which results in the release of hemoglobin and heme. The ratio of heme to HPX is inversely associated with disease severity and the 6-month mortality rate (64). Over the past 30 years, the incidence of severe dengue hemorrhagic fever cases has increased, with many patients succumbing due to a lack of timely clinical intervention. In DHF, fibronectin, HPX, and transferrin levels significantly rise in all three phases compared to Dengue Fever (DF) (65). Besides, a 2014 study revealed increased levels of HPX and vitronectin in both DF and DHF compared to healthy controls (66), suggesting HPX as a potential biomarker to distinguish between uncomplicated dengue fever and dengue hemorrhagic fever (5).

However, HPX does not always act as a protective factor in infection-related hemolysis. For instance, in a mouse model of Shiga toxin-induced hemolytic-uremic syndrome (HUS), HPX deficiency was protective in resolving HUS pathology (67). HPX$^{-/-}$ mice exhibited higher survival rates when challenged with Shiga toxin, with reduced renal inflammation characterized by decreased macrophage and neutrophil recruitment and C3c deposition [66]. This finding aligns with a previous study by Spiller et al., which concluded that HPX deficiency was protective in sepsis (68).

Hemopexin's role in hemorrhagic diseases

Hemopexin's role in intracerebral hemorrhage

Intracerebral hemorrhage is the most common type of hemorrhagic stroke and has the highest mortality rate of all stroke subtypes (69, 70). The rapid accumulation of blood within the brain parenchyma leads to the disruption of the normal anatomy and the increase of local pressure (71–73). Heme has been identified as a proinflammatory substance in the brain, and HPX can target it effectively (73).

HPX is present in the plasma and expressed by neurons and glia in the central nervous system. Intrathecally produced HPX represents another source of HPX in the cerebrospinal fluid (CSF) (74). However, HPX levels in the CSF are approximately tenfold lower than those in circulation, suggesting a relatively low capacity for heme binding in the brain, which can become easily overwhelmed (75). An *ex vivo* study supported the neuroprotective effects of HPX, as it protects neurons and glial cells from blood-related injuries through antioxidation and downregulation of HO-1 and caspase-3 (76). Preclinical research indicated that higher levels of HPX in the brain improve outcomes after ICH in a mouse model. Elevated local HPX levels were associated with smaller lesion volumes, reduced perihematomal tissue injury, and trends toward decreased hematoma volumes (77). Additionally, mice with higher HPX levels experienced no significant changes in brain iron levels and HO-1 but exhibited increased microgliosis and decreased astrogliosis and lipid peroxidation. This suggests the potential synergy of central and peripheral heme clearance (77).

Co-administration of hemopexin effectively mitigated heme-derived toxicity at both molecular and cellular levels (73). However, an *in vitro* study revealed increased globin-mediated neurotoxicity when Hp was absent after hemopexin treatment. In contrast, when used in combination with Hp, the neurotoxicity was notably reduced (78). This observation supports the notion that Hp-CD163 plays an

important role in activating detoxification pathways. Another hypothesis suggests that hemopexin may destabilize Hb in the absence of haptoglobin, leading to globin precipitation and iron deposition, ultimately exacerbating iron-dependent oxidative cell injury (Figure 3) (78). Consequently, it has been proposed that a combined therapy involving hemopexin and haptoglobin may be more favorable following intracerebral hemorrhage than a hemopexin supplement alone[77]. When administered systemically through intraperitoneal injection, hemopexin exhibited a reduction in blood-brain barrier (BBB) disruption on day 3 in ICH mouse models. However, it had no significant effect on striatal heme content on days 3 or 7, and it did not alleviate neurological deficits, inflammatory cell infiltration, or the viability of perihematomal cells on day 8 (79). This suggests that the administration of hemopexin in this manner is inadequate for allowing hemopexin to penetrate the BBB, which likely accounts for these results.

Hemopexin's role in subarachnoid hemorrhage

Subarachnoid hemorrhage is a type of hemorrhagic stroke primarily resulting from the rupture of saccular aneurysms, accounting for 3% of all stroke cases (80). The presence of hemoglobin and its breakdown products in the brain, combined with the toxic cascade initiated during early brain injury, has been extensively studied and is strongly linked to the development of delayed brain injury (81). In a study involving 30 SAH patients, free heme was still detectable in the cerebrospinal fluid after SAH, suggesting saturation of the HPX-CD91 system following SAH (74). Interestingly, elevated HPX levels in the CSF after SAH were associated with a higher likelihood of delayed cerebral ischemia and poorer neurological outcomes, which differed from the effects of HPX in other diseases (74). The underlying mechanism remains to be elucidated, but a possible explanation is that when the level of hemopexin in the CSF is excessively high, it may become deleterious as it impedes the efflux of heme due to its high heme affinity, resulting in intracellular heme/iron overload, which can be toxic to neurons and glia (74). It is worth noting that while bleed size and severity may be controlled, the subtypes of Hp were not in a recent review, emphasizing the need for more studies (82). In addition, CD91 is responsible for ApoE uptake, and reduced ApoE levels were associated with more severe neurological injury and worse outcomes after SAH (83–86). Thus, Hp-HPX replenishment could scavenge Hb and heme while limiting undesired ApoE uptake (82).

Hemopexin's role in atherosclerosis and thrombosis

Atherothrombotic diseases have long been a leading cause of death worldwide, accounting for over a quarter of all global deaths (87). Although the components involved in thrombosis and atherosclerosis differ, it is increasingly recognized that they are closely intertwined in biochemical and cellular mechanisms, particularly concerning platelet function (88). Notably, small platelets, as opposed to their larger counterparts, are rich in proteins associated with iron homeostasis, including HPX, Hp, α-1 anti-trypsin, transferrin, and vitronectin (89, 90). It is highly conceivable that small platelets take up these plasma proteins via the open canalicular system (OCS) and store them in α-granules (91). Since platelets release their contents upon activation (92), small platelets may play a role in iron homeostasis during thrombosis. *In vitro* studies have indicated that incubation of platelets with heme leads to ferroptosis and platelet activation. These effects are driven

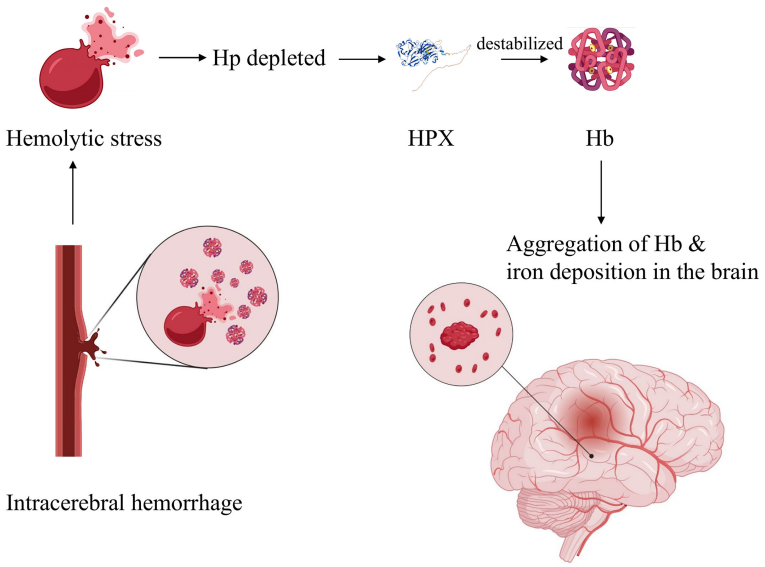

FIGURE 3
Hypothetic mechanism of globin-mediated neurotoxicity in the absence of Hp upon HPX treatment. Briefly, in the absence of Hp, application of HPX destabilizes Hb, resulting in globin precipitation and iron deposition, therefore exacerbating oxidative cell injury. Created with Biorender.com.

by ROS-driven proteasomal activity and lipid peroxidation and can be mitigated by melatonin. However, the role of HPX in this process requires further investigation (93, 94). It is hypothesized that the ferroptosis of smaller platelets may lead to the release of HPX, helping to mitigate ion toxicity.

Heme toxicity contributes to the progression of atherosclerosis in multiple ways. With its hydrophobic nature distributed within lipid compartments like lipoproteins, heme initiates peroxidative reactions, promoting atherosclerosis and elevating iron levels in advanced atherosclerotic lesions (95, 96). Besides, vascular endothelial injury in atherosclerosis leads to platelet adhesion and subsequent pro-thrombotic and pro-inflammatory effects. Studies have shown that HPX-related therapy alleviates endothelial activation and oxidation in SCD mice (22). After intraplaque hemorrhage, local cells were exposed to heme-induced oxidative damage, such as endoplasmic reticulum (ER) stress, which worsened atherosclerosis. An *in vitro* study demonstrated that HPX could significantly mitigate heme-induced ER stress in human aortic smooth muscle cells, indicating the protective role of HPX in atherosclerosis (97).

The protective role of hemopexin in clotting diseases has been validated by pre-clinical studies. An *in vivo* study by Wang et al. found that high doses of heme led to a dose-dependent increase in the plasma level of thrombin-antithrombin complexes, indicating an ongoing tissue factor-dependent coagulation process in SCD mice. Recombinant hemopexin treatment partially inhibited this coagulation activation (98). An *ex vivo* study revealed that heme-induced contractile dysfunction of human cardiomyocytes could be alleviated by hemopexin (99). Furthermore, in HPX-null mice with venous thrombosis induced by ligation of the inferior vena cava (IVCL), the clot size and weight were substantially greater than those in wild-type IVCL mice, underscoring the protective role of HPX in venous thrombosis (100). Both RT-PCR and Western blot analysis showed higher HPX expression in the IVCL group compared to the sham group (100). However, clinical studies on HPX therapy for these diseases are still lacking.

The timely detection and assessment of plaque presence and stability are critical, as the rupture of atherosclerotic plaques can have dire consequences. Quantitative proteomics analysis revealed that the serum concentration of hemopexin was elevated in individuals with coronary heart disease (CHD) and coronary atherosclerosis compared to healthy controls (101). Mass spectrometric analysis further indicated that hemopexin concentration was lower in serum from patients with unstable atherosclerotic plaques compared to those with stable atherosclerotic plaques, suggesting a connection between plaque stability and hemopexin concentration (102). In addition, serum proteomics analysis showed increased HPX levels on day 3 after ST-elevation myocardial infarction (103). Furthermore, a higher level of hemopexin (isotypes 1 and 2) was associated with future cardiovascular mortality in the healthy population (104). Further research into the role of hemopexin in the diagnosis and prognosis of atherothrombotic diseases is warranted.

Clinical application of hemopexin

Potential biomarkers to assess heme load and disease prognosis

In various hemolytic diseases, heme overload often significantly decreases HPX plasma levels, diminishing HPX's ability to scavenge heme effectively. Identifying an increase in plasma heme levels can aid in diagnosing and developing targeted plasma-based therapeutics (5). The level of HPX is considered a biomarker to assess heme load in many hemolytic pathologies. It was first proposed in 1975 that plasma HPX levels could indicate the severity of hemolysis, and this parameter has since been established to assess the level of hemolysis. For instance, in SCD, HPX levels in plasma increased as hemolysis levels declined in response to hydroxycarbamide treatment (105). Patients with septic shock who experienced lethal outcomes and severe organ injury were found to have reduced HPX concentrations (62, 64). In the case of malaria, the heme to HPX ratio negatively correlated with disease severity, as estimated by severe anemia, respiratory distress, stage 3 acute kidney injury, and the 6-month mortality rate (56). However, the levels of HPX increased significantly in all three phases of dengue hemorrhagic fever, which contradicts serum HPX changes in several other diseases. A higher level of HPX in the CSF was associated with better outcomes in ICH but worse prognosis in SAH (74, 77). The next step may involve measuring HPX levels at different stages of hemolytic diseases to further establish its role in prognosis and treatment in clinical scenarios.

Hemopexin replenishment therapy

Considering an average plasma concentration of 770 μg/ml of HPX in adults, each milliliter of plasma can bind 6.3 μg of heme, and higher heme levels can deplete HPX unless recycling or rapid compensatory synthesis occurs (1). As discussed earlier, HPX has been evaluated as a therapeutic agent in various heme overload diseases, including SCD, blood transfusions, sepsis, malaria, hemolytic-uremic syndrome, ICH, and SAH. The preponderance of data supporting HPX as a therapeutic target suggests that HPX replenishment remains an adjuvant therapy for hemolytic disorders with high heme stress (Figure 4). Over the years, preclinical models have been employed to evaluate potentially applicable scenarios. Notably, a phase 1 clinical trial is investigating HPX dosage in patients with sickle cell anemia, focusing on safety, tolerability, and pharmacokinetics (NCT04285827). However, HPX administration has only been approved for SCD by the European Commission and FDA in 2020 (20).

Beyond its application in SCD, preclinical trials have provided proof of concept for using HPX in other clinical settings. For example, in transfusion-induced hemolysis, the administration of HPX upon stored RBC transfusions in mice was shown to be partially effective, as discussed earlier. In the context of ICH and

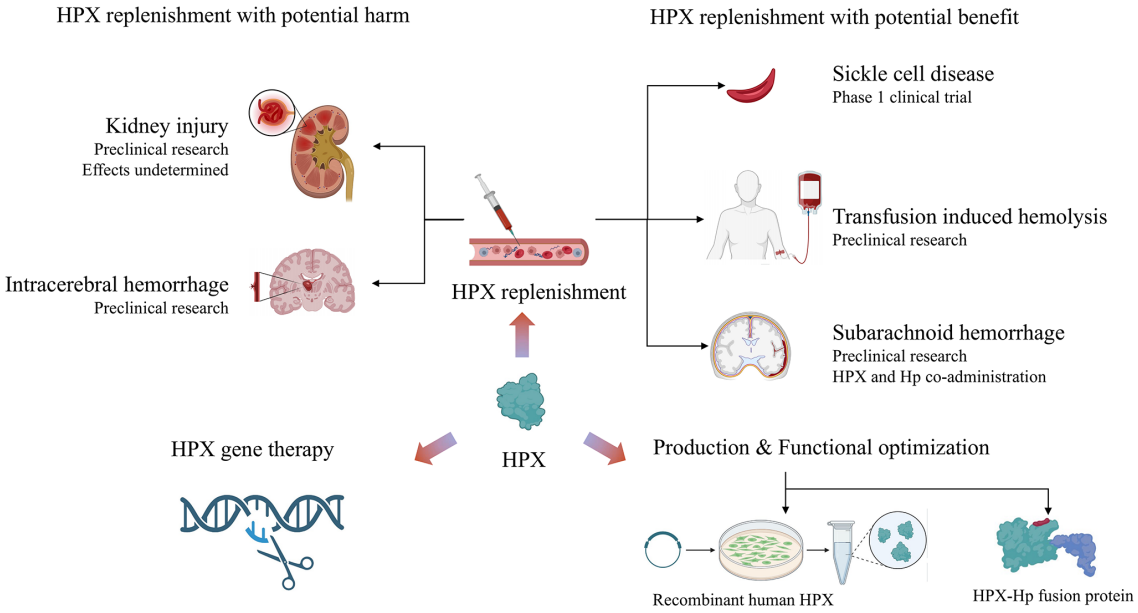

FIGURE 4
Summary of current research on the therapeutic potential of HPX: HPX replenishment therapy shows double-edged function in homological disorders. Novel directions include production and functional optimization of HPX, as well as HPX gene therapy. Created with Biorender.com.

SAH, HPX replenishment alone exhibited deleterious effects in several preclinical studies, promoting the administration of both Hp and HPX. Furthermore, the potential benefits of Hb/HPX replacement have been highlighted in β-thalassemia major and intermedia and hereditary spherocytosis (106).

The limited application of HPX in clinical settings can be partially attributed to its dual effects in different pathologies. For example, renal injury and resultant impairment of renal function are common complications of various hemolytic diseases. However, the effects of HPX on renal function remain to be elucidated. A study found that HPX could prevent complement activation in the kidneys of patients (or mice) with phenylhydrazine-induced hemolysis, substantiating the beneficial effects of HPX as a therapeutic agent, given that C3 deposition is associated with kidney injury (26). However, HPX does not always serve a protective role in hemolysis-associated renal injury. While HPX deficiency promotes AKI in sickle cell mice under hemolytic stress, HPX injection did not alter hemoglobinuria (24, 25). In a Shiga-toxin–induced HUS mouse model, HPX knockout mice displayed improved survival and reduced tubular iron deposition compared to wild-type mice (67).

Aside from HPX-mediated potential harm to the kidney, HPX increases the concentration of Hb in the CNS and promotes the aggregation of Hb or globin, consistent with findings observed in the kidneys. HPX-Hb increases iron-dependent neurotoxicity, which can be attenuated by Hp. These effects have also been shown to be deleterious to the brain, resulting in memory deficits in young mice (107). Therefore, HPX supplementation alone is not indicated for certain hemolytic conditions, while HPX plus Hp supplementation is more advisable when encountering toxicity mediated by iron or heme in pathological conditions. Plasmapheresis is a symptomatic treatment for autoimmune diseases and was investigated as a treatment for SCD patients with multiple organ dysfunction. In a case report, SCD patients refractory to RBC exchange were treated with plasmapheresis. Patients with a significant rise in plasma HPX and Hp levels showed clinical relief, in contrast to patients with minimal increases in HPX and Hp levels (108).

Recently, a hemopexin-Hp fusion protein with binding affinity and detoxification capacity for both heme and Hb was produced, which may contribute to the development of hemopexin-Hp therapies (109). This bifunctional fusion protein was generated using transient mammalian gene expression of Hp integrated with the pro-haptoglobin processing protease C1r-LP co-transfection for recombinant Hp-variant generation. This technology can likely be harnessed to generate multifunctional fusion proteins involved in the entire process of Hb and heme detoxification and clearance (110). Another study focused on increasing HPX yield and enhancing the interaction between heme and HPX (110). Utilizing a recombinant production strategy in human cell lines, Elena Karnaukhova et al. produced recombinant human HPX (rhHPX) by constructing an rhHPX expression plasmid and transfecting it into an HEK293 mammalian cell line (110).

The specific patient populations for which HPX-Hp replenishment is indicated and the degree of effectiveness achievable are beyond our current knowledge. Indeed, more research should be directed towards investigations into the role of HPX in various heme-related diseases and prospective clinical studies.

Hemopexin gene therapy

Historically, early efforts in HPX replacement therapy primarily focused on protein and plasma HPX levels. However, researchers have shifted their focus in recent years toward upregulating HPX expression and generating recombinant human HPX in eukaryotic cell expression systems (111). In mouse models of SCD, upregulating the endogenous hepatic synthesis of hemopexin through gene therapy has ameliorated inflammation and vaso-occlusion. This was demonstrated by quantifying hepatic nuclear Nrf2 expression, HO-1 activity, and NF-κB levels (112). Inspired by the success of gene therapy with adeno-associated virus (AAV) in hemophilia treatment, long-term expression of human HPX (hHPX) with AAV vectors was developed (113, 114). These vectors integrated with the full cDNA sequence of hHPX to prompt continuous hHPX expression for 58 days. Subjects exposed to heme challenges induced by heme infusions and phenylhydrazine survived (114). With the application of precision medicine and genome sequencing, the relationship between HPX genes and individualized drug side effects as well as tumorigenesis needs to be further investigated (115, 116).

Conclusion and perspectives

Heme overload is typically observed following hemolysis. Under physiological conditions, heme is quickly scavenged by the immune system in the plasma, preventing adverse pathophysiology driven by heme. HPX, one of the heme-binding proteins with the highest affinity, has broadened the therapeutic possibilities in hemolytic and thrombotic-related conditions because its administration can reverse the toxic effects of heme. This review summarized the double-edged functions of HPX in various hematological-related pathologies that cause heme overload based on current studies, such as SCD, transfusion-induced hemolysis, sepsis, ICH, SAH, atherosclerosis, and more. With an update of current preclinical and clinical studies, the review has outlined the potential of HPX as a biomarker for assessing the severity of certain diseases and its therapeutic value based on the pros and cons of its replenishment.

Initially, there has been much uncertainty due to the conflicting outcomes stemming from HPX supplementation. However, a possible hypothesis was proposed after a comprehensive understanding of HPX functions based on current studies. HPX replenishment can be protective when the heme clearance system is significantly undermined. In pathological conditions that mainly cause inflammation, HPX probably promotes precipitation and destabilization of Hb and HPX-Hb. Consequently, disassociated Hb can induce iron toxicity and oxidative stress, causing additional organ injury. Under such circumstances, HPX administration is detrimental. However, the border line between the two edges of HPX remains a scientific gap that requires further investigation. More research into the effects of HPX on different organs with heme overload due to systemic infection by fungi is expected. Additionally, ongoing investigations are being conducted to explore the diseases for which HPX administration is relevant.

In addition to its role as a therapeutic agent, new technologies for producing HPX protein using gene therapy were briefly introduced. The advancement in generating recombinant human HPX and fusion proteins offers new insights into the analysis of HPX-heme interactions and the neutralization of heme and its precursor, Hb. In this regard, the administration of a hemopexin-haptoglobin fusion protein may help avoid the deleterious effects caused by the sole administration of HPX, though further verification is needed.

Overall, the optimization of HPX therapy represents a novel and promising direction in the field of hematology. Recent progress includes upregulating endogenous HPX gene expression, producing recombinant HPX, and developing multifunctional fusion proteins with binding affinity and detoxification capacity for both heme and Hb.

Author contributions

YL: Writing – original draft, Conceptualization, Data curation, Formal Analysis. RC: Data curation, Writing – original draft. CW: Data curation, Writing – review & editing. JD: Writing – review & editing. SL: Conceptualization, Funding acquisition, Supervision, Writing – review & editing.

Funding

The author(s) declare financial support was received for the research, authorship, and/or publication of this article. This work was supported by the National Natural Science Foundations of China (SL, No. 82070136).

Conflict of interest

The authors declare that the research was conducted in the absence of any commercial or financial relationships that could be construed as a potential conflict of interest.

Publisher's note

References

1. Muller-Eberhard U, Javid J, Liem HH, Hanstein A, Hanna M. Plasma concentrations of hemopexin, haptoglobin and heme in patients with various hemolytic diseases. *Blood* (1968) 32(5):811–5. doi: 10.1182/blood.V32.5.811.811

2. Tolosano E, Altruda F. Hemopexin: structure, function, and regulation. *DNA Cell Biol* (2002) 21(4):297–306. doi: 10.1089/104454902753759717

3. Alves de Souza RW, Gallo D, Lee GR, Katsuyama E, Schaufler A, Weber J, et al. Skeletal Muscle Heme Oxygenase-1 Activity Regulates Aerobic Capacity. *Cell Rep* (2021) 35(3):109018. doi: 10.1016/j.celrep.2021.109018

4. Ashouri R, Fangman M, Burris A, Ezenwa MO, Wilkie DJ, Dore S. Critical role of hemopexin mediated cytoprotection in the pathophysiology of sickle cell disease. *Int J Mol Sci* (2021) 22(12):9285–9. doi: 10.3390/ijms22126408

5. Smith A, McCulloh RJ. Hemopexin and haptoglobin: allies against heme toxicity from hemoglobin not contenders. *Front Physiol* (2015) 6:187. doi: 10.3389/fphys.2015.00187

6. Balla J, Jacob HS, Balla G, Nath K, Eaton JW, Vercellotti GM. Endothelial-cell heme uptake from heme proteins: induction of sensitization and desensitization to oxidant damage. *Proc Natl Acad Sci U.S.A.* (1993) 90(20):9285–9. doi: 10.1073/pnas.90.20.9285

7. Tolosano E, Fagoonee S, Morello N, Vinchi F, Fiorito V. Heme scavenging and the other facets of hemopexin. *Antioxid Redox Signal* (2010) 12(2):305–20. doi: 10.1089/ars.2009.2787

8. Albrecht JH, Muller-Eberhard U, Kren BT, Steer CJ. Influence of transcriptional regulation and mrna stability on hemopexin gene expression in regenerating liver. *Arch Biochem Biophys* (1994) 314(1):229–33. doi: 10.1006/abbi.1994.1434

9. Wicher KB, Fries E. Haptoglobin, a hemoglobin-binding plasma protein, is present in bony fish and mammals but not in frog and chicken. *Proc Natl Acad Sci USA* (2006) 103(11):4168–73. doi: 10.1073/pnas.0508723103

10. Muller-Eberhard U. Hemopexin. *N Engl J Med* (1970) 283(20):1090–4. doi: 10.1056/nejm197011122832007

11. Ascenzi P, Bocedi A, Visca P, Altruda F, Tolosano E, Beringhelli T, et al. Hemoglobin and heme scavenging. *IUBMB Life* (2005) 57(11):749–59. doi: 10.1080/15216540500380871

12. Miller YI, Shaklai N. Kinetics of hemin distribution in plasma reveals its role in lipoprotein oxidation. *Biochim Biophys Acta* (1999) 1454(2):153–64. doi: 10.1016/s0925-4439(99)00027-7

13. Grinshtein N, Bamm VV, Tsemakhovich VA, Shaklai N. Mechanism of low-density lipoprotein oxidation by hemoglobin-derived iron. *Biochemistry* (2003) 42 (23):6977–85. doi: 10.1021/bi020647r

14. Mehta NU, Reddy ST. Role of hemoglobin/heme scavenger protein hemopexin in atherosclerosis and inflammatory diseases. *Curr Opin Lipidol* (2015) 26(5):384–7. doi: 10.1097/mol.0000000000000208

15. Buehler PW, Karnaukhova E. When might transferrin, hemopexin or haptoglobin administration be of benefit following the transfusion of red blood cells? *Curr Opin Hematol* (2018) 25(6):452–8. doi: 10.1097/moh.0000000000000458

16. Aygun B, Odame I. A global perspective on sickle cell disease. *Pediatr Blood Cancer* (2012) 59(2):386–90. doi: 10.1002/pbc.24175

17. Gladwin MT, Kato GJ. Cardiopulmonary complications of sickle cell disease: role of nitric oxide and hemolytic anemia. *Hematol Am Soc Hematol Educ Program* (2005) 2005(1):51–7. doi: 10.1182/asheducation-2005.1.51

18. Buehler PW, Swindle D, Pak DI, Ferguson SK, Majka SM, Karoor V, et al. Hemopexin dosing improves cardiopulmonary dysfunction in murine sickle cell disease. *Free Radic Biol Med* (2021) 175:95–107. doi: 10.1016/j.freeradbiomed.2021.08.238

19. Yildirim N, Unal S, Yalcinkaya A, Karahan F, Oztas Y. Evaluation of the relationship between intravascular hemolysis and clinical manifestations in sickle cell disease: decreased hemopexin during vaso-occlusive crises and increased inflammation in acute chest syndrome. *Ann Hematol* (2022) 101(1):35–41. doi: 10.1007/s00277-021-04667-w

20. Gentinetta T, Belcher JD, Brügger-Verdon V, Adam J, Ruthsatz T, Bain J, et al. Plasma-derived hemopexin as a candidate therapeutic agent for acute vaso-occlusion in sickle cell disease: preclinical evidence. *J Clin Med* (2022) 11(3). doi: 10.3390/jcm11030630

21. Merle NS, Grunenwald A, Rajaratnam H, Gnemmi V, Frimat M, Figueres ML, et al. Intravascular hemolysis activates complement via cell-free heme and heme-loaded microvesicles. *JCI Insight* (2018) 3(12). doi: 10.1172/jci.insight.96910

22. Vinchi F, De Franceschi L, Ghigo A, Townes T, Cimino J, Silengo L, et al. Hemopexin therapy improves cardiovascular function by preventing heme-induced endothelial toxicity in mouse models of hemolytic diseases. *Circulation* (2013) 127 (12):1317–29. doi: 10.1161/circulationaha.112.130179

23. Alishlash AS, Sapkota M, Ahmad I, Maclin K, Ahmed NA, Molyvdas A, et al. Chlorine inhalation induces acute chest syndrome in humanized sickle cell mouse model and ameliorated by postexposure hemopexin. *Redox Biol* (2021) 44:102009. doi: 10.1016/j.redox.2021.102009

24. Ghosh S, Orikogbo O, Hazra R, Flage B, Crosby D, Ofori-Acquah SF. Hemopexin replacement therapy protects sickle cell disease mice from acute kidney injury. *Blood* (2019) 134(Supplement_1):78. doi: 10.1182/blood-2019-127161

25. Ofori-Acquah SF, Hazra R, Orikogbo OO, Crosby D, Flage B, Ackah EB, et al. Hemopexin deficiency promotes acute kidney injury in sickle cell disease. *Blood* (2020) 135(13):1044–8. doi: 10.1182/blood.2019002653

26. Poillerat V, Gentinetta T, Leon J, Wassmer A, Edler M, Torset C, et al. Hemopexin as an inhibitor of hemolysis-induced complement activation. *Front Immunol* (2020) 11:1684. doi: 10.3389/fimmu.2020.01684

27. Gerogianni A, Dimitrov JD, Zarantonello A, Poillerat V, Chonat S, Sandholm K, et al. Heme interferes with complement factor I-dependent regulation by enhancing alternative pathway activation. *Front Immunol* (2022) 13:901876. doi: 10.3389/fimmu.2022.901876

28. Gotardo É MF, Brito PL, Gushiken LFS, Chweih H, Leonardo FC, Costa FF, et al. Molecular and cellular effects of in vivo chronic intravascular hemolysis and anti-inflammatory therapeutic approaches. *Vascul Pharmacol* (2023) 150:107176. doi: 10.1016/j.vph.2023.107176

29. Risbano MG, Kanias T, Triulzi D, Donadee C, Barge S, Badlam J, et al. Effects of aged stored autologous red blood cells on human endothelial function. *Am J Respir Crit Care Med* (2015) 192(10):1223–33. doi: 10.1164/rccm.201501-0145OC

30. Donadee C, Raat NJ, Kanias T, Tejero J, Lee JS, Kelley EE, et al. Nitric oxide scavenging by red blood cell microparticles and cell-free hemoglobin as a mechanism for the red cell storage lesion. *Circulation* (2011) 124(4):465–76. doi: 10.1161/circulationaha.110.008698

31. Yoshida T, Prudent M, D'Alessandro A. Red blood cell storage lesion: causes and potential clinical consequences. *Blood Transfus* (2019) 17(1):27–52. doi: 10.2450/2019.0217-18

32. Hébert PC, Chin-Yee I, Fergusson D, Blajchman M, Martineau R, Clinch J, et al. A pilot trial evaluating the clinical effects of prolonged storage of red cells. *Anesth Analg* (2005) 100(5):1433–58. doi: 10.1213/01.Ane.0000148690.48803.27

33. Wagener BM, Hu PJ, Oh JY, Evans CA, Richter JR, Honavar J, et al. Role of heme in lung bacterial infection after trauma hemorrhage and stored red blood cell transfusion: A preclinical experimental study. *PloS Med* (2018) 15(3):e1002522. doi: 10.1371/journal.pmed.1002522

34. Pietropaoli AP, Henrichs KF, Cholette JM, Spinelli SL, Phipps RP, Refaai MA, et al. Total plasma heme concentration increases after red blood cell transfusion and predicts mortality in critically ill medical patients. *Transfusion* (2019) 59:2007–15. doi: 10.1111/trf.15218

35. Graw JA, Mayeur C, Rosales I, Liu Y, Sabbisetti VS, Riley FE, et al. Haptoglobin or hemopexin therapy prevents acute adverse effects of resuscitation after prolonged storage of red cells. *Circulation* (2016) 134(13):945–60. doi: 10.1161/circulationaha.115.019955

36. Jacques M. Comment on the microreview by B. Craig lee (Quelling the red menace: haem capture by bacteria). *Mol Microbiol* (1996) 20(1):238. doi: 10.1111/j.1365-2958.1996.tb02506.x

37. Braun V, Killmann H. Bacterial solutions to the iron-supply problem. *Trends Biochem Sci* (1999) 24(3):104–9. doi: 10.1016/s0968-0004(99)01359-6

38. Hod EA, Brittenham GM, Billote GB, Francis RO, Ginzburg YZ, Hendrickson JE, et al. Transfusion of human volunteers with older, stored red blood cells produces extravascular hemolysis and circulating non-transferrin-bound iron. *Blood* (2011) 118 (25):6675–82. doi: 10.1182/blood-2011-08-371849

39. Furlaneto MC, Góes HP, Perini HF, Dos Santos RC, Furlaneto-Maia L. How much do we know about hemolytic capability of pathogenic candida species? *Folia Microbiol (Praha)* (2018) 63(4):405–12. doi: 10.1007/s12223-018-0584-5

40. Wiseman GM. The hemolysins of staphylococcus aureus. *Bacteriol Rev* (1975) 39 (4):317–44. doi: 10.1128/br.39.4.317-344.1975

41. Cassat JE, Skaar EP. Iron in infection and immunity. *Cell Host Microbe* (2013) 13 (5):509–19. doi: 10.1016/j.chom.2013.04.010

42. Hanson MS, Pelzel SE, Latimer J, Muller-Eberhard U, Hansen EJ. Identification of a genetic locus of haemophilus influenzae type B necessary for the binding and utilization of heme bound to human hemopexin. *Proc Natl Acad Sci USA* (1992) 89 (5):1973–7. doi: 10.1073/pnas.89.5.1973

43. Cope LD, Thomas SE, Latimer JL, Slaughter CA, Müller-Eberhard U, Hansen EJ. The 100 kda haem:Haemopexin-binding protein of haemophilus influenzae: structure and localization. *Mol Microbiol* (1994) 13(5):863–73. doi: 10.1111/j.1365-2958.1994.tb00478.x

44. Cope LD, Yogev R, Muller-Eberhard U, Hansen EJ. A gene cluster involved in the utilization of both free heme and heme:Hemopexin by haemophilus influenzae type B. *J Bacteriol* (1995) 177(10):2644–53. doi: 10.1128/jb.177.10.2644-2653.1995

45. Fournier C, Smith A, Delepelaire P. Haem release from haemopexin by hxua allows haemophilus influenzae to escape host nutritional immunity. *Mol Microbiol* (2011) 80(1):133–48. doi: 10.1111/j.1365-2958.2011.07562.x

46. Olczak T, Simpson W, Liu X, Genco CA. Iron and heme utilization in porphyromonas gingivalis. *FEMS Microbiol Rev* (2005) 29(1):119–44. doi: 10.1016/j.femsre.2004.09.001

47. Sroka A, Sztukowska M, Potempa J, Travis J, Genco CA. Degradation of host heme proteins by lysine- and arginine-specific cysteine proteinases (Gingipains) of

porphyromonas gingivalis. *J Bacteriol* (2001) 183(19):5609–16. doi: 10.1128/JB.183.19.5609-5616.2001

48. Weissman Z, Kornitzer D. A family of candida cell surface haem-binding proteins involved in haemin and haemoglobin-iron utilization. *Mol Microbiol* (2004) 53(4):1209–20. doi: 10.1111/j.1365-2958.2004.04199.x

49. Nasser L, Weissman Z, Pinsky M, Amartely H, Dvir H, Kornitzer D. Structural basis of haem-iron acquisition by fungal pathogens. *Nat Microbiol* (2016) 1(11):16156. doi: 10.1038/nmicrobiol.2016.156

50. Sakamoto K, Kim YG, Hara H, Kamada N, Caballero-Flores G, Tolosano E, et al. Il-22 controls iron-dependent nutritional immunity against systemic bacterial infections. *Sci Immunol* (2017) 2(8). doi: 10.1126/sciimmunol.aai8371

51. Kuznets G, Vigonsky E, Weissman Z, Lalli D, Gildor T, Kauffman SJ, et al. A relay network of extracellular heme-binding proteins drives C. Albicans iron acquisition from hemoglobin. *PloS Pathog* (2014) 10(10):e1004407. doi: 10.1371/journal.ppat.1004407

52. Pinsky M, Roy U, Moshe S, Weissman Z, Kornitzer D. Human serum albumin facilitates heme-iron utilization by fungi. *Mbio* (2020) 11(2). doi: 10.1128/mBio.00607-20

53. Rudd KE, Johnson SC, Agesa KM, Shackelford KA, Tsoi D, Kievlan DR, et al. Global, regional, and national sepsis incidence and mortality, 1990-2017: analysis for the global burden of disease study. *Lancet* (2020) 395(10219):200–11. doi: 10.1016/S0140-6736(19)32989-7

54. Effenberger-Neidnicht K, Hartmann M. Mechanisms of hemolysis during sepsis. *Inflammation* (2018) 41(5):1569–81. doi: 10.1007/s10753-018-0810-y

55. Piagnerelli M, Boudjeltia KZ, Vanhaeverbeek M, Vincent JL. Red blood cell rheology in sepsis. *Intensive Care Med* (2003) 29(7):1052–61. doi: 10.1007/s00134-003-1783-2

56. Arias CF, Arias CF. How do red blood cells know when to die? *R Soc Open Sci* (2017) 4(4):160850. doi: 10.1098/rsos.160850

57. Parker MW, Feil SC. Pore-forming protein toxins: from structure to function. *Prog Biophys Mol Biol* (2005) 88(1):91–142. doi: 10.1016/j.pbiomolbio.2004.01.009

58. Janz DR, Bastarache JA, Peterson JF, Sills G, Wickersham N, May AK, et al. Association between cell-free hemoglobin, acetaminophen, and mortality in patients with sepsis: an observational study. *Crit Care Med* (2013) 41(3):784–90. doi: 10.1097/CCM.0b013e3182741a54

59. Adamzik M, Hamburger T, Petrat F, Peters J, de Groot H, Hartmann M. Free hemoglobin concentration in severe sepsis: methods of measurement and prediction of outcome. *Crit Care* (2012) 16(4):R125. doi: 10.1186/cc11425

60. Janz DR, Bastarache JA, Sills G, Wickersham N, May AK, Bernard GR, et al. Association between haptoglobin, hemopexin and mortality in adults with sepsis. *Crit Care* (2013) 17(6):R272. doi: 10.1186/cc13108

61. Jung JY, Kwak YH, Kim KS, Kwon WY, Suh GJ. Change of hemopexin level is associated with the severity of sepsis in endotoxemic rat model and the outcome of septic patients. *J Crit Care* (2015) 30(3):525–30. doi: 10.1016/j.jcrc.2014.12.009

62. Larsen R, Gozzelino R, Jeney V, Tokaji L, Bozza FA, Japiassu AM, et al. A central role for free heme in the pathogenesis of severe sepsis. *Sci Transl Med* (2010) 2(51):51ra71. doi: 10.1126/scitranslmed.3001118

63. Detzel MS, Schmalohr BF, Steinbock F, Hopp MT, Ramoji A, Paul George AA, et al. Revisiting the interaction of heme with hemopexin. *Biol Chem* (2021) 402(6):675–91. doi: 10.1515/hsz-2020-0347

64. Elphinstone RE, Conroy AL, Hawkes M, Hermann L, Namasopo S, Warren HS, et al. Alterations in systemic extracellular heme and hemopexin are associated with adverse clinical outcomes in Ugandan children with severe malaria. *J Infect Dis* (2016) 214(8):1268–75. doi: 10.1093/infdis/jiw357

65. Kumar Y, Liang C, Bo Z, Rajapakse JC, Ooi EE, Tannenbaum SR. Serum proteome and cytokine analysis in a longitudinal cohort of adults with primary dengue infection reveals predictive markers of dhf. *PloS Negl Trop Dis* (2012) 6(11):e1887. doi: 10.1371/journal.pntd.0001887

66. Poole-Smith BK, Gilbert A, Gonzalez AL, Beltran M, Tomashek KM, Ward BJ, et al. Discovery and characterization of potential prognostic biomarkers for dengue hemorrhagic fever. *Am J Trop Med Hyg* (2014) 91(6):1218–26. doi: 10.4269/ajtmh.14-0193

67. Pirschel W, Mestekemper AN, Wissuwa B, Krieg N, Kröller S, Daniel C, et al. Divergent roles of haptoglobin and hemopexin deficiency for disease progression of shiga-toxin-induced hemolytic-uremic syndrome in mice. *Kidney Int* (2022) 101(6):1171–85. doi: 10.1016/j.kint.2021.12.024

68. Spiller F, Costa C, Souto FO, Vinchi F, Mestriner FL, Laure HJ, et al. Inhibition of neutrophil migration by hemopexin leads to increased mortality due to sepsis in mice. *Am J Respir Crit Care Med* (2011) 183(7):922–31. doi: 10.1164/rccm.201002-0223OC

69. Schlunk F, Greenberg SM. The pathophysiology of intracerebral hemorrhage formation and expansion. *Transl Stroke Res* (2015) 6(4):257–63. doi: 10.1007/s12975-015-0410-1

70. Chen S, Yang Q, Chen G, Zhang JH. An update on inflammation in the acute phase of intracerebral hemorrhage. *Transl Stroke Res* (2015) 6(1):4–8. doi: 10.1007/s12975-014-0384-4

71. Aronowski J, Zhao X. Molecular pathophysiology of cerebral hemorrhage: secondary brain injury. *Stroke* (2011) 42(6):1781–6. doi: 10.1161/strokeaha.110.596718

72. Baechli H, Behzad M, Schreckenberger M, Buchholz HG, Heimann A, Kempski O, et al. Blood constituents trigger brain swelling, tissue death, and reduction of glucose metabolism early after acute subdural hematoma in rats. *J Cereb Blood Flow Metab* (2010) 30(3):576–85. doi: 10.1038/jcbfm.2009.230

73. Buzzi RM, Akeret K, Schwendinger N, Klohs J, Vallelian F, Hugelshofer M, et al. Spatial transcriptome analysis defines heme as a hemopexin-targetable inflammatoxin in the brain. *Free Radic Biol Med* (2022) 179:277–87. doi: 10.1016/j.freeradbiomed.2021.11.011

74. Garland P, Durnford AJ, Okemefuna AI, Dunbar J, Nicoll JA, Galea J, et al. Heme-hemopexin scavenging is active in the brain and associates with outcome after subarachnoid hemorrhage. *Stroke* (2016) 47(3):872–6. doi: 10.1161/strokeaha.115.011956

75. Hvidberg V, Maniecki MB, Jacobsen C, Højrup P, Møller HJ, Moestrup SK. Identification of the receptor scavenging hemopexin-heme complexes. *Blood* (2005) 106(7):2572–9. doi: 10.1182/blood-2005-03-1185

76. Liu Y, Tan C, Li W, Liu X, Wang X, Gui Y, et al. Adenoviral transfer of hemopexin gene attenuates oxidative stress and apoptosis in cultured primary cortical neuron cell exposed to blood clot. *Neuroreport* (2020) 31(15):1065–71. doi: 10.1097/wnr.0000000000001510

77. Leclerc JL, Santiago-Moreno J, Dang A, Lampert AS, Cruz PE, Rosario AM, et al. Increased brain hemopexin levels improve outcomes after intracerebral hemorrhage. *J Cereb Blood Flow Metab* (2018) 38(6):1032–46. doi: 10.1177/0271678x16679170

78. Chen-Roetling J, Ma SK, Cao Y, Shah A, Regan RF. Hemopexin increases the neurotoxicity of hemoglobin when haptoglobin is absent. *J Neurochem* (2018) 145(6):464–73. doi: 10.1111/jnc.14328

79. Chen-Roetling J, Li Y, Cao Y, Yan Z, Lu X, Regan RF. Effect of hemopexin treatment on outcome after intracerebral hemorrhage in mice. *Brain Res* (2021) 1765:147507. doi: 10.1016/j.brainres.2021.147507

80. Go AS, Mozaffarian D, Roger VL, Benjamin EJ, Berry JD, Blaha MJ, et al. Heart disease and stroke statistics–2014 update: A report from the american heart association. *Circulation* (2014) 129(3):e28–e292. doi: 10.1161/01.cir.0000441139.02102.80

81. Akeret K, Buzzi RM, Saxenhofer M, Bieri K, Chiavi D, Thomson BR, et al. The hemoval study protocol: A prospective international multicenter cohort study to validate cerebrospinal fluid hemoglobin as a monitoring biomarker for aneurysmal subarachnoid hemorrhage related secondary brain injury. *BMC Neurol* (2022) 22(1):267. doi: 10.1186/s12883-022-02789-w

82. Griffiths S, Clark J, Adamides AA, Ziogas J. The role of haptoglobin and hemopexin in the prevention of delayed cerebral ischaemia after aneurysmal subarachnoid haemorrhage: A review of current literature. *Neurosurg Rev* (2020) 43(5):1273–88. doi: 10.1007/s10143-019-01169-2

83. Kay A, Petzold A, Kerr M, Keir G, Thompson E, Nicoll J. Temporal alterations in cerebrospinal fluid amyloid beta-protein and apolipoprotein E after subarachnoid hemorrhage. *Stroke* (2003) 34(12):e240–3. doi: 10.1161/01.Str.0000100157.88508.2f

84. Kay A, Petzold A, Kerr M, Keir G, Thompson E, Nicoll J. Decreased cerebrospinal fluid apolipoprotein E after subarachnoid hemorrhage: correlation with injury severity and clinical outcome. *Stroke* (2003) 34(3):637–42. doi: 10.1161/01.Str.0000057579.25430.16

85. Guo ZD, Sun XC, Zhang JH. The role of apolipoprotein E in the pathological events following subarachnoid hemorrhage: A review. *Acta Neurochir Suppl* (2011) 110(Pt 2):5–7. doi: 10.1007/978-3-7091-0356-2_1

86. Lanterna LA, Biroli F. Significance of apolipoprotein E in subarachnoid hemorrhage: neuronal injury, repair, and therapeutic perspectives–a review. *J Stroke Cerebrovasc Dis* (2009) 18(2):116–23. doi: 10.1016/j.jstrokecerebrovasdis.2008.09.006

87. Jackson SP. Arterial thrombosis–insidious, unpredictable and deadly. *Nat Med* (2011) 17(11):1423–36. doi: 10.1038/nm.2515

88. Davì G, Patrono C. Platelet activation and atherothrombosis. *N Engl J Med* (2007) 357(24):2482–94. doi: 10.1056/NEJMra071014

89. Handtke S, Steil L, Palankar R, Conrad J, Cauhan S, Kraus L, et al. Role of platelet size revisited-function and protein composition of large and small platelets. *Thromb Haemost* (2019) 119(3):407–20. doi: 10.1055/s-0039-1677875

90. Montecinos L, Eskew JD, Smith A. What is next in this "Age" of heme-driven pathology and protection by hemopexin? An update and links with iron. *Pharm (Basel)* (2019) 12(4):144. doi: 10.3390/ph12040144

91. Handtke S, Thiele T. Large and small platelets-(When) do they differ? *J Thromb Haemost* (2020) 18(6):1256–67. doi: 10.1111/jth.14788

92. Xu XR, Zhang D, Oswald BE, Carrim N, Wang X, Hou Y, et al. Platelets are versatile cells: new discoveries in hemostasis, thrombosis, immune responses, tumor metastasis and beyond. *Crit Rev Clin Lab Sci* (2016) 53(6):409–30. doi: 10.1080/10408363.2016.1200008

93. NaveenKumar SK, Hemshekhar M, Kemparaju K, Girish KS. Hemin-induced platelet activation and ferroptosis is mediated through ros-driven proteasomal activity and inflammasome activation: protection by melatonin. *Biochim Biophys Acta Mol Basis Dis* (2019) 1865(9):2303–16. doi: 10.1016/j.bbadis.2019.05.009

94. NaveenKumar SK, SharathBabu BN, Hemshekhar M, Kemparaju K, Girish KS, Mugesh G. The role of reactive oxygen species and ferroptosis in heme-mediated activation of human platelets. *ACS Chem Biol* (2018) 13(8):1996–2002. doi: 10.1021/acschembio.8b00458

95. Bosseboeuf E, Raimondi C. Signalling, metabolic pathways and iron homeostasis in endothelial cells in health, atherosclerosis and alzheimer's disease. *Cells* (2020) 9(9). doi: 10.3390/cells9092055

96. Vallelian F, Buehler PW, Schaer DJ. Hemolysis, free hemoglobin toxicity, and scavenger protein therapeutics. *Blood* (2022) 140(17):1837–44. doi: 10.1182/blood.2022015596

97. Gáll T, Pethő D, Nagy A, Hendrik Z, Méhes G, Potor L, et al. Heme induces endoplasmic reticulum stress (Hier stress) in human aortic smooth muscle cells. *Front Physiol* (2018) 9:1595. doi: 10.3389/fphys.2018.01595

98. Sparkenbaugh EM, Chantrathammachart P, Wang S, Jonas W, Kirchhofer D, Gailani D, et al. Excess of heme induces tissue factor-dependent activation of coagulation in mice. *Haematologica* (2015) 100(3):308–14. doi: 10.3324/haematol.2014.114728

99. Alvarado G, Jeney V, Tóth A, Csősz É, Kalló G, Huynh AT, et al. Heme-induced contractile dysfunction in human cardiomyocytes caused by oxidant damage to thick filament proteins. *Free Radic Biol Med* (2015) 89:248–62. doi: 10.1016/j.freeradbiomed.2015.07.158

100. Nath KA, Grande JP, Belcher JD, Garovic VD, Croatt AJ, Hillestad ML, et al. Antithrombotic effects of heme-degrading and heme-binding proteins. *Am J Physiol Heart Circ Physiol* (2020) 318(3):H671–h81. doi: 10.1152/ajpheart.00280.2019

101. Stakhneva EM, Meshcheryakova IA, Demidov EA, Starostin KV, Peltek SE, Voevoda MI, et al. Changes in the proteomic profile of blood serum in coronary atherosclerosis. *J Med Biochem* (2020) 39(2):208–14. doi: 10.2478/jomb-2019-0022

102. Stakhneva EM, Kashtanova EV, Polonskaya YV, Striukova EV, Shramko VS, Sadovski EV, et al. The search for associations of serum proteins with the presence of unstable atherosclerotic plaque in coronary atherosclerosis. *Int J Mol Sci* (2022) 23(21):12795. doi: 10.3390/ijms232112795

103. Cubedo J, Suades R, Padro T, Martin-Yuste V, Sabate-Tenas M, Cinca J, et al. Erythrocyte-Heme proteins and stemi: implications in prognosis. *Thromb Haemost* (2017) 117(10):1970–80. doi: 10.1160/th17-05-0314

104. Melander O, Modrego J, Zamorano-León JJ, Santos-Sancho JM, Lahera V, López-Farré AJ. New circulating biomarkers for predicting cardiovascular death in healthy population. *J Cell Mol Med* (2015) 19(10):2489–99. doi: 10.1111/jcmm.12652

105. Brewin J, Tewari S, Menzel S, Kirkham F, Inusa B, Renney G, et al. The effects of hydroxycarbamide on the plasma proteome of children with sickle cell anaemia. *Br J Haematol* (2019) 186(6):879–86. doi: 10.1111/bjh.15996

106. Vinchi F, Sparla R, Passos ST, Sharma R, Vance SZ, Zreid HS, et al. Vasculotoxic and pro-inflammatory action of unbound haemoglobin, haem and iron in transfusion-dependent patients with haemolytic anaemias. *Br J Haematol* (2021) 193(3):637–58. doi: 10.1111/bjh.17361

107. Nagase T, Tohda C. Skeletal muscle atrophy-induced hemopexin accelerates onset of cognitive impairment in alzheimer's disease. *J Cachexia Sarcopenia Muscle* (2021) 12(6):2199–210. doi: 10.1002/jcsm.12830

108. Louie JE, Anderson CJ, Fayaz MFK, Henry A, Killeen T, Mohandas N, et al. Case series supporting heme detoxification via therapeutic plasma exchange in acute multiorgan failure syndrome resistant to red blood cell exchange in sickle cell disease. *Transfusion* (2018) 58(2):470–9. doi: 10.1111/trf.14407

109. Buzzi RM, Owczarek CM, Akeret K, Tester A, Pereira N, Butcher R, et al. Modular platform for the development of recombinant hemoglobin scavenger biotherapeutics. *Mol Pharm* (2021) 18(8):3158–70. doi: 10.1021/acs.molpharmaceut.1c00433

110. Karnaukhova E, Owczarek C, Schmidt P, Schaer DJ, Buehler PW. Human plasma and recombinant hemopexins: heme binding revisited. *Int J Mol Sci* (2021) 22(3):1199. doi: 10.3390/ijms22031199

111. Song L, Ke Y, Zhang ZQ. High level expression and purification of recombinant pex protein in cultured skeletal muscle cell expression system. *Biochem Biophys Res Commun* (2007) 357(1):258–63. doi: 10.1016/j.bbrc.2007.03.137

112. Vercellotti GM, Zhang P, Nguyen J, Abdulla F, Chen C, Nguyen P, et al. Hepatic overexpression of hemopexin inhibits inflammation and vascular stasis in murine models of sickle cell disease. *Mol Med* (2016) 22:437–51. doi: 10.2119/molmed.2016.00063

113. Nathwani AC. Gene therapy for hemophilia. *Hematol Am Soc Hematol Educ Program* (2019) 2019(1):1–8. doi: 10.1182/hematology.2019000007

114. de Lima F, Hounkpe BW, de Moraes CRP, Borba-Junior IT, Costa FF, De Paula EV. Safety and feasibility of the gene transfer of hemopexin for conditions with increased free heme. *Exp Biol Med (Maywood)* (2023) 248(13):1103–11. doi: 10.1177/15353702231182199

115. Liu W, Lu L, Pan H, He X, Zhang M, Wang N, et al. Heme oxygenase-1 and hemopexin gene polymorphisms and the risk of anti-tuberculosis drug-induced hepatotoxicity in China. *Pharmacogenomics* (2022) 23(7):431–41. doi: 10.2217/pgs-2022-0015

116. Cine N, Baykal AT, Sunnetci D, Canturk Z, Serhatli M, Savli H. Identification of apoa1, hpx and potee genes by omic analysis in breast cancer. *Oncol Rep* (2014) 32(3):1078–86. doi: 10.3892/or.2014.3277

frontiers | Frontiers in Immunology

TYPE Review
PUBLISHED 16 February 2024
DOI 10.3389/fimmu.2024.1327035

OPEN ACCESS

EDITED BY
Stefan Eugen Szedlacsek,
Institute of Biochemistry of the Romanian Academy, Romania

REVIEWED BY
Shigeo Fuji,
Osaka International Cancer Institute, Japan
Pranali Shah,
Brigham and Womens Hospital and Harvard Medical School, United States

*CORRESPONDENCE
Cristina Adela Iuga
iugac@umfcluj.ro

†These authors have contributed equally to this work and share first authorship

‡These authors have contributed equally to this work and share last authorship

RECEIVED 25 October 2023
ACCEPTED 01 February 2024
PUBLISHED 16 February 2024

CITATION
Iacobescu M, Pop C, Uifălean A, Mogoşan C, Cenariu D, Zdrenghea M, Tănase A, Bergthorsson JT, Greiff V, Cenariu M, Iuga CA, Tomuleasa C and Tătaru D (2024) Unlocking protein-based biomarker potential for graft-versus-host disease following allogenic hematopoietic stem cell transplants. *Front. Immunol.* 15:1327035. doi: 10.3389/fimmu.2024.1327035

Unlocking protein-based biomarker potential for graft-versus-host disease following allogenic hematopoietic stem cell transplants

Maria Iacobescu[1†], Cristina Pop[2†], Alina Uifălean[3], Cristina Mogoşan[2], Diana Cenariu[4], Mihnea Zdrenghea[5], Alina Tănase[6], Jon Thor Bergthorsson[7], Victor Greiff[8], Mihai Cenariu[9], Cristina Adela Iuga[1,3*], Ciprian Tomuleasa[4,5‡] and Dan Tătaru[10‡]

[1]Department of Proteomics and Metabolomics, MEDFUTURE Research Center for Advanced Medicine, "Iuliu Hatieganu" University of Medicine and Pharmacy, Cluj-Napoca, Romania, [2]Department of Pharmacology, Physiology and Pathophysiology, Faculty of Pharmacy, "Iuliu Hatieganu" University of Medicine and Pharmacy, Cluj-Napoca, Romania, [3]Department of Pharmaceutical Analysis, Faculty of Pharmacy, "Iuliu Hatieganu" University of Medicine and Pharmacy, Cluj-Napoca, Romania, [4]Department of Translational Medicine, MEDFUTURE Research Center for Advanced Medicine, "Iuliu Hatieganu" University of Medicine and Pharmacy, Cluj-Napoca, Romania, [5]Department of Hematology, Faculty of Medicine, "Iuliu Hatieganu" University of Medicine and Pharmacy, Cluj-Napoca, Romania, [6]Department of Stem Cell Transplantation, Fundeni Clinical Institute, Bucharest, Romania, [7]Department of Laboratory Hematology, Stem Cell Research Unit, Biomedical Center, School of Health Sciences, University Iceland, Reykjavik, Iceland, [8]Department of Immunology, University of Oslo, Oslo, Norway, [9]Department of Animal Reproduction, University of Agricultural Sciences and Veterinary Medicine, Cluj-Napoca, Romania, [10]Department of Internal Medicine, Faculty of Medicine, "Iuliu Hatieganu" University of Medicine and Pharmacy, Cluj-Napoca, Romania

Despite the numerous advantages of allogeneic hematopoietic stem cell transplants (allo-HSCT), there exists a notable association with risks, particularly during the preconditioning period and predominantly post-intervention, exemplified by the occurrence of graft-versus-host disease (GVHD). Risk stratification prior to symptom manifestation, along with precise diagnosis and prognosis, relies heavily on clinical features. A critical imperative is the development of tools capable of early identification and effective management of patients undergoing allo-HSCT. A promising avenue in this pursuit is the utilization of proteomics-based biomarkers obtained from non-invasive biospecimens. This review comprehensively outlines the application of proteomics and proteomics-based biomarkers in GVHD patients. It delves into both single protein markers and protein panels, offering insights into their relevance in acute and chronic GVHD. Furthermore, the review provides a detailed examination of the site-specific involvement of GVHD. In summary, this article explores the potential of proteomics as a tool for timely and accurate intervention in the context of GVHD following allo-HSCT.

KEYWORDS

allogenic stem cell transplantation, graft-versus-host-disease, biomarker, proteomics, biofluids

10.3389/fimmu.2024.1327035

1 Background on graft-versus-host-disease

In hematology, precision medicine has made strides, particularly in bone marrow transplants (BMT) and targeted therapies transforming blood disorder management. BMTs recent safety profile, with transplant-related mortality below 30% and a 30 to 70% risk of graft-versus-host disease (GVHD), positions it as a universal option. However, advances in genetics, molecular biology, and immunology have led to targeted therapeutics, reducing BMT necessity in some cases.

Currently, allogenic hematopoietic stem cell transplants (allo-HSCT), using bone marrow, peripheral blood stem cells (PBSCs), or cord blood, are increasingly performed globally. Allo-HSCT holds a great potential of curing many malignant and non-malignant hematologic disorders, subjected to specific conditions (1). Risk factors include human leukocyte antigen (HLA) mismatch, female donors for male recipients, and total body irradiation. Complications post-allo-HSCT involve infections, GVHD, and relapse, with risk assessment relying on clinical characteristics (2, 3).

GVHD is a life-threatening complication that can occur after the allo-HSCT. About 30 to 80% of allo-HSCT recipients develop acute GVHD (aGVHD) and around 50% chronic GVHD (cGVHD) (4). In this context, GVHD arises when immunocompetent T cells from the donated tissue (the graft) identify the recipient (the host) as foreign. This recognition triggers an immune response that activates donor T cells, enabling them to develop cytolytic capacity and attack the recipients cells carrying foreign antigens (5). In hematological malignancies, there is a fine balance between the harmful consequences of GVHD and the therapeutic effects produced when donor lymphocytes attack recipient malignant cells, in graft versus leukemia/tumor (GVL) effect.

In aGVHD, the skin, liver or gastrointestinal tract can be affected in about 2 to 12 weeks after allo-HSCT, but there are situations when aGVHD appears before or after this interval. A cascade of events initiated by the activation of innate immune cells and subsequent tissue injury induces aGVHD, which is additionally exacerbated by the engagement of adaptive immune responses. The hallmark of aGVHD is the infiltration of activated donor T cells, predominantly CD4+ cells, into host tissues, driven by their recognition of the recipients tissues as allo-antigenic. This process results in severe inflammation that further amplifies the immune response, leading to a cytokine storm. In cytokine storm, elevated levels of circulating cytokines and immune cell hyperactivation occurs. The intricate interplay between innate and adaptive immunity during aGVHD underscores the multifaceted nature of this condition, necessitating a comprehensive understanding of the underlying immunological mechanisms for the development of effective therapeutic strategies. The dynamics of aGVHD pathogenesis, particularly the contributions of specific immune cell subsets and the cytokine storm, is crucial for both understanding the disease and for identifying new biomarkers to help early diagnosis, prognosis and targeted interventions to improve clinical outcomes.

Additionally, cGVHD can develop within 4 to 6 months post-allo-HSCT, following aGVHD or in patients without any prior complications. This condition is similar to an autoimmune disease, involving, besides donor T cells, extensive B cell activation, the release of pro-inflammatory cytokines that can affect the skin, mouth, eyes, gastrointestinal tract and the liver. The pathophysiology of cGVHD involved 3 stages (1): high production of inflammatory cytokines (interleukin-1 (IL-1), IL-6, TNF-α) and expression of antigens of the major histocompatibility complex (MHC) that stimulate antigen-presenting cells to interact with the donor T cells (2), this interaction leads to the activation of T cells which then release additional inflammatory cytokines (IL-2, Interferon- γ (INF-γ)) and (3) the migration of cytotoxic T lymphocytes and natural killer cells to specific organs, producing tissue damage (6).

GVHD is an important cause of non-relapse mortality (NRM), accounting for about 11% deaths in patients receiving allo-HSCT (7). The need for risk stratification for GVHD is high, due to problems associated with immunosuppression. It is either not aggressive enough leaving patients with a high GVHD risk vulnerable, or it is too aggressive leading to infections and other complications (3, 8).

A major concern consists in the development of tools capable of (i) timely identification of patients at risk for GVHD, (ii) invasive procedures avoidance and (iii) timely intervention, one such option could be a biomarker. Currently, there is no validated specific biomarker for GVHD. In the clinical scenario the diagnosis is confirmed through analysis of the biospecimen of the involved site.

As such, fast and organ-specific diagnosis of GVHD based on biomarkers can lead to targeted interventions, and prognosis biomarkers can assist in the process of decision making for treatment. Until recently, biomarkers were identified by hypothesis-driven approaches, considering the pathophysiologic role of specific molecules in GVHD, such as miRNAs and cellular biomarkers for GVHD (2, 9).

The aim of this paper is to review the potential candidate biomarkers derived from unbiased approaches, facilitated by the recent advancements in proteomics a robust high-throughput technique. These biomarkers may or may not have a direct pathophysiologic link to GVHD; instead, they might emerge due to the condition itself or other unexplored interactions.

2 Proteomics as the key strategy for maximizing minimally invasive biopsies towards biomarker discovery

A biomarker is defined by the Food and Drug Administration - National Institute of Health (FDA-NIH) Biomarker Working Group as "a characteristic that is measured as an indicator of normal biological processes, pathogenic ones, or a response to an exposure or intervention" (10). Biomarkers have diverse applications, guiding healthcare interventions for maximum patient advantage. They are commonly utilized for disease diagnosis, risk-based population screening, evaluating disease complications and therapy effectiveness. Furthermore, they

facilitate disease trajectory prediction, aid therapy selection, and assess novel drug effectiveness and safety. Thus, biomarkers can be diagnostic biomarkers, prognostic biomarkers and theranostic biomarkers (11).

An ideal biomarker should be easily quantifiable, allowing for simple procurement of biological specimens and employing a financially viable quantification method. It is crucial for a biomarker assay to demonstrate reproducibility, sensitivity (SEN), and specificity (SPE), providing accurate results for clinicians to make informed therapeutic decisions. The efficacy of a biomarker depends on its strong correlation with treatment responses. To establish clinical applicability, a comprehensive series of assays in both preclinical and clinical settings is necessary. Following the identification of a prospective biomarker candidate, validation processes, rigorous evaluation, and refinement through clinical investigations are conducted before approval and commercialization (11).

In the development of GVHD biomarkers, optimizing statistical test performance and determining cut points are critical. *Bidgoli et al.* (12) emphasized the importance of Receiver Operating Characteristic (ROC) curves and Area Under the Curve (AUC) in assessing assay performance. SEN and SPE, represented by ROC curves, reflect true positive and true negative rates, respectively. Positive and negative predictive values are calculated considering both cut points and GVHD incidence, with the latter being particularly relevant in HCT. Tailoring biomarker cut points for clinical use involves testing multiple values to balance intervention efficacy and toxicity. Hazard ratio (HR) is another key parameter used to gauge the impact of an intervention on a specific outcome over time. In biomarker discovery, HR helps evaluate the link between a biomarkers expression and the timing of an event, suggesting its potential as a prognostic indicator (13). Clinical trials using biomarkers for patient selection have a higher likelihood of success compared to those lacking biomarkers (14).

2.1 Proteins as a valuable biomarker source

Despite advances in genomics and technology, clinical biomarker discovery faces persistent challenges. Solely focusing on genetic abnormalities does not fully capture the complexity of disease biology, involving interactions between genetic anomalies, epigenetics, post-translational modifications, and immune responses (15). Proteins, as structural and signaling entities, are pivotal in understanding disease characteristics and serve as key drug intervention targets. Exploring the proteome, representing the entire set of proteins expressed under specific conditions, provides valuable insights into their functions, interactions, and roles in biological systems. Notably, identifying proteins and monitoring their levels in biological samples dynamically reflects the cumulative impact of genetic and epigenetic changes, crucial for understanding functional disease biology and guiding therapeutic strategies (16, 17).

Exploring biomarkers from both membrane-bound and soluble protein forms is intriguing. Membrane-bound proteins are crucial for signaling, transport, and adhesion, with changes indicating disease signatures (18). Simultaneously, measuring soluble proteins in bodily fluids offers a non-invasive and dynamic approach for biomarker discovery, providing real-time insights into physiological states. This versatile method applies across diseases, identifying diagnostic, prognostic, and therapeutic indicators. Soluble biomarkers, exemplified by soluble immune checkpoints, have emerged as dynamic molecules with significant physiological roles. The intricate network of immune checkpoints, encompassing diverse stimulatory and inhibitory pathways, plays a pivotal role in fine-tuning immune responses. Notably, molecules like Programmed Cell Death Protein 1 (PD-1), Cytotoxic T-lymphocyte associated protein 4 (CTLA4), and their ligands have emerged as focal points for anti-cancer immunotherapy, while other checkpoint pathways contribute to the immunopathogenesis of human diseases as critically analyzed by *Riva A* (19). Beyond the traditional view of membrane-bound systems, immune checkpoints also manifest as soluble forms (sCRs), actively regulating immune responses both locally and systemically. In a comprehensive review by *Niu et al.* (20), the roles of sPD-1 and sPD-L1 in cancer are explored, shedding light on their synthesis, release, and alternative mRNA splicing mechanisms. The study suggests that PD-1 may function as an immune stimulator, in contrast to its membrane-bound counterpart, while sPD-L1 retains suppressive activity. The review also proposes the intriguing idea that sCRs could act as decoy sponges for therapeutic blocking antibodies, impacting resistance to immunotherapy and disease progression. The complexity of sCR networks, disease-specific signatures, and the persistence of sCR "imprinting" post-treatment pose challenges (21–24). The articles collectively support the hypothesis that soluble isoforms of immune checkpoints may exhibit distinct functions compared to their membrane-bound counterparts. Furthermore, the existence of various isoforms for each sCR and soluble receptor-ligand complexes underscores the need for standardized measurement criteria and open comparisons of antibody clones. In conclusion, unraveling the intricacies of the sCR system holds promise for advancing both basic and translational research, providing valuable insights into their roles as disease biomarkers and potential targets for pharmacological interventions and immunotherapy. Nevertheless, analyzing both forms enhances our understanding of disease biology, supporting precision medicine. This dual approach boosts the potential for discovering robust biomarkers, influencing disease diagnosis, prognosis, and treatment (12).

2.2 Proteomics as a discovery instrument

Proteomics, an 'omics strategy, is crucial for profiling and quantifying proteins in a biospecimen under specific conditions. This involves investigating protein abundances, protein-protein interactions, and the functional roles of proteins in diverse conditions. Proteomics methodologies are classified as low-throughput and high-throughput. Low-throughput approaches include antibody-based techniques like Enzyme-Linked Immunosorbent Assay (ELISA) and Western blotting (WB), relying on antigen-antibody interactions for protein detection. Electrophoresis methods, such as two-dimensional gel

electrophoresis and sodium dodecyl-sulfate polyacrylamide gel electrophoresis (SDS-PAGE), separate proteins based on characteristics like mass, charge, or isoelectric point, followed by identification using molecular weight standards or mass spectrometry (MS). Chromatography, another separation technique, aids in isolating and purifying proteins through ion-exchange, size exclusion, and affinity chromatography. Downstream analyses, including MS, contribute to protein identification and quantification post-separation (25).

High-throughput methodologies in proteomics involve affinity binder techniques and MS. Affinity binder techniques, such as microarrays and multiplex arrays, use specific antibodies and aptamers to capture target proteins (26). Microarray research, particularly in the context of cancer and hematologic disorders, has identified candidate diagnostic biomarkers for GVHD. MS, employed in both top-down (intact protein analysis) and bottom-up (protein digestion to peptides before analysis) settings, involves ionization, separation, and detection of proteins or peptides. Ionization modes like electrospray ionization and matrix assisted laser desorption/ionization (MALDI), along with mass analyzers like time-of-flight and quadrupole, contribute to accurate protein identification, including isoforms and posttranslational modifications. MS-based protein quantification, especially with tandem MS (MS/MS), is highly accurate and relies on mass spectra matched to sequence databases (27). Best practices for protein-based biomarker discovery and validation are discussed elsewhere (28). The preferred high-throughput approaches for biomarker discovery, including those for GVHD, involve bottom-up proteomics and affinity-based methods (29). Figure 1 illustrates the advantages and disadvantages of these proteomics methods in the context of GVHD biomarker discovery. Proteomics, as a prominent 'omics technology, has witnessed significant progress, overcoming challenges and contributing to the pursuit of protein-based biomarkers for precision medicine in recent years (30).

2.3 Biomarker panels

Efficiently measuring multiple markers can be achieved through multiplexing techniques, which allow simultaneous detection of various biomolecules in a single assay. Multiplexing enhances throughput, conserves sample volume, and reduces costs compared to running individual assays for each marker. Technologies such as multiplex immunoassays, microarrays, and MS enable the detection of multiple markers within a single experimental run. Additionally, advances in high-throughput screening methods and automation contribute to efficiency by streamlining the workflow. Choosing an appropriate multiplexing platform based on the characteristics of the markers and the research objectives ensures a comprehensive and resource-effective approach to measuring multiple biomarkers simultaneously (31).

Measurements of individual candidate levels are not always relevant or specific. That is why their use in combination of multi-marker panels can bring an increase in SEN and SPE. MS based proteome studies towards biomarker discovery for GVHD accurately distinguished GVHD samples from both posttransplant non-GVHD samples and pretransplant samples. Furthermore, distinct serum proteomic signatures were identified to distinguish pretransplant from posttransplant non-GVHD samples, opening up new insights towards biomarker panel discoveries (32). For aGVHD protein-based biomarker panel discovery, saliva and plasma were the non-invasive biofluids investigated and the identified panels are further presented.

2.4 Valuable biomarker sources

Proteome analysis of biospecimens offers insights into physiological processes, aiding the identification of actionable approaches, including biomarkers applicable at the bedside. Primary sources of protein markers include tissues and body fluids such as serum, plasma, saliva, urine, and bone marrow. While bone

Methods used for proteome-based biomarker discovery


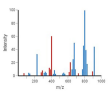
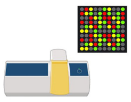

Low-throughput methods	High-throughput methods	
Enzyme-linked immunosorbent assay ELISA	Liquid chromatography coupled to mass spectrometry LC-MS	Affinity binding methods (microarrays, multiplex arrays)
advantages		
✓ high specificity ✓ low costs ✓ standardized method ✓ complex samples ✓ quantitative analysis ✓ fast ✓ can be automatized	✓ high sensitivity ✓ high throughput ✓ highly multiplex ✓ high dynamic range of peptides and proteins ✓ low amount of sample ✓ complex samples ✓ protein isoforms and post-translational modifications	✓ high sensitivity ✓ high specificity ✓ High throughput ✓ low abundance protein detection ✓ high number of proteins ✓ complex samples ✓ automatization
disadvantages		
↘ limited complexity ↘ high amount of sample ↘ unable to analyze protein isoforms and post-translational modifications	↘ high cost ↘ highly trained personnel ↘ complex data analysis	↘ detects only predefined proteins ↘ high costs ↘ unable to analyze protein isoforms and post-translational modifications

FIGURE 1
Advantages and disadvantages of methods used for proteome-based biomarker discovery studies for GVHD.

marrow provides heightened diagnostic precision, non-invasive biospecimens, like plasma and serum, present advantages in terms of patient compliance and reduced procedural risks.

Plasma and serum, being popular biofluids for biomarker discovery, offer easy acquisition and broad molecular representation due to systemic circulation. Challenges like sample standardization and accessing low-abundance proteins can impact proteomics studies, but the Human Proteome Organization (HUPO) provides Biomarker Discovery Protocols for addressing these issues (33). Tears, a non-invasive biospecimen, are gaining attention, particularly for ocular involvement in GVHD. In gastrointestinal GVHD, feces can serve as a useful biospecimen, providing insights into intestinal inflammation. Skin biopsies, obtained minimally invasively, are valuable for identifying specific biomarkers related to skin manifestations of GVHD. Urine, an alternative to blood samples, offers advantages such as ease of collection, larger quantities, and a less complex protein mixture with low abundance variation. However, its limitation lies in providing information primarily about diseases in the organs directly involved in its production and excretion, like the kidneys, rather than systemic diseases.

Proteomics, aiming to translate discoveries into clinical practice, focuses on uncovering minimally invasive biofluid-based biomarkers (34, 35). Examples of biospecimens for GVHD biomarker studies are detailed in the following sections.

3 Protein-based biomarkers for GVHD following allo-HSCT

Technological advancements have facilitated the comprehensive profiling of proteins within a given biological system. Unbiased investigations have yielded intriguing findings that might have been overlooked using narrower analytical approaches. Diverse biomarkers, when evaluated prior to BMT, play a pivotal role in the selection of suitable candidates for intervention, particularly in cases of unfavorable prognostics, resistance to chemotherapy, or heightened susceptibility to drug-induced toxicities. Furthermore, post- HSCT biomarkers offer valuable information regarding prognosis and the likelihood of complications. The diagnosis of GVHD is still dependent on clinical criteria in most of the part and requires the realization of skin biopsy, colonoscopy, bronchoscopy and bronchoalveolar lavage. aGVHD is the main cause of morbidity after transplant, being responsible for 15 to 40% of the post-transplant deaths. Mortality in GVHD is caused by the difficulty in giving a diagnosis and planning the optimal moment for therapy start (1, 36). As previously mentioned, GVHD markers can facilitate quick diagnosis of this complication and quick start of the therapy, which would increase the survival rate. Also, based on stratification biomarkers, the patients can get a more or less aggressive immunosuppressive regime reducing the costs and the long-term toxicity (34). Different strategies have been approached towards GVHD biomarker discovery targeting proteins. Strategies include single biomarker as well as multi-marker panel scouting and using different biospecimen. A comprehensive overview is further presented.

3.1 Protein based biomarkers for aGVHD

3.1.1 Cytokine-based biomarkers for aGVHD

Cytokines are important in both protection after HSCT, notably in graft-versus-leukemia and in disease, notably in GVHD. Acute GVHD is a complex pathologic process that involves many types of T-cells that secrete cytokines: Th1, Th2, TH17 and CD8+ T cells. Most cytokines associated with aGVHD include ILs, TNF-α and IFN-γ. Many cytokines are also important in the inflammatory cytokine storm that is specific to aGVHD, including the proinflammatory cytokines IL-12, IL-17, IL-21, IL-33, and the protective cytokines IL-10, IL-22, and TGF-β (37). Even more, the involvement of soluble interleukin-2 receptor (sIL-2R) in the physiopathology of GVHD has led to the development of targeted therapies with monoclonal antibodies, like daclizumab and conjugates like denileukin diftitox (38). The administration of anti-IL-6 receptor antibodies was associated to a drop in GVHD mortality (39). Thus, because of the role of cytokines in systemic inflammation during aGVHD, they were studied as potential biomarkers with diagnostic or predictive value. Mostly, they were studied from serum or plasma by employing ELISA methods. The cytokine-based biomarkers for aGVHD are presented in Table 1.

3.1.2 Other emerging protein-based biomarkers for aGVHD

In addition to cytokines, extensive research has been conducted on various protein-based biomarkers, and their promising utility as potential indicators of aGVHD is currently on the rise. The suppression of tumorigenicity 2 (ST2) is a receptor included in the IL-1 family, which binds specifically to IL-33. ST2 has two isoforms: a transmembrane (mST2) and a soluble form (sST2). During aGVHD, an increase in IL-33 has been observed, leading to specific inflammation and tissue damage (45). The sST2 receptors are expressed in different cells and act as decoy receptors, sequestering free IL-33, thereby preventing IL-33-mediated proinflammatory actions (46). Studies have found an increase of sST2 which could be correlated with GVHD severity in patients. A possible explanation given by earlier studies was that the release of sST2 in the serum occurs very late in the inflammatory response resulting in the inability of sST2 to sequester circulating IL-33. This could make sST2 an interesting biomarker for aGVHD and NRM (47). Also, *Vander Lugt et al.* found by quantitative liquid chromatography coupled with MS/MS and further ELISA validation that ST2 could be a prognostic marker for GVHD with endpoints such as treatment resistance or death 6 months after therapy, with SEN and SPE for six-month post-transplant NRM in an independent set of 70 and 64 respectively (48).

Another marker is vascular endothelial growth factor (VEGF). Studies that have evaluated the prognostic value of VEGF levels in GVHD presented with controversial results (49). Some studies have reported that high VEGF levels were associated with the development or severity of GVHD in a mouse model study (50), whereas others have found that VEGF either has a protective effect against severe aGVHD (AUC 0.69) (51) or no correlation with GVHD (52). Low VEGF levels after allo-HSCT were found to be

TABLE 1 Cytokine-based biomarkers for aGVHD.

Cytokine	Specimen	Method	Clinical relevance	SEN/SPE	Ref.
Diagnostic biomarker					
IL-7	serum	ELISA	Raised serum IL-7 at 7 to 14 days after transplant are associated with aGVHD.	86/100	(40)
sIL-7, sIL-7R	plasma	ELISA	Reduced sIL-7R levels may indicate an elevated risk of GVHD, suggesting insufficient availability for the IL-7 'buffer system. Assessing plasma sIL-7R levels, along with IL-7, could help identify individuals at higher risk for GVHD and potentially CMV infection.	–	(41)
IL-8, IFN-γ	plasma	ELISA	Reduced levels of IL-8 on day +7 and IFN-γ post-engraftment were linked to the occurrence of grade II-IV aGVHD and severe aGVHD. Additionally, decreased IFN-γ after engraftment was connected to a higher risk of NRM.	–	(42)
IL-12, IFN-γ	mononuclear cells	microbead array technology	Donor IL-12 and IFN-γ were associated with aGVHD.	IL-12: 100/50 INF-γ: 96.8%/-	(43)
Prognostic biomarker					
IL-18	serum	ELISA	Increased pre-transplant levels of free IL-18 correlated with lower risks of both NRM (HR 1.24) and overall mortality (HR 1.22) following allo-HSCT.	–	(44)

SEN, sensitivity; SPE, specificity; -, not available; CMV, Cytomegalovirus infection; HR, hazard ratio; Ref, reference.

associated with NRM due to severe exacerbation of aGVHD, implying the biomarker utility of VEGF. VEGF monitoring after allo-HSCT might identify those patients at risk of severe transplant-related mortality (53).

Another interesting molecule is T cell immunoglobulin and mucin domain 3 (TIM3). TIM3 is a transmembrane receptor protein expressed on T cells that produce IFN-gamma, Tregs, myeloid cells, natural killer cells, and mast cells, where it inhibits cytokine expression (54). Although the physiopathology concerning the involvement of TIM3 in aGVHD is not fully understood, and only preclinical studies have given hints regarding the regulation of hepatic CD8+ T cells by TIM3 (55), clinical proteomics studies have shown that the levels of the soluble extracellular domain of Tim-3 exhibited an elevation in the bloodstream of individuals preceding the clinical manifestation of aGVHD. Furthermore, these levels demonstrated a correlation with the severity of gut GVHD (AUC of 0.79) (56).

Finally, macrophage migration inhibitory factor (MIF), a pleiotropic protein, is known to participate in inflammatory and immune responses by regulating TNF-α production. Elevated peak serum MIF at acute GVHD onset and increased mean serum MIF in patients developing extensive cGVHD within 6 months suggest heightened MIF levels during active phases of both GVHD types (57).

3.1.3 Salivary protein panels for aGVHD

Towards salivary protein panel discovery, the salivary proteome was analyzed by gel electrophoresis with subsequent MS/MS analysis and ELISA. MS identified significant salivary protein fluctuations lasting at least 2 months posttransplant. High salivary levels of lactoferrin, cystatin SN, albumin and salivary amylase have been identified in patients with GVHD with oral cavity involvement. High levels of these proteins indicate pathophysiological processes that take place in GVHD with oral cavity involvement, like salivary glands infiltration, activation of immunomodulatory processes and increasing the permeability of the oral cavity mucosa and plasma extravasation (58). Also by MS, proteins from the S100 protein family was found to play a role in aGVHD diagnosis: S100A8, S100A7 and S100A9 showing SEN of 60% and SPE of 88% (59).

3.1.4 Plasma protein panels for aGVHD

Another strategy to identify biomarker panels was to screen a large set of proteins by antibody array and to validate the results by ELISA. This was done for four plasmatic diagnostic markers: IL-2-receptor-alpha (IL-2Rα), tumor-necrosis-factor-receptor-1 (TNFR1), IL-8 (IL-8), and hepatocyte growth factor (HGF). The 4 biomarkers panel confirmed their potential for diagnosis of GVHD in patients at onset of clinical symptoms and provided prognostic information independent of GVHD severity with AUC of 0.86 (60). Elafin, a skin-specific marker and regenerating islet-derived 3-α (Reg3α), a gastrointestinal tract-specific marker was added later to the 4-parameter panel. The panel was studied for its potential to discriminate between therapy responsive and nonresponsive patients and predict survival in patients receiving GVHD therapy. Even more, the 6 biomarker panel demonstrated potential to be used for early identification of patients at high or low risk for treatment non responsiveness or death, and provided opportunities for early intervention and improved survival after HSCT (61). Also in pediatric patients with aGVHD a biomarker panel of TNFR1, IL-2Rα, HGF, CCL8, IL-8 and IL-12p70 demonstrated its utility following HSCT (62). Another combination of proteins, namely a panel composed of ST2 and REG3α was found to be able to identify patients at high risk for lethal aGVHD and NRM with an AUC of 0.68, SEN of 40% and SPE of 83% (63). Including also cells to sIL-2R, a 5-parameter biomarker score based on CD4+ T cells, CD8+ T cells, CD19− CD21+ precursor B cells, CD4/CD8 T cell ratio, and sIL-2R was used to predict GVHD onset with AUC of 0.90, SEN of 88.2% and SPE of 66.7% (64). Aiming to identify and evaluate

candidate biomarkers potentially predictive of response to treatment with itacitinib plus corticosteroid in aGVHD, plasma monocyte-chemotactic protein (MCP)3, pro-calcitonin/calcitonin (ProCALCA/CALCA), REG3α, ST2, and TNFR1 were found (65).

aGVHD treatment relies on corticosteroid immunosuppression, with initial response guiding further decisions. Analysis of 507 patients from 17 Mount Sinai Acute GVHD International Consortium (MAGIC) centers revealed a validated biomarker algorithm, consisting of ST2 and REG3α measured by ELISA, predicting outcomes in steroid resistant GVHD. MAGIC biomarker probabilities after 1 week of systemic GVHD treatment outperform clinical criteria (AUC 0.82), aiding in the development of improved treatment strategies (66).

3.2 Protein based biomarkers for cGVHD

cGVHD usually starts more than 3 months after a transplant and can last for as long as a lifetime (67). Preclinical studies and translational research on human biospecimen have revealed some possible biological pathways in cGvHD. This has opened the way for the exploration of diagnostic, prognostic and predictive biomarkers in both hypothesis-driven and discovery-based testing (68). Biomarkers for cGVHD are presented in Table 2.

3.2.1 Biomarker panels for cGVHD

Besides the identification of individual biomarkers for cGVHD, efforts are being made to validate panels of biomarkers (Table 3), with a much higher accuracy of diagnosis or prognosis.

3.3 Protein based biomarkers for site-specific involvement in GVHD

Site-specific involvement represents a critical facet of GVHD and manifests in distinct anatomical regions, such as the skin, gastrointestinal tract, the eyes, and the lungs, with varying degrees of severity. The skin, often the initial site of presentation, can exhibit rashes, blistering, and itching (79). Clinical aspects of skin lesions in GVHD are illustrated in Figure 2.

Ocular symptoms of GVHD can include dry eyes, redness, and sensitivity to light. Oral symptoms of GVHD can manifest as painful mouth sores and difficulty in swallowing (80). Gastrointestinal GVHD may lead to diarrhea, abdominal pain, and even malabsorption. Liver involvement may result in elevated liver enzymes and jaundice. Cough, shortness of breath, and lung inflammation are frequent manifestations of pulmonary site involvement of GVHD (36).

Understanding the site-specific manifestations of GVHD is essential for early diagnosis and tailored treatment strategies, as the severity and response to therapy can differ significantly depending on the affected organ. In this context, site-specific involvement represents a critical aspect of managing GVHD to optimize patient outcomes, one potential option being the protein-based biomarker deciphered below.

3.3.1 Protein biomarkers of GVHD with skin involvement

Tissue biopsies can help identify useful GVHD biomarkers, that can ultimately be sought in biofluids that can be sampled in a less invasive way. For example, skin biopsies can be used for skin GHVD biomarker identification.

Elafin, also known as skin-derived antileukoprotease (SKLP), is an inhibitor of epidermic protease induced by TNF-α and identified at the level of inflamed epidermis in autoimmune diseases such as psoriasis (1, 81). *Mahabal et al.* used skin biopsies and revealed that tissue elafin could be a useful biomarker of aGVHD with skin manifestations (SEN and SPE of 100% and 75%, respectively) (82). Additionally, proteomics studies have highlighted the potential of elafin as a plasmatic biomarker for skin GVHD (83), although the results may be controversial and need further evaluation in larger patient groups (84). *Paczesny et al.* found by quantitative liquid chromatography coupled with MS and further ELISA validation that elafin exhibited increased expression in GVHD skin biopsies. Elevated plasma elafin levels at skin GVHD onset, correlating with the maximum GVHD grade, were linked to a higher mortality risk (HR 1.78). This underscores the diagnostic and prognostic significance of elafin as a biomarker for skin GVHD (85).

3.3.2 Protein biomarkers of GVHD with ocular involvement

Another non-invasive biospecimen, the tears, is in the spotlight of researchers (86, 87). In a recent study focused on cGVHD with ocular symptoms, a team of researchers identified a tear cytokine panel comprising IL-8, IL-10, IFN-γ, CXCL9, CCL17, and CCL19 as promising biomarkers for early diagnosis of ocular GVHD. Moreover, the levels of IL-10, IFN-γ, and CXCL9 were found to be indicative of the severity of ocular GVHD following allo-HSCT (AUCs > 0.6) (88). Furthermore, in a separate investigation, the prognostic role of cytokine levels in tears prior to HSCT was examined in the context of ocular cGVHD. This pilot study included 25 patients who were prospectively monitored, with 19 cytokines measured using a multiplex bead assay. A multistate model, considering four states (HSCT, systemic cGVHD, ocular cGVHD, and death), was constructed to pinpoint cytokines linked to each transition probability. Fractalkine, IL-1Rα, and IL-6 emerged as key contributors with optimal prognostic value (AUC 67% to 80%) for predicting the development of ocular cGVHD after HSCT (89). In advancing understanding of ocular GVHD, a predictive model was developed by multiplex-bead assay at the tear molecule level. Analyzing a cytokine panels correlation with clinical features, the best model, incorporating IL-8/CXCL8, IP-10/CXCL10 tear levels, age, and sex, achieved an AUC of 0.9004, with 86.36% SEN and 95.24% SPE (87). Presence and role of autoantibodies after stem-cell transplantation and their association with cGVHD was also addressed (90) and anticardiolipin antibodies high plasmatic levels have been found to correlate with cGVHD with ocular involvement (91).

10.3389/fimmu.2024.1327035

TABLE 2 Diagnostic and prognostic plasma and serum biomarkers of cGVHD.

Biomarker	Specimen	Method	Clinical relevance	SEN/ SPE	AUC	HR	Ref.
Diagnostic biomarker							
CXCL9	Plasma	antibody microarray	**CXCL9** is a significant diagnostic biomarker for cGVHD.	–	0.83	–	(69)
IL-10	Plasma	ELISA	High plasmatic levels of **IL-10** have been associated with the presence of cGVHD.	–	–	–	(70)
Fibronectin	Plasma	ELISA	The level of **plasma fibronectin**, a ligand of CD29, correlated with the number of IL-10 spot-forming cells.	–	–	–	(70)
CD29	Plasma	ELISA	**CD29** expression on monocytes in patients with active cGVHD was elevated.	–	–	–	(70)
CXCL9	Serum	ELISA	**CXCL9** predicts development of severe cGVHD.	–	–	1.33	(71)
Prognostic biomarker							
sBAFF	Plasma	ELISA	**sBAFF** were found to correlate with the severity of cGVHD, but also with the presence of autoimmune disease.	–	–	–	(72)
			sBAFF levels at the time of cGVHD diagnosis were also associated with NRM and could be potentially useful for risk stratification.	–	–	5	(73)
CD13	Plasma	ELISA	The presence of the soluble and active form of this protein in the plasma is correlated with cGVHD. Currently, the implication of **CD13** in cGVHD is being studied and the possibility that actinonin, a specific **CD13** inhibitor, can be used as therapeutic agent.	–	–	–	(74)
			High **CD163** concentration was associated with a higher cumulative incidence of *de novo*-onset cGVHD.		0.73		(75)

SEN, sensitivity; SPE, specificity; -, not available; HR, hazard ratio; Ref, reference.

TABLE 3 MS-based biomarker panels for diagnosis and prediction of cGVHD.

Biomarker panel	Specimen	Clinical relevance	Ref.
sBAFF, anti-dsDNA antibody, sIL-2Rα, and sCD13	Plasma	Useful for diagnosis, early response evaluation, disease management.	(76)
ST2, OPN, MMP3, CXCL9	Plasma	Useful for diagnosis, severity prediction, and NRM.	(77)
cGvHD_MS14 comprising 14 differentially excreted peptides, including fragments from thymosin β-4, eukaryotic translation initiation factor 4γ2, fibrinogen β-chain, or collagens.	Urine	This pattern facilitates the prediction of cGVHD with a SEN and SPE of 84% and 76%, respectively.	(78)
		When integrated with relevant clinical variables in a logistic regression model, the SEN increased to 93%.	
		Notably, cGvHD_MS14 allowed for the prediction of cGVHD up to 55 days before clinical diagnosis and did not recognize acute GvHD. Serving as an independent diagnostic criterion, this pattern showed the potential for early therapeutic intervention	

Ref, reference.

3.3.3 Protein biomarkers of GVHD with oral involvement

Because both aGVHD and cGVHD may present with oral alterations such as gingivitis, mucositis, xerostomia, mucosal atrophy, and ulcers, saliva is a target biofluid used in precision medicine approaches. Modification in salivary function is irreversible and reflects systemic GVHD, making saliva sampling and analysis a useful source of diagnostic biomarkers. Salivary proteins with potential biomarker role for oral cGVHD have been studied by MS and confirmed by ELISA or targeted label-free quantification. IL-1Rα and cystatin B distinguished oral cGVHD with a SEN of 85% and SPE of 60%. Particularly, in newly diagnosed patients assessed within 12 months of allo-HSCT, the markers exhibited enhanced discrimination (SEN 92% and SPE 73%) (92). A decline in salivary lactoperoxidase, lactotransferrin, and various proteins within the cysteine proteinase inhibitor family indicated compromised oral antimicrobial host immunity in patients with cGVHD (93). Also, high levels of lactoferrin and lactoperoxidase have been identified in the saliva of patients with GVHD with oral cavity involvement (92).

3.3.4 Protein biomarkers of GVHD with gastrointestinal involvement

GVHD with gastrointestinal involvement has been considered the major cause of morbidity, compared to all the other GVHD manifestations. Several biomarkers have been evaluated for their

10.3389/fimmu.2024.1327035

FIGURE 2
Clinical aspects of GVHD skin lesions **(A)** axillar region; **(B)** ear; **(C)** foot; **(D)** calfs; **(E)** thorax; **(F)** feet.

utility in gastrointestinal GVHD. Recently, the Reg3α has been identified as a potential biomarker for GVHD with intestinal involvement. Reg3α is a protein involved in cellular differentiation and proliferation and in defense against Gram-positive infections of the intestinal tract (1). Quantitative LC-MS analysis identified plasma Reg3α as a valuable predictor for diagnosing gastrointestinal aGVHD. Produced by Paneth cells in the gastrointestinal tract, Reg3α serves as an antimicrobial peptide with bactericidal properties against Gram-positive bacteria and antiapoptotic effects for Paneth cells (94). IL-22, secreted by lymphoid cells in the crypts of the gastrointestinal tract, stimulates Reg3α secretion. In the context of gastrointestinal GVHD, damage to the intestinal mucosa releases Reg3α into the bloodstream, making it a biomarker for gastrointestinal GVHD. Utilizing quantitative LC-MS, the predictive capability of plasma Reg3α for diagnosing gastrointestinal aGVHD was confirmed (AUC 0.80). Furthermore, combining Reg3α with clinical stage and histologic grade enhances risk stratification for patients (95).

Additionally, elevated plasma levels of TIM3, IL-6, and sTNFR1 demonstrated predictive value for the development of peak grade 3-4 GVHD (AUC 0.88). Plasma ST2 and sTNFR1 served as predictors for NRM within 1-year post-transplantation (AUC 0.90). In a landmark analysis, plasma TIM3 predicts subsequent grade 3-4 GVHD (AUC 0.76). Thus plasma levels of TIM3, sTNFR1, ST2, and IL-6 proved to be valuable in predicting more severe GVHD and NRM (96). In liver GVHD without gastrointestinal involvement, a rare occurrence (3% of GVHD patients), REG3α and HGF concentrations were elevated compared to asymptomatic patients but were like liver gastrointestinal GVHD, non-GVHD hyperbilirubinemia, and isolated skin GVHD. KRT18 concentrations were significantly higher in liver GVHD patients than in others, except those with non-GVHD liver complications. However, none of the three biomarkers effectively distinguished liver GVHD from non-GVHD liver complications. Including patients with concomitant gastrointestinal and liver involvement at GVHD onset, REG3α emerged as a stronger diagnostic biomarker for liver gastrointestinal GVHD compared to HGF and Keratin 18 (KRT18). REG3α, HGF, and KRT18 predicted day 28 nonresponse to therapy, while REG3α and HGF are good prognostic markers for 1-year NRM in liver-gastrointestinal GVHD patients (97).

The predictive value of two biomarkers, ST2 and Reg3α, in the case of NRM and GVHD, in allotransplant patients was highlighted. High concentrations of the two biomarkers tested in day 7 after transplant were associated with high GVHD related mortality and more frequent intestinal GVHD, demonstrating their usefulness in the prediction of GVHD before the clinical signs appear (63). Also, another study showed that higher levels of plasma Reg3α were found in patients with gastrointestinal-cGVHD, suggesting the utility of Reg3a as a prognostic biomarker of gastrointestinal-cGVHD (98).

Besides plasma, one more potentially useful source of biomarkers in the context of gastrointestinal GVHD is feces. Intestinal inflammation can be observed by accessing markers of leukocyte activation into the mucosa. A trial aimed to assess the dynamics of fecal biomarkers calprotectin and α1-antitrypsin (α1-AT) in GVHD. Steroid-refractory patients initially exhibited higher biomarker levels, which consistently increased throughout GVHD progression. In cortico-sensitive GvHD, calprotectin and α1-AT showed low and decreasing levels. Second-line treatment in refractory patients did not have predictive biomarker levels, but subsequent responders showed a progressive decrease in calprotectin, while non-responders maintained high levels. α1-AT values had a weaker correlation with treatment response, remaining elevated in both non-responders and responders. Monitoring calprotectin levels proved to be beneficial in managing immunosuppressive treatment for gastrointestinal GVHD (99). While there was a noticeable trend towards elevated serum calprotectin levels in GVHD development and gut involvement, statistical significance was not achieved, unlike fecal calprotectin. Therefore, fecal calprotectin, rather than serum calprotectin, may be considered a potential biomarker for gut GVHD as shown by *Metafuni et al.* (100).

3.3.5 Protein biomarkers of GVHD with pulmonary involvement

Pulmonary cGVHD can present with obstructive and/or restrictive disease. Severity ranges from subclinical pulmonary

impairment to respiratory insufficiency with bronchiolitis obliterans, a feature of pulmonary cGVHD. Early diagnosis may improve clinical outcome, and regular post-transplant follow-ups are recommended (101).

In recent proteomics studies, regulatory proteins of the extracellular matrix have been identified as candidate biomarkers for the diagnostic and prognosis of bronchiolitis obliterans syndrome (BOS) and GVHD with pulmonary involvement. Plasmatic levels of matrix metalloproteinase 3 (MMP3) have been associated with the presence of BOS and could be correlated with disease severity (102). In another study, the diagnostic value of the lead candidate, MMP3, was evaluated by ELISA in plasma and was found to differ significantly between patients with and without BOS (AUC 0.77) (102). Moreover, in another study, the specific BOS biomarker potential of osteopontin (OPN) was explored in patients with cGVHD. Using immunohistochemistry, *Williams et al.* showed that elevated OPN plasma levels observed in patients with BOS, potentially originating from alveolar macrophages, correlated with disease severity. These findings, supported by lung immunohistochemistry, could be valuable for diagnosing and prognosing BOS after HSCT (103).

4 Conclusions

In summary, the exploration of protein-based biomarkers for GVHD post-allo-HSCT is crucial for improving diagnostic accuracy and treatment outcomes. Proteomics, with its ability to increase the potential of minimally invasive biopsies, serves as a powerful strategy for biomarker discovery by analyzing intricate protein profiles. Proteins, ranging from cytokines to emerging candidates, play a pivotal role as valuable biomarker sources. The strategies outlined, such as focusing on cytokine-based biomarkers, emerging protein-based markers, and biomarker panels for acute and chronic GVHD, as well as for site specific involvement of GVHD, offer a roadmap for future research, promising improved diagnostic precision and personalized treatment approaches. Nevertheless, the existing literature on GVHD protein-based biomarkers is characterized by substantial heterogeneity in reports, a lack of standardized study protocols, and inconsistent inclusion of patients. This heterogeneity and variability in methodology represent significant challenges that contribute to the observed disparity between the multitude of promising biomarkers identified in individual studies and the limited number of biomarkers poised for clinical translation. Consequently, the immediate focus may not solely be on the discovery of novel molecules and pathways, but rather on the critical task of validating or exposing the efficacy of existing methods. Addressing these challenges is imperative for bridging the gap between bench side research and clinical application in the near term.

However, the integration of proteomics into GVHD research not only enhances our understanding of the disease but also positions us at the forefront of transformative advancements in clinical practice. Collaborative efforts and technological advancements in proteomic analysis are essential for realizing the full potential of protein-based biomarkers, paving the way for a future where GVHD diagnosis and treatment are increasingly personalized and effective.

Author contributions

MI: Writing – original draft, Writing – review & editing. CP: Writing – original draft, Writing – review & editing. AU: Writing – original draft, Writing – review & editing. CM: Writing – original draft, Writing – review & editing. DC: Writing – original draft, Writing – review & editing. MZ: Writing – original draft, Writing – review & editing. AT: Writing – original draft, Writing – review & editing. JB: Writing – original draft, Writing – review & editing. VG: Writing – original draft, Writing – review & editing. MC: Writing – original draft, Writing – review & editing. CI: Writing – original draft, Writing – review & editing, Conceptualization, Formal analysis, Funding acquisition, Resources, Supervision. CT: Writing – original draft, Writing – review & editing, Conceptualization, Formal analysis, Resources, Supervision. DT: Writing – original draft, Writing – review & editing, Conceptualization, Formal analysis, Supervision.

Funding

The author(s) declare that no financial support was received for the research, authorship, and/or publication of this article.

Acknowledgments

Continuous Flow Interchange of Communication and Knowledge in Biomedical 533 University Research—FLOW", No. 21-COP-0034.

Conflict of interest

The authors declare that the research was conducted in the absence of any commercial or financial relationships that could be construed as a potential conflict of interest.

Publisher's note

References

1. Ahmed SS, Wang XN, Norden J, Pearce K, El-Gezawy E, Atarod S, et al. Identification and validation of biomarkers associated with acute and chronic graft versus host disease. *Bone Marrow Transplant*. (2015) 50:1563–71. doi: 10.1038/bmt.2015.191

2. He FC, Holtan SG. Biomarkers in graft-versus-host disease: from prediction and diagnosis to insights into complex graft/host interactions. *Curr Hematol Malig Rep*. (2018) 13:44–52. doi: 10.1007/s11899-018-0433-2

3. Lee CJ, Wang T, Chen K, Arora M, Brazauskas R, Spellman SR, et al. Severity of chronic graft-versus-host disease and late effects following allogeneic hematopoietic cell transplantation for adults with hematologic Malignancy. *Transplant Cell Ther* (2023) 30(1):97.E1–97.E14. doi: 10.1016/j.jtct.2023.10.010

4. Jacobsohn DA, Vogelsang GB. Acute graft versus host disease. *Orphanet J Rare Dis*. (2007) 2:35. doi: 10.1186/1750-1172-2-35

5. Zeiser R, Blazar BR. Acute graft-versus-host disease — Biologic process, prevention, and therapy. *N Engl J Med*. (2017) 377:2167–79. doi: 10.1056/NEJMra1609337

6. Zeiser R, Blazar BR. Pathophysiology of chronic graft-versus-host disease and therapeutic targets. *N Engl J Med*. (2017) 377:2565–79. doi: 10.1056/NEJMra1703472

7. Presland RB. Application of proteomics to graft-versus-host disease: from biomarker discovery to potential clinical applications. *Expert Rev Proteomics*. (2017) 14:997–1006. doi: 10.1080/14789450.2017.1388166

8. Konuma T, Matsuda K, Shimomura Y, Tanoue S, Sugita J, Inamoto Y, et al. Effect of graft-versus-host disease on post-transplantation outcomes following single cord blood transplantation compared with haploidentical transplantation with post-transplantation cyclophosphamide for adult acute myeloid leukemia. *Transplant Cell Ther*. (2023) 29:365. doi: 10.1016/j.jtct.2023.03.001.

9. Tomuleasa C, Fuji S, Cucuianu A, Kapp M, Pileczki V, Petrushev B, et al. MicroRNAs as biomarkers for graft-versus-host disease following allogeneic stem cell transplantation. *Ann Hematol*. (2015) 94:1081–92. doi: 10.1007/s00277-015-2369-0

10. FDA-NIH Biomarker Working Group. *BEST (Biomarkers, EndpointS, and other Tools) Resource [Internet]*. Silver Spring (MD): Food and Drug Administration (US) (2016). Available from: https://www.ncbi.nlm.nih.gov/books/NBK326791/ Co-published by National Institutes of Health (US), Bethesda (MD).

11. Bravo-Merodio L, Acharjee A, Russ D, Bisht V, Williams JA, Tsaprouni LG, et al. Chapter Four - Translational biomarkers in the era of precision medicine. In: *Makowski GSBT-A in CC*. Amsterdam, The Netherlands: Elsevier (2021). p. 191–232. Available at: https://www.sciencedirect.com/science/article/pii/S0065242320300913.

12. Bidgoli A, DePriest BP, Saatloo MV, Jiang H, Fu D, Paczesny S. Current definitions and clinical implications of biomarkers in graft-versus-host disease. *Transplant Cell Ther*. (2022) 28:657–66. doi: 10.1016/j.jtct.2022.07.008

13. Spruance SL, Reid JE, Grace M, Samore M. Hazard ratio in clinical trials. *Antimicrob Agents Chemother*. (2004) 48:2787–92. doi: 10.1128/AAC.48.8.2787-2792.2004.

14. Wong CH, Siah KW, Lo AW. Estimation of clinical trial success rates and related parameters. *Biostatistics [Internet]*. (2019) 20:273–86. doi: 10.1093/biostatistics/kxx069

15. Wang J, Ma Z, Carr SA, Mertins P, Zhang H, Zhang Z, et al. Proteome profiling outperforms transcriptome profiling for coexpression based gene function prediction. *Mol Cell Proteomics*. (2017) 16:121–34. doi: 10.1074/mcp.M116.060301.

16. DAdamo GL, Widdop JT, Giles EM. The future is now? Clinical and translational aspects of "Omics" technologies. *Immunol Cell Biol*. (2021) 99:168–76. doi: 10.1111/imcb.12404

17. Qian L, Dima D, Berce C, Liu Y, Rus I, Raduly L-Z, et al. Protein dysregulation in graft versus host disease. *Oncotarget*. (2018) 9:1483–91. doi: 10.18632/oncotarget.v9i1.

18. Varady G, Cserepes J, Nemeth A, Szabo E, Sarkadi B. Cell surface membrane proteins as personalized biomarkers: where we stand and where we are headed. *biomark Med*. (2013) 7:803–19. doi: 10.2217/bmm.13.90.

19. Riva A. Editorial: Soluble immune checkpoints: Novel physiological immunomodulators. *Front Immunol*. (2023) 14:1178541. doi: 10.3389/fimmu.2023.1178541

20. Khan M, Zhao Z, Arooj S, Fu Y, Liao G. Soluble PD-1: predictive, prognostic, and therapeutic value for cancer immunotherapy. *Front Immunol*. (2020) 11:587460. doi: 10.3389/fimmu.2020.587460

21. Landeira-Vinuela A, Arias-Hidalgo C, Juanes-Velasco P, Alcoceba M, Navarro-Bailon A, Pedreira CE, et al. Unravelling soluble immune checkpoints in chronic lymphocytic leukemia: Physiological immunomodulators or immune dysfunction. *Front Immunol*. (2022) 13:965905. doi: 10.3389/fimmu.2022.965905

22. Wang Q, He Y, Li W, Xu X, Hu Q, Bian Z, et al. Soluble immune checkpoint-related proteins in blood are associated with invasion and progression in non-small cell lung cancer. *Front Immunol*. (2022) 13:887916. doi: 10.3389/fimmu.2022.887916

23. Noubissi Nzeteu GA, Schlichtner S, David S, Ruppenstein A, Fasler-Kan E, Raap U, et al. Macrophage differentiation and polarization regulate the release of the immune checkpoint protein V-domain ig suppressor of T cell activation. *Front Immunol*. (2022) 13:837097. doi: 10.3389/fimmu.2022.837097

24. Li W, Syed F, Yu R, Yang J, Xia Y, Relich RF, et al. Soluble immune checkpoints are dysregulated in COVID-19 and heavy alcohol users with HIV infection. *Front Immunol*. (2022) 13:833310. doi: 10.3389/fimmu.2022.833310

25. Cui M, Cheng C, Zhang L. High-throughput proteomics: a methodological mini-review. *Lab Investig [Internet]*. (2022) 102:1170–81. doi: 10.1038/s41374-022-00830-7

26. Chen G, Yang L, Liu G, Zhu Y, Yang F, Dong X, et al. Research progress in protein microarrays: Focussing on cancer research. *Proteomics Clin Appl*. (2023) 17:2200036. doi: 10.1002/prca.202200036

27. Marcus K, Eisenacher M, Sitek B. *Quantitative methods in proteomics*. Humana New York, NY: Springer Nature (2021). p. 2228. doi: 10.1007/978-1-0716-1024-4.

28. Nakayasu ES, Gritsenko M, Piehowski PD, Gao Y, Orton DJ, Schepmoes AA, et al. Tutorial: best practices and considerations for mass-spectrometry-based protein biomarker discovery and validation. *Nat Protoc [Internet]*. (2021) 16:3737–60. doi: 10.1038/s41596-021-00566-6

29. Bader JM, Albrecht V, Mann M. MS-based proteomics of body fluids: the end of the beginning. *Mol Cell Proteomics*. (2023) 22:100577. doi: 10.1016/j.mcpro.2023.100577

30. Mundt F, Albrechtsen NJW, Mann SP, Treit P, Ghodgaonkar-Steger M, OFlaherty M, et al. Foresight in clinical proteomics: current status, ethical considerations, and future perspectives. *Open Res Eur*. (2023) 3:59. doi: 10.12688/openreseurope.

31. Van Gool A, Corrales F, Colović M, Krstić D, Oliver-Martos B, Martinez-Caceres E, et al. Analytical techniques for multiplex analysis of protein biomarkers. *Expert Rev Proteomics*. (2020) 17:257–73. doi: 10.1080/14789450.2020.1763174

32. Srinivasan R, Daniels J, Fusaro V, Lundqvist A, Killian JK, Geho D, et al. Accurate diagnosis of acute graft-versus-host disease using serum proteomic pattern analysis. *Exp Hematol*. (2006) 34:796–801. doi: 10.1016/j.exphem.2006.02.013

33. Deutsch EW, Vizcaino JA, Jones AR, Binz P-A, Lam H, Klein J, et al. Proteomics standards initiative at twenty years: current activities and future work. *J Proteome Res*. (2023) 22:287–301. doi: 10.1021/acs.jproteome.2c00637

34. Paczesny S. Discovery and validation of graft-versus-host disease biomarkers. *Blood*. (2013) 121:585–94. doi: 10.1182/blood-2012-08-355990

35. Dayon L, Cominetti O, Affolter M. Proteomics of human biological fluids for biomarker discoveries: technical advances and recent applications. *Expert Rev Proteomics*. (2022) 19:131–51. doi: 10.1080/14789450.2022.2070477

36. Logan BR, Fu D, Howard A, Fei M, Kou J, Little MR, et al. Validated graft-specific biomarkers identify patients at risk for chronic graft-versus-host disease and death. *J Clin Invest*. (2023) 133:e168575. doi: 10.1172/JCI168575.

37. Kumar S, Mohammadpour H, Cao X. Targeting cytokines in GVHD therapy. *J Immunol Res Ther*. (2017) 2:90–9.

38. Shen M-Z, Li J-X, Zhang X-H, Xu L-P, Wang Y, Liu K-Y, et al. Meta-analysis of interleukin-2 receptor antagonists as the treatment for steroid-refractory acute graft-versus-host disease. *Front Immunol*. (2021) 12:749266. doi: 10.3389/fimmu.2021.749266

39. Tvedt THA, Ersvaer E, Tveita AA, Bruserud Ø. Interleukin-6 in allogeneic stem cell transplantation: its possible importance for immunoregulation and as a therapeutic target *Front Immunol*. (2017) 8:667. doi: 10.3389/fimmu.2017.00667

40. Dean RM, Fry T, Mackall C, Steinberg SM, Hakim F, Fowler D, et al. Association of serum interleukin-7 levels with the development of acute graft-versus-host disease. *J Clin Oncol Off J Am Soc Clin Oncol*. (2008) 26:5735–41. doi: 10.1200/JCO.2008.17.1314.

41. Poiret T, Rane L, Remberger M, Omazic B, Gustafsson-Jernberg A, Vudattu NK, et al. Reduced plasma levels of soluble interleukin-7 receptor during graft-versus-host disease (GVHD) in children and adults. *BMC Immunol*. (2014) 15:25. doi: 10.1186/1471-2172-15-25

42. Pirogova OV, Moiseev IS, Surkova EA, Lapin SV, Bondarenko SN, Kulagin AD, et al. Profiles of pro-inflammatory cytokines in allogenic stem cell transplantation with post-transplant cyclophosphamide. *Cytokine*. (2017) 99:148–53. doi: 10.1016/j.cyto.2017.08.016.

43. Kamel AM, Elsharkawy NM, Abdelfattah EK, Abdelfattah R, Samra MA, Wallace P, et al. IL12 and IFNγ secretion by donor mononuclear cells in response to host antigens may predict acute GVHD after HSCT. *Immunobiology*. (2019) 224:659–65. doi: 10.1016/j.imbio.2019.07.001.

44. Radujkovic A, Kordelas L, Dai H, Schult D, Majer-Lauterbach J, Beelen D, et al. Interleukin-18 and outcome after allogeneic stem cell transplantation: A retrospective cohort study. *eBioMedicine*. (2019) 49:202–12. doi: 10.1016/j.ebiom.2019.10.024

45. Liew FY, Pitman NI, McInnes IB. Disease-associated functions of IL-33: the new kid in the IL-1 family. *Nat Rev Immunol*. (2010) 10:103–10. doi: 10.1038/nri2692.

46. Ito S, Barrett AJ. ST2: the biomarker at the heart of GVHD severity. *Blood*. (2015) 125:10–1. doi: 10.1182/blood-2014-11-611780.

47. Miyazaki T, Matsumura A, Tachibana T, Ando T, Koyama M, Koyama S, et al. Predictive values of early ST2 for acute graft-versus-host disease and transplant-related complications after allogeneic stem cell transplantation. *Blood*. (2019) 134:1976. doi: 10.1182/blood-2019-123262

48. Vander Lugt MT, Braun TM, Hanash S, Ritz J, Ho VT, Antin JH, et al. ST2 as a marker for risk of therapy-resistant graft-versus-host disease and death. *N Engl J Med*. (2013) 369:529–39. doi: 10.1056/NEJMoa1213299

49. Azarpira N, Dehghani M, Darai M. The interleukin-6 and vascular endothelial growth factor in hematopoietic stem cell transplantation. *Saudi J Kidney Dis Transplant an Off Publ Saudi Cent Organ Transplantation Saudi Arab*. (2012) 23:521–5.

50. Riesner K, Shi Y, Jacobi A, Krater M, Kalupa M, McGearey A, et al. Initiation of acute graft-versus-host disease by angiogenesis. *Blood*. (2017) 129:2021–32. doi: 10.1182/blood-2016-08-736314

51. Holtan SG, Verneris MR, Schultz KR, Newell LF, Meyers G, He F, et al. Circulating angiogenic factors associated with response and survival in patients with acute graft-versus-host disease: results from blood and marrow transplant clinical trials network 0302 and 0802. *Biol Blood Marrow Transplant*. (2015) 21:1029–36. doi: 10.1016/j.bbmt.2015.02.018

52. Souza LN, Carneiro MA, De Azevedo WM, Gomez RS. Vascular endothelial growth factor (VEGF) and chronic graft-versus-host disease (cGVHD) in salivary glands of bone marrow transplant (BMT) recipients. *J Oral Pathol Med*. (2004) 33:13–6. doi: 10.1111/j.1600-0714.2004.00035.x

53. Min C-K, Kim SY, Lee MJ, Eom KS, Kim YJ, Kim HJ, et al. Vascular endothelial growth factor (VEGF) is associated with reduced severity of acute graft-versus-host disease and nonrelapse mortality after allogeneic stem cell transplantation. *Bone Marrow Transplant*. (2006) 38:149–56. doi: 10.1038/sj.bmt.1705410

54. Banerjee H, Kane LP. Immune regulation by tim-3. *F1000Research*. (2018) 7:316. doi: 10.12688/f1000research.

55. Oikawa T, Kamimura Y, Akiba H, Yagita H, Okumura K, Takahashi H, et al. Preferential involvement of Tim-3 in the regulation of hepatic CD8+ T cells in murine acute graft-versus-host disease. *J Immunol*. (2006) 177:4281–7. doi: 10.4049/jimmunol.177.7.4281.

56. Hansen JA, Hanash SM, Tabellini L, Baik C, Lawler RL, Grogan BM, et al. A novel soluble form of Tim-3 associated with severe graft-versus-host disease. *Biol Blood marrow Transplant J Am Soc Blood Marrow Transplant*. (2013) 19:1323–30. doi: 10.1016/j.bbmt.2013.06.011.

57. Toubai T, Shono Y, Nishihira J, Ibata M, Suigita J, Kato N, et al. Serum macrophage migration inhibitory factor (MIF) levels after allogeneic hematopoietic stem cell transplantation. *Int J Lab Hematol*. (2009) 31:161–8. doi: 10.1111/j.1751-553X.2007.01016.x.

58. Imanguli MM, Atkinson JC, Harvey KE, Hoehn GT, Ryu OH, Wu T, et al. Changes in salivary proteome following allogeneic hematopoietic stem cell transplantation. *Exp*. (2007) 35:184–92. doi: 10.1016/j.exphem.2006.10.009

59. Chiusolo P, Giammarco S, Fanali C, Bellesi S, Metafuni E, Sica S, et al. Salivary Proteomic Analysis and Acute Graft-versus-Host Disease after Allogeneic Hematopoietic Stem Cell Transplantation. *Biol Blood Marrow Transplant*. (2013) 19:888–92. doi: 10.1016/j.bbmt.2013.03.011

60. Paczesny S, Krijanovski OI, Braun TM, Choi SW, Clouthier SG, Kuick R, et al. A biomarker panel for acute graft-versus-host disease. *Blood*. (2009) 113:273–8. doi: 10.1182/blood-2008-07-167098

61. Levine JE, Logan BR, Wu J, Alousi AM, Bolanos-Meade J, Ferrara JLM, et al. Acute graft-versus-host disease biomarkers measured during therapy can predict treatment outcomes: a Blood and Marrow Transplant Clinical Trials Network study. *Blood*. (2012) 119:3854–60. doi: 10.1182/blood-2012-01-403063

62. Berger M, Signorino E, Muraro M, Quarello P, Biasin E, Nesi F, et al. Monitoring of TNFR1, IL-2Rα, HGF, CCL8, IL-8 and IL-12p70 following HSCT and their role as GVHD biomarkers in paediatric patients. *Bone Marrow Transplant*. (2013) 48:1230–6. doi: 10.1038/bmt.2013.41.

63. Hartwell MJ, Ozbek U, Holler E, Renteria AS, Major-Monfried H, Reddy P, et al. An early-biomarker algorithm predicts lethal graft-versus-host disease and survival. *JCI Insight*. (2017) 2:e89798. doi: 10.1172/jci.insight.89798.

64. Budde H, Papert S, Maas J-H, Reichardt HM, Wulf G, Hasenkamp J, et al. Prediction of graft-versus-host disease: a biomarker panel based on lymphocytes and cytokines. *Ann Hematol*. (2017) 96:1127–33. doi: 10.1007/s00277-017-2999-5

65. Pratta M, Paczesny S, Socie G, Barkey N, Liu H, Owens S, et al. A biomarker signature to predict complete response to itacitinib and corticosteroids in acute graft-versus-host disease. *Br J Haematol*. (2022) 198:729–39. doi: 10.1111/bjh.18300.

66. Major-Monfried H, Renteria AS, Pawarode A, Reddy P, Ayuk F, Holler E, et al. MAGIC biomarkers predict long-term outcomes for steroid-resistant acute GVHD. *Blood*. (2018) 131:2846–55. doi: 10.1182/blood-2018-01-822957.

67. Presland RB.Biology of chronic graft-vs-host disease: Immune mechanisms and progress in biomarker discovery. *World J Transplant*. (2016) 6:608–19. doi: 10.5500/wjt.v6.i4.608.

68. Wolff D, Greinix H, Lee SJ, Gooley T, Paczesny S, Pavletic S, et al. Biomarkers in chronic graft-versus-host disease: quo vadis? *Bone Marrow Transplant*. (2018) 53:832–7. doi: 10.1038/s41409-018-0092-x

69. Kitko CL, Levine JE, Storer BE, Chai X, Fox DA, Braun TM, et al. Plasma CXCL9 elevations correlate with chronic GVHD diagnosis. *Blood [Internet]*. (2014) 123:786–93. doi: 10.1182/blood-2013-08-520072

70. Hirayama M, Azuma E, Nakagawa-Nakazawa A, Kumamoto T, Iwamoto S, Amano K, et al. Interleukin-10 spot-forming cells as a novel biomarker of chronic graft-versus-host disease. *Haematologica*. (2013) 98:41–9. doi: 10.3324/haematol.2012.069815.

71. Giesen N, Schwarzbich M-A, Dischinger K, Becker N, Hummel M, Benner A, et al. CXCL9 predicts severity at the onset of chronic graft-versus-host disease. *Transplantation*. (2020) 104:2354–9. doi: 10.1097/TP.0000000000003108.

72. Sarantopoulos S, Stevenson KE, Kim HT, Bhuiya NS, Cutler CS, Soiffer RJ, et al. High levels of B-cell activating factor in patients with active chronic graft-versus-host disease. *Clin Cancer Res an Off J Am Assoc Cancer Res*. (2007) 13:6107–14. doi: 10.1158/1078-0432.CCR-07-1290.

73. Saliba RM, Sarantopoulos S, Kitko CL, Pawarode A, Goldstein SC, Magenau J, et al. B-cell activating factor (BAFF) plasma level at the time of chronic GvHD diagnosis is a potential predictor of non-relapse mortality. *Bone Marrow Transplant*. (2017) 52:1010–5. doi: 10.1038/bmt.2017.73

74. Cuvelier GDE, Kariminia A, Fujii H, Aslanian S, Wall D, Goldman F, et al. Anti-CD13 Abs in children with extensive chronic GVHD and their relation to soluble CD13 after allogeneic blood and marrow transplantation from a Childrens Oncology Groups Study, ASCT0031. *Bone Marrow Transplant*. (2010) 45:1653–7. doi: 10.1038/bmt.2010.15.

75. Inamoto Y, Martin PJ, Paczesny S, Tabellini L, Momin AA, Mumaw CL, et al. Association of plasma CD163 concentration with *de novo*-onset chronic graft-versus-host disease. *Biol Blood marrow Transplant J Am Soc Blood Marrow Transplant*. (2017) 23:1250–6. doi: 10.1016/j.bbmt.2017.04.019.

76. Fujii H, Cuvelier G, She K, Aslanian S, Shimizu H, Kariminia A, et al. Biomarkers in newly diagnosed pediatric-extensive chronic graft-versus-host disease: a report from the Childrens Oncology Group. *Blood*. (2008) 111:3276–85. doi: 10.1182/blood-2007-08-106286

77. Yu J, Storer BE, Kushekhar K, Abu Zaid M, Zhang Q, Gafken PR, et al. Biomarker panel for chronic graft-versus-host disease. *J Clin Oncol*. (2016) 34:2583–90. doi: 10.1200/JCO.2015.65.9615

78. Weissinger EM, Human C, Metzger J, Hambach L, Wolf D, Greinix HT, et al. The proteome pattern cGvHD_MS14 allows early and accurate prediction of chronic GvHD after allogeneic stem cell transplantation. *Leukemia [Internet]*. (2017) 31:654–62. doi: 10.1038/leu.2016.259

79. Hong J, Fraebel J, Yang Y, Tkacyk E, Kitko C, Kim TK. Understanding and treatment of cutaneous graft-versus-host-disease. *Bone Marrow Transplant*. (2023) 58, 1298–313. doi: 10.1038/s41409-023-02109-x.

80. Cheng X, Huang R, Huang S, Fan W, Yuan R, Wang X, et al. Recent advances in ocular graft-versus-host disease. *Front Immunol*. (2023) 14:1092108. doi: 10.3389/fimmu.2023.1092108.

81. Qian L, Wu Z, Shen J. Advances in the treatment of acute graft-versus-host disease. *J Cell Mol Med*. (2013) 17:966–75. doi: 10.1111/jcmm.12093

82. Mahabal GD, George L, Peter D, Bindra M, Thomas M, Srivastava A, et al. Utility of tissue elafin as an immunohistochemical marker for diagnosis of acute skin graft-versus-host disease: a pilot study. *Clin Exp Dermatol*. (2019) 44:161–8. doi: 10.1111/ced.13678

83. Paczesny S, Levine JE, Hogan J, Crawford J, Braun T, Wang H, et al. Elafin is a biomarker of graft versus host disease of the skin. *Blood*. (2008) 112:716. doi: 10.1182/blood.V112.11.716.716

84. George L, Mahabal G, Mohanan E, Balasubramanian P, Peter D, Pulimood S, et al. Limited utility of plasma elafin as a biomarker for skin graft-versus-host disease following allogeneic stem cell transplantation. *Clin Exp Dermatol*. (2021) 46:1482–7. doi: 10.1111/ced.14785

85. Paczesny S, Braun TM, Levine JE, Hogan J, Crawford J, Coffing B, et al. Elafin is a biomarker of graft-versus-host disease of the skin. *Sci Transl Med*. (2010) 2:13ra2–2. doi: 10.1126/scitranslmed.3000406

86. Jung JW, Han SJ, Song MK, Kim T-I, Kim EK, Min YH, et al. Tear cytokines as biomarkers for chronic graft-versus-host disease. *Biol Blood marrow Transplant J Am Soc Blood Marrow Transplant*. (2015) 21:2079–85. doi: 10.1016/j.bbmt.2015.08.020.

87. Cocho L, Fernandez I, Calonge M, Martinez V, Gonzalez-Garcia MJ, Caballero D, et al. Biomarkers in ocular chronic graft versus host disease: tear cytokine- and chemokine-based predictive model. *Invest Ophthalmol Vis Sci*. (2016) 57:746–58. doi: 10.1167/iovs.15-18615

88. Cheng X, Huang R, Fan W, Huang S, Zeng L, Wu T, et al. The tear cytokine panel is a useful biomarker for early diagnosis and severity-evaluating of ocular chronic graft-versus-host disease. *Bone Marrow Transplant [Internet]*. (2023) 58:732–4. doi: 10.1038/s41409-023-01952-2

89. Cocho L, Fernandez I, Calonge M, Sainz de la Maza M, Rovira M, Stern ME, et al. Prehematopoietic stem cell transplantation tear cytokines as potential susceptibility biomarkers for ocular chronic graft-versus-host disease. *Invest Ophthalmol Vis Sci*. (2017) 58:4836–46. doi: 10.1167/iovs.17-21670.

90. Wechalekar A, Cranfield T, Sinclair D, Ganzckowski M. Occurrence of autoantibodies in chronic graft vs. host disease after allogeneic stem cell transplantation. *Clin Lab Haematol*. (2005) 27:247–9. doi: 10.1111/j.1365-2257.2005.00699.x

91. Quaranta S, Shulman H, Ahmed A, Shoenfeld Y, Peter J, McDonald GB, et al. Autoantibodies in human chronic graft-versus-host disease after hematopoietic cell transplantation. *Clin Immunol*. (1999) 91:106–16. doi: 10.1006/clim.1998.4666.

92. Devic I, Shi M, Schubert MM, Lloid M, Izutsu KT, Pan C, et al. Proteomic analysis of saliva from patients with oral chronic graft-versus-host disease. *Biol Blood Marrow Transplant*. (2014) 20:1048–55. doi: 10.1016/j.bbmt.2014.03.031

93. Bassim CW, Ambatipudi KS, Mays JW, Edwards DA, Swatkoski S, Fassil H, et al. Quantitative salivary proteomic differences in oral chronic graft-versus-host disease. *J Clin Immunol*. (2012) 32:1390–9. doi: 10.1007/s10875-012-9738-4

94. Shin JH, Seeley RJ. Reg3 proteins as gut hormones? *Endocrinology*. (2019) 160:1506–14. doi: 10.1210/en.2019-00073

95. Ferrara JLM, Harris AC, Greenson JK, Braun TM, Holler E, Teshima T, et al. Regenerating islet-derived 3-alpha is a biomarker of gastrointestinal graft-versus-host disease. *Blood*. (2011) 118:6702–8. doi: 10.1182/blood-2011-08-375006

96. McDonald GB, Tabellini L, Storer BE, Lawler RL, Martin PJ, Hansen JA. Plasma biomarkers of acute GVHD and nonrelapse mortality: predictive value of measurements before GVHD onset and treatment. *Blood*. (2015) 126:113–20. doi: 10.1182/blood-2015-03-636753

97. Harris AC, Ferrara JLM, Braun TM, Holler E, Teshima T, Levine JE, et al. Plasma biomarkers of lower gastrointestinal and liver acute GVHD. *Blood*. (2012) 119:2960–3. doi: 10.1182/blood-2011-10-387357.

98. DePriest BP, Li H, Bidgoli A, Onstad L, Couriel D, Lee SJ, et al. Regenerating islet-derived protein 3-α is a prognostic biomarker for gastrointestinal chronic graft-versus-host disease. *Blood Adv*. (2022) 6:2981–6. doi: 10.1182/bloodadvances.2021005420

99. OMeara A, Kapel N, Xhaard A, Sicre de Fontbrune F, Manene D, Dhedin N, et al. Fecal calprotectin and α1-antitrypsin dynamics in gastrointestinal GvHD. *Bone Marrow Transplant*. (2015) 50:1105–9. doi: 10.1038/bmt.2015.109

100. Metafuni E, Giammarco S, De Ritis DG, Rossi M, De Michele T, Zuppi C, et al. Fecal but not serum calprotectin is a potential marker of GVHD after stem cell transplantation. *Ann Hematol*. (2017) 96:929–33. doi: 10.1007/s00277-017-2974-1

101. Hildebrandt GC, Fazekas T, Lawitschka A, Bertz H, Greinix H, Halter J, et al. Diagnosis and treatment of pulmonary chronic GVHD: report from the consensus conference on clinical practice in chronic GVHD. *Bone Marrow Transplant*. (2011) 46:1283–95. doi: 10.1038/bmt.2011.35

102. Liu X, Yue Z, Yu J, Daguindau E, Kushekhar K, Zhang Q, et al. Proteomic characterization reveals that MMP-3 correlates with bronchiolitis obliterans syndrome following allogeneic hematopoietic cell and lung transplantation. *Am J Transplant*. (2016) 16:2342–51. doi: 10.1111/ajt.13750

103. Williams KM, Hakim FT, Rosenberg A, Kleiner D, Mitchell SA, Tamm M, et al. Plasma Osteopontin Is a Biomarker Specifically Associated with Bronchiolitis Obliterans Syndrome after HCT. *Biol Blood Marrow Transplant*. (2016) 22:S417–8. doi: 10.1016/j.bbmt.2015.11.955

frontiers | Frontiers in Pharmacology

TYPE Original Research
PUBLISHED 10 May 2024
DOI 10.3389/fphar.2024.1382399

OPEN ACCESS

EDITED BY
Susheel Kumar Nethi,
Iowa State University, United States

REVIEWED BY
Ketki Bhise,
Biotech Industry, United States
Suresh Kumar Gulla,
University of Oklahoma Health Sciences Center, United States

*CORRESPONDENCE
Diana Gulei,
diana.c.gulei@gmail.com
Ciprian Tomuleasa,
ciprian.tomuleasa@umfcluj.ro
Sanda Boca,
sanda.boca@ubbcluj.ro

†These authors have contributed equally to this work

RECEIVED 05 February 2024
ACCEPTED 18 April 2024
PUBLISHED 10 May 2024

CITATION
Munteanu R-A, Tigu AB, Feder R, Tatar A-S, Gulei D, Tomuleasa C and Boca S (2024), *In vivo* imaging system (IVIS) therapeutic assessment of tyrosine kinase inhibitor-loaded gold nanocarriers for acute myeloid leukemia: a pilot study.
Front. Pharmacol. 15:1382399.
doi: 10.3389/fphar.2024.1382399

In vivo imaging system (IVIS) therapeutic assessment of tyrosine kinase inhibitor-loaded gold nanocarriers for acute myeloid leukemia: a pilot study

Raluca-Andrada Munteanu[1†], Adrian Bogdan Tigu[1†], Richard Feder[1], Andra-Sorina Tatar[2,3], Diana Gulei[1*], Ciprian Tomuleasa[1,4*] and Sanda Boca[2,3*]

[1]Medfuture Research Center for Advanced Medicine, Iuliu Hatieganu University of Medicine and Pharmacy, Cluj-Napoca, Romania, [2]Interdisciplinary Research Institute in Bio-Nano-Sciences, Babes-Bolyai University, Cluj-Napoca, Romania, [3]Molecular and Biomolecular Physics Department, National Institute for Research and Development of Isotopic and Molecular Technologies, Cluj-Napoca, Romania, [4]Department of Hematology, Ion Chiricuta Oncology Institute, Cluj-Napoca, Romania

Acute myeloid leukemia (AML) is a malignancy in the myeloid lineage that is characterized by symptoms like fatigue, bleeding, infections, or anemia, and it can be fatal if untreated. In AML, mutations in tyrosine kinases (TKs) lead to enhanced tumor cell survival. The most frequent mutations in TKs are reported in *Fms*-like tyrosine kinase 3 (FLT3), Janus kinase 2 (JAK2), and KIT (tyrosine-protein kinase KIT), making these TKs potential targets for TK inhibitor (TKI) therapies in AML. With 30% of the mutations in TKs, mutated FLT3 is associated with poor overall survival and an increased chance of resistance to therapy. FLT3 inhibitors are used in FLT3-mutant AML, and the combination with hypomethylating agents displayed promising results. Midostaurin (MDS) is the first targeted therapy in FLT3-mutant AML, and its combination with chemotherapy showed good results. However, chemotherapies induce several side effects, and an alternative to chemotherapy might be the use of nanoparticles for better drug delivery, improved bioavailability, reduced drug resistance and induced toxicity. The herein study presents MDS-loaded gold nanoparticles and compares its efficacy with MDS alone, on both *in vitro* and *in vivo* models, using the FLT3-ITD-mutated AML cell line *MV-4-11 Luc2* transfected to express luciferin. Our preclinical study suggests that MDS-loaded nanoparticles have a better tumor inhibitory effect than free drugs on *in vivo* models by controlling tumor growth in the first half of the treatment, while in the second part of the therapy, the tumor size was comparable to the cohort that was treatment-free.

KEYWORDS

acute myeloid leukemia, tyrosine kinases, gold nanoparticles, drug delivery, *in vivo* models, *in vivo* imaging system

1 Introduction

Acute Myeloid Leukemia (AML) is a stem cell precursor malignancy in the myeloid lineage that can be fatal if untreated, with common symptoms such as fatigue, anemia, infections, or bleeding (Stubbins et al., 2022). In AML, the main tyrosine kinase (TK) mutations can lead to the upregulation of several biological pathways, which can enhance tumor cell survival (Wilson et al., 2018). TK mutations are mainly produced in *Fms-like tyrosine kinase 3* (FLT3), *Janus kinase 2* (JAK2), and KIT (*tyrosine-protein kinase KIT–CD117*); thus, some TK inhibitors (TKIs) could be used as targeted therapies (Altman et al., 2013). Mutations that occur in FLT3 account for 30% of all cases, mostly with FLT3 internal tandem duplication. These mutations in FLT3 are associated with the aggressiveness of AML, reduce overall survival (Kottaridis et al., 2001), and increase the chances of resistance to therapy and relapse (Rombouts et al., 2000). FLT3 inhibitors are promising therapeutic agents, with midostaurin (MDS) and gilteritinib approved by the FDA to be used in FLT3-mutant AML, both in first-line and salvage settings. Midostaurin was a path-breaker for gilteritinib; thus, the combination of FLT3 inhibitors with hypomethylating agents such as decitabine or azacitidine shows good results, and other FLT3 inhibitors are now undergoing clinical testing (Galanis et al., 2012; Levis, 2017; Perl, 2019; Smith, 2019). MDS is the first targeted therapy for AML with the FLT3 mutation, aiming to improve overall survival. MDS combined with chemotherapy showed good results in high-risk AML FLT3-mutant patients (Starr, 2016). RATIFY (NCT00651261), a phase III trial, showed that MDS addition to chemotherapy improves survival in FLT3-mutated patients (Stone et al., 2017). Although TKI first-line therapy is used for myelosuppression to induce a hematological response, several side effects like liver dysfunction, edema, fluid retention, fatigue, and gastrointestinal symptoms (Guilhot et al., 2012; Qosa et al., 2018; Mauro, 2021) might occur. On the other hand, chemotherapy usually induces serious side effects that augment in combination with other drugs by becoming acute. For example, the RADIUS_X study (NCT02624570) showed that half of the patients treated with midostaurin reported adverse events, with the most common being diarrhea and neutropenia (Roboz et al., 2020).

Chemotherapy alternatives tend to use nanoparticles for drug delivery to improve bioavailability and reduce drug resistance and toxicity (Yan et al., 2020). Our previous studies showed that FLT3 inhibitors loaded on Pluronic–gold nanoparticles inhibit tumor growth and have a superior therapeutic effect compared to bare drugs (Simon et al., 2015). In another study, we showed that FLT3 inhibitors loaded on gelatin-coated gold nanoparticles had an increased antitumor effect compared to the drug alone (Suarasan et al., 2016). Gold nanoparticles loaded with FLT3 inhibitors had an increased transmembrane delivery in AML cells, and the *in vitro* evaluation indicates that the *FLT3-IDT* gene was downregulated, leading to tumor cell suppression (Petrushev et al., 2016). Thus, MDS internalization in nanocarriers could improve its bioavailability and reduce its overall side effects.

In recent work, we have shown that the MDS loading and controlled release behavior greatly depend on the stimuli-responsive properties of the polymer that is conjugated onto a gold nanoparticle core (Tatar et al., 2023). Herein, we took a step forward by extending our studies toward preclinical *in vivo* investigations. For this, we employed a protocol based on data generated by an *in vivo* imaging system (IVIS) (Lim et al., 2009; Nakayama et al., 2020; Iluta et al., 2021), which allows us to track tumor cells and evaluate the drug effect in mice in a non-invasive manner over a longer time scale. Our findings show that the group treated with MDS-loaded nanoparticles had a better outcome than the group treated with MDS alone after 2 weeks of drug administration at a dosage approximately 10 times lower than the one given in clinical settings, considering the human-to-animal conversion. However, one can notice that the antitumor effect is more pronounced in the first half of the treatment, as after 4 weeks, the tumors have similar sizes in all treated groups. We attribute this effect to the significantly low concentration of MDS in loaded nanoparticles and, implicitly, to the overall dosage. Thus, further optimization of the nanoparticle formulation is a prerequisite for a better and more sustained outcome and the minimization of any potential relapse.

2 Materials

Hydrogen tetrachloroaurate (III) trihydrate ($HAuCl_4{\cdot}3H_2O$, 99.99%), sodium citrate tribasic dihydrate, citric acid, Pluronic F-127 (Pluronic), midostaurin hydrate (>98%) (MDS), and L-glutathione reduced ≥98.0% (GSH) were obtained from Sigma-Aldrich. Thiolated polyethylene glycol of 5000 kDa molecular mass was obtained from Iris Biotech, Germany. The phosphate-buffered saline solution was purchased from Gibco®. All the other reagents used during the experiments are of analytical grade and were used without further purification. The aqueous solutions were prepared with ultrapure water (R = 18.2 MΩ cm) from a Milli-Q Purification System (Millipore, Merck). Ultrapure water was used for rinsing and cleaning procedures.

3 Methods

3.1 Gold nanoparticle synthesis and loading with the midostaurin drug

Gold nanoparticles were fabricated by chemical synthesis based on the Turkevich–Frens protocol (Boca et al., 2009). In brief, 100 mL of 1 mM $HAuCl_4{\cdot}3H_2O$ were heated until boiling. Under vigorous stirring, 10 mL of 38.8 mM sodium citrate were quickly added. During the boiling process, the solution changed color from yellow to an intense burgundy-red. Then, the solution was removed from the heat, and the stirring continued for another 10–15 min until the formation of nanoparticles. For the loading of the drug, 40 ul of midostaurin (1 mg/mL) were added to 1 mL of the synthesized nanoparticles in an aqueous solution, followed by the rapid addition of 2 mM Pluronic polymer to the nanoparticle–drug mixture. The mixture underwent 1 h of stirring at room temperature, after which the drug-loaded nanoparticles were purified by centrifugation and resuspension in phosphate-buffered saline (PBS). The amount of the drug that was loaded onto GNPs was obtained by measuring the drug content of the supernatant after particle purification. The loading efficiency (LE) was calculated using the following formula:

$$\%LE = \frac{T_{Drug} - S_{Drug}}{T_{Drug}} * 100,$$

where T_{drug} is the total amount of the drug added and S_{drug} represents the amount of the drug in the supernatant (Simon et al., 2015). Drug loading was calculated by estimating the free drug content of the supernatant. The drug concentrations were determined by measuring the supernatant absorbance (area under the curve in the 300–380 nm range) and comparing it with a free drug solution calibration curve (ESI Supplementary Figure S1). Based on these, the drug content in the nanoparticle formulation was 30.534 μg/mL, while the gold quantity per particle was calculated to be 8.07E-17 g, considering the 3.67E+8 M extinction coefficient for 20-nm spherical nanoparticles. The purified drug loaded sample (GNP-MDS-PLU) was kept at 8°C until further use. The control sample of drug-free nanoparticles (GNP-PLU) was prepared by mixing the colloidal nanoparticles with Pluronic under similar conditions but by adding the PEG polymer as a particle pre-stabilizer before the Pluronic coating.

3.2 Drug release evaluation

To evaluate the release of the drug from the nanocarriers, the particles were re-suspended in buffer solutions mimicking the physiological environment (lysosomes and extracellular fluids): (i) acidic citrate buffer (pH 4.5); (ii) acidic citrate buffer (pH 4.5) containing a GSH; and (iii) PBS (pH 7.4). The nano-MDS samples were incubated at 37°C in the three buffers above for various time intervals: 1, 3, 8, and 24 h. At the selected time checkpoints, the samples were centrifuged to separate the nanoparticles from the supernatant containing the released drug molecules. The two fractions were spectroscopically measured for drug quantification, and the concentration of the released drug and that of the drug remaining within the nanoparticle were calculated based on calibration curves previously obtained for the MDS molecule. MDS quantification was based on the area under the curve measurements.

3.3 Physico-chemical characterization of the drug nanocarriers

UV-Vis-NIR extinction spectra of free and drug-loaded nanoparticles were acquired using a JASCO V-670 UV-Vis-NIR spectrometer at 1-nm spectral resolution in 2-mm path length quartz cuvettes. Particle size distribution and zeta potential were measured at 25°C using the Zetasizer Nano ZS90 from Malvern Instruments. Analysis was performed at a scattering angle of 90° and a temperature of 25°C. Particle morphology was imaged by transmission electron microscopy using a JEOL model JEM 1010 microscope.

3.4 Cell culture

The FLT3-ITD-mutated MV-4-11 AML cell line transfected to express luciferin MV-4-11 Luc2 (original cell line CRL-9591—MV-4-11) was cultured in sterile cell flasks at 37°C and 5% CO_2 in a humidified chamber. The RPMI 1640 culture medium, supplemented with 10% fetal bovine serum (FBS), 1% penicillin/streptomycin, and 1% glutamine, was used for maintaining the MV-4-11 Luc2 cells under optimal growth conditions. All the cell culture reagents were purchased from Gibco.

3.5 Cell toxicity

The cell toxicity assay was performed using the CyQUANT XTT Cell Viability Assay Kit (Invitrogen, Carlsbad, CA, United States of America) with the experimental conditions set at 15 × 10^3 cells/well in a 100 μL culture medium in a sterile and flat bottomed 96-well plate. After 24 h of incubation, different concentrations of nanoparticles of various formulations (polymer and polymer–drug conjugates) were added to the cells. The cells were incubated with the treatment for another 24 h, followed by 4 h of incubation with the XTT reagent mixed with an electron-coupling reagent at 37°C, protected from light. The cell viability was measured at 450 nm and 660 nm using the Tecan Spark 10M spectrophotometer (TECAN, Austria GmbH, Grodig, Austria). Data analysis and graphical representation were performed using GraphPad Prism 8, and the result was expressed as the mean ± standard deviation (GraphPad Software, San Diego, CA, United States of America).

3.6 MV-4-11 Luc cell morphological analysis

The morphological changes in the cells and cell clustering after 24 h of treatment were evaluated in bright field using a Zeiss Axio Vert. A1 inverted microscope (Zeiss, Jena, Germany) with a ×5 objective. The images were captured using ZEN software (Zeiss, Jena, Germany).

3.7 *In vivo* protocols

Eight-week-old male and female athymic nude mice were included in the study. The mice were purchased from Charles River Laboratories and maintained in an authorized animal facility at the Medfuture Research Center for Advanced Medicine, Iuliu Hatieganu University of Medicine and Pharmacy, Cluj-Napoca. The mice were accommodated at a standard temperature of 22°C ± 2°C and a relative humidity of 55% ± 10% in a 12:12 h light:dark cycle. The housing was made in an IVC2-SM-56-IIL rack system (Acellabor) with individually ventilated cages supplied with HEPA-filtered air (II L Cages) with autoclaved bedding and *ad libitum* access to autoclaved water and pelleted food. All experimental protocols were approved by the Ethics Committee of Iuliu Hatieganu University of Medicine and Pharmacy and were conducted in accordance with EU Directive 63/2010.

Sixteen mice were included in the study and tagged with metallic ear tags for identification. The animals were injected with approximately 2 × 10^6 MV4-11 luciferase-positive cells in the knee joint while kept under gas anesthesia. The tumors were allowed to develop for 14 days, and at day 14, the size of the xenograft was measured using the IVIS SPECTRUM–IVIS

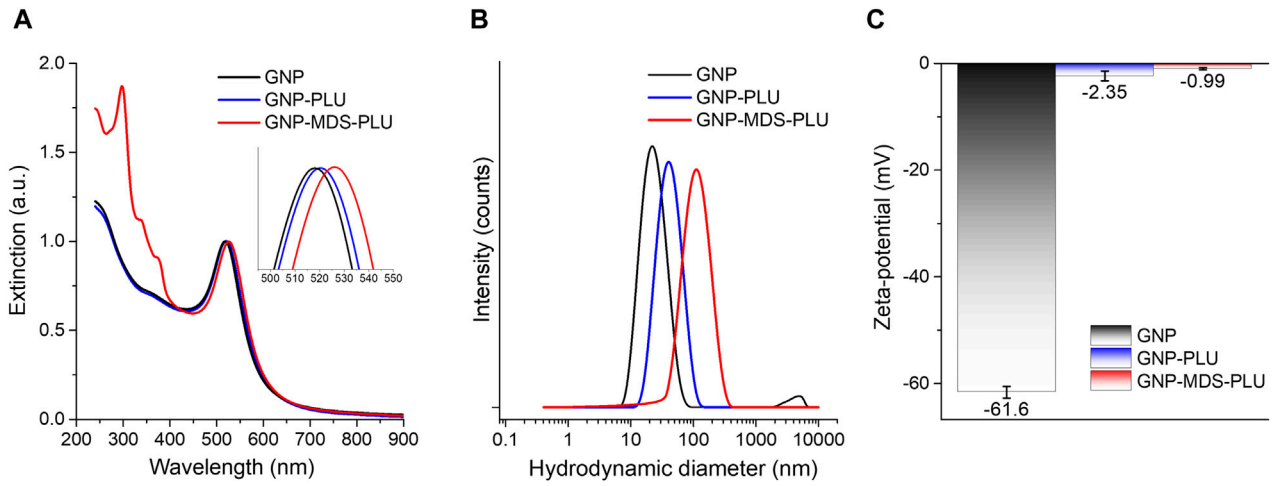

FIGURE 1
(A) UV-Vis-NIR extinction spectra of Pluronic nanoconjugates of various composition. Inset: LSPR (the spectra are normalized to unity). **(B)** DLS hydrodynamic diameter data of nanoconjugates. **(C)** Zeta potential values of nanoconjugates. Black, pristine GNPs; blue, Pluronic-conjugated nanoparticles; red, MDS-loaded nanoparticles.

Imaging System (PerkinElmer) using a systemically injected bioluminescent reporter optimized for *in vivo* imaging–RediJect D-Luciferin (XenoLight, PerkinElmer). Out of the 16 mice, 11 developed relatively uniform tumors and were divided into four experimental groups as follows: control (2n), nano-control (3n), midostaurin control (3n), and nano-midostaurin (3n). We have chosen to include the fewest number of mice in the control group considering that the main purpose of the study was to demonstrate the superiority of the treatment loaded with nanoparticles compared with the standard free drug and not to demonstrate the feasibility of the actual treatment that was already tested in clinical trials. Control mice received 200 µL of buffer solution, nano-control mice received 200 µL of unloaded nanoparticles (GNP-PLU), midostaurin control mice received 200 µL of the equivalent dosage of a free drug, and nano-MDS mice received 200 µL of nanoparticles loaded with MDS in a PBS solution (GNP-MDS-PLU). All treatments were administered intraperitoneally (IP). The treatments were administered daily for 14 consecutive days, except for control mice that did not survive until the end of the experiment and received only seven doses of treatment. The evolution of the tumors was monitored *via* bioluminescent imaging at days 1, 8, and 15 for all treatment groups, except for the control mice that were followed until day 8. Bioluminescent images were processed using Living Image® 4.5.2 software. The same software program was used to automatically measure the signal intensity within the region of interest (ROI) using the automatic contour tool.

4 Results and discussion

4.1 Characterization of midostaurin nanocarriers

The synthesized gold nanoparticles have a spherical shape and sizes of approximately 20 nm, as indicated by the morphological characterization of the TEM micrograph (ESI Supplementary Figure S2). The particles were purified by centrifugation and resuspension in ultrapure water and used for further functionalization. Figure 1 presents the UV-Vis-NIR spectra of the particles in different formulations (free, conjugated with Pluronic, and loaded with MDS drug). The characteristic peaks of midostaurin are visible in the 300–380 nm region. The nanoconjugates have a very high MDS loading efficiency (94.65%) facilitated by the midostaurin, which, being an organic hetero-octacyclic compound, is capable of participating in less than five hydrogen bonds, so it is mostly hydrophobic. Pluronic molecules are hydrophilic–hydrophobic–hydrophilic block copolymers of poly(ethylene oxide) (PEO) and poly(propylene oxide) (PPO). Taking these into consideration, the mechanism by which MDS-loaded gold nanoparticles are formed is based on the self-assembly of Pluronic and MDS into amphiphilic structures that engulf the nanoparticles suspended in an aqueous solution. The hydrophobic area of MDS is captured in the PPO layer of the Pluronic via hydrophobic interactions, and the outer hydrophilic shell ensures the solubility and stability of the system. The LSPR position is red-shifted by several nm after conjugation with the polymer and drug molecules, respectively, confirming that the drug and polymer molecules are conjugated onto the nanoparticle surface. DLS measurements corroborate the results, as the measured hydrodynamic diameter systematically increases after each round of functionalization from approximately 25 nm in the case of bare nanoparticles to 45 nm and 123 nm, respectively, for polymer and MDS-polymer-coated ones. The zeta potential also modifies, showing a value of −61.6 ± 1.1 mV for the pristine GNPs, while after Pluronic shielding, the value increases to −2.35 ± 0.9 mV. The presence of MDS in the nanoparticle formulation further modifies the zeta potential of the particles to values approaching neutral charge. Still, the nanoparticles remain stable in a biologically compatible buffer solution due to the presence of the polymer, which provides steric stability to the nanocomplexes.

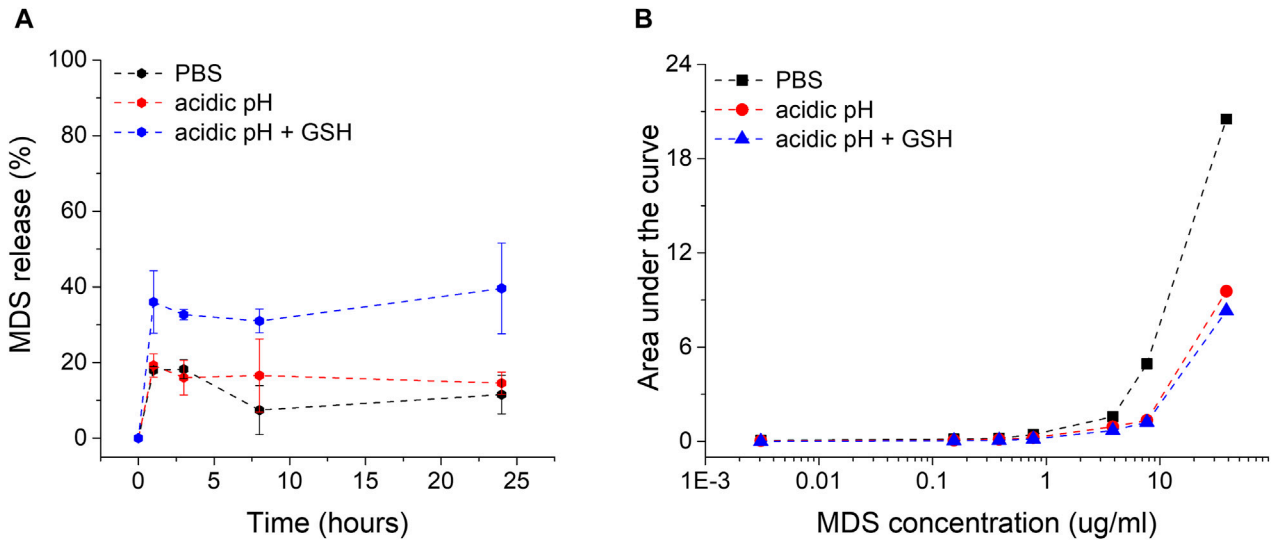

FIGURE 2
(A) Representation of the MDS drug release rates from midostaurin-loaded Pluronic conjugated gold nanoparticles (GNP-MDS-PLU) in function of time in various incubation media. **(B)** Calibration curves for MDS quantification in all three release media solutions (black, PBS; red, acidic pH; blue, GSH presence in acidic pH).

4.2 Evaluation of the drug release profile

The particles were subjected to *ex vivo* release buffers simulating relevant intracellular microenvironment conditions. PBS is commonly used due to its resemblance to extracellular fluid pH of 7.4 and ionic strength. A citrate-based acidic buffer with a pH of 4.5 resembles lysosomal pH conditions, as GNPs are engulfed by cells mostly based on endocytosis through the endo-lysosomal internalization system. For an even more accurate simulation of the intra-lysosomal microenvironment where GNP-MDS-PLUs are located after internalization, we added 10 mM of glutathione (GSH), an important component of the lysosomal fluid and the most abundant thiol in animal cells. Due to its chemical composition, Pluronic is a pH-non-sensitive polymer, and Pluronic-coated nanoparticles are relatively stable under both PBS (7.4 pH) and acidic (pH 4.5) conditions (Figure 2). Similar results regarding the stability of conjugated nanoparticles in the PBS buffer were previously obtained and demonstrated in our group (Simon et al., 2015; Tatar et al., 2023). Herein, we expand the evaluation by testing the stability of the particles over a 3-day time period. The results indicate the high stability of the drug nanocomplex since both the particle LSPR band position and the spectral characteristics of the drug molecules are conserved (ESI Supplementary Figure S3). The drug release experiments showed a burst release in the first hour of incubation for all release buffers but barely reached 16%–17% MDS release after 24 h of incubation under non-GSH conditions. In contrast, the presence of glutathione leads to release rates of 50% after 24 h due to the molecules' high affinity to the gold surface of the particles, leading to a major displacement of the adsorbed MDS and Pluronic (Figure 2). The released MDS is most likely captured in Pluronic micelles within the hydrophobic core.

4.3 *In vitro* cytotoxicity evaluation

In vitro toxicity of MDS, GNP-PLU, and GNP-MDS-PLU on MV-4-11 Luc2 leukemia cells was evaluated at 24 h after treatment. The cytotoxicity was assessed at different concentrations of the above-mentioned nanocompounds by adding different volumes of the colloid containing either nanoparticles or the free drug in culture media (volume range 2.5–100 µL), as presented in Figures 3A, B. The GNP-PLU concentration as particles/mL was adapted to match that of GNP-MDS-PLU, which was loaded with MDS as an anti-FLT3 compound.

The MTS results indicate that the GNPs without drug load showed no toxicity on MV-4-11 Luc2 cells, while the MDS alone and GNP-MDS-PLU treatments inhibited leukemia cell growth in a dose-dependent manner. Furthermore, it is notable that at a very low dose of the free midostaurin drug and midostaurin-loaded nanoparticles, the inhibition effect is significant, downstreaming the viability by almost 50%. This aspect highlights the high antitumor effect of midostaurin. The reduced cell population was evaluated by bright-field microscopy, and the results are presented in the Supplementary Material attached to the article (ESI Supplementary Figure S4). The nonlinear regression fit of the obtained data indicates a low IC_{50} value, confirming that the compound can inhibit half of the MV-4-11 Luc2 cells at a very low dose in a short period of treatment of 24 h, while the unloaded GNPs showed no toxicity (ESI Supplementary Figure S5).

4.4 *In vivo* cytotoxicity evaluation

In order to demonstrate the improved efficiency of the treatment loaded into the particles in a preclinical experimental setup closer to the patients' scenario, we used athymic nude mice with tumor xenografts as models for the evolution of the disease. Once we

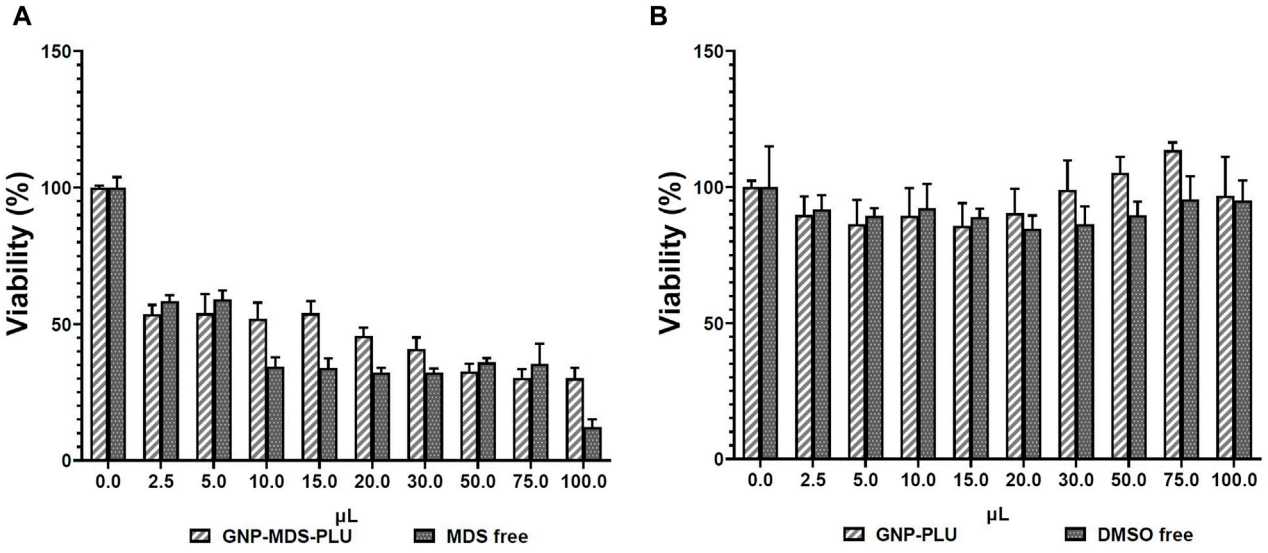

FIGURE 3
(A) Cytotoxicity evaluation by the XTT assay of GNP-MDS-PLU and MDS and **(B)** GNP-PLU and DMSO on MV-4-11 Luc2 cells after 24 h of treatment.

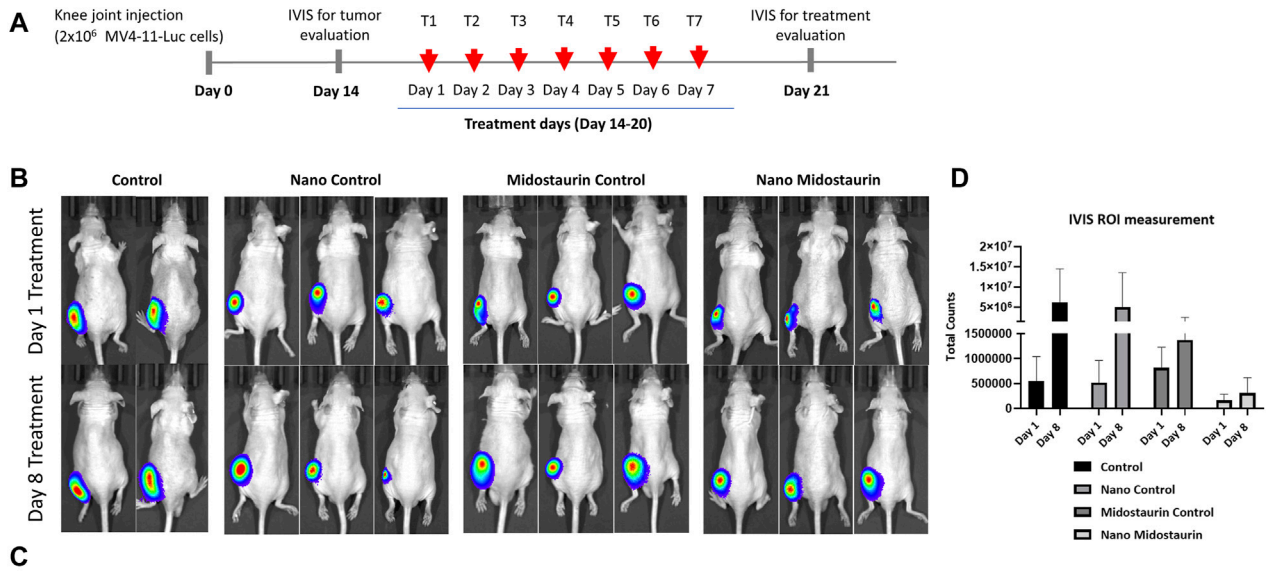

C

	Total Counts (Image Overlay)										
	Control		Nano Control			Midostaurin Control			Nano Midostaurin		
	1	2	1	2	3	1	2	3	1	2	3
Day 1	8.95E+05	1.94E+05	9.11E+05	6.02E+05	3.73E+04	1.27E+06	7.14E+05	4.61E+05	2.53E+05	2.09E+05	2.11E+04
Day 8	1.21E+07	3.97E+05	1.49E+07	5.00E+04	5.77E+04	2.33E+06	1.63E+06	1.46E+05	1.44E+05	1.10E+05	6.63E+05

FIGURE 4
In vivo evaluation of systemic efficiency of various gold nanocarrier formulations—14 days of continued acute myeloid leukemia treatment. **(A)** Scheme of tumor development, treatment administration, and imagistic evaluation schedule. **(B)** *In vivo* bioluminescent evaluation of mice grafted with MV4-11-Luc cells in the knee joint divided into four experimental groups: control, nano-control, midostaurin control, and nano-midostaurin. *In vivo* imaging was done before treatment administration (day 1 of treatment) and after the last dose of treatment (day 8 of treatment). **(C)** Measurement of bioluminescent signal intensity within the region of interest of the tumor graft before treatment administration (day 1) and after the last dose of treatment (day 8) of the four experimental groups: control, nano-control, midostaurin control, and nano-midostaurin. **(D)** Graphical representation of the bioluminescent signal intensity of ROI according to the values presented at Figure 4C.

observed a significant tumor formation, we administered systemically via IP injection control buffer (control), free nanoparticles (nano-control), free drug (midostaurin control), and particles loaded with the drug (nano-midostaurin) (Figure 4). The treatment was administered daily for 14 days (ESI Supplementary Figure S6) and evaluated on days 1, 8, and 15 using the IVIS. The therapy delivery approach was chosen according to its pharmacokinetic and pharmacodynamic properties to ensure appropriate therapeutic plasma levels. The daily intraperitoneal dose for 14 consecutive days was chosen to ensure consistent exposure to the therapy, which is important to determine its therapeutic effect. This strategy was informed by existing literature data, suggesting that such a regimen could minimize toxicity while maximizing tumor inhibition (Lu et al., 2022). Moreover, we hypothesized that nanoparticles might exhibit delayed effects on tumor progression or interact differently with the tumor microenvironment over an extended period. The control group that did not receive any form of treatment died under anesthesia at the second IVIS evaluation (day 8), stopping the experiment on day 7 of treatment (Figure 4). As can be seen in Figure 4, in the case of control mice that received only buffer solution or nanoparticles alone, the xenografts developed significantly without any signs of tumor inhibition. In the third control group, meaning the mice that were injected with the free drug, the malignant formation decreased at day 8 compared with the other two control cohorts; however, the treatment did not manage to completely stop tumor evolution. Finally, when midostaurin was loaded into the particles and administered systemically (nano-midostaurin), we observed a significant improvement in terms of tumor development, where the new formulation managed to significantly minimize tumor growth compared with the other three control situations, including the free drug cohort.

Despite losing the control group in the first half of the experiment, we continued the protocol until day 14 of the treatment with the other three cohorts, considering that the main purpose of the preclinical evaluation consisted of demonstrating the improved efficiency of the new particles loaded with the drug compared with the drug alone. Moving past day 7 of treatment, we observed a sudden rapid tumor growth also in the nano-midostaurin cohort, similar to the one from the midostaurin control and nano-control groups (ESI Supplementary Figure S6). We attributed this change to the highly aggressive character of the tumor but also to the fact that, at this point, we were unable to load into the particles a clinically equivalent dose of midostaurin. To establish our dosing strategy, we used an approved therapeutic regimen, and we consulted the RATIFY clinical trial (Stone et al., 2017), where midostaurin was administered at 50 mg orally twice daily in adult AML patients with FLT3 mutations. Considering the pharmacokinetic and pharmacodynamic differences between humans and mice, we used a scaled dose that was approximately 10 times lower than the human equivalent dose when adjusted for the body surface area. This adjustment is consistent with standard practices for translating human doses to mouse doses, ensuring relevance and safety in our preclinical investigation. Hence, the dosage was calculated according to the human–animal dose conversion, being limited by the volume that can be administered to a mouse. However, the new therapeutic formulation has managed to keep the tumor under control for half of the therapeutic scheme, a fact that did not happen in the case of the standard treatment that is currently used in the clinic.

5 Discussions and future perspectives

Our preclinical study shows that midostaurin in the nanoparticle formulation has improved effects on tumor inhibition compared to the free drug *in vivo*, managing to keep tumor formation under control with no significant tumor growth within the first half of the treatment (ESI Supplementary Figure S7). However, starting with the second half of the therapy, the tumor growth intensified even under the new nanoparticle-based formulation, reaching similar levels to those observed in the free midostaurin cohort. We mainly attribute this spurt to an insufficient drug concentration, being limited by the volume of treatment that can be injected into a mouse and, implicitly, the particle concentration. It is, therefore, notable that the administered drug quantity with positive results was approximately 10 times lower than the one given in the clinic after the human-to-animal conversion. However, in the case of a patient, this limitation does not exist anymore since a much higher tolerance can be applied in terms of treatment volume. To overcome these limitations, we plan to conduct further research with an expanded sample size and investigate different statistical approaches. Furthermore, considering the challenges in maintaining consistent drug concentrations due to the limitations in treatment volume that can be administered in a mouse model, future studies will also focus on optimizing the nanoparticle formulation. This will improve the bioavailability and sustained release of midostaurin, potentially increasing the efficacy of the treatment throughout the entire research period.

Data availability statement

The raw data supporting the conclusion of this article will be made available by the authors, without undue reservation.

Ethics statement

The animal study was approved by the Ethics Committee of Iuliu Hatieganu University of Medicine and Pharmacy and conducted in accordance with EU Directive 63/2010. The study was conducted in accordance with the local legislation and institutional requirements.

Author contributions

R-AM: formal analysis, investigation, methodology, visualization, and writing–original draft. AT: formal analysis, investigation, methodology, validation, and writing–original draft. RF: formal analysis, investigation, methodology, writing–review and editing, and visualization. A-ST: formal analysis, investigation, methodology, and writing–original draft. DG: conceptualization, formal analysis, investigation, methodology, supervision, validation, visualization, and writing–review and editing. CT: conceptualization, supervision, validation, visualization, and writing–review and editing. SB: conceptualization, formal analysis, funding acquisition, investigation, methodology, project administration, resources, supervision, validation, visualization, writing–original draft, and writing–review and editing.

Funding

The author(s) declare that financial support was received for the research, authorship, and/or publication of this article. This work was supported by CNCS-UEFISCDI, project number PN-III-P1-1.1-TE-2016-0919 within PNCDI III and Babes-Bolyai University under the project SRG-UBB 32985/23.06.2023—Starting Research Grants.

Conflict of interest

The authors declare that the research was conducted in the absence of any commercial or financial relationships that could be construed as a potential conflict of interest.

Publisher's note

Supplementary material

The Supplementary Material for this article can be found online at: https://www.frontiersin.org/articles/10.3389/fphar.2024.1382399/full#supplementary-material

References

Altman, J. K., Szilard, A. K., and Platanias, L. C. (2013). Tyrosine kinase inhibition in acute myeloid leukemia. *Leukemia Lymphoma* 54, 1351–1352. doi:10.3109/10428194.2012.754889

Boca, S. C., Farcau, C., and Astilean, S. (2009). The study of Raman enhancement efficiency as function of nanoparticle size and shape. *Nucl. Instrum. Methods Phys. Res. Sect. B Beam Interact. Mater. Atoms* 267, 406–410. doi:10.1016/j.nimb.2008.10.020

Galanis, A., Rajkhowa, T., Muralidhara, C., Ramachandran, A., and Levis, M. J. (2012). Crenolanib is A highly potent, selective, FLT3 TKI with activity against D835 mutations. *Blood* 120, 1341. doi:10.1182/blood.V120.21.1341.1341

Guilhot, F., Hughes, T. P., Cortes, J., Druker, B. J., Baccarani, M., Gathmann, I., et al. (2012). Plasma exposure of imatinib and its correlation with clinical response in the tyrosine kinase inhibitor optimization and selectivity trial. *Haematologica* 97, 731–738. doi:10.3324/haematol.2011.045666

Iluta, S., Pasca, S., Gafencu, G., Jurj, A., Terec, A., Teodorescu, P., et al. (2021). Azacytidine plus olaparib for relapsed acute myeloid leukaemia, ineligible for intensive chemotherapy, diagnosed with a synchronous malignancy. *J. Cell Mol. Med.* 25, 6094–6102. doi:10.1111/jcmm.16513

Kottaridis, P. D., Gale, R. E., Frew, M. E., Harrison, G., Langabeer, S. E., Belton, A. A., et al. (2001). The presence of a FLT3 internal tandem duplication in patients with acute myeloid leukemia (AML) adds important prognostic information to cytogenetic risk group and response to the first cycle of chemotherapy: analysis of 854 patients from the United Kingdom Medical Research Council AML 10 and 12 trials. *Blood* 98, 1752–1759. doi:10.1182/blood.V98.6.1752

Levis, M. (2017). Midostaurin approved for FLT3-mutated AML. *Blood* 129, 3403–3406. doi:10.1182/blood-2017-05-782292

Lim, E., Modi, K. D., and Kim, J. (2009). *In vivo* bioluminescent imaging of mammary tumors using IVIS spectrum. *J. Vis. Exp. JoVE*, 1210. doi:10.3791/1210

Lu, H., Weng, X.-qin, Sheng, Y., Wu, J., Xi, H.-min, and Cai, X. (2022). *Combination of midostaurin and ATRA exerts dose-dependent dual effects on acute myeloid leukemia cells with wild type FLT3*. *BMC Cancer* 22, 749. 749. doi:10.1186/s12885-022-09828-2

Mauro, M. J. (2021). Lifelong TKI therapy: how to manage cardiovascular and other risks. *Hematology* 2021, 113–121. doi:10.1182/hematology.2021000239

Nakayama, J., Saito, R., Hayashi, Y., Kitada, N., Tamaki, S., Han, Y., et al. (2020). High sensitivity *in vivo* imaging of cancer metastasis using a near-infrared luciferin analogue seMpai. *Int. J. Mol. Sci.* 21, 7896. doi:10.3390/ijms21217896

Perl, A. E. (2019). Availability of FLT3 inhibitors: how do we use them? *Blood* 134, 741–745. doi:10.1182/blood.2019876821

Petrushev, B., Boca, S., Simon, T., Berce, C., Frinc, I., Dima, D., et al. (2016). Gold nanoparticles enhance the effect of tyrosine kinase inhibitors in acute myeloid leukemia therapy. *Int. J. Nanomedicine* 11, 641–660. doi:10.2147/IJN.S94064

Qosa, H., Avaritt, B. R., Hartman, N. R., and Volpe, D. A. (2018). *In vitro* UGT1A1 inhibition by tyrosine kinase inhibitors and association with drug-induced hyperbilirubinemia. *Cancer Chemother. Pharmacol.* 82, 795–802. doi:10.1007/s00280-018-3665-x

Roboz, G. J., Strickland, S. A., Litzow, M. R., Dalovisio, A., Perl, A. E., Bonifacio, G., et al. (2020). Updated safety of midostaurin plus chemotherapy in newly diagnosed FLT3 mutation-positive acute myeloid leukemia: the RADIUS-X expanded access program. *Leuk. Lymphoma* 61, 3146–3153. doi:10.1080/10428194.2020.1805109

Rombouts, W. J. C., Blokland, I., Löwenberg, B., and Ploemacher, R. E. (2000). Biological characteristics and prognosis of adult acute myeloid leukemia with internal tandem duplications in the Flt3 gene. *Leukemia* 14, 675–683. doi:10.1038/sj.leu.2401731

Simon, T., Tomuleasa, C., Bojan, A., Berindan-Neagoe, I., Boca, S., and Astilean, S. (2015). Design of FLT3 inhibitor - gold nanoparticle conjugates as potential therapeutic agents for the treatment of acute myeloid leukemia. *Nanoscale Res. Lett.* 10, 466. doi:10.1186/s11671-015-1154-2

Smith, C. C. (2019). The growing landscape of FLT3 inhibition in AML. *Hematol. Am. Soc. Hematol. Educ. Program* 2019, 539–547. doi:10.1182/hematology.2019000058

Starr, P. (2016). Midostaurin the first targeted therapy to improve survival in AML: potentially practice-changing. *Am. Health Drug Benefits* 9, 1–21.

Stone, R. M., Mandrekar, S. J., Sanford, B. L., Laumann, K., Geyer, S., Bloomfield, C. D., et al. (2017). Midostaurin plus chemotherapy for acute myeloid leukemia with a FLT3 mutation. *N. Engl. J. Med.* 377, 454–464. doi:10.1056/NEJMoa1614359

Stubbins, R. J., Francis, A., Kuchenbauer, F., and Sanford, D. (2022). Management of acute myeloid leukemia: a review for general practitioners in oncology. *Curr. Oncol.* 29, 6245–6259. doi:10.3390/curroncol29090491

Suarasan, S., Simon, T., Boca, S., Tomuleasa, C., and Astilean, S. (2016). Gelatin-coated gold nanoparticles as carriers of FLT3 inhibitors for acute myeloid leukemia treatment. *Chem. Biol. Drug Des.* 87, 927–935. doi:10.1111/cbdd.12725

Tatar, A.-S., Nagy-Simon, T., Tigu, A. B., Tomuleasa, C., and Boca, S. (2023). Optimization of tyrosine kinase inhibitor-loaded gold nanoparticles for stimuli-triggered antileukemic drug release. *J. Funct. Biomater.* 14, 399. doi:10.3390/jfb14080399

Wilson, L. J., Linley, A., Hammond, D. E., Hood, F. E., Coulson, J. M., MacEwan, D. J., et al. (2018). New perspectives, opportunities, and challenges in exploring the human protein kinome. *Cancer Res.* 78, 15–29. doi:10.1158/0008-5472.CAN-17-2291

Yan, L., Shen, J., Wang, J., Yang, X., Dong, S., and Lu, S. (2020). Nanoparticle-based drug delivery system: a patient-friendly chemotherapy for oncology. *Dose Response* 18, 1559325820936161. doi:10.1177/1559325820936161

frontiers | Frontiers in Pharmacology

TYPE Original Research
PUBLISHED 22 July 2024
DOI 10.3389/fphar.2024.1418456

OPEN ACCESS

EDITED BY
Gregory Wiedman,
Seton Hall University, United States

REVIEWED BY
Fatemeh Saheb Sharif-Askari,
University of Sharjah, United Arab Emirates
Adrian Bogdan Tigu,
University of Medicine and Pharmacy Iuliu Hatieganu, Romania

*CORRESPONDENCE
Ping Xu,
zishanshuxu@sina.com
Wenhan Wu,
wuwenhan88@126.com

RECEIVED 16 April 2024
ACCEPTED 28 May 2024
PUBLISHED 22 July 2024

CITATION
Zhang C, Zheng J, Liu J, Li Y, Xing G, Zhang S, Chen H, Wang J, Shao Z, Li Y, Jiang Z, Pan Y, Liu X, Xu P and Wu W (2024), Pan-cancer analyses reveal the molecular and clinical characteristics of TET family members and suggests that TET3 maybe a potential therapeutic target.
Front. Pharmacol. 15:1418456.
doi: 10.3389/fphar.2024.1418456

Pan-cancer analyses reveal the molecular and clinical characteristics of TET family members and suggests that TET3 maybe a potential therapeutic target

Chunyan Zhang[1,2,3], Jie Zheng[4], Jin Liu[5], Yanxia Li[2,3], Guoqiang Xing[1], Shupeng Zhang[1], Hekai Chen[1], Jian Wang[1], Zhijiang Shao[1,3], Yongyuan Li[1,3], Zhongmin Jiang[4], Yingzi Pan[6], Xiaozhi Liu[2,3], Ping Xu[3,7]* and Wenhan Wu[1,2,3,8]*

[1]Department of General Surgery, Tianjin Fifth Central Hospital, Tianjin, China, [2]Tianjin Key Laboratory of Epigenetics for Organ Development of Premature Infants, Tianjin Fifth Central Hospital, Tianjin, China, [3]High Altitude Characteristic Medical Research Institute, Huangnan Tibetan Autonomous Prefecture People's Hospital, Huangnan Prefecture, Qinghai, China, [4]Department of Pathology, Tianjin Fifth Central Hospital, Tianjin, China, [5]North China University of Science and Technology, Tangshan, Hebei, China, [6]Department of Ophthalmology, Peking University First Hospital, Beijing, China, [7]Department of Pharmacy, Tianjin Fifth Central Hospital, Tianjin, China, [8]Department of General Surgery, Peking University First Hospital, Beijing, China

The Ten-Eleven Translocation (TET) family genes are implicated in a wide array of biological functions across various human cancers. Nonetheless, there is a scarcity of studies that comprehensively analyze the correlation between TET family members and the molecular phenotypes and clinical characteristics of different cancers. Leveraging updated public databases and employing several bioinformatics analysis methods, we assessed the expression levels, somatic variations, methylation levels, and prognostic values of TET family genes. Additionally, we explored the association between the expression of TET family genes and pathway activity, tumor microenvironment (TME), stemness score, immune subtype, clinical staging, and drug sensitivity in pan-cancer. Molecular biology and cytology experiments were conducted to validate the potential role of TET3 in tumor progression. Each TET family gene displayed distinct expression patterns across at least ten detected tumors. The frequency of Single Nucleotide Variant (SNV) in TET genes was found to be 91.24%, primarily comprising missense mutation types, with the main types of copy number variant (CNV) being heterozygous amplifications and deletions. TET1 gene exhibited high methylation levels, whereas TET2 and TET3 genes displayed hypomethylation in most cancers, which correlated closely with patient prognosis. Pathway activity analysis revealed the involvement of TET family genes in multiple signaling pathways, including cell cycle, apoptosis, DNA damage response, hormone AR, PI3K/AKT, and RTK. Furthermore, the expression levels of TET family genes were shown to impact the clinical staging of tumor patients, modulate the sensitivity of chemotherapy drugs, and thereby influence patient prognosis by participating in the regulation of the tumor microenvironment, cellular stemness potential, and immune subtype. Notably, TET3 was identified to promote cancer

progression across various tumors, and its silencing was found to inhibit tumor malignancy and enhance chemotherapy sensitivity. These findings shed light on the role of TET family genes in cancer progression and offer insights for further research on TET3 as a potential therapeutic target for pan-cancer.

KEYWORDS

TET family genes, pan-cancer analysis, tumor microenvironment, drug sensitivity, therapeutic target

Introduction

Epigenetics, including DNA methylation, histone modifications, and non-coding RNA regulation, plays a crucial role in human disease, particularly cancer, by orchestrating gene expression dynamics without altering DNA sequence. Aberrant epigenetic changes, such as hypermethylation of tumor suppressor gene promoters and dysregulated histone modifications, disrupt normal cellular processes, fostering tumor initiation, progression, and metastasis. Despite the continuous advancements in surgical and targeted therapies in recent years, a considerable portion of tumor patients still present with advanced and widespread metastasis at the time of diagnosis, resulting in a bleak prognosis (Golemis et al., 2018). Consequently, conducting comprehensive research into the molecular mechanisms underlying cancer development holds paramount importance for tumor prevention, early screening and diagnosis, clinical treatment, as well as enhancing patient prognosis and survival rates (Alqahtani et al., 2019; Ban et al., 2021; Rodriguez et al., 2022).

Genetic variations and epigenetic changes play pivotal roles in the initiation and progression of tumors (Talib et al., 2021). Nearly all tumors involve single or tandem mutations in one or multiple genes (Kossenas and Constantinou, 2021). To devise precise treatment strategies capable of effectively targeting tumor cells while minimizing damage to normal tissues, from the myriad of small molecule chemical drugs available, a comprehensive understanding of the underlying mechanisms of the implicated genes is imperative (Srivastava and Goodwin, 2020). The advent and advancement of modern bioinformatics methodologies offer a streamlined approach for humanity to efficiently explore and analyze tumor occurrences within established gene information databases, thereby providing guidance for tumor treatment (Nooter and Stoter, 1996; Zaridze, 2008; Gonçalves et al., 2021).

Recent studies have revealed that epigenetic regulations, such as DNA methylation and demethylation modifications, are intricately linked to the onset and progression of human cancers (Kulis and Esteller, 2010; Klutstein, Nejman, Greenfield and Cedar, 2016; Nishiyama and Nakanishi, 2021). DNA methylation often occurs on the CpG islands of the promoter regions, resulting in the activation of oncogenes and the inactivation of tumor suppressor genes (Kulis and Esteller, 2010; Papanicolau-Sengos and Aldape, 2022). Aberrant DNA methylation can disrupt the apoptosis process of cells, render tumor cells insensitive to growth inhibition signals, and induce uncontrolled replication of tumor cells (Pan et al., 2018). Consequently, epigenetic research, particularly focusing on DNA methylation, holds significant value for tumor molecular diagnosis, prevention, and treatment, as well as predicting therapeutic outcomes and prognosis (C. Chen et al., 2022; Meng et al., 2015).

Studies indicate that both hypermethylation and hypomethylation play crucial roles in tumor development. The Ten-Eleven Translocation (TET) enzymes facilitate the oxidation of 5-methylcytosines (5mCs) and promote site-specific reversal of DNA methylation (Kohli and Zhang, 2013). TET family genes, including TET1, TET2, and TET3, exhibit diverse vital biological functions in mammals (Kinney and Pradhan, 2013; Zeng and Chen, 2019; Joshi, Liu, Breslin and Zhang, 2022). At their core, TET family genes consist of α-Ketoglutaric acid (α-KG) and Fe2+-dependent dioxygenases, which regulate DNA demethylation, modulate gene transcription, and influence various life processes such as embryonic development, as well as the onset of various diseases including tumors (Rasmussen and Helin, 2016; Ma et al., 2021). Additionally, studies have demonstrated that TET family genes not only facilitate active DNA demethylation but also impede methylation propagation by maintaining a low DNA methylation state, thus closely associating them with tumorigenesis (Shekhawat et al., 2021). Notably, TET family genes exhibit a dual role in different tumors, displaying both carcinogenic and anticancer effects.

While TET family genes are known to play an indispensable role in the progression of numerous tumors, there is currently scarce literature on pan-cancer analysis of these genes. Therefore, in this study, we conducted an analysis of the relationship between TET family genes and pan-cancer, exploring various aspects including mRNA expression levels, somatic cell variations, DNA methylation patterns, pathway activities, survival rates and prognoses, immune subtypes specific to individual tumors, tumor microenvironment (TME), stem cell indices, and drug sensitivities. Our aim is to provide valuable reference data and constructive suggestions based on a comprehensive understanding of the landscape.

Results

Expression and differential analysis of TET family genes in pan-cancer

Firstly, utilizing transcriptome data from 33 tumors available in the UCSC Xena database, we conducted an extraction and analysis of the expression profiles of the target genes belonging to the TET family (specifically, TET1, TET2, and TET3) across various types of cancer. The results depicted in the Boxplot revealed that the expression level of the TET3 gene ranked highest across pan-cancer samples, followed by TET2, with TET1 exhibiting the lowest expression (Figure 1A, Supplementary Table S1).

Next, we screened 18 types of tumors, each containing at least five corresponding normal samples, and analyzed the expression differences of TET family members in pan-cancer and its normal

10.3389/fphar.2024.1418456

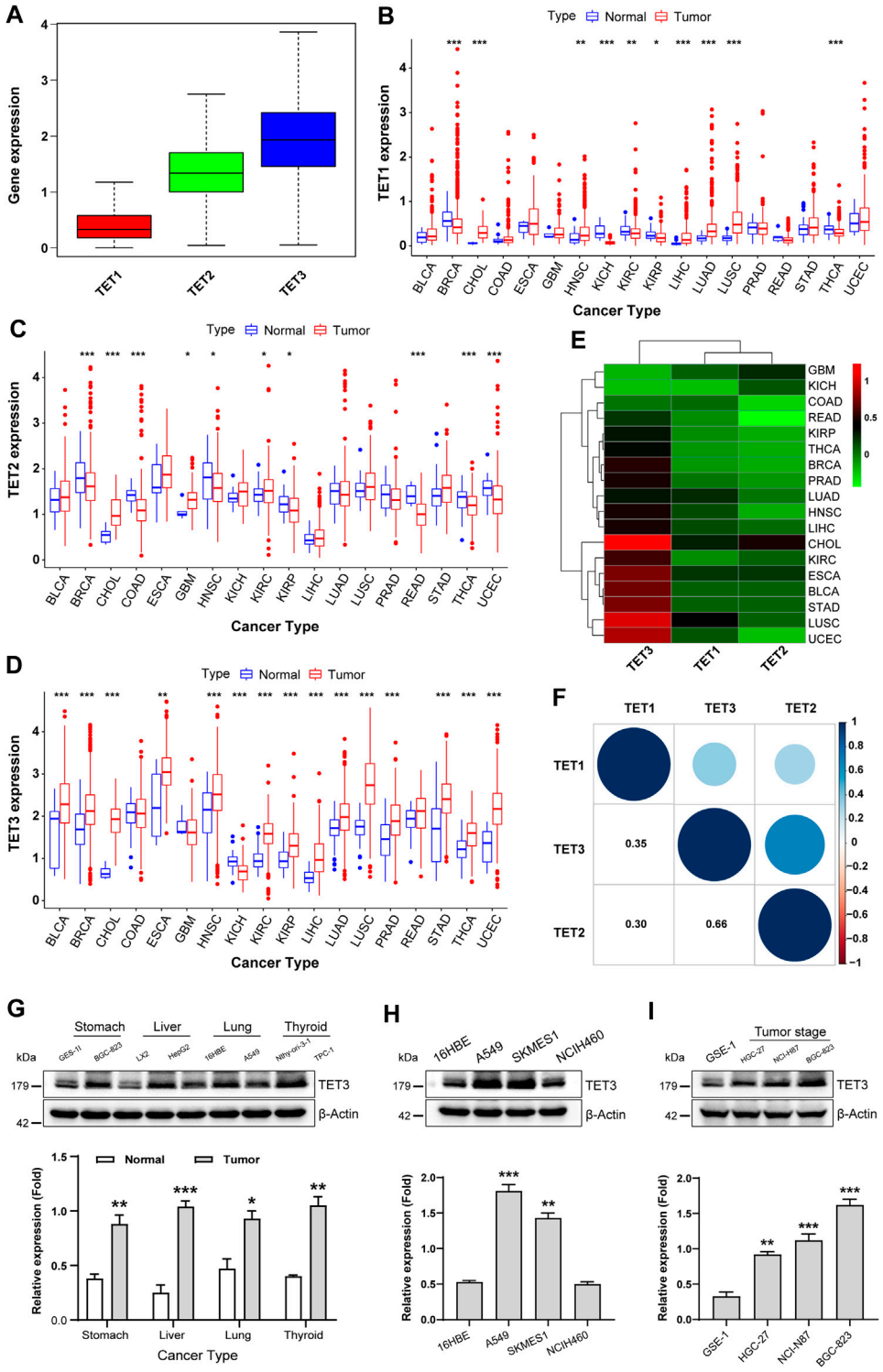

FIGURE 1
Expression and differential analysis of TET family genes in pan-cancer. **(A)** TET1, TET2, and TET3 expression was assessed across pan-cancer samples. **(B–D)** Differences in TET1-3 expression between pan-cancer and normal tissues were analyzed. **(E)** A heatmap visualized expression disparities among tumors using Wilcox analysis. **(F)** The expression correlation among TET family genes was analyzed in pan-cancer. **(G–I)** TET3 protein expression was evaluated across various cancer cell types **(G)**, lung tumor subtypes **(H)**, and gastric cancer cell differentiation levels **(I)**. Data are shown as mean ± SD, with statistical significance denoted as *$p < 0.05$, **$p < 0.01$, ***$p < 0.001$.

TABLE 1 Differential expression of TET family members in various tumors.

CancerType	TET1	TET2	TET3
BLCA	0.096236305	0.101847392	0.716234375
BRCA	−0.065518523	−0.144760041	0.506621202
CHOL	0.283859336	0.49181886	1.242806426
COAD	0.065707243	−0.283057513	0.027092671
ESCA	0.211017314	0.209220152	0.772441549
GBM	0.075892311	0.246159584	−0.18453126
HNSC	0.140153387	−0.137649947	0.479021335
KICH	−0.222646071	0.105693609	−0.22620435
KIRC	−0.030193499	0.079717096	0.589176718
KIRP	−0.044008843	−0.153032274	0.3255915
LIHC	0.165642026	0.057092953	0.501816772
LUAD	0.261827716	0.026681648	0.315641285
LUSC	0.399485757	0.093571817	1.013154683
PRAD	0.016403461	−0.083845777	0.483879586
READ	−0.039904543	−0.431725117	0.209207574
STAD	0.078809067	0.089785518	0.754909001
THCA	−0.066662138	−0.14246154	0.363362479
UCEC	0.121399047	−0.207671334	0.881939819

tissues. As shown in Figure 1B, TET1 exhibited abnormal expression in 10 types of tumors, with significantly downregulated expression observed in BRCA, KICH, KIRC, KIRP, and THCA, and upregulated expression noted in CHOL, HNSC, LIHC, LUAD, and LUSC tumors compared to their corresponding normal samples. The expression of TET2, in tumor samples such as BRCA, COAD, HNSC, KIRP, READ, and THCA, was lower, while in CHOL, GBM, KIRC, and UCEC tumors, it was significantly higher than that in corresponding normal control tissues (Figure 1C). The expression of the TET3 gene varied across 15 tumors and corresponding normal samples, including BLCA, BRCA, CHOL, ESCA, HNSC, KIRC, KIRP, LIHC, LUAD, LUSC, PRAD, STAD, THCA, UCEC, and KICH. Among these, except for KICH, TET3 was significantly overexpressed in all 14 other tumors (Figure 1D). These findings suggest that the high expression of TET3 may serve as a key factor in the occurrence, development, and poor prognosis of various clinical tumors.

To further elucidate the differential expression patterns of TET family members in various tumors, we conducted Wilcox analysis on the expression differences in each tumor and obtained the aforementioned differential expression cluster analysis graph (Figure 1E; Table 1). As previously mentioned, TET3 was significantly upregulated, while TET1 and TET2 were downregulated in most tumors. It remains unclear whether there is a correlation between the expression of the three members of the TET family in pan-cancer. Therefore, we conducted a detailed analysis of the correlation between TET family genes in pan-cancer. As illustrated in Figure 1F, the expression of TET1, TET2, and TET3 positively correlated in pan-cancer, with a stronger positive correlation observed between TET2 and TET3.

Given the high expression of TET3 in numerous tumors, we speculate that it may represent a potential therapeutic target. Consequently, we assessed the expression of TET3 protein in four tumor cell lines (BGC-823, HepG2, A549, TPC-1) and their corresponding normal cell lines (GES-1, LX2, 16HBE, Nthy-ori-3-1). The results demonstrated higher expression levels of TET3 in all four tumor cell lines compared to the corresponding control cell lines (Figures 1G–I). Subsequently, we examined the expression of TET3 protein in three different pathological subtypes of lung cancer cell lines (A549, SKMES1, NCIH460). The findings revealed significantly higher expression levels of TET3 protein in lung adenocarcinoma A549 and lung squamous cell carcinoma SKMES1 compared to normal controls and large cell lung cancer cell lines. This observation suggests differential expression of TET3 protein within the same type of tumors with varying pathological subtypes. Finally, we evaluated the expression of TET3 protein in gastric cancer cell lines (NCI-N87, BGC-823, HGC-27) with differing degrees of differentiation. The results indicated that as the degree of cell differentiation decreased, the expression of TET3 protein gradually increased. This implies that the expression intensity of TET3 protein may serve as an indicator of the malignant level of gastric cancer.

Somatic cell variation landscape of TET family genes

To comprehend the genomic alterations of TET1-3 in tumors, we scrutinized single nucleotide variant data (SNV, Table 2) and copy number variant data (CNV, Table 3) from a total of 10,289 pan-cancer samples spanning 33 types of tumors, and illustrated SNV and CNV landscapes.

Initially, we analyzed the SNP data pertaining to the TET gene to ascertain the frequency and variant types across each cancer subtype. As depicted in Figures 2A, B, among these cancers, the SNV frequency of UCEC, SKCM, and COAD ranges from 19% to 57%. The SNV frequency of the TETs gene collectively is 91.24% (1052/1153). Variant analysis unveiled missense mutation as the predominant SNP type. SNV percentage analysis revealed mutation rates of 23%, 17%, and 16% for TET1-3, respectively.

To elucidate the mutation pattern of CNV, we examined the CNV data of TETs genes in the TCGA database. The distribution of CNV pie charts illustrated heterozygous amplification and heterozygous deletion as the primary types (Figure 2C). CNV percentage analysis unveiled heterozygous amplification rates of TET1 in ACC and UCS, TET2 in ACC and KICH, and TET3 in ESCA, LUSC, OV, TGCT, and UCS, all exceeding 20% (Figure 2D). However, homozygous amplification was weak, observed solely in CHOL for TET1 (Figure 2E). Heterozygous deletions of TET1 in GBM, KICH, SARC, SKCM, and TGCT, TET2 in CHOL, ESCA, LIHC, LUSC, MESO, OV, READ, TGCT, and UCS, and TET3 in KICH and SARC, all surpassed 40% (Figure 2D). No homozygous deletions were noted across all tumors (Figure 2E).

TABLE 2 The single nucleotide variants index of TETs in the tumor genome.

Cancertype	Symbol	Effective Mut	Non Effective Mut	sample_size	Percentage	Entrez
ACC	TET1	2	1	92	2.173913043	80312
ACC	TET2	1	3	92	1.086956522	54790
ACC	TET3	1	1	92	1.086956522	200424
BLCA	TET1	26	8	411	6.326034063	80312
BLCA	TET2	9	4	411	2.189781022	54790
BLCA	TET3	11	4	411	2.676399027	200424
BRCA	TET1	14	11	1026	1.364522417	80312
BRCA	TET2	14	5	1026	1.364522417	54790
BRCA	TET3	12	6	1026	1.169590643	200424
CESC	TET1	11	3	291	3.780068729	80312
CESC	TET2	6	15	291	2.06185567	54790
CESC	TET3	8	3	291	2.749140893	200424
CHOL	TET2	0	1	36	0	54790
CHOL	TET3	1	0	36	2.777777778	200424
COAD	TET1	26	10	407	6.388206388	80312
COAD	TET2	19	30	407	4.668304668	54790
COAD	TET3	26	9	407	6.388206388	200424
DLBC	TET1	1	1	37	2.702702703	80312
DLBC	TET2	3	1	37	8.108108108	54790
DLBC	TET3	0	1	37	0	200424
ESCA	TET1	4	3	185	2.162162162	80312
ESCA	TET2	4	5	185	2.162162162	54790
ESCA	TET3	3	4	185	1.621621622	200424
GBM	TET1	8	2	403	1.985111663	80312
GBM	TET2	4	2	403	0.992555831	54790
GBM	TET3	5	1	403	1.240694789	200424
HNSC	TET1	9	4	509	1.768172888	80312
HNSC	TET2	7	5	509	1.37524558	54790
HNSC	TET3	9	1	509	1.768172888	200424
KICH	TET1	1	0	66	1.515151515	80312
KICH	TET2	0	1	66	0	54790
KICH	TET3	0	1	66	0	200424
KIRC	TET1	3	3	370	0.810810811	80312
KIRC	TET2	5	0	370	1.351351351	54790
KIRC	TET3	2	1	370	0.540540541	200424
KIRP	TET1	7	0	282	2.482269504	80312
KIRP	TET2	2	2	282	0.709219858	54790
KIRP	TET3	2	2	282	0.709219858	200424

(Continued on following page)

TABLE 2 (*Continued*) The single nucleotide variants index of TETs in the tumor genome.

Cancertype	Symbol	Effective Mut	Non Effective Mut	sample_size	Percentage	Entrez
LAML	TET1	1	0	85	1.176470588	80312
LGG	TET1	2	1	526	0.380228137	80312
LGG	TET2	5	2	526	0.950570342	54790
LGG	TET3	1	2	526	0.190114068	200424
LIHC	TET1	7	0	365	1.917808219	80312
LIHC	TET2	2	11	365	0.547945205	54790
LIHC	TET3	4	0	365	1.095890411	200424
LUAD	TET1	25	7	567	4.409171076	80312
LUAD	TET2	11	3	567	1.940035273	54790
LUAD	TET3	13	3	567	2.292768959	200424
LUSC	TET1	20	7	485	4.12371134	80312
LUSC	TET2	19	1	485	3.917525773	54790
LUSC	TET3	14	6	485	2.886597938	200424
MESO	TET1	1	0	82	1.219512195	80312
MESO	TET2	0	1	82	0	54790
OV	TET1	6	3	412	1.45631068	80312
OV	TET2	1	1	412	0.242718447	54790
OV	TET3	7	1	412	1.699029126	200424
PAAD	TET1	1	0	178	0.561797753	80312
PAAD	TET2	1	0	178	0.561797753	54790
PAAD	TET3	2	0	178	1.123595506	200424
PRAD	TET1	4	1	498	0.803212851	80312
PRAD	TET2	1	1	498	0.200803213	54790
PRAD	TET3	4	1	498	0.803212851	200424
READ	TET1	8	3	149	5.369127517	80312
READ	TET2	4	7	149	2.684563758	54790
READ	TET3	4	3	149	2.684563758	200424
SARC	TET1	2	3	239	0.836820084	80312
SARC	TET2	6	1	239	2.510460251	54790
SARC	TET3	3	2	239	1.255230126	200424
SKCM	TET1	52	21	468	11.111111111	80312
SKCM	TET2	37	14	468	7.905982906	54790
SKCM	TET3	42	25	468	8.974358974	200424
STAD	TET1	22	8	439	5.011389522	80312
STAD	TET2	17	2	439	3.872437358	54790
STAD	TET3	21	8	439	4.783599089	200424
TGCT	TET1	4	1	151	2.649006623	80312
THCA	TET1	2	0	500	0.4	80312

(Continued on following page)

TABLE 2 (*Continued*) The single nucleotide variants index of TETs in the tumor genome.

Cancertype	Symbol	Effective Mut	Non Effective Mut	sample_size	Percentage	Entrez
THCA	TET2	1	0	500	0.2	54790
THCA	TET3	2	2	500	0.4	200424
THYM	TET1	1	1	123	0.81300813	80312
THYM	TET2	1	0	123	0.81300813	54790
THYM	TET3	1	0	123	0.81300813	200424
UCEC	TET1	57	29	531	10.734463277	80312
UCEC	TET2	46	45	531	8.662900188	54790
UCEC	TET3	51	43	531	9.604519774	200424
UCS	TET1	1	1	57	1.754385965	80312
UCS	TET2	1	1	57	1.754385965	54790
UCS	TET3	1	0	57	1.754385965	200424
UVM	TET3	1	0	80	1.25	200424

Correlation analysis revealed a positive association between the mRNA expression of TETs and CNV, notably with TET2 in CHOL and ACC. Conversely, TET2 in LAML and TET3 in THMY exhibited negative correlations with CNV (Figure 2F; Table 4). This suggests that CNV of the TETs genes mediate abnormal expression in pan-cancer, potentially playing a pivotal role in cancer progression.

Methylation variation in TET family genes across pan-cancer

We delved into the methylation levels of TET genes across various cancers to decipher their epigenetic regulation. Our findings revealed heterogeneity in the methylation levels of TET family genes among different tumors. Specifically, TET1 gene exhibited hypermethylation in most cancers, with hypomethylation observed solely in LIHC. Conversely, TET2 and TET3 genes displayed hypomethylation in the majority of tumors, except for instances of hypermethylation in THCA, COAD, and KIRP for TET2 (Figure 3A). Correlation analysis between methylation and mRNA expression unveiled a negative correlation between the expression of these genes and their methylation levels across pan-cancer (Figure 3B; Table 2). Furthermore, survival analysis indicated that methylation of TET1 was linked to a lower survival rate in ACC and a higher survival rate in UVM; methylation of TET2 was associated with increased survival rates in ACC, KIRP, and PCPG; while methylation of TET3 correlated with decreased survival rates in SARC and BLCA (Figure 3C, Supplementary Table S2). These observations suggest that the methylation levels of TET genes are primarily associated with the survival outcomes of a limited number of tumors.

Pathway activity analysis of TET family genes in pan-cancer

Pathway activity analysis revealed significant involvement of TETs in cancer-related signaling pathways, including Cell Cycle, Apoptosis, DNA Damage Response, Hormone AR, PI3K/AKT, and RTK. Notably, TET1 primarily activated the DNA Damage Response pathway (19% activation vs. 0% inhibition), while TET2 mainly participated in the Cell Cycle (4% activation vs. 28% inhibition) and DNA Damage Response pathways (10% activation vs. 9% inhibition). TET3 showed activation primarily in the PI3K/AKT (19%) and the RTK pathway (16% activation vs. 6% inhibition) (Figure 4A; Table 5).

Given the significance of TET3, we modulated its expression in the NCI-N87 gastric cancer cell line. Overexpression of TET3 led to increased phosphorylation levels of AKT (Ser 308 and Ser 473) and mTOR (Ser2448), suppressed P21 expression, and enhanced HIF1α and c-Myc protein expression, whereas silencing TET3 exhibited the opposite effect (Figure 4B).

Sunitinib, a selective multi-target tyrosine kinase inhibitor, was employed to assess whether TET3 affects tumor behavior via the RTK pathway. We tested the therapeutic sensitivity of three different pathological subtypes of lung cancer cell lines (A549, SKMES1, NCIH460) to sunitinib. The results showed that A549 and SKMES1 cell lines with relatively high expression of TET3 exhibited higher sensitivity to sunitinib (Figure 4C). Similarly, we also tested the therapeutic sensitivity of gastric cancer cell lines (NCI-N87, BGC-823, HGC-27) with different degrees of differentiation to sunitinib. The results revealed that those with higher TET3 expression exhibited increased sensitivity to the drug (Figure 4D). These findings underscore the involvement of TET3 in regulating the PI3K/AKT and RTK pathways during tumor progression.

Influence of TET gene family on pan-cancer survival and prognosis

We conducted an analysis to assess the correlation between TET gene expression levels and the survival outcomes of patients across 33 types of tumors using data from the TCGA database. Kaplan-Meier survival curve analysis revealed that high expression of TET1 in ACC, KIRP, LIHC, SARC, and STAD was associated with shorter patient survival, while low expression in LGG and THYM indicated reduced survival. Similarly, high expression of

TABLE 3 The copy number variant index of TETs in the tumor genome.

Cancertype	Symbol	a_total	d_total	a_hete	d_hete	a_homo	d_homo	Entrez
ACC	TET1	27.7777778	13.3333333	27.7777778	13.3333333	0	0	80312
ACC	TET2	38.8888889	12.2222222	38.8888889	12.2222222	0	0	54790
ACC	TET3	15.5555556	20	15.5555556	18.8888889	0	1.1111111	200424
BLCA	TET1	10.7843137	35.0490196	9.8039216	33.8235294	0.9803922	1.2254902	80312
BLCA	TET2	7.5980392	37.0098039	7.1078431	36.7647059	0.4901961	0.245098	54790
BLCA	TET3	33.0882353	8.0882353	31.6176471	8.0882353	1.4705882	0	200424
BRCA	TET1	12.5925926	21.7592593	12.037037	21.5740741	0.5555556	0.1851852	80312
BRCA	TET2	9.537037	29.4444444	9.0740741	29.0740741	0.462963	0.3703704	54790
BRCA	TET3	16.2962963	15	15.7407407	14.9074074	0.5555556	0.0925926	200424
CESC	TET1	5.7627119	25.0847458	5.7627119	25.0847458	0	0	80312
CESC	TET2	6.1016949	32.2033898	6.1016949	31.8644068	0	0.3389831	54790
CESC	TET3	23.0508475	5.7627119	23.0508475	5.7627119	0	0	200424
CHOL	TET1	16.6666667	13.8888889	11.1111111	13.8888889	5.5555556	0	80312
CHOL	TET2	5.5555556	44.4444444	5.5555556	44.4444444	0	0	54790
CHOL	TET3	11.1111111	5.5555556	11.1111111	5.5555556	0	0	200424
COAD	TET1	5.5432373	19.5121951	5.3215078	19.5121951	0.2217295	0	80312
COAD	TET2	3.7694013	29.9334812	3.7694013	29.7117517	0	0.2217295	54790
COAD	TET3	17.9600887	1.5521064	17.9600887	1.5521064	0	0	200424
DLBC	TET1	10.4166667	6.25	10.4166667	6.25	0	0	80312
DLBC	TET2	0	10.4166667	0	10.4166667	0	0	54790
DLBC	TET3	12.5	6.25	10.4166667	2.0833333	2.0833333	4.1666667	200424
ESCA	TET1	19.5652174	27.7173913	18.4782609	27.7173913	1.0869565	0	80312
ESCA	TET2	10.8695652	52.7173913	10.8695652	52.7173913	0	0	54790
ESCA	TET3	39.673913	4.3478261	38.5869565	4.3478261	1.0869565	0	200424
GBM	TET1	0.3466205	87.3483536	0.3466205	86.8284229	0	0.5199307	80312
GBM	TET2	4.6793761	10.745234	4.6793761	10.5719237	0	0.1733102	54790
GBM	TET3	6.2391681	6.7590988	6.2391681	6.7590988	0	0	200424
HNSC	TET1	8.2375479	23.9463602	7.6628352	23.9463602	0.5747126	0	80312
HNSC	TET2	9.3869732	30.4597701	9.3869732	30.2681992	0	0.1915709	54790
HNSC	TET3	21.2643678	4.789272	20.8812261	4.789272	0.3831418	0	200424
KICH	TET1	4.5454545	72.7272727	4.5454545	72.7272727	0	0	80312
KICH	TET2	34.8484848	1.5151515	34.8484848	1.5151515	0	0	54790
KICH	TET3	3.030303	69.6969697	3.030303	69.6969697	0	0	200424
KIRC	TET1	2.2727273	16.8560606	2.2727273	16.8560606	0	0	80312
KIRC	TET2	2.2727273	14.2045455	2.0833333	14.0151515	0.1893939	0.1893939	54790
KIRC	TET3	14.3939394	2.6515152	14.3939394	2.6515152	0	0	200424
KIRP	TET1	2.4305556	5.9027778	2.4305556	5.9027778	0	0	80312
KIRP	TET2	3.8194444	9.0277778	3.8194444	9.0277778	0	0	54790

(Continued on following page)

TABLE 3 (*Continued*) The copy number variant index of TETs in the tumor genome.

Cancertype	Symbol	a_total	d_total	a_hete	d_hete	a_homo	d_homo	Entrez
KIRP	TET3	14.9305556	2.4305556	14.9305556	2.0833333	0	0.3472222	200424
LAML	TET1	1.5706806	0.5235602	1.5706806	0.5235602	0	0	80312
LAML	TET2	2.0942408	1.5706806	2.0942408	1.0471204	0	0.5235602	54790
LAML	TET3	1.0471204	0	1.0471204	0	0	0	200424
LGG	TET1	0.7797271	19.6881092	0.7797271	19.6881092	0	0	80312
LGG	TET2	1.1695906	20.0779727	0.7797271	19.6881092	0.3898635	0.3898635	54790
LGG	TET3	2.5341131	4.288499	2.5341131	4.288499	0	0	200424
LIHC	TET1	11.8918919	21.0810811	11.3513514	21.0810811	0.5405405	0	80312
LIHC	TET2	1.8918919	47.027027	1.8918919	46.2162162	0	0.8108108	54790
LIHC	TET3	11.8918919	10	11.8918919	10	0	0	200424
LUAD	TET1	15.8914729	25.5813953	15.1162791	25.1937984	0.7751938	0.3875969	80312
LUAD	TET2	9.6899225	31.3953488	9.496124	31.3953488	0.1937984	0	54790
LUAD	TET3	28.875969	5.2325581	28.2945736	5.2325581	0.5813953	0	200424
LUSC	TET1	12.1756487	44.510978	11.7764471	43.7125749	0.3992016	0.7984032	80312
LUSC	TET2	5.5888224	60.2794411	5.3892216	60.0798403	0.1996008	0.1996008	54790
LUSC	TET3	48.3033932	2.1956088	46.3073852	2.1956088	1.996008	0	200424
MESO	TET1	3.4482759	19.5402299	2.2988506	19.5402299	1.1494253	0	80312
MESO	TET2	1.1494253	44.8275862	1.1494253	44.8275862	0	0	54790
MESO	TET3	5.7471264	8.045977	5.7471264	8.045977	0	0	200424
OV	TET1	24.5250432	26.2521589	22.4525043	25.9067358	2.0725389	0.3454231	80312
OV	TET2	4.6632124	72.193437	4.3177893	70.984456	0.3454231	1.208981	54790
OV	TET3	35.4058722	10.1899827	33.5060449	10.0172712	1.8998273	0.1727116	200424
PAAD	TET1	7.6086957	15.2173913	7.0652174	15.2173913	0.5434783	0	80312
PAAD	TET2	5.4347826	15.7608696	5.4347826	15.7608696	0	0	54790
PAAD	TET3	7.6086957	5.9782609	7.6086957	5.9782609	0	0	200424
PCPG	TET1	6.1728395	0.617284	6.1728395	0.617284	0	0	80312
PCPG	TET2	3.0864198	6.1728395	1.8518519	6.1728395	1.2345679	0	54790
PCPG	TET3	3.0864198	6.7901235	3.0864198	6.7901235	0	0	200424
PRAD	TET1	4.4715447	10.5691057	4.0650407	9.7560976	0.4065041	0.8130081	80312
PRAD	TET2	2.4390244	6.300813	2.4390244	4.6747967	0	1.6260163	54790
PRAD	TET3	3.0487805	7.5203252	2.8455285	6.300813	0.203252	1.2195122	200424
READ	TET1	5.4545455	22.4242424	4.8484848	22.4242424	0.6060606	0	80312
READ	TET2	3.030303	44.2424242	3.030303	43.6363636	0	0.6060606	54790
READ	TET3	23.030303	7.2727273	23.030303	7.2727273	0	0	200424
SARC	TET1	3.8910506	56.4202335	3.5019455	55.2529183	0.3891051	1.1673152	80312
SARC	TET2	15.1750973	24.9027237	14.7859922	24.9027237	0.3891051	0	54790
SARC	TET3	12.4513619	32.6848249	11.6731518	32.6848249	0.7782101	0	200424
SKCM	TET1	1.0899183	60.4904632	1.0899183	60.4904632	0	0	80312

(Continued on following page)

TABLE 3 (*Continued*) The copy number variant index of TETs in the tumor genome.

Cancertype	Symbol	a_total	d_total	a_hete	d_hete	a_homo	d_homo	Entrez
SKCM	TET2	12.5340599	26.1580381	11.9891008	25.8855586	0.5449591	0.2724796	54790
SKCM	TET3	17.7111717	13.6239782	17.4386921	13.6239782	0.2724796	0	200424
STAD	TET1	18.8208617	16.7800454	17.4603175	16.3265306	1.3605442	0.4535147	80312
STAD	TET2	4.7619048	39.2290249	4.7619048	38.5487528	0	0.6802721	54790
STAD	TET3	20.4081633	4.0816327	20.1814059	4.0816327	0.2267574	0	200424
TGCT	TET1	4	52	4	52	0	0	80312
TGCT	TET2	0	73.3333333	0	73.3333333	0	0	54790
TGCT	TET3	32.6666667	6	32.6666667	6	0	0	200424
THCA	TET1	0.4008016	2.2044088	0.4008016	1.4028056	0	0.8016032	80312
THCA	TET2	1.002004	0.4008016	1.002004	0.4008016	0	0	54790
THCA	TET3	0.4008016	1.8036072	0.4008016	1.8036072	0	0	200424
THYM	TET1	1.6260163	1.6260163	1.6260163	1.6260163	0	0	80312
THYM	TET2	1.6260163	3.2520325	1.6260163	3.2520325	0	0	54790
THYM	TET3	0.8130081	0.8130081	0.8130081	0.8130081	0	0	200424
UCEC	TET1	22.4489796	10.0185529	21.5213358	10.0185529	0.9276438	0	80312
UCEC	TET2	1.8552876	20.9647495	1.6697588	20.593692	0.1855288	0.3710575	54790
UCEC	TET3	20.0371058	2.0408163	18.3673469	1.8552876	1.6697588	0.1855288	200424
UCS	TET1	39.2857143	33.9285714	39.2857143	33.9285714	0	0	80312
UCS	TET2	3.5714286	69.6428571	3.5714286	69.6428571	0	0	54790
UCS	TET3	44.6428571	5.3571429	44.6428571	5.3571429	0	0	200424
UVM	TET1	0	1.25	0	1.25	0	0	80312
UVM	TET2	5	5	5	5	0	0	54790
UVM	TET3	12.5	0	12.5	0	0	0	200424

TET2 in OV, PCPG, and UCS was linked to shorter survival, whereas low expression in KIRC correlated with decreased survival. Additionally, high expression of TET3 in ACC, MESO, and PCPG was associated with shorter survival, while low expression in THCA indicated reduced survival (Figure 5, Supplementary Table S3).

Furthermore, we evaluated the relationship between TET expression and cancer prognosis (Figure 6). COX regression analysis across 33 cancer types revealed that high expression of TET1 in ACC, BLCA, CESC, LIHC, PCPG, and SARC was indicative of poor prognosis, while in LGG, THYM, and UVM, it suggested a favorable prognosis. Conversely, in KIRC, high expression of TET2 was associated with a favorable prognosis. Notably, high expression of TET3 in ACC alone indicated a poor prognosis among tumor patients.

Correlation between TET family genes expression and immune subtypes in pan-cancer and single tumors

To elucidate the association between TETs and immune responses, we conducted a pan-cancer analysis correlating TETs expression with immune subtypes using the TCGA database. As depicted in Figure 7A, TETs expression exhibited a significant positive correlation with pan-cancer immune subtypes ($p < 0.05$): notably, TET1 and TET2 were markedly upregulated in immune subtype C5, whereas their expression remained stable in other subtypes; TET3 displayed variable expression levels across immune subtypes. To further delineate the specific immune subtype associations with TETs, we performed KS test correlation analysis in eight common tumors. Results indicated significant correlations between TETs expression and immune subtypes in most tumors ($p < 0.05$), with TET1 consistently exhibiting the lowest expression across all subtypes, while TET3 demonstrated high expression levels (Figure 7B). In STAD, LIHC, and LUAD, TETs expression showed significant positive correlations with various immune responses. Notably, TET1 displayed highest expression in STAD's C3 subtype and minimal expression in C2, while TET2 was consistently upregulated across all subtypes. Conversely, in LIHC, TET1 and TET3 exhibited decreasing expression trends across subtypes, with TET1 almost absent in C6, and TET2 lowest in C2. In LUAD, TET1 expression remained stable, while TET2 peaked in C3 and declined in C4, and TET3 expression was highest in C1 and lowest in C4. However,

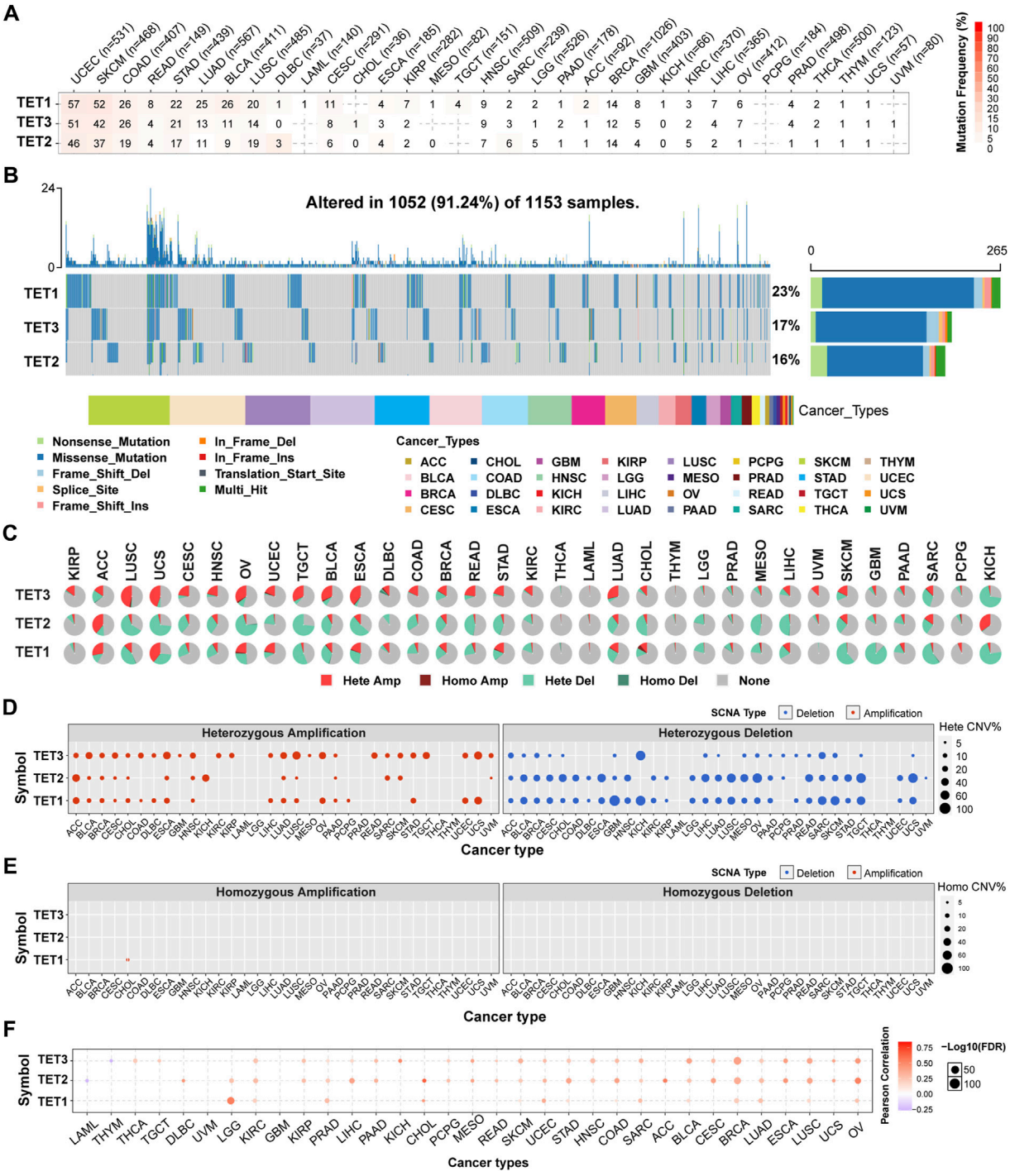

FIGURE 2
Somatic mutations in TET family genes were analyzed. **(A)** Single Nucleotide Variants (SNV) frequencies of TETs across cancers are presented in a table, indicating mutated gene counts per cancer type. '0' indicates that there was no mutation in the gene coding region, and no number indicates there was no mutation in any region of the gene. **(B)** SNV variant types of TETs illustrate mutation distribution and categorization. **(C)** copy number variant (CNV) distribution across 33 cancers is depicted in pie charts, showing combined heterozygous/homozygous CNV proportions for each gene in each cancer. Hete Amp = heterozygous amplification; Hete Del = heterozygous deletion; Homo Amp = homozygous amplification; Homo Del = homozygous deletion; None = no CNV. **(D, E)** Heterozygous and homozygous CNV profiles display the percentage of CNV, including amplification and deletion, for each gene in each cancer. Only genes with >5% CNV in a given cancer are shown as a point on figure. **(F)** CNV correlation with mRNA expression is depicted through Person's correlation analysis, with point size indicating statistical significance. FDR, false discovery rate.

COAD and LUSC immune subtypes showed significant correlations only with TET1 and TET3 expression. TET1 was highly expressed across all COAD immune subtypes, while TET3 was least expressed in C3. In LUSC, TET1 displayed minimal expression in C3 and C4, while TET3 was lowest in C6 and stable in other subtypes. In summary, TET1 exhibited consistently low expression across

TABLE 4 The correlation between CNV and their mRNA expression.

Cancertype	Symbol	Spm	fdr	Entrez
ACC	TET1	0.430415695	0.000382089	80312
ACC	TET2	0.511309337	0.000012999	54790
ACC	TET3	0.051295551	0.745616362	200424
BLCA	TET1	0.114024143	0.033251141	80312
BLCA	TET2	0.336644723	1.10974382E-11	54790
BLCA	TET3	0.340550181	6.120072297E-12	200424
BRCA	TET1	0.17684712	9.213854436E-09	80312
BRCA	TET2	0.315899282	5.853643734E-26	54790
BRCA	TET3	0.383294576	1.790536808E-38	200424
CESC	TET1	−0.011925245	0.873039475	80312
CESC	TET2	0.433545123	4.588165373E-14	54790
CESC	TET3	0.271741685	0.000006056254999	200424
CHOL	TET1	0.428258757	0.038654288	80312
CHOL	TET2	0.561405786	0.003283608	54790
CHOL	TET3	0.056461562	0.848010845	200424
COAD	TET1	0.073510305	0.297222482	80312
COAD	TET2	0.352256129	4.196154549E-09	54790
COAD	TET3	0.253839	0.000038277	200424
DLBC	TET1	0.275888429	0.263041898	80312
DLBC	TET2	0.295977236	0.218166997	54790
DLBC	TET3	0.095479039	0.784130723	200424
ESCA	TET1	−0.019454847	0.83412304	80312
ESCA	TET2	0.4619393	2.010983006E-10	54790
ESCA	TET3	0.372357854	0.0000006135376908	200424
GBM	TET1	−0.053067272	0.63830057	80312
GBM	TET2	−0.08313632	0.433185966	54790
GBM	TET3	0.076977807	0.472044777	200424
HNSC	TET1	0.023066842	0.657651986	80312
HNSC	TET2	0.251620139	1.746877379E-08	54790
HNSC	TET3	0.306192782	3.865545249E-12	200424
KICH	TET1	0.148008977	0.377833687	80312
KICH	TET2	0.05092177	0.794830274	54790
KICH	TET3	0.529190704	0.000065305	200424
KIRC	TET1	0.147881527	0.001647943	80312
KIRC	TET2	0.17761043	0.000127103	54790
KIRC	TET3	0.117307811	0.014200842	200424
KIRP	TET1	−0.007483698	0.926764006	80312
KIRP	TET2	0.189767588	0.002997358	54790

(Continued on following page)

TABLE 4 (*Continued*) The correlation between CNV and their mRNA expression.

Cancertype	Symbol	Spm	fdr	Entrez
KIRP	TET3	0.188767054	0.00317016	200424
LAML	TET1	0.149963407	0.334679172	80312
LAML	TET2	−0.003409614	0.990688679	54790
LAML	TET3	−0.137435668	0.391747523	200424
LGG	TET1	0.467842231	5.692491551E-28	80312
LGG	TET2	0.079155919	0.114763564	54790
LGG	TET3	0.046883491	0.375849928	200424
LIHC	TET1	0.110406029	0.056609338	80312
LIHC	TET2	0.411352746	1.740150257E-15	54790
LIHC	TET3	0.230812946	0.00002128	200424
LUAD	TET1	0.241128773	7.011929884E-08	80312
LUAD	TET2	0.318284609	4.396339316E-13	54790
LUAD	TET3	0.225184712	0.0000005295820664	200424
LUSC	TET1	0.154795317	0.000812676	80312
LUSC	TET2	0.415485507	1.074058287E-21	54790
LUSC	TET3	0.381062315	3.352834713E-18	200424
MESO	TET1	0.089110139	0.542886691	80312
MESO	TET2	0.421938585	0.000298081	54790
MESO	TET3	0.381702164	0.001299683	200424
OV	TET1	0.234019939	0.000066111	80312
OV	TET2	0.551932491	7.243171248E-25	54790
OV	TET3	0.431378446	1.043908895E-14	200424
PAAD	TET1	−0.061448553	0.515955742	80312
PAAD	TET2	0.199723579	0.016853621	54790
PAAD	TET3	0.142297603	0.100590146	200424
PCPG	TET1	0.018434753	0.886632411	80312
PCPG	TET2	0.145142755	0.139559512	54790
PCPG	TET3	0.166062429	0.084315004	200424
PRAD	TET1	0.154472002	0.002081839	80312
PRAD	TET2	−0.003035538	0.965320811	54790
PRAD	TET3	0.02348171	0.711296619	200424
READ	TET1	0.016981146	0.916053342	80312
READ	TET2	0.383910653	0.000470645	54790
READ	TET3	0.241234307	0.03995682	200424
SARC	TET1	0.295420904	0.000004026630119	80312
SARC	TET2	0.199937606	0.002495798	54790
SARC	TET3	0.303585043	0.000002051512803	200424
SKCM	TET1	0.119676377	0.033771157	80312

(Continued on following page)

TABLE 4 (*Continued*) The correlation between CNV and their mRNA expression.

Cancertype	Symbol	Spm	fdr	Entrez
SKCM	TET2	0.193024785	0.000387309	54790
SKCM	TET3	0.223515543	0.000033163	200424
STAD	TET1	0.150082077	0.003950941	80312
STAD	TET2	0.374310942	1.742633898E-14	54790
STAD	TET3	0.295686853	2.760124327E-09	200424
TGCT	TET1	0.076588277	0.449268635	80312
TGCT	TET2	0.138882271	0.143924951	54790
TGCT	TET3	0.208033963	0.022204873	200424
THCA	TET1	0.096471699	0.120203443	80312
THCA	TET2	0.006562727	0.943305456	54790
THCA	TET3	−0.021385958	0.79793012	200424
THYM	TET1	−0.001319092	0.994135125	80312
THYM	TET2	0.172829062	0.166760439	54790
THYM	TET3	−0.046292677	0.763030306	200424
UCEC	TET1	0.313307531	0.000070915	80312
UCEC	TET2	0.323505359	0.000038654	54790
UCEC	TET3	0.262893322	0.001039668	200424
UCS	TET1	0.249431789	0.112968663	80312
UCS	TET2	0.41846238	0.003818614	54790
UCS	TET3	0.408150735	0.004958962	200424
UVM	TET1	−0.013131937	0.954523434	80312
UVM	TET2	0.110891607	0.536029019	54790
UVM	TET3	−0.012770116	0.956015278	200424

various tumors, while TET3 showed highest expression levels, both closely associated with pan-cancer immune subtypes.

Correlation analysis of TET family genes expression with tumor microenvironment (TME) and stem cell index across pan-cancer

The efficacy of radiotherapy, chemotherapy, and immunotherapy in treating tumors is greatly influenced by the Tumor Microenvironment (TME). Utilizing the ESTIMATE algorithm, we assessed TME characteristics across 33 tumor types by computing Stromal Score, Immune Score, and ESTIMATE Score. Analysis from Figures 8A–C reveals that TET1 exhibits higher Stromal Scores in COAD, ESCA, KIRP, MESO, PAAD, and STAD, with elevated Immune and ESTIMATE Scores observed specifically in PAAD. These findings suggest that upregulating TET1 expression may enhance TME in PAAD, potentially suppressing tumor invasion, metastasis, and augmenting immunotherapy sensitivity. Conversely, heightened TET1 expression may exacerbate TME conditions in GBM, LGG, and TGCT, potentially escalating invasion, metastasis, and drug resistance.

Similarly, TET2 displays elevated Stromal Scores in CHOL, LAML, and MESO, alongside increased Immune Scores in DLBC and LAML, and higher ESTIMATE Scores in DLBC and LAML. Conversely, reduced Stromal Scores are noted in BLCA and GBM, while diminished Immune Scores are observed in ACC, BLCA, GBM, PCPG, SARC, and THYM, collectively translating to overall lower scores in ACC, BLCA, GBM, and PCPG. This suggests that restoring TET2 expression may ameliorate TME in LAML, potentially suppressing invasion, metastasis, and bolstering immunotherapy sensitivity. However, it may exacerbate TME conditions in BLCA and GBM, fostering invasion, metastasis, and drug resistance.

Meanwhile, TET3 exhibits heightened Stromal, Immune, and ESTIMATE Scores in KICH, KIRC, and LAML, while displaying diminished Stromal Scores in BLCA, ESCA, GBM, LUSC, and STAD, alongside reduced Immune Scores in BLCA, CESC, ESCA, GBM, LUSC, and UCEC, culminating in overall lower scores in BLCA,

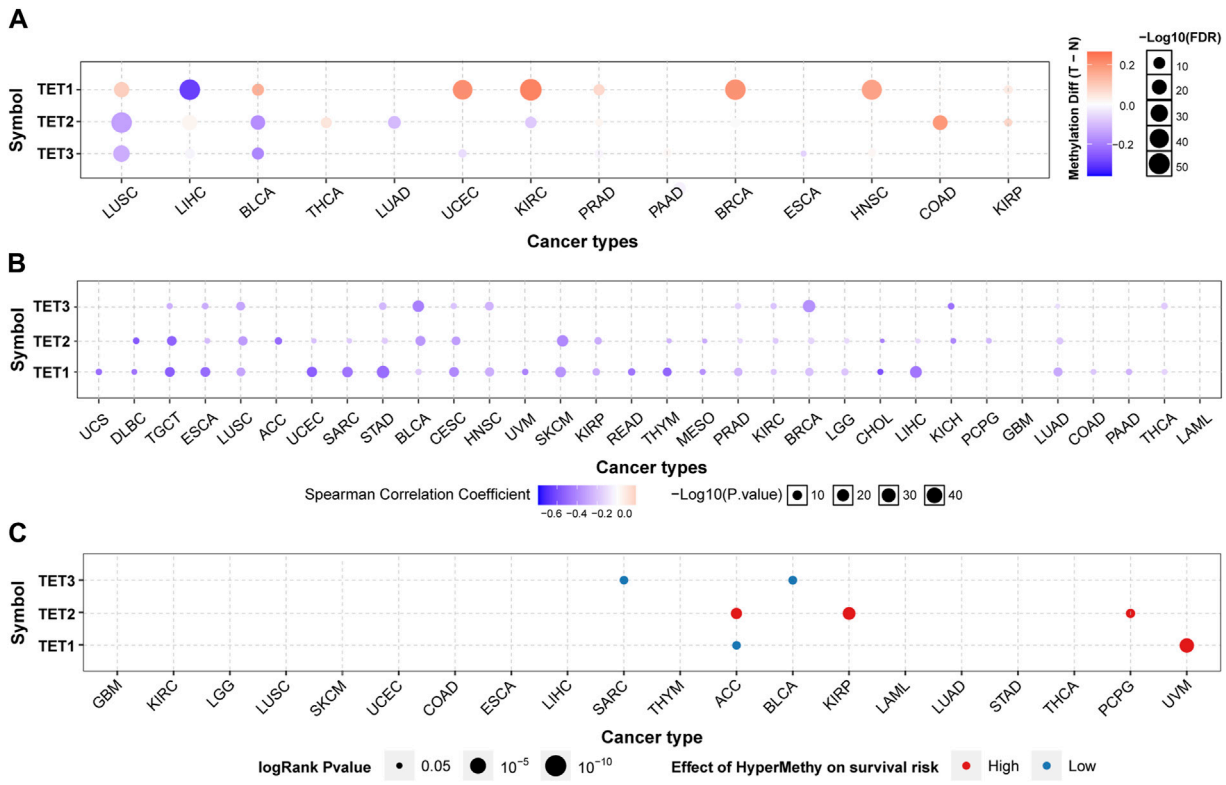

FIGURE 3
Methylation analysis of TET family genes in pan-cancer. **(A)** Methylation levels of TETs genes were examined to assess epigenetic regulation. **(B)** Correlation between methylation and mRNA expression of TETs genes in pan-cancer was analyzed. Then, association of survival rate with methylation level of TETs genes was investigated **(C)**.

TABLE 5 Signaling pathways that are significantly correlated with TETs.

Gene	CancerType	*p*-value
TET3	ACC	0.00000227
TET1	ACC	0.0000117
TET1	LGG	0.000108119
TET2	KIRC	0.001101312
TET1	THYM	0.005565956
TET1	LIHC	0.009310381
TET2	OV	0.012079857
TET1	STAD	0.012577951
TET1	SARC	0.016864357
TET2	UCS	0.018971079
TET3	MESO	0.027885901
TET3	THCA	0.033935782
TET2	PCPG	0.033970023
TET3	PCPG	0.039436326
TET1	KIRP	0.043112406

CESC, ESCA, GBM, LUSC, and UCEC. This suggests that inducing TET3 expression may enhance TME in KICH, KIRC, and LAML, potentially suppressing invasion, metastasis, and augmenting immunotherapy sensitivity. Conversely, it may deteriorate TME conditions in BLCA, CESC, ESCA, GBM, LUSC, and UCEC, fostering invasion, metastasis, and drug resistance.

Moreover, the therapeutic efficacy of radiotherapy, chemotherapy, and immunotherapy is closely linked to the tumor stem cell index. Figures 8D, E indicates that TET1 expression is positively correlated with RNAss in LGG and TGCT, while negatively correlated with KIRC, PAAD, and STAD. TET2 levels are negatively correlated with RNAss in CHOL, KIRP, and THYM. Conversely, TET3 levels are negatively correlated in KICH, KIRP, THCA, and THYM, and positively correlated in BLCA, BRCA, and PRAD. Additionally, TET1 expression is positively correlated with DNAss in GBM and TGCT, but negatively correlated with LGG, OV, and THYM. TET2 shows a positive correlation in TGCT and a negative correlation in OV, while TET3 exhibits a negative correlation in OV.

Next, we conducted a detailed analysis of the tumor microenvironment and stem cell index of eight common clinical cancers (Figure 9). The results showed that for tumor microenvironment-related scores, TET1 was significantly positively correlated with the three scores of PAAD, and

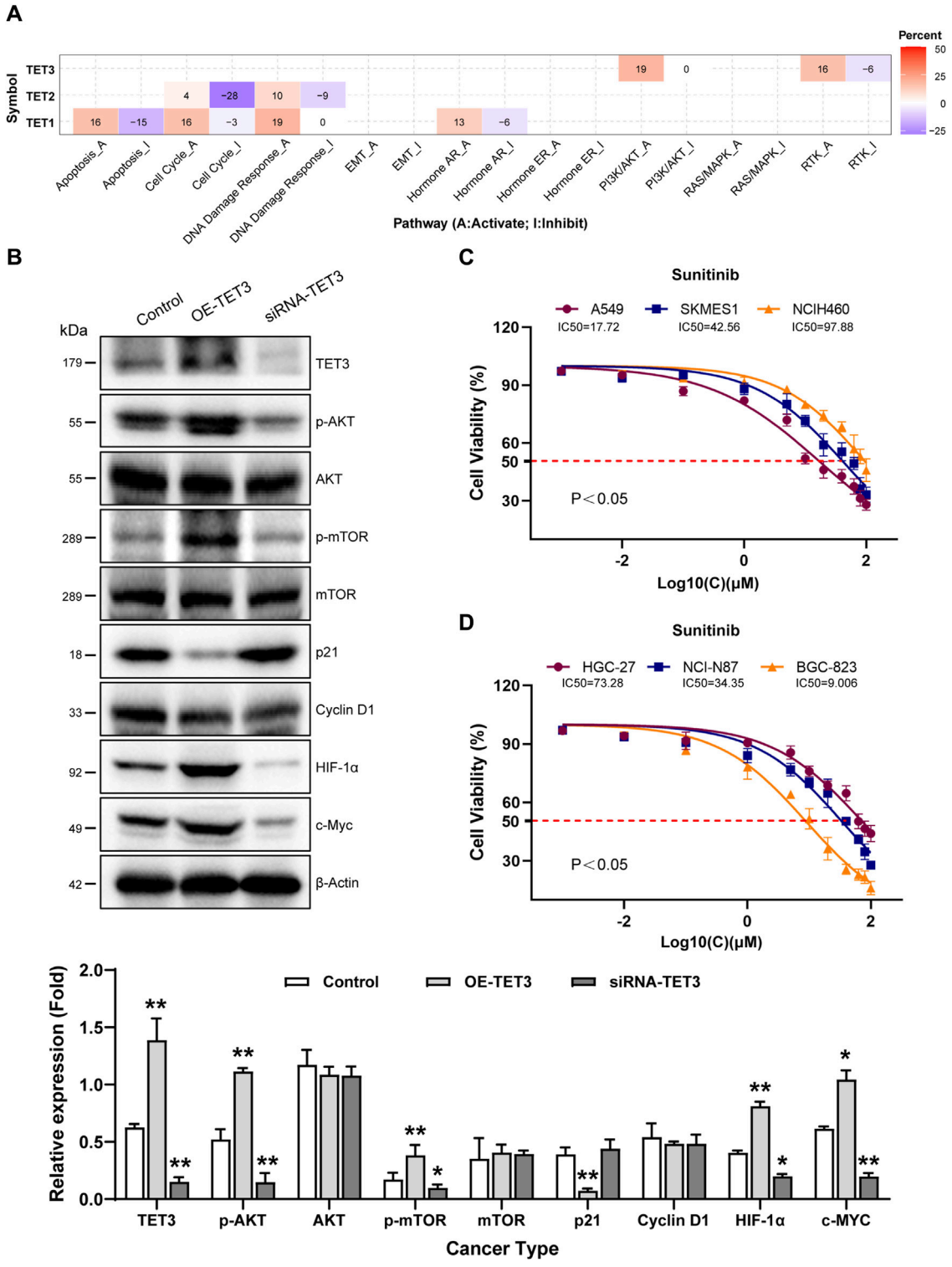

FIGURE 4
Pathway activity analysis of TET family genes in pan-cancer. **(A)** Combined percentage of TET genes' effect on pathway activity is depicted. Red indicates activation, while blue indicates inhibition. Numbers in the table represent the percentage of pathway activity on TETs. Red represents activate effect and blue represents inhibition. **(B)** Impact of TET3 on protein expression levels of key signaling pathway members was assessed via Western blot. **(C, D)** Therapeutic sensitivity of lung and gastric cancer cells to Sunitinib, a multi-target tyrosine kinase inhibitor, was tested to elucidate the role of TET3 in regulating the RTK pathway as shown in Figure 4A.

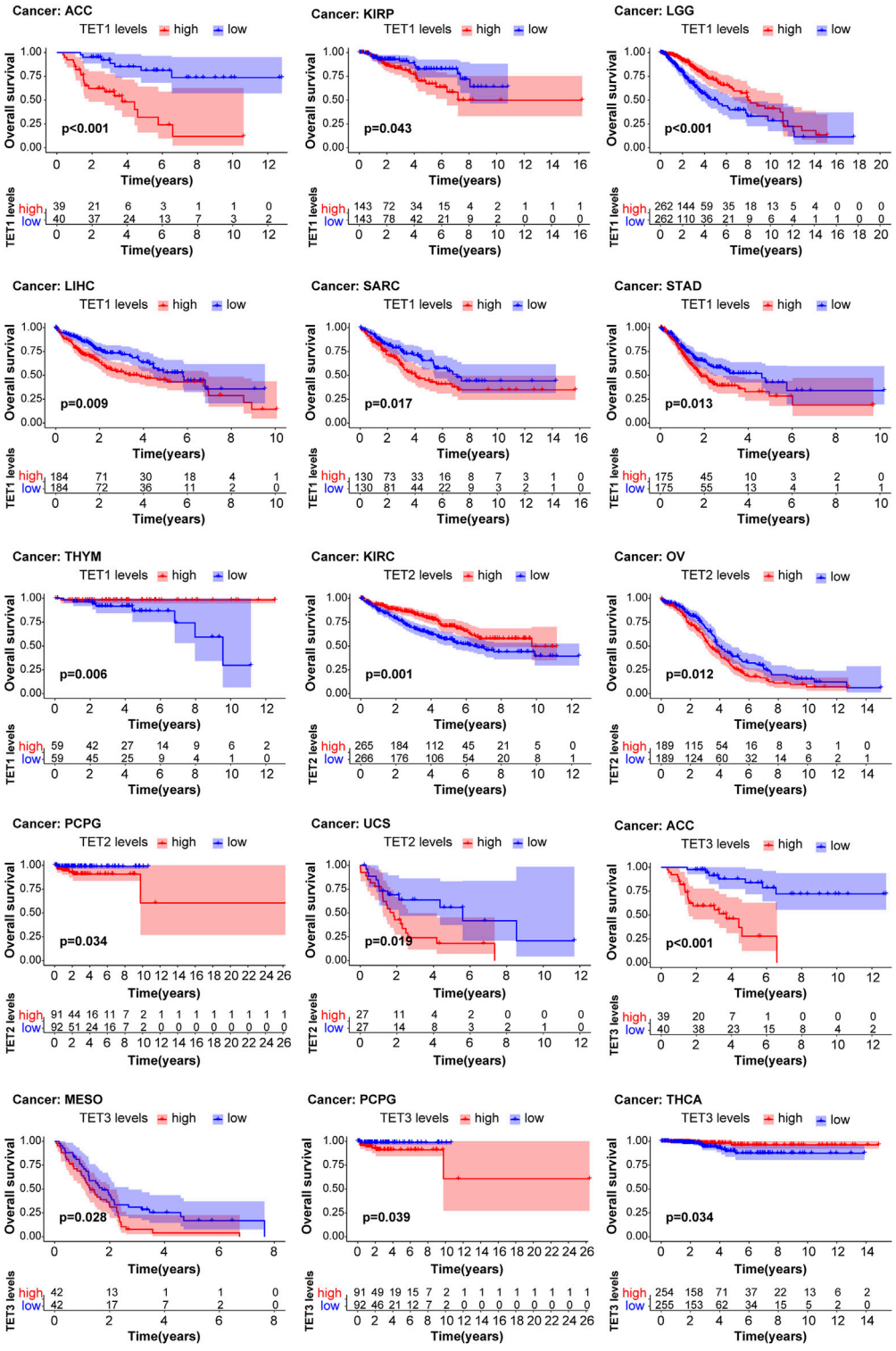

FIGURE 5
Analysis of TET family genes expression and patient prognosis using univariate KM risk proportional regression model.

negatively in LUAC. Its stem cell index is negatively correlated in STAD and COAD, and positively in LUAD and LUAC. TET2 shows a significant positive correlation with the TME score in COAD, and a negative correlation with the stem cell index in PAAD. TET3 is significantly negatively correlated with TME scores in STAD and LUAC, and positively with the stem cell index in STAD, LUAD, and LUAC. In addition, several tumors had no significant correlation with their microenvironment score and stem cell index.

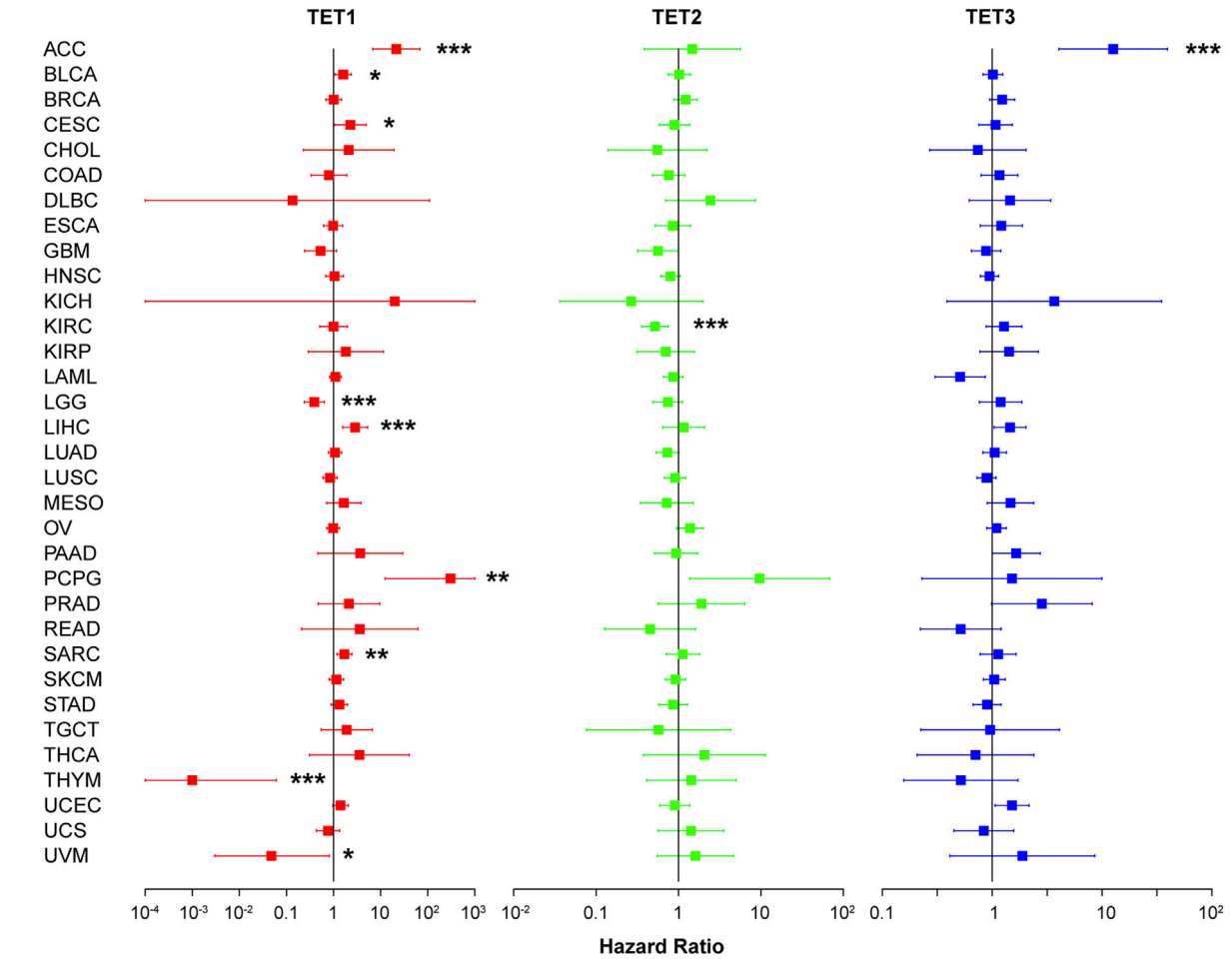

FIGURE 6
Impact of TET family genes on pan-cancer prognosis through COX regression analysis.

TET family genes expression was correlated with clinical stages across various cancers, indicating their potential as prognostic markers

These findings underscore the close relationship between TET gene expression and both the tumor microenvironment and tumor stemness potential. Further analysis revealed distinct correlations between TET gene expression and clinical stages across eight common tumor types. As shown in Figure 10, there was no significant difference between the expression level of TETs genes and clinical stage of tumors in COAD and READ. Notably, TET2 and TET3 exhibited significant correlations with clinical stages in LIHC, with elevated expression in Stage III and reduced expression in Stage IV. Similarly, in LUSC, TET1 and TET3 expression levels were notably associated with clinical stages, showing upregulation in Stage III and downregulation in Stage IV. Furthermore, TET2 expression levels were significantly linked to clinical staging in STAD and LUAD, with varying expressions across different stages. In PAAD, TET3 expression levels exhibited significant correlation with clinical characteristics, displaying the lowest expression in Stage III and the highest expression in Stage IV. These results maybe highlight the distinctive correlations between TET gene expression and clinical stages across various tumors.

TET family genes levels were analyzed for their impact on drug sensitivity

Using the CellMiner ™ database, we conducted an analysis to explore potential correlations between gene expression levels of TET family members and drug sensitivity across various human tumors (Figure 11A, Supplementary Table S4). We identified the top 16 chemotherapy-sensitive drugs exhibiting the highest correlation coefficients with TETs genes. Notably, the expression level of TET1 displayed significant positive correlations with drug sensitivity to Arsenic trioxide, Fenretinide, Dimethylaminophenhenolide, Daunorubicin, Homoharringtonine, Imatinib, Testolactone, Pipapperone, and Lomustine. Conversely, TET2 expression was positively correlated with drug sensitivity to Fulvestrant and Raloxifene but significantly negatively correlated with Vemurafenib and Dabrafenib. Moreover, the expression level of TET3 exhibited significant positive correlations with drug sensitivity to Lapatinib, AZD-9291, and (+)-JQ1.

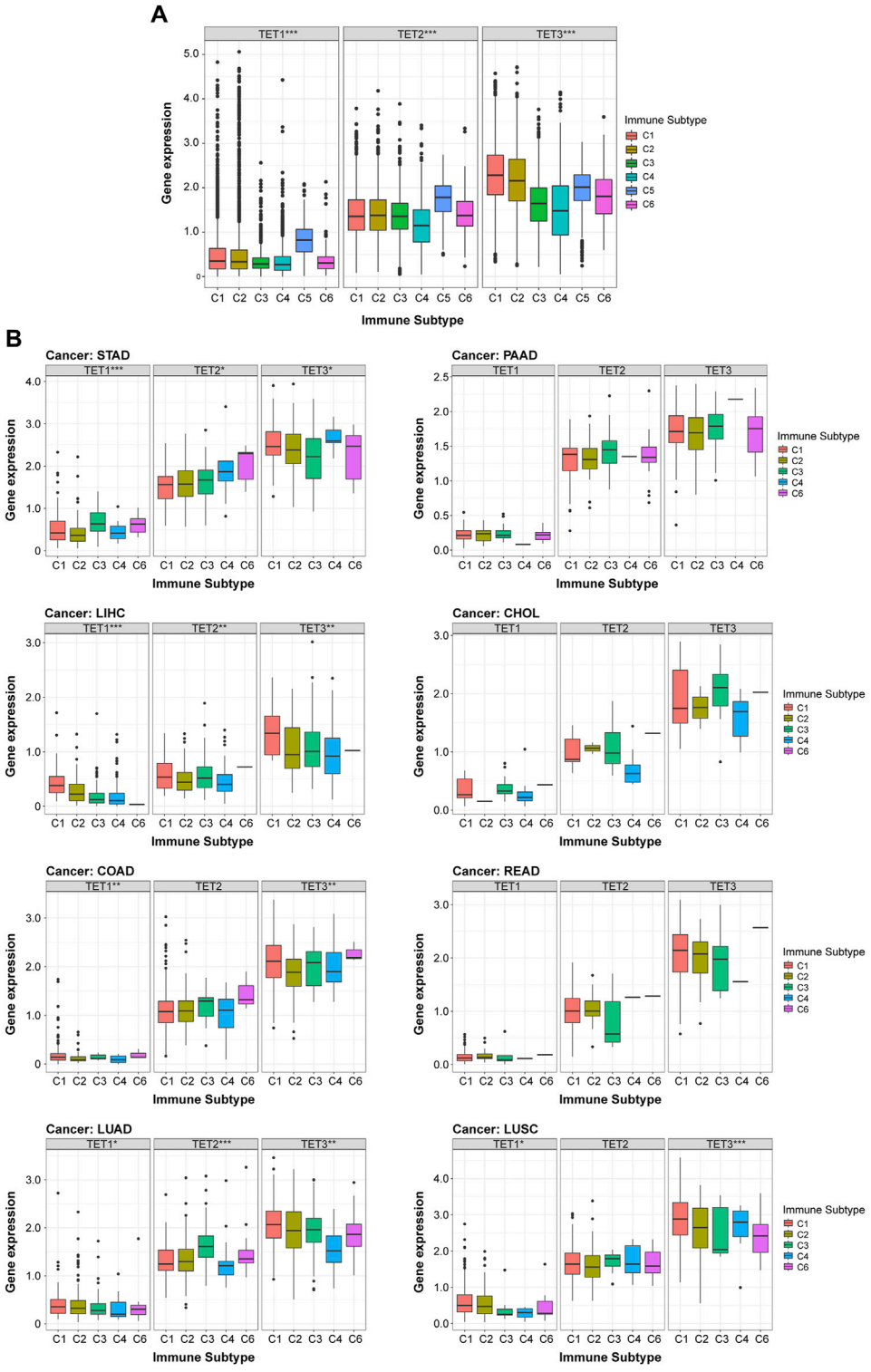

FIGURE 7
Correlation between expression of TET family members and immune subtypes. **(A)** Analysis of the relationship between TET family genes expression and immune subtypes across pan-cancer, based on the TCGA database. **(B)** Further analysis of the correlation between immune subtypes of eight common clinical tumors and TETs expression levels. Data are presented as the mean ± SD. *$p < 0.05$, **$p < 0.01$, ***$p < 0.001$.

Furthermore, we assessed the therapeutic sensitivity of three distinct pathological subtypes of lung cancer cell lines (A549, SKMES1, NCIH460) to Lapatinib, AZD-9291, and (+)-JQ1. The findings indicated that the therapeutic efficacy of these drugs on tumor cells positively correlated with the expression level of TET3 (Figure 11B).

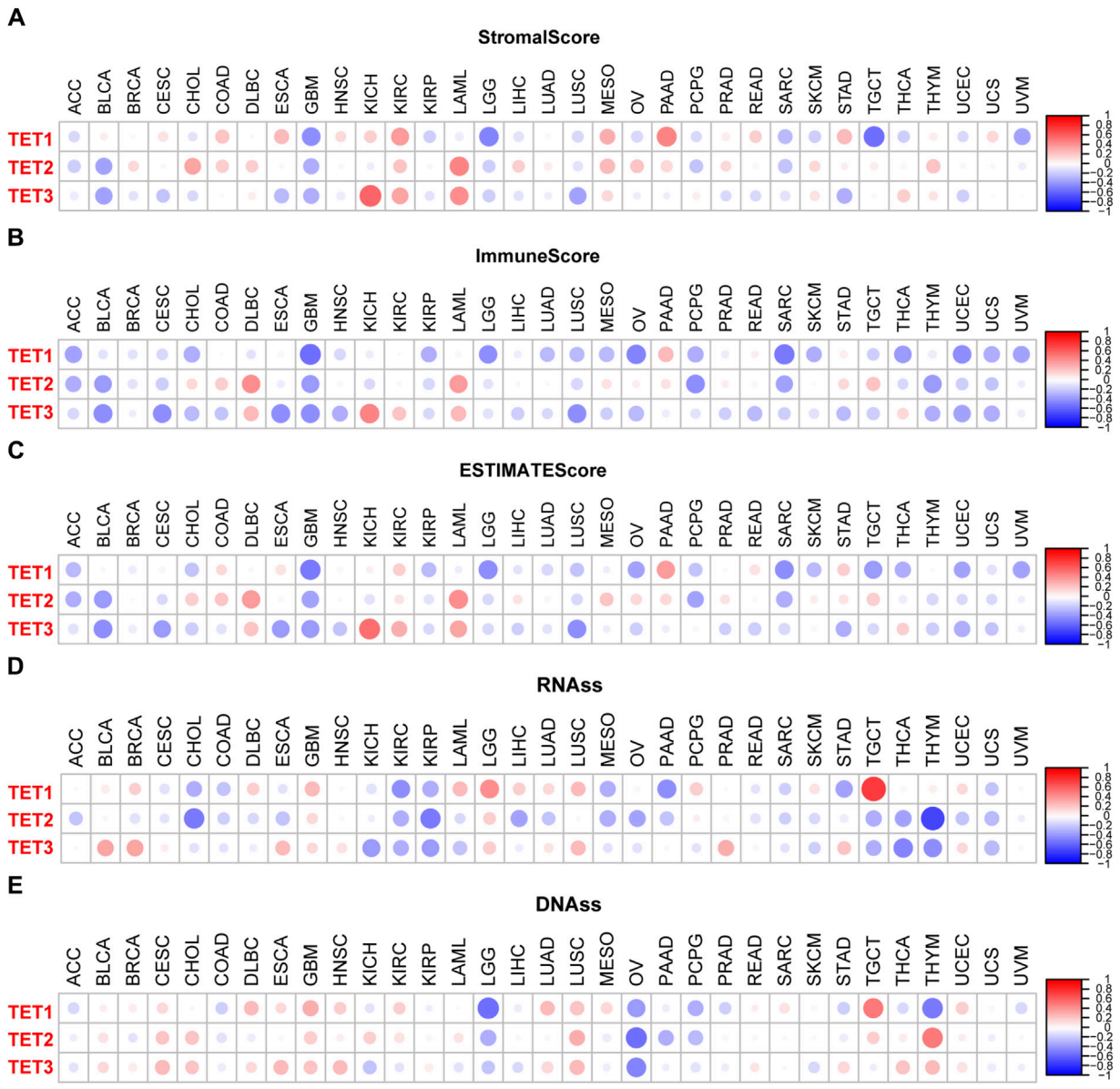

FIGURE 8
TET family members and tumor microenvironment in pan-cancer. **(A–C)** Association between TET family genes expression and tumor microenvironment parameters including tumor matrix score, immune score, and tumor purity score in pan-cancer. **(D, E)** Relationship between TET family genes expression and RNAs and DNAs in pan-cancer.

Silencing TET3 effectively suppresses the malignant behavior of tumor cells

Following our comprehensive analysis spanning various cancer types, TET3 has emerged as a prime candidate for targeted therapeutic intervention. In subsequent experiments, where we selectively silenced TET3 expression in four distinct tumor cell lines (BGC-823, HepG2, A549, TPC-1) (Figure 12A), we observed a profound attenuation of multiple malignant phenotypes. Specifically, the inhibition of TET3 led to a notable reduction in clone formation capacity (Figure 12B), as well as a significant impairment in cell migration and invasion abilities (Figures 12C, D). Furthermore, TET3 silencing induced cell cycle arrest (Figure 12E), resulting in decreased proliferation rates, while simultaneously promoting apoptosis (Figure 12F). These compelling findings underscore the pivotal oncogenic role of TET3 across various tumor contexts and highlight the potential of TET3-targeted therapies as a promising avenue for effective cancer treatment.

Discussion

DNA methylation patterns impact gene expression and are often disrupted in diseases like inflammation, hypertension, diabetes, and tumors (Bowman and Levine, 2017; Ismail et al., 2020; Bray et al., 2021; Matuleviciute et al., 2021). TET enzymes catalyze the oxidation of 5-

FIGURE 9
TET family members and stem cell index in eight common clinical tumors.

methylcytosine to stable epigenetic modifications, playing crucial roles in gene regulation (Delatte et al., 2014; Scott-Browne et al., 2017; Bray et al., 2021; Matuleviciute et al., 2021; Joshi et al., 2022). These oxidized 5-methylcytosine derivatives serve as stable epigenetic modification that exert distinctive regulatory roles (Kao et al., 2016). Dysregulated TET protein expression is common in various cancers (Pan et al., 2015; Smeets et al., 2018; Kunimoto and Nakajima, 2021).

In our analysis of transcriptome data from 33 tumors in the UCSC Xena database, we found distinct expression patterns among TET genes across different cancer types. Specifically, TET1 showed

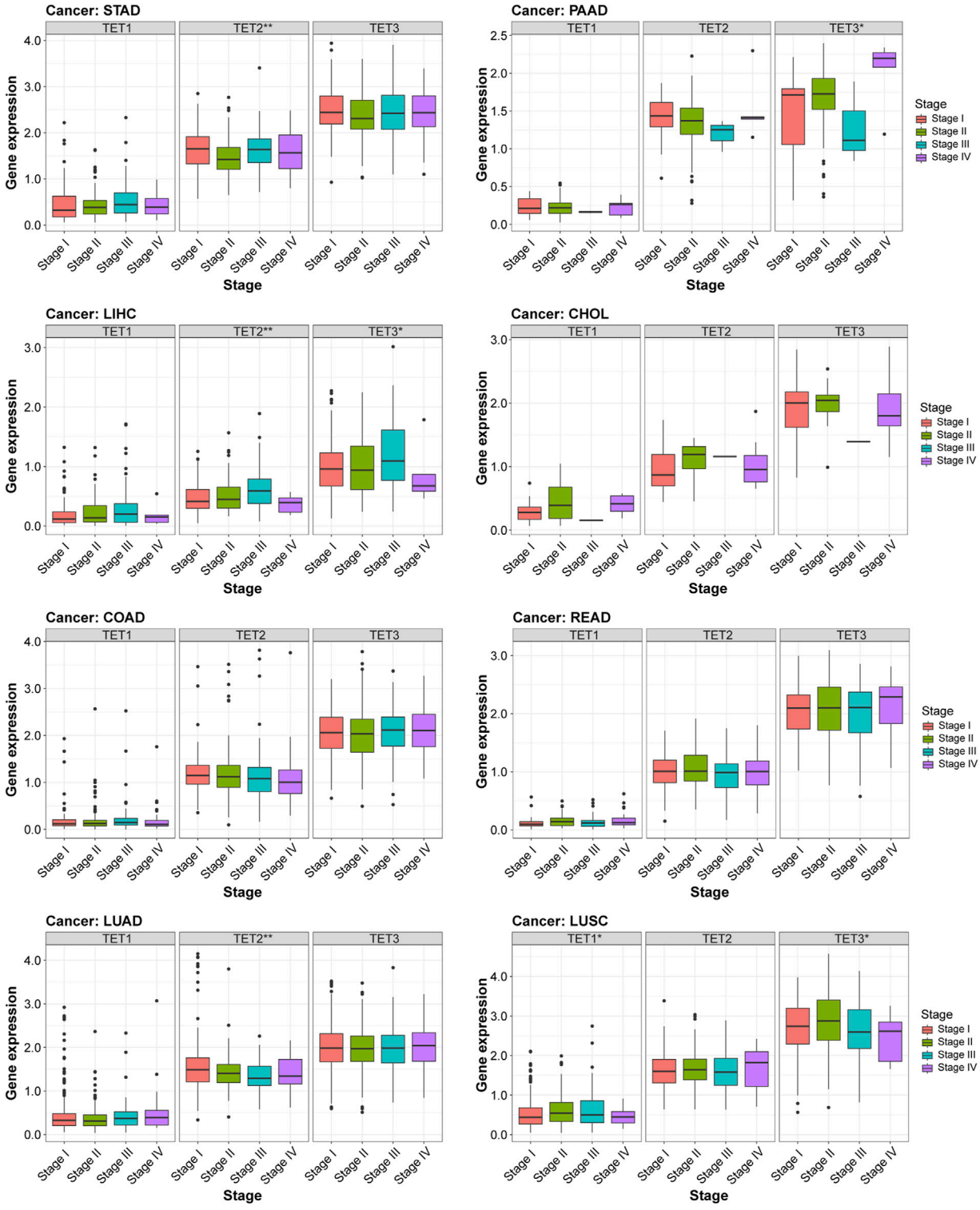

FIGURE 10
Relationship between TET gene family expression and clinical characteristics in eight common tumors.

notable overexpression in epithelioid squamous cell carcinoma (HNSC and LUSC) and hepatobiliary duct tissue (CHOL and LIHC), while consistently exhibiting low expression in various kidney-derived tumors (KICH, KIRC, and KIRP). Conversely, TET2 was predominantly expressed in adenocarcinomas (BRCA, COAD, READ, and THCA). In contrast, TET3 demonstrated widespread high expression across most tumors, with the exception of KICH. These expression patterns may hold significance for clinical diagnostics and the development of targeted therapies.

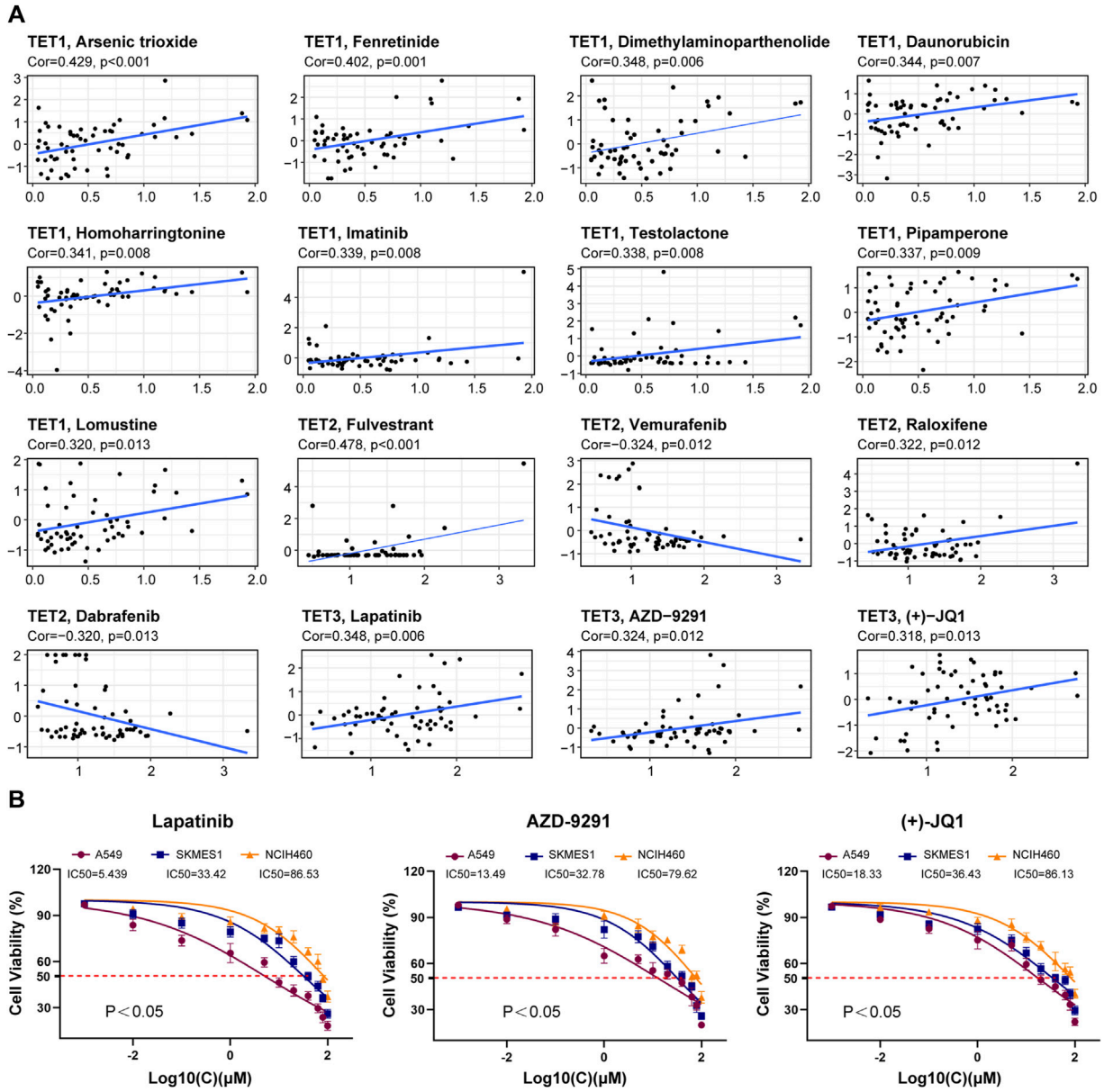

FIGURE 11
Correlation analysis between TET gene family expression and drug sensitivity. **(A)** The potential correlation between gene expression levels and drug sensitivity of TET family members were analyzed based on the CellMiner™ database. **(B)** We tested the therapeutic sensitivity of three different pathological subtypes of lung cancer cell lines to Lapatinib, AZD-9291, and (+) - JQ1.

Certain SNPs within genes can directly impact protein structure or expression levels, potentially influencing tumor genetic mechanisms (Kuhlen et al., 2019). In this study, we conducted a systematic analysis of somatic cell variations in TET gene family members. We observed a high frequency of Single Nucleotide Variants (SNV) and found that the main type of copy number variant (CNV) was heterozygous amplification and deletion. Correlation analysis revealed positive associations between TET2 expression and CNV in CHOL and ACC, while TET2 in LAML and TET3 in THMY showed negative correlations with CNV. Identifying pathogenic CNV and interpreting their clinical significance will be crucial for future research, despite the challenges associated with this endeavor.

In general, the extent of whole-genome hypomethylation in tumor cells correlates closely with disease progression, tumor size, and malignancy (Esteller and Herman, 2002). DNA methylation holds significant value in assessing tumor malignancy and guiding targeted drug selection. The TET family genes, pivotal in modulating the methylation levels of numerous genes, contribute to the complexity of gene expression regulation due to their own methylation status. Although these mechanisms enhance gene regulation accuracy, they pose challenges for researchers. Despite the negative correlation between TET family genes expression and methylation levels in pan-cancer, unique patterns were observed, such as high methylation of TET1 in most analyzed cancers (except LIHC) and low methylation of TET2 and TET3 in most tumors. Further

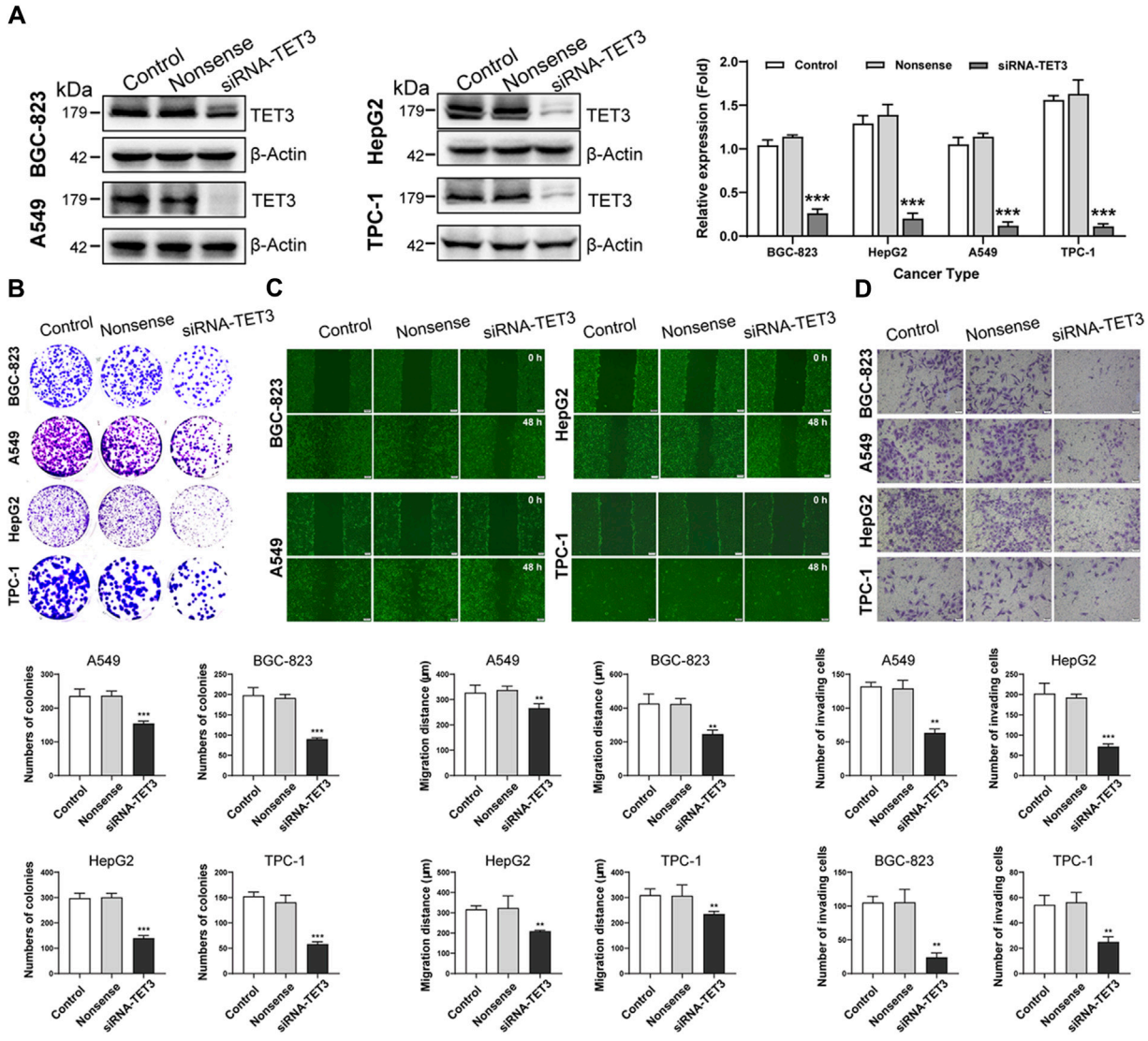

FIGURE 12
(Continued).

investigation is required to elucidate whether this differential expression pattern suggests functional compensation among TET family genes. Notably, the state of DNA methylation evolves during tumor progression, necessitating dynamic and cautious interpretation of its clinical significance (Miyamoto and Ushijima, 2003).

Our analysis of TET family genes in pan-cancer revealed their involvement in various signaling pathways. Notably, TET1 was found to predominantly activate the PI3K/AKT pathway. Prior studies have highlighted TET1's role in driving the proliferation of insulin-dependent endometrial cancer by enhancing G protein-coupled estrogen receptor expression and PI3K/AKT pathway activation (Xie et al., 2017). Moreover, research by Huang elucidated TET1's impact on stem cell development through modulation of the Wnt and PI3K-Akt pathways, while TET2 deficiency in mice led to a progressive reduction in spermatogonia stem cells (Huang et al., 2020). TET2 plays a pivotal role in cell cycle regulation and DNA damage responses. Studies by Zhong have revealed that 5 mC oxidation is cell-cycle dependent, occurring primarily during the S and G2/M phases. Notably, TET2 depletion diminishes the observed elevation in 5hmC, indicating its dependence on TET2, particularly in response to idarubicin stimulation, a topoisomerase II inhibitor (Panigrahi et al., 2015). Additionally, Chen found that SMAD nuclear interacting protein one recruits TET2 to regulate c-MYC target genes and the cellular DNA damage response (Chen et al., 2018). TET3, a pivotal enzyme, showcases its versatility within cellular processes, including the cell cycle, apoptosis, hormone AR regulation, and the DNA damage response. Research led by Jiang and colleagues revealed that upon DNA damage, ATR kinase activation leads to TET3 phosphorylation in mammalian cells. This phosphorylation enhances DNA demethylation and the accumulation of 5-hydroxymethylcytosine, underlining TET3's essential role in DNA repair and cell survival (Jiang et al., 2017).

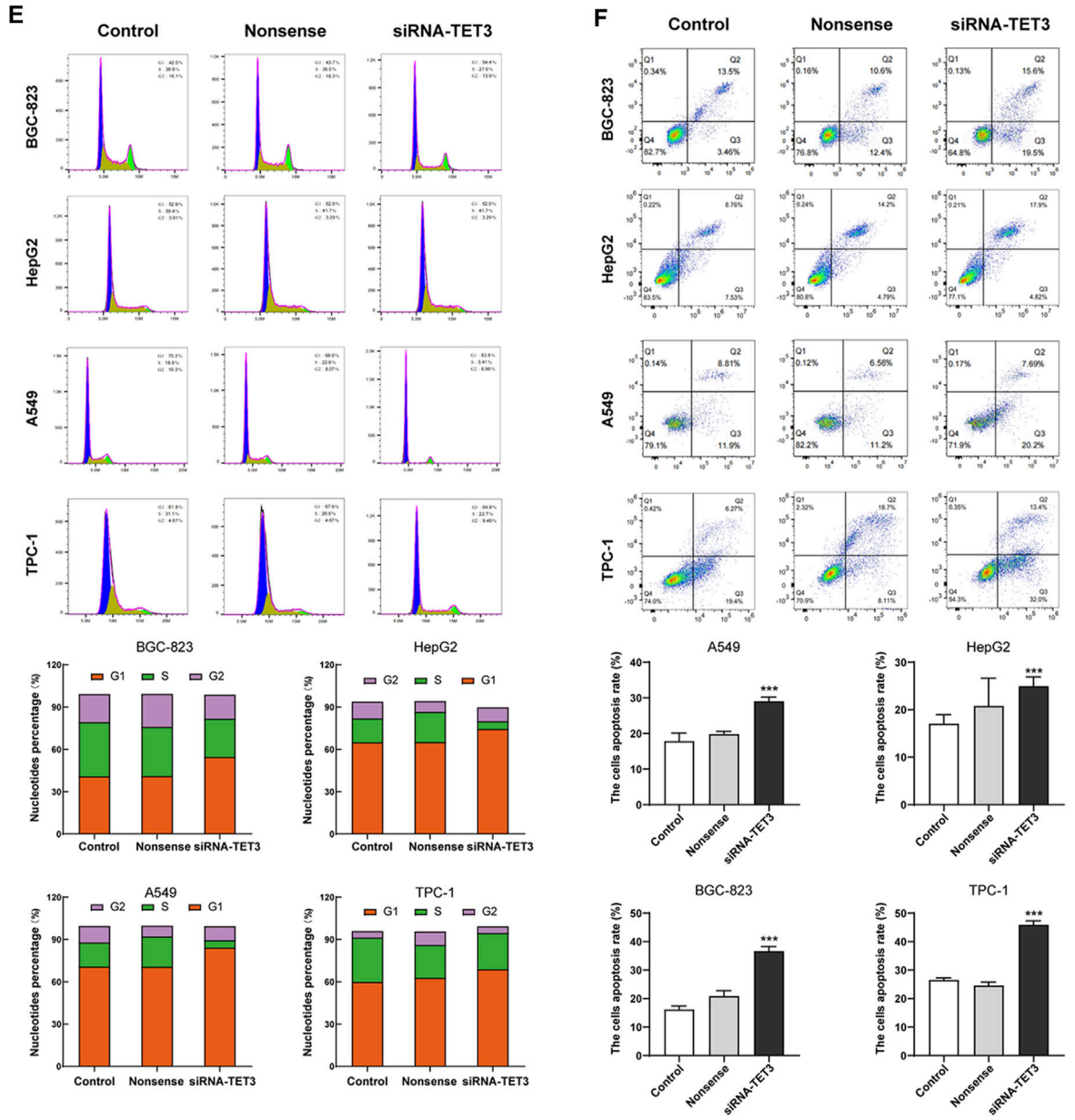

FIGURE 12
(Continued). Silencing TET3 can inhibit the malignant behavior of tumor cells. **(A)** The expression of TET3 in four tumor cell lines (BGC-823, HepG2, A549, TPC-1) was silenced. **(B–F)** Silencing TET3 significantly inhibited tumor cell clone formation ability **(B)**, migration ability **(C)**, and invasion ability **(D)**; and also inhibited the cell proliferation cycle **(E)** while increased cell apoptosis **(F)**.

In the landscape of cancer, the expression levels of the TET family offer prognostic insights. Elevated TET1 expression correlates with worse outcomes in solid organ tumors such as ACC, KIRP, LIHC, and SARC, yet it signifies better prognoses in LGG and THYM cancers. Similarly, increased TET2 expression suggests poorer outcomes in tumors of the female reproductive system, including OV and UCS, but predicts favorable outcomes in KIRC. Notably, high TET3 expression is linked to unfavorable prognoses in ACC but indicates better survival rates in THCA. These observations underscore the multifaceted roles that TET enzymes play in the vast expanse of cancer prognosis.

Diving deeper into the complex interplay between TET enzyme expression and immune subtypes, this pan-cancer study unveils their pivotal influence within the tumor immune microenvironment. The findings suggest that TET1 and TET2, especially upregulated in the C5 immune subtype known for its inflammatory profile, might influence immune evasion or activation. TET3, with its variable expression, appears to affect a broad range of immune responses across tumors. The distinct expression patterns of TET enzymes across different cancers and immune subtypes underscore their potential in modulating tumor immunity, progression, and therapy response. This research not

only sheds light on the complex interactions between TET enzymes and the immune system but also emphasizes the importance of TET genes as biomarkers and therapeutic targets in cancer. It advances our understanding of the tumor immune microenvironment, paving the way for novel immunotherapeutic strategies.

Building on this understanding, the study further explores the relationship between TET expression and the TME, a critical factor in tumor survival, immune evasion, and drug resistance (Arneth, 2019). For instance, augmenting TET1 expression may improve the TME in PAAD while potentially exacerbating it in GBM, LGG, and TGCT. Insights from Li suggest that TET1 could inhibit epithelial-mesenchymal transition and increase PAAD cells' sensitivity to chemotherapy agents like 5FU and gemcitabine (Li et al., 2020). However, the impact of TET1 overexpression on GBM, LGG, and TGCT TME remains unexplored. Secondly, TET2 expression restoration may improve LAML's TME but worsen that of BLCA and GBM. Cimmino et al. found that TET2 restoration might reverse aberrant hematopoietic stem and progenitor cell self-renewal *in vitro* and *in vivo* (Cimmino et al., 2017). Similarly, the effect of inducing TET2 expression on BLCA and GBM TME remains unclear. Lastly, inducing TET3 expression could enhance KICH, KIRC, and LAML TME while deteriorating BLCA, CESC, ESCA, GBM, LUSC, and UCEC TME. This comprehensive analysis sheds further light on the nuanced roles of TET enzymes in the TME, highlighting their potential as biomarkers and therapeutic targets in the ongoing battle against cancer.

Further investigation into the tumor stem cell index revealed a positive correlation between heightened TET1 expression and increased levels of ribonucleic acid synthesis (RNAss) and deoxyribonucleic acid synthesis (DNAss) in testicular germ cell tumors (TGCT). Notably, Benešová et al. observed a marked increase in TET1 dioxygenase expression in most seminomas, suggesting its potential utility as a marker for seminomas and mixed germ cell tumors (Benešová et al., 2017). These findings underscore the potential of TET1 as a pivotal indicator for evaluating stemness maintenance and chemoradiotherapy resistance in TGCT tumor stem cells.

The examination of TET family genes expression concerning the clinical staging of common tumors reveals nuanced patterns. While TET1 demonstrates only limited correlation with tumor staging, TET2 exhibits significant associations in STAD, LIHC, and LUAD ($p < 0.01$). Similarly, TET3 shows correlations with staging in PAAD, LIHC, and LUSC ($p < 0.05$). These findings are in line with the research by Liu, indicating decreased genomic 5hmC and 5 fC contents in early LIHC stages, with further reductions in late stages. Moreover, the significantly positive correlations among the expression levels of TET2 in para-tumor tissues were generally attenuated or even disappeared in LIHC tumor tissues (Liu et al., 2019). Moreover, Sajadian underscore the impaired expression and activity of TET2 and TET3 in hepatocellular carcinoma, further validating our analysis (Sajadian et al., 2015). These conclusions are close to our analysis results.

Effective cancer treatment relies on understanding drug sensitivity, a cornerstone of personalized therapy and precision medicine advancement (Chaudhry and Asselin, 2009). Yet, due to individual variations and disparate drug responses, optimal resource utilization remains a challenge (Panczyk, 2014). Therefore, investigating molecules influencing drug reactions is essential for refining treatment strategies. Our study delves into the interplay between TET family genes expression and drug sensitivity, yielding significant insights. Notably, we find that TET genes expression levels correlate with the efficacy of specific drugs, highlighting the importance of assessing TET1, TET2, and TET3 expression for informed clinical drug selection.

Our study delved into the intricate role of TET family genes across various aspects of cancer biology. We identified TET1, TET2, and TET3 as pivotal players influencing tumor progression, prognosis, immune response, tumor microenvironment, and drug sensitivity. Notably, the analysis reveals that each TET family member, including TET3, displays unique expression patterns in at least ten detected tumor types. This heterogeneity suggests that TET3 may play distinct roles in different cancer subtypes. Furthermore, the finding that TET3 genes display hypomethylation in most cancers, which correlates closely with patient prognosis, highlights its potential involvement in cancer progression and metastasis. The association between TET3 expression and various cancer-related factors, such as pathway activity, tumor microenvironment, stemness score, immune subtype, clinical staging, and drug sensitivity, further underscores its relevance as a potential therapeutic target. The results from molecular biology and cytology experiments validating the potential role of TET3 in tumor progression strengthen this argument.

In summary, studying TET3 in different cancers is highly relevant due to its potential as a therapeutic target. The comprehensive pan-cancer analysis presented in the manuscript provides a foundation for future research aimed at developing targeted therapies that may improve cancer treatment outcomes.

Conclusion

The comprehensive analysis of TET family genes in pan-cancer unveiled their multifaceted roles. Through transcriptome data analysis, distinct expression patterns were observed across various tumor types, indicating their potential diagnostic significance. Moreover, correlation with prognosis highlighted their prognostic value, while associations with the tumor microenvironment and drug sensitivity underscored their therapeutic implications. These findings suggest that TET genes could serve as valuable targets for precision medicine approaches in cancer treatment.

Materials and methods

Data download preparation

Based on data obtained from the UCSC Xena database, RNA-Seq and clinical data for 33 tumor types prefixed with "GDC TCGA" were downloaded. This includes "HTSeq FPKM (n = 151) GDC Hub" data for gene expression RNAseq, as well as "Phenotype (n = 697) GDC Hub (Clinical Traits)" and "Survival Data (n = 626) GDC Hub" under the Phenotype category. TCGA pan-cancer (PANCAN) data, such as "Immune subtype" under Phenotype and "Stemness score (DNA methylation based) pan-cancer Atlas Hub" and

"Stemness score (RNA based) pan-cancer Atlas Hub" under Signatures, was also retrieved. Additionally, drug sensitivity information was obtained from the CellMiner™ database (https://discover.nci.mih.gov/cellminer/home.do).

Differential analysis of gene expression

Utilize Perl software to extract, transform, and integrate the 'HTSeq FPKM (n = 151) GDC Hub' data obtained from the Gene expression RNAseq item. Generate boxplots to illustrate the expression profiles of TET family genes across diverse tumor samples. Next, filter samples with a minimum of five normal controls per tumor type and create gene expression boxplots accordingly. Conduct expression difference analysis of TET family genes in different cancer types using the 'Wilcox. test' method, with statistical significance levels indicated by '*', '**', and '***' for $p < 0.05$, <0.01, and <0.001, respectively. Utilize the R package 'Pheatmap' to generate a heatmap based on the resulting *p*-values. Finally, examine the correlation between genes within the TET family using the R package 'Coreplot'.

Somatic mutation analysis

Data on single nucleotide variant (SNV) and copy number variant (CNV) for 33 tumor types were retrieved from the TCGA database through the Xena Functional Genomics Explorer (https://xenabrowser.net/datapages/). The SNV data encompasses various non-silent mutations, including Missense_Mutation, Nonsense_Mutation, Frame_Shift_Del, Splice_Site, Frame_Shift_Ins, In_Frame_Del, In_Frame_Ins, Translation_Start_Site, and Multi_Hit. The SNV mutation frequency (%) for each gene coding region is calculated as the number of mutation samples divided by the total number of cancer samples. Finally, SNV landscape maps were generated using Maftools.

For CNV analysis, we classified CNV into two types: homozygous and heterozygous, representing amplifications and deletions, respectively. We then computed the percentage statistics for each CNV subtype using GISTIC processed CNV data. Next, we investigated the correlation between CNV and mRNA expression levels. Genes with CNV exceeding 5% were identified, and their association with TET expression was explored. Utilizing the method described by Tyagi (Tyagi et al., 2024), we assessed the correlation between mRNA expression and CNV percentage samples using Pearson's product-moment correlation coefficient, with *p*-values corrected for false discovery rate (FDR).

Methylation analysis

To perform methylation analysis, we initially obtained DNA methylation data from the UCSC Xena database. We focused on 14 tumor types with a minimum of 10 paired samples of tumor and normal tissues. Differential methylation between tumor and normal samples was assessed using Student's t-test, with *p*-values adjusted for false discovery rate (FDR). Significance was determined at FDR <0.05. Subsequently, we integrated the methylation data with TET gene expression data. Spearman correlation coefficient was computed to evaluate the correlation between methylation levels and gene expression.

Further analysis involved categorizing the median methylation level of genes into two groups. This categorization was based on the threshold defined by the median methylation level. Cox regression analysis was then conducted to estimate the hazard ratio (HR) of gene methylation, considering covariates specific to each cancer type. A Cox coefficient >0 indicated worse survival rates for the high methylation group, hence defining it as high-risk, while a Cox coefficient ≤0 indicated low-risk. Additionally, we compared the distribution of the two methylation groups using the log-rank test to assess their association with clinical outcomes. A significance level of $p < 0.05$ was considered statistically significant in these comparisons.

Signal pathway activity analysis

The reverse protein array (RPPA) data from the UCSC Xena database within TCGA is leveraged to assess pathway activity across various tumor samples. Nine key pathways associated with cancer progression are scrutinized, including Apoptosis, Cell cycle, DNA Damage Response, Epithelial Mesenchyme Transition (EMT), Hormone androgen receptor (AR), Hormone estrogen receptor (ER), Phosphatidylinositol-4,5-bisphosphate-3-kinase (PI3K)/protein kinase B (AKT), Rasopathies (RAS)/mitogen-activated protein kinase (MAPK), and Receptor Tyrosine Kinase (RTK).

Pathway activity scores are calculated by summing the relative protein levels of positive regulatory components and subtracting those of negative regulatory components within each pathway. Following this, employing methodologies outlined in prior studies, such as those by Akbani and Ye. (Akbani et al., 2014), pathway activity scores (PAS) are derived. A higher PAS in one group compared to another suggests an activating effect of certain genes on the pathway, while a lower PAS indicates an inhibitory effect.

Survival and prognostic analysis

We performed expression survival analysis by integrating mRNA expression data of TETs genes with clinical survival data across 33 cancer types, utilizing the Survival Data (n = 626) GDC Hub from the UCSC Xena database. Employing the Kaplan-Meier method and log-rank test ($p < 0.05$), tumor samples were stratified into high and low expression groups based on median gene expression levels.

Subsequently, we applied a univariate Cox proportional hazards regression model to investigate the relationship between TET family genes expression and patient prognosis across various cancers. Finally, the results were visualized using forest plots generated with the "survival" and "Forestplot" R packages.

Immunological subtype analysis

Utilizing the "Immune subtype" data from the Phenotype category within the TCGA pan-cancer (PANCAN) dataset available on the UCSC Xena database, we conducted immune subtype analysis on the TETs genes. Employing R packages "Limma", "Ggplot2", and "Reshape2", we applied the Kruskal–Wallis (KS) test method to detect expression differences among various immune subtypes. A significance threshold of $p < 0.05$ was set for statistical significance.

Analysis of tumor microenvironment and stem cell index

Using the "Stemness score (DNA methylation based) pan-cancer Atlas Hub" and "Stemness score (RNA based) pan-cancer Atlas Hub" data within the Signatures section of TCGA pan-cancer (PANCAN), we employed R packages "Estimate" and "Limma" to predict Stromal Score, Immune Score, and ESTIMATE Score for 33 tumor types, enabling an analysis of tumor purity. Following this, we conducted a correlation analysis between TETs gene expression levels and ESTIMATE Scores across the 33 tumor types using Spearman's correlation coefficient. Additionally, we performed Spearman correlation tests based on transcriptional data and stemness scores (RNA expression and DNA methylation levels).

Drug sensitivity analysis

Download drug sensitivity data from the CellMiner™ database and preprocess it using R packages such as "Input", "Limma", "Ggplot2", and "Ggpubr" to ensure accurate analysis and visualization. Utilize the Cor. Test function to perform correlation analysis on the data, considering a significance level of $p < 0.05$ as indicative of significant drug sensitivity.

Evaluate the sensitivity of tumor cells to drugs using the Cell Counting Kit-8 (CCK-8) assay following the manufacturer's protocol (Yeasen, Shanghai, China). This involves treating cultured tumor cells with various drugs and assessing cell viability using the CCK-8 assay.

Cell culture, plasmids, and transfections

All cell lines utilized in this study, including those derived from gastric mucosa (GES-1), liver (LX2), lung epithelium (16HBE), thyroid (Nthy-ori-3-1), as well as various cancer cell lines like BGC-823 (poorly differentiated gastric cancer), HepG2 (hepatoblastoma), A549 (lung adenocarcinoma), TPC-1 (papillary thyroid cancer), SKMES1 (lung squamous cell carcinoma), NCIH460 (large cell lung cancer), NCI-N87 (moderately differentiated gastric cancer), and HGC-27 (undifferentiated gastric cancer), were procured from the American Type Culture Collection (ATCC; United States). These cell lines were cultured following ATCC's recommended protocols.

TET3-targeting interfering RNAs (siRNA-TET3) and TET3 overexpression plasmid (pcDNA3.1-3*Flag-TET3) were synthesized by GenePharma Co., Ltd (Shanghai, China) and transfected into cells at a concentration of 20 nM using Lipofectamine RNAiMax (Invitrogen, United States). The siRNA sequence used was: siRNA-TET3: 5′-GGAAAGAGCUCCCGC GGUUTT-3'. The plasmid was constructed using the Fast MultiSite Mutagenesis System Kit (FM201-01, TransGen Biotech, China) according to the manufacturer's instructions. Transfections of the mentioned plasmids were performed using Lipofectamine 2000 reagent (Thermo Fisher Scientific, United States), and the transfected cells were utilized in experiments 48 h post-transfection.

Western blot

Cell lysates were prepared using RIPA lysis buffer, and protein concentration was determined with a BCA kit (Beyotime, Shanghai, China, P0010) following the manufacturer's instructions. Protein samples were separated on SDS-PAGE gels, transferred to PVDF membranes, and blocked with 5% skimmed milk powder. Primary antibodies were applied overnight at 4°C, followed by secondary antibodies at room temperature. Immunoreactive bands were visualized using ECL (Thermo Fisher Scientific, 34580) and imaged with a ChemiDoc™ MP Imaging System (BioRad, United States of America).

The antibodies used for Western blotting were as follows: TET3 (Abcam, ab153724, 1:1000), β-Actin (CST, #3700, 1:1000), p-AKT (CST, #4060, 1:2000), AKT (CST, #9272, 1:1000), p-mTOR (CST, #2974, 1:1000), mTOR (CST, #2983, 1:1000), p21 (Invitrogen, MA5-14949, 1:1000), Cyclin D1 (Invitrogen, MA5-16356, 1:200), HIF-1α (CST, #3716, 1:1000), c-Myc (Invitrogen, MA1-980, 1:1000).

Behavioral detection of tumor cells

According to the experimental requirements, the flat plate cloning experiment, wound healing assay, cell invasion assay, flow cytometry cell cycle and apoptosis detection involved in this project were all implemented according to standard methods as follows:

The colony formation assay, cells are first seeded at low density into culture dishes or plates and allowed to grow undisturbed for a period of time, typically several days to weeks, depending on the cell type and experimental requirements. During this time, individual cells proliferate and form colonies derived from a single progenitor cell. Once the colonies have reached a suitable size, the cells are fixed and stained to visualize them. Finally, the number of colonies and their size are quantified using microscopy or image analysis software, providing valuable information about cell proliferation, survival, and clonogenic potential. This assay is commonly used to assess the effects of various treatments or genetic manipulations on cell growth and survival.

The wound healing, cells are first cultured in a monolayer until they reach confluence. Then, a scratch or wound is created in the cell layer using a pipette tip or specialized tool. The cells are then washed to remove debris and allowed to incubate in fresh media. Images of the scratch are taken at regular intervals over a specified period, allowing researchers to monitor and measure cell migration into the scratch area. Finally, data analysis involves quantifying the extent of

scratch closure or the rate of migration, typically by measuring the remaining scratch width using image analysis software. This assay provides insights into cell migration dynamics and can be used to assess the effects of various factors on cell motility.

The Transwell assay, cells are seeded into the upper chamber of a Transwell insert, while the lower chamber is filled with medium containing chemoattractant. The cells are allowed to migrate or invade through the porous membrane of the insert towards the lower chamber for a specified period of time. After incubation, non-migratory or non-invasive cells on the upper surface of the membrane are removed, while cells that have migrated or invaded to the lower surface are fixed, stained, and counted under a microscope. The number of migrated or invaded cells is quantified to assess the migratory or invasive capacity of the cells in response to different experimental conditions or treatments.

Flow cytometry analysis of the cell cycle and apoptosis, cells are typically harvested, fixed, and permeabilized to preserve their structural integrity. For cell cycle analysis, the fixed cells are treated with DNA intercalating dyes, such as propidium iodide (PI), to stain DNA. The stained cells are then subjected to flow cytometry analysis to measure the DNA content, allowing for the identification of cells in different phases of the cell cycle. Conversely, for apoptosis analysis, cells are stained with fluorescent dyes that selectively bind to apoptotic cells, such as Annexin V and PI. The stained cells are then analyzed by flow cytometry to quantify the percentage of apoptotic cells based on their fluorescence properties. By comparing treated samples to untreated controls, the effects of various treatments or experimental conditions on the cell cycle progression and apoptosis induction can be assessed.

Statistics methods

Each validation experiment included three replicates and was repeated thrice for reliability. Data analysis and graphing were performed using GraphPad software v.5.01, with results displayed as mean ± SEM. Student's t-test compared two independent groups, while One-way ANOVA assessed multiple groups. Statistical significance was set at $p < 0.05$, denoted as $^{*}p < 0.05$, $^{**}p < 0.01$, $^{***}p < 0.001$, and ns for no significant difference.

Data availability statement

The datasets presented in this study can be found in online repositories. The names of the repository/repositories and accession number(s) can be found in the article/Supplementary Material.

Author contributions

CZ: Methodology, Writing–original draft. JZ: Methodology, Writing–original draft. JL: Software, Validation, Writing–original draft. YL: Methodology, Validation, Writing–original draft. GX: Software, Writing–review and editing. SZ: Validation, Writing–review and editing. HC: Formal Analysis, Writing–original draft. JW: Formal Analysis, Writing–review and editing. ZS: Data curation, Writing–review and editing. YL: Methodology, Software, Writing–original draft. ZJ: Resources, Writing–original draft. YP: Data curation, Writing–review and editing. XL: Writing–review and editing. PX: Project administration, Writing–review and editing. WW: Project administration, Writing–review and editing.

Funding

The author(s) declare that financial support was received for the research, authorship, and/or publication of this article. This study was supported by grant from National Natural Science Foundation of China (Grant No. 82272880), Beijing Natural Science Foundation (Grant No. 7212112), Tianjin Municipal Science and Technology Plan Project (Grant No. 22ZYQYSY00030), Tianjin Municipal Natural Science Foundation (Grant No. 21JCZDJC01270), Tianjin Health Technology Project (TJWJ2022XK041, TJWJ2022XK042,TJWJ2022XK043, TJWJ2022MS051, TJWJ2022QN101, TJWJ2023MS053), Tianjin Binhai New Area Health Commission Science and Technology Project (2022BWKQ003), Bethune Charity Foundation Project (B-0307-H20200302), Tianjin Municipal Health Commission research project on the integration of traditional and Western medicine (2021061, 2023062), and also funded by Tianjin Key Medical Discipline (Specialty) Construction Project (TJYXZDXK-062B, TJYXZDXK-079D).

Acknowledgments

We thank the databases of TCGA, Kaplan-Meier Plotter, PrognoScan, and CellMiner™ for the availability of the data. We also would like to express my sincere gratitude to ChatGPT 3.5 for its invaluable assistance in correcting the language aspects of this article.

Conflict of interest

The authors declare that the research was conducted in the absence of any commercial or financial relationships that could be construed as a potential conflict of interest.

Publisher's note

Supplementary material

The Supplementary Material for this article can be found online at: https://www.frontiersin.org/articles/10.3389/fphar.2024.1418456/full#supplementary-material

References

Akbani, R., Ng, P. K. S., Werner, H. M. J., Shahmoradgoli, M., Zhang, F., Ju, Z., et al. (2014). A pan-cancer proteomic perspective on the Cancer Genome Atlas. *Nat. Commun.* 5, 3887. doi:10.1038/ncomms4887

Alqahtani, A., Khan, Z., Alloghbi, A., Said Ahmed, T. S., Ashraf, M., and Hammouda, D. M. (2019). Hepatocellular carcinoma: molecular mechanisms and targeted therapies. *Med. Kaunas.* 55, 526. doi:10.3390/medicina55090526

Arneth, B. (2019). Tumor microenvironment. *Med. Kaunas.* 56, 15. doi:10.3390/medicina56010015

Ban, J., Fock, V., Aryee, D. N. T., and Kovar, H. (2021). Mechanisms, diagnosis and treatment of bone metastases. *Cells* 10, 2944. doi:10.3390/cells10112944

Benešová, M., Trejbalová, K., Kučerová, D., Vernerová, Z., Hron, T., Szabó, A., et al. (2017). Overexpression of TET dioxygenases in seminomas associates with low levels of DNA methylation and hydroxymethylation. *Mol. Carcinog.* 56, 1837–1850. doi:10.1002/mc.22638

Bowman, R. L., and Levine, R. L. (2017). TET2 in normal and malignant hematopoiesis. *Cold Spring Harb. Perspect. Med.* 7, a026518. doi:10.1101/cshperspect.a026518

Bray, J. K., Dawlaty, M. M., Verma, A., and Maitra, A. (2021). Roles and regulations of TET enzymes in solid tumors. *Trends Cancer* 7, 635–646. doi:10.1016/j.trecan.2020.12.011

Chaudhry, P., and Asselin, E. (2009). Resistance to chemotherapy and hormone therapy in endometrial cancer. *Endocr. Relat. Cancer* 16, 363–380. doi:10.1677/erc-08-0266

Chen, C., Wang, Z., Ding, Y., Wang, L., Wang, S., Wang, H., et al. (2022). DNA methylation: from cancer biology to clinical perspectives. *Front. Biosci. Landmark Ed.* 27, 326. doi:10.31083/j.fbl2712326

Chen, L. L., Lin, H. P., Zhou, W. J., He, C. X., Zhang, Z. Y., Cheng, Z. L., et al. (2018). SNIP1 recruits TET2 to regulate c-MYC target genes and cellular DNA damage response. *Cell Rep.* 25, 1485–1500. doi:10.1016/j.celrep.2018.10.028

Cimmino, L., Dolgalev, I., Wang, Y., Yoshimi, A., Martin, G. H., Wang, J., et al. (2017). Restoration of TET2 function blocks aberrant self-renewal and leukemia progression. *Cell* 170, 1079–1095. doi:10.1016/j.cell.2017.07.032

Delatte, B., Deplus, R., and Fuks, F. (2014). Playing TETris with DNA modifications. *Embo J.* 33, 1198–1211. doi:10.15252/embj.201488290

Esteller, M., and Herman, J. G. (2002). Cancer as an epigenetic disease: DNA methylation and chromatin alterations in human tumours. *J. Pathol.* 196, 1–7. doi:10.1002/path.1024

Golemis, E. A., Scheet, P., Beck, T. N., Scolnick, E. M., Hunter, D. J., Hawk, E., et al. (2018). Molecular mechanisms of the preventable causes of cancer in the United States. *Genes Dev.* 32, 868–902. doi:10.1101/gad.314849.118

Gonçalves, A. C., Richiardone, E., Jorge, J., Polónia, B., Xavier, C. P. R., Salaroglio, I. C., et al. (2021). Impact of cancer metabolism on therapy resistance - clinical implications. *Drug Resist Updat* 59, 100797. doi:10.1016/j.drup.2021.100797

Huang, G., Liu, L., Wang, H., Gou, M., Gong, P., Tian, C., et al. (2020). Tet1 deficiency leads to premature reproductive aging by reducing spermatogonia stem cells and germ cell differentiation. *iScience* 23, 100908. doi:10.1016/j.isci.2020.100908

Ismail, J. N., Ghannam, M., Al Outa, A., Frey, F., and Shirinian, M. (2020). Ten-eleven translocation proteins and their role beyond DNA demethylation - what we can learn from the fly. *Epigenetics* 15, 1139–1150. doi:10.1080/15592294.2020.1767323

Jiang, D., Wei, S., Chen, F., Zhang, Y., and Li, J. (2017). TET3-mediated DNA oxidation promotes ATR-dependent DNA damage response. *EMBO Rep.* 18, 781–796. doi:10.15252/embr.201643179

Joshi, K., Liu, S., Breslin, S. J. P., and Zhang, J. (2022). Mechanisms that regulate the activities of TET proteins. *Cell Mol. Life Sci.* 79, 363. doi:10.1007/s00018-022-04396-x

Joshi, K., Zhang, L., Breslin, S. J. P., Kini, A. R., and Zhang, J. (2022). Role of TET dioxygenases in the regulation of both normal and pathological hematopoiesis. *J. Exp. Clin. Cancer Res.* 41, 294. doi:10.1186/s13046-022-02496-x

Kao, S. H., Wu, K. J., and Lee, W. H. (2016). Hypoxia, epithelial-mesenchymal transition, and TET-mediated epigenetic changes. *J. Clin. Med.* 5, 24. doi:10.3390/jcm5020024

Kinney, S. R., and Pradhan, S. (2013). Ten eleven translocation enzymes and 5-hydroxymethylation in mammalian development and cancer. *Adv. Exp. Med. Biol.* 754, 57–79. doi:10.1007/978-1-4419-9967-2_3

Klutstein, M., Nejman, D., Greenfield, R., and Cedar, H. (2016). DNA methylation in cancer and aging. *Cancer Res.* 76, 3446–3450. doi:10.1158/0008-5472.CAN-15-3278

Kohli, R. M., and Zhang, Y. (2013). TET enzymes, TDG and the dynamics of DNA demethylation. *Nature* 502, 472–479. doi:10.1038/nature12750

Kossenas, K., and Constantinou, C. (2021). Epidemiology, molecular mechanisms, and clinical trials: an update on research on the association between red meat consumption and colorectal cancer. *Curr. Nutr. Rep.* 10, 435–467. doi:10.1007/s13668-021-00377-x

Kuhlen, M., Taeubner, J., Brozou, T., Wieczorek, D., Siebert, R., and Borkhardt, A. (2019). Family-based germline sequencing in children with cancer. *Oncogene* 38, 1367–1380. doi:10.1038/s41388-018-0520-9

Kulis, M., and Esteller, M. (2010). DNA methylation and cancer. *Adv. Genet.* 70, 27–56. doi:10.1016/b978-0-12-380866-0.60002-2

Kunimoto, H., and Nakajima, H. (2021). TET2: a cornerstone in normal and malignant hematopoiesis. *Cancer Sci.* 112, 31–40. doi:10.1111/cas.14688

Li, H., Jiang, W., Liu, X. N., Yuan, L. Y., Li, T. J., Li, S., et al. (2020). TET1 downregulates epithelial-mesenchymal transition and chemoresistance in PDAC by demethylating CHL1 to inhibit the Hedgehog signaling pathway. *Oncogene* 39, 5825–5838. doi:10.1038/s41388-020-01407-8

Liu, J., Jiang, J., Mo, J., Liu, D., Cao, D., Wang, H., et al. (2019). Global DNA 5-hydroxymethylcytosine and 5-formylcytosine contents are decreased in the early stage of hepatocellular carcinoma. *Hepatology* 69, 196–208. doi:10.1002/hep.30146

Ma, C., Seong, H., Liu, Y., Yu, X., Xu, S., and Li, Y. (2021). Ten-eleven translocation proteins (TETs): tumor suppressors or tumor enhancers? *Front. Biosci. Landmark Ed.* 26, 895–915. doi:10.52586/4996

Matuleviciute, R., Cunha, P. P., Johnson, R. S., and Foskolou, I. P. (2021). Oxygen regulation of TET enzymes. *Febs J.* 288, 7143–7161. doi:10.1111/febs.15695

Meng, H., Cao, Y., Qin, J., Song, X., Zhang, Q., Shi, Y., et al. (2015). DNA methylation, its mediators and genome integrity. *Int. J. Biol. Sci.* 11, 604–617. doi:10.7150/ijbs.11218

Miyamoto, K., and Ushijima, T. (2003). DNA methylation and cancer--DNA methylation as a target of cancer chemotherapy. *Gan Kagaku Ryoho* 30, 2021–2029.

Nishiyama, A., and Nakanishi, M. (2021). Navigating the DNA methylation landscape of cancer. *Trends Genet.* 37, 1012–1027. doi:10.1016/j.tig.2021.05.002

Nooter, K., and Stoter, G. (1996). Molecular mechanisms of multidrug resistance in cancer chemotherapy. *Pathol. Res. Pract.* 192, 768–780. doi:10.1016/s0344-0338(96)80099-9

Pan, F., Weeks, O., Yang, F. C., and Xu, M. (2015). The TET2 interactors and their links to hematological malignancies. *IUBMB Life* 67, 438–445. doi:10.1002/iub.1389

Pan, Y., Liu, G., Zhou, F., Su, B., and Li, Y. (2018). DNA methylation profiles in cancer diagnosis and therapeutics. *Clin. Exp. Med.* 18, 1–14. doi:10.1007/s10238-017-0467-0

Panczyk, M. (2014). Pharmacogenetics research on chemotherapy resistance in colorectal cancer over the last 20 years. *World J. Gastroenterol.* 20, 9775–9827. doi:10.3748/wjg.v20.i29.9775

Panigrahi, G. K., Yadav, A., Srivastava, A., Tripathi, A., Raisuddin, S., and Das, M. (2015). Mechanism of rhein-induced apoptosis in rat primary hepatocytes: beneficial effect of cyclosporine A. *Chem. Res. Toxicol.* 28, 1133–1143. doi:10.1021/acs.chemrestox.5b00063

Papanicolau-Sengos, A., and Aldape, K. (2022). DNA methylation profiling: an emerging paradigm for cancer diagnosis. *Annu. Rev. Pathol.* 17, 295–321. doi:10.1146/annurev-pathol-042220-022304

Rasmussen, K. D., and Helin, K. (2016). Role of TET enzymes in DNA methylation, development, and cancer. *Genes Dev.* 30, 733–750. doi:10.1101/gad.276568.115

Rodriguez, R., Schreiber, S. L., and Conrad, M. (2022). Persister cancer cells: iron addiction and vulnerability to ferroptosis. *Mol. Cell* 82, 728–740. doi:10.1016/j.molcel.2021.12.001

Sajadian, S. O., Ehnert, S., Vakilian, H., Koutsouraki, E., Damm, G., Seehofer, D., et al. (2015). Induction of active demethylation and 5hmC formation by 5-azacytidine is TET2 dependent and suggests new treatment strategies against hepatocellular carcinoma. *Clin. Epigenetics* 7, 98. doi:10.1186/s13148-015-0133-x

Scott-Browne, J. P., Lio, C. J., and Rao, A. (2017). TET proteins in natural and induced differentiation. *Curr. Opin. Genet. Dev.* 46, 202–208. doi:10.1016/j.gde.2017.07.011

Shekhawat, J., Gauba, K., Gupta, S., Choudhury, B., Purohit, P., Sharma, P., et al. (2021). Ten-eleven translocase: key regulator of the methylation landscape in cancer. *J. Cancer Res. Clin. Oncol.* 147, 1869–1879. doi:10.1007/s00432-021-03641-3

Smeets, E., Lynch, A. G., Prekovic, S., Van den Broeck, T., Moris, L., Helsen, C., et al. (2018). The role of TET-mediated DNA hydroxymethylation in prostate cancer. *Mol. Cell Endocrinol.* 462, 41–55. doi:10.1016/j.mce.2017.08.021

Srivastava, S. P., and Goodwin, J. E. (2020). Cancer biology and prevention in diabetes. *Cells* 9, 1380. doi:10.3390/cells9061380

Talib, W. H., Mahmod, A. I., Kamal, A., Rashid, H. M., Alashqar, A. M. D., Khater, S., et al. (2021). Ketogenic diet in cancer prevention and therapy: molecular targets and therapeutic opportunities. *Curr. Issues Mol. Biol.* 43, 558–589. doi:10.3390/cimb43020042

Tyagi, N., Roy, S., Vengadesan, K., and Gupta, D. (2024). Multi-omics approach for identifying CNV-associated lncRNA signatures with prognostic value in prostate cancer. *Noncoding RNA Res.* 9, 66–75. doi:10.1016/j.ncrna.2023.10.001

Xie, B. Y., Lv, Q. Y., Ning, C. C., Yang, B. Y., Shan, W. W., Cheng, Y. L., et al. (2017). TET1-GPER-PI3K/AKT pathway is involved in insulin-driven endometrial cancer cell proliferation. *Biochem. Biophys. Res. Commun.* 482, 857–862. doi:10.1016/j.bbrc.2016.11.124

Zaridze, D. G. (2008). Molecular epidemiology of cancer. *Biochem. (Mosc)* 73, 532–542. doi:10.1134/s0006297908050064

Zeng, Y., and Chen, T. (2019). DNA methylation reprogramming during mammalian development. *Genes (Basel)* 10, 257. doi:10.3390/genes10040257

frontiers | Frontiers in Pharmacology

TYPE Review
PUBLISHED 05 August 2024
DOI 10.3389/fphar.2024.1409210

OPEN ACCESS

EDITED BY
Adrian Bogdan Tigu,
University of Medicine and Pharmacy Iuliu Hatieganu, Romania

REVIEWED BY
Gábor Barna,
Semmelweis University, Hungary
Madhu M. Ouseph,
Cornell University, United States

*CORRESPONDENCE
Natalia Baran,
nbaran@ihit.waw.pl,
nbaran@mdanderson.org

†These authors have contributed equally to this work

RECEIVED 16 April 2024
ACCEPTED 08 July 2024
PUBLISHED 05 August 2024

CITATION
Chomczyk M, Gazzola L, Dash S, Firmanty P, George BS, Mohanty V, Abbas HA and Baran N (2024), Impact of p53-associated acute myeloid leukemia hallmarks on metabolism and the immune environment.
Front. Pharmacol. 15:1409210.
doi: 10.3389/fphar.2024.1409210

Impact of p53-associated acute myeloid leukemia hallmarks on metabolism and the immune environment

Monika Chomczyk[1†], Luca Gazzola[2†], Shubhankar Dash[1], Patryk Firmanty[1], Binsah S. George[3], Vakul Mohanty[4], Hussein A. Abbas[5] and Natalia Baran[1,5*]

[1]Department of Experimental Hematology, Institute of Hematology and Transfusion Medicine, Warsaw, Poland, [2]Department of Biomedical and Neuromotor Sciences, University of Bologna, Bologna, Italy, [3]Department of Hematology-oncology, The University of Texas Health Sciences, Houston, TX, United States, [4]Department of Bioinformatics and Computational Biology, The University of Texas MD Anderson Cancer Center, Houston, TX, United States, [5]Department of Leukemia, The University of Texas MD Anderson Cancer Center, Houston, TX, United States

Acute myeloid leukemia (AML), an aggressive malignancy of hematopoietic stem cells, is characterized by the blockade of cell differentiation, uncontrolled proliferation, and cell expansion that impairs healthy hematopoiesis and results in pancytopenia and susceptibility to infections. Several genetic and chromosomal aberrations play a role in AML and influence patient outcomes. *TP53* is a key tumor suppressor gene involved in a variety of cell features, such as cell-cycle regulation, genome stability, proliferation, differentiation, stem-cell homeostasis, apoptosis, metabolism, senescence, and the repair of DNA damage in response to cellular stress. In AML, *TP53* alterations occur in 5%–12% of *de novo* AML cases. These mutations form an important molecular subgroup, and patients with these mutations have the worst prognosis and shortest overall survival among patients with AML, even when treated with aggressive chemotherapy and allogeneic stem cell transplant. The frequency of *TP53*-mutations increases in relapsed and recurrent AML and is associated with chemoresistance. Progress in AML genetics and biology has brought the novel therapies, however, the clinical benefit of these agents for patients whose disease is driven by *TP53* mutations remains largely unexplored. This review focuses on the molecular characteristics of *TP53*-mutated disease; the impact of *TP53* on selected hallmarks of leukemia, particularly metabolic rewiring and immune evasion, the clinical importance of *TP53* mutations; and the current progress in the development of preclinical and clinical therapeutic strategies to treat *TP53*-mutated disease.

KEYWORDS

AML, *TP53* mutations, drug resistance, immunosuppression, metabolic rewiring, therapeutic approaches

1 Introduction

1.1 Acute myeloid leukemia

Acute myeloid leukemia (AML) is a malignant, clonal, hematological disease (Caruso et al., 2022) that develops from transformed hematopoietic stem cells (HSCs) and is characterized by cells' uncontrolled proliferation, expansion, and an unlimited capacity for self-renewal (George et al., 2021). AML occurs mainly in adults over 40 years old, with the peak incidence in patients above 70 years of age (Daver et al., 2023a). Most patients with AML harbor mutations that cause cells' malignant proliferation and enhance their ability to evade cell death (Chen et al., 2022). AML shows different metabolic and physiologic hallmarks, depending on the types of harbored mutations (Kennedy and Lowe, 2022). The most commonly mutated genes related to AML initiation and progression include FMS-related receptor tyrosine kinase 3 (*FLT3*), DNA methyltransferase three alpha (*DNMT3A*), nucleophosmin 1 (*NPM1*), and tet methylcytosine dioxygenase 2 (*TET2*) (Villatoro et al., 2020). AML mutations, together with cytogenetic abnormalities, have critical implications for clinical outcomes (Olivier et al., 2010). It is estimated that 50% of *de novo* AML cases show cytogenetic abnormalities, and the number and frequency of mutations increase in patients developing therapy-related AML, who have been treated previously with cytotoxic therapies such as alkylating agents, topoisomerase II inhibitors, and radiotherapy (Hong et al., 2016). Therapy-related AML is also frequently characterized by complex karyotypes and mutations in the tumor protein p53 (*TP53*) gene (Olivier et al., 2010; Hong et al., 2016). The incidence of *TP53* mutations in AML can vary. While the frequency of *TP53* mutations is estimated to account for 10% of *de novo* AML cases, it rises strikingly in therapy-related AML or relapsing/refractory (R/R) AML cases, reaching up to 30% and 25%, respectively, in these groups (Daver et al., 2023a). An even higher frequency of mutant *TP53* is associated with the complex karyotype subtype of AML, in which the frequency of *TP53* mutations reaches up to 70%, mainly due to selective pressure caused by acquired resistance to DNA damage following chemotherapy and radiotherapy.

Identifying potential therapeutic vulnerabilities and therapeutic targets in AML is challenging due to AML's genetic heterogeneity (Zhou et al., 2020). The exploration of novel genomic targets has led to the development of only a few potent targeted therapies, such as IDH, FLT3, or KMT2A inhibitors for genomically defined AML subsets (Appelbaum et al., 2024). However, due to the genotypic and phenotypic diversity of mutant *TP53,* finding targeted therapies against *TP53* remains an unresolved challenge.

1.2 TP53

TP53 is a 20-kbp gene located on chromosome 17p13.1 (Olivier et al., 2010). So far, 15 isoforms of p53 have been identified (Haaland et al., 2021). Despite some differences, each p53 isoform consists of five common domains: an *N*-terminal, a proline-rich domain, a DNA-binding domain (DBD), a regulatory domain, and a C-terminal (George et al., 2021). Activation of p53 occurs in response to diverse cellular stress factors such as hypoxia, DNA damage, oncogene expression, or replicative stress (Daver et al., 2022; Wang H. et al., 2023). Through its DBD domain, p53 regulates the transcription of genes involved in cell-cycle regulation, genome stability, proliferation, stem-cell homeostasis and differentiation, and cell-death regulation (Daver et al., 2022; Wang H. et al., 2023). P53 also has antiangiogenic properties; it represses metastases, controls tumor-promoting inflammation, facilitates the immune response, promotes replicative senescence, enhances the effects of growth suppressors, and regulates energetics and metabolism (Daver et al., 2022; Wang H. et al., 2023). The p53 inhibitors MDM2 and MDM4, which control p53 s ubiquitination and ubiquitin–proteasome system activity, tightly regulate p53 levels. (Wang H. et al., 2023). In AML, p53 is mainly silenced by the upregulation of MDM2, MDM4/MDMX, ARF, and E6 (Abramowitz et al., 2017; Latif et al., 2021; Tashakori et al., 2022). The precisely controlled level of p53 might be also disturbed due to somatic mutations in *TP53* or to imbalances in the gene products interacting with p53, leading to its inactivation (Olivier et al., 2010). Most somatic mutations occur mainly as point missense mutations, frameshift insertions or deletions, splice sites, and nonsense mutations; these mutations are observed in leukemia and in many other types of cancer (Olivier et al., 2010). Studies have shown that almost 90% of *TP53* mutations detected in patients with therapy-related myeloid neoplasms have variant allele frequencies (VAFs) greater than 10%, and that these VAFs frequently occurred with the loss of 17p across the *TP53* locus (loss of heterozygosity) or as copy-neutral loss of heterozygosity (Donehower et al., 2019; Shah et al., 2023). Compared to wild-type *TP53*, *TP53* mutation with a VAF greater than10% was associated with inferior outcomes and worse survival (Donehower et al., 2019; Shah et al., 2023).

TP53 mutations are a strong indicator of prognosis, and studies have shown that, in AML, multi-hit mutated *TP53* is associated with genomic instability, thrombocytopenia, and a higher blast count, independent of the VAF (Deng et al., 2020). Further studies have shown that, unlike AML cells that carry multi-hit mutated *TP53*, those that carry monoallelic *TP53* mutations frequently harbor co-mutations in genes like tet methylcytosine dioxygenase 2 (*TET2*), splicing factor 3b subunit 1 (*SF3B1*), ASXL transcriptional regulator 1 (*ASXL1*), RUNX family transcription factor 1 (*RUNX1*), isocitrate dehydrogenase (NADP(+)) 2 (*IDH2*), serine and arginine rich splicing factor 2 (*SRSF2)* (Shah et al., 2023), Mitogen-activated protein kinase kinase kinase 7 (*TAK1*), BCL6 corepressor (*BCOR*), and Cbl proto-oncogene (*CBL*) (Daver et al., 2023a). Finally, *TP53* monoallelic mutations with co-mutated *RUNX1*, KRAS proto-oncogene, GTPase (*KRAS*), or *CBL* are correlated with poor prognosis more frequently than monoallelic *TP53* mutations (Daver et al., 2023a). Although performing a *TP53* status analysis is not yet considered standard procedure, Cox multivariate hazard models have shown that heavy alterations of *TP53* allele status independently predict a poor prognosis (Daver et al., 2023a). The 2022 findings of European LeukemiaNet support the consideration of a *TP53* mutation as a distinct AML entity with a "very-adverse" risk profile like that listed for European LeukemiaNet in the 2022 International Consensus Classification (Tashakori et al., 2022; Fleming et al., 2023).

1.2.1 Alteration of the *TP53* gene in AML and other cancers

In AML, *TP53* mutations are mainly found in 6 DBD hotspots: R175H, G245S, R248Q/W, R249S, R273H/S, and R282W (Kennedy and Lowe, 2022). These mutations lead to reduced activity, complete

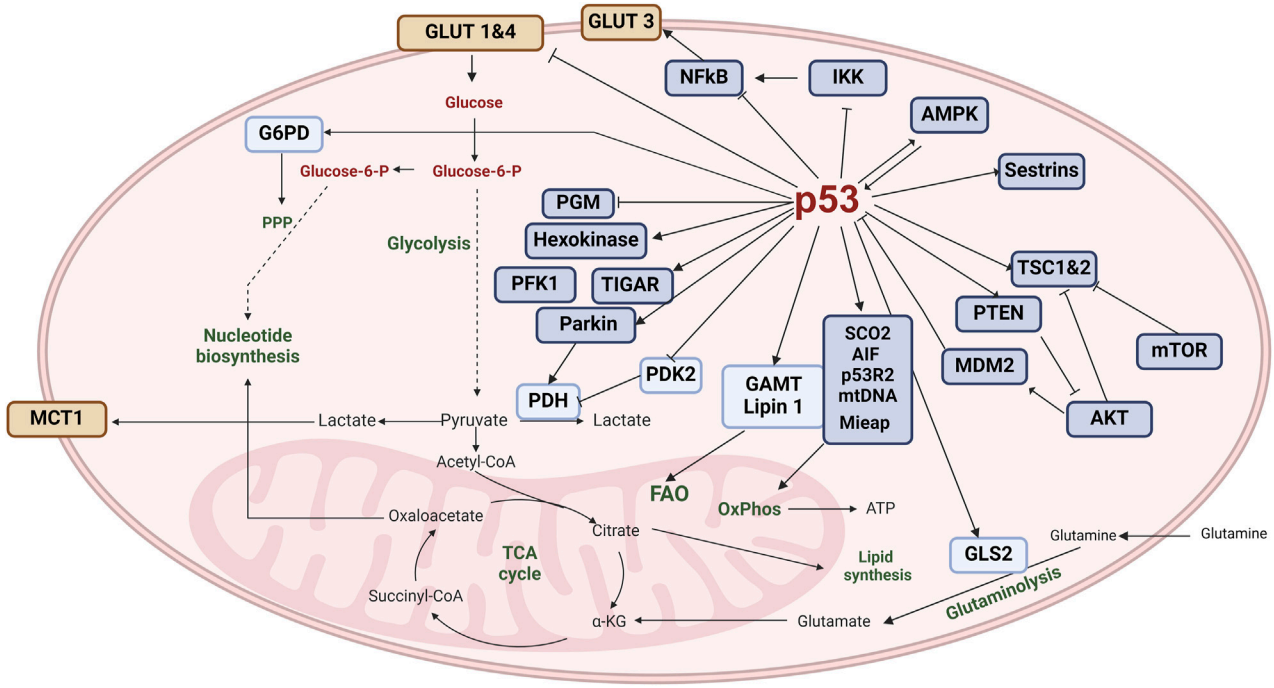

FIGURE 1
The role of p53 in the hallmarks of acute myeloid leukemia. The wild-type and mutant forms of p53 play distinct roles in controlling the diverse hallmarks of cancer. Wild-type p53 (wtp53) maintains effective anti-tumor immunity, mainly through its role in cell death (apoptosis or autophagy), senescence, or regulation of reactive oxygen species (ROS). It is also involved in regulating the immune response. In contrast, mutant p53 exerts negative effects on the immune environment by activating inflammatory pathways; this process can be enhanced by an excessive production of ROS. In consequence, mutant p53 contributes to cancer-associated chronic inflammation and protects leukemia cells from immune-mediated destruction and phagocytosis. It causes genome instability and the accumulation of new mutations that further perturbate the DNA repair machinery and enable uncontrolled growth and arrest of the cell cycle. Mutant p53 also sustains proliferative signaling, leading to replicative immortality, resistance to cell death, and finally metabolic rewiring to meet new energetic and biosynthetic demands. (Image created with BioRender.com).

loss of function (LOF), or, less frequently, to a switch or gain of function (GOF), suggesting that there may be some tissue-specific requirements for the loss of wild-type (wt) or gain of mutant p53 functions (Boettcher et al., 2019; Daver et al., 2022; Kennedy and Lowe, 2022).

Beyond the most common *TP53* mutations, the Y220C mutation frequently appears in various solid tumors and leukemias (Barnoud et al., 2021). Research suggests that this mutation is the ninth-most-frequent p53 cancer mutation (Barnoud et al., 2021; Hassin and Oren, 2023). It creates a cavity on the p53's surface, making it highly unstable. Interestingly, the Y220C mutation has been linked to 3 cases of familial cancer, and it appears to grant the p53 new cancer-promoting abilities. These abilities include stimulating the growth of blood vessels (angiogenesis) and making cancer cells resistant to the chemotherapy drug doxorubicin (Loke et al., 2022).

In general, *TP53* mutations substantially impact tumor development. In fact, over half of all human cancers have some form of *TP53* mutation. The mutations can be particularly severe in Li-Fraumeni syndrome, in which a mutated *TP53* gene dramatically increases the risk of cancers like osteosarcoma, leukemia, breast cancer, brain tumors, and adrenal tumors (Vaddavalli and Schumacher, 2022). Since p53 plays a role in many cellular processes, mutations in this gene can disrupt a wide range of functions and ultimately make cells more likely to acquire the characteristics needed to become cancerous, as illustrated in Figure 1.

Mutations in *TP53* affect homeostasis, not only via altering protein activity, but also by altering the isoforms ratio, which may diminish a patient's response to chemotherapy (Haaland et al., 2021). Among the most common *TP53* mutations, mutations in the hotspots R175 and R248 are frequently detected in diverse solid tumors but occur less frequently in AML (Barnoud et al., 2021). Interestingly, AML patients with heterozygous *TP53* mutations have shown similar responses to therapy as those harboring wt *TP53* (Barnoud et al., 2021; Kennedy and Lowe, 2022; Daver et al., 2023a). However, the sequential acquisition of the mutation of one allele, followed by mutation of the other allele or loss of the entire 17p chromosome, leads to a complete LOF of wt *TP53* and has been identified as the key progression mechanism involving *TP53* mutation. (Hong et al., 2016; Boettcher et al., 2019; Yang et al., 2022; Shah et al., 2023). Furthermore, wt *TP53* LOF is seen in patients with Li-Fraumeni syndrome; affected individuals develop AML at a frequency comparable to that of healthy individuals with other *TP53* mutations, but they manifest more aggressive disease (Prokocimer et al., 2017; Boettcher et al., 2019; Daver et al., 2022; Shah et al., 2023). *TP53* LOF is often correlated with nonautonomous effects on the tumor immune microenvironment; it subverts the wt p53 effect and allows the evasion of attack from the immune system (Prokocimer et al., 2017; Loizou et al., 2019; Hassin and Oren, 2023; Rajagopalan et al., 2023). Many point mutations in *TP53* have been studied by overexpressing the missense allele in *TP53* null tumor cells; specifically, an increase in growth independence, tumor progression, metastasis, and drug resistance (Singh et al., 2019). These changes

TABLE 1 Differences between the loss-of-function and gain-of-function mutations affecting the p53 protein.

Mutation characteristic	Mutations affecting the p53 protein	
	LOF	GOF
Frequency	Common	Less frequent
Effect	Mutations inactivate the p53 protein and decreased its ability to suppress tumor growth	Mutations inactivate p53's tumor-suppressor function and promote tumor growth
Mechanism	Mutations occur in various ways (e.g., insertions/deletions of genetic material, point mutations that change amino acids in the protein). These changes disrupt the protein's structure or its ability to bind to DNA, hindering its function as a tumor suppressor	Mutations often occur in the DNA-binding domain of p53. These mutations alter how the protein interacts with DNA, allowing it to bind to different genetic sites and regulate genes that favor tumorigenesis
Impact	Cells with nonfunctional p53 protein lack the normal cell-cycle arrest or apoptosis (programmed cell death) mechanisms triggered by DNA damage	GOF-mutant p53 can promote metastasis, induce resistance to therapy, and help cancer cells evade the immune system
Summary	LOF mutations prevent cells from damaged DNA	GOF mutations alter DNA binding, which not only makes cells ineffective at their original functions but also allows them to actively assist cancer progression

GOF, gain-of-function; LOF, loss-of-function.

have been associated with missense *TP53* variants, indicating that they have novel functions that promote tumor growth and contribute to tumorigenesis. (Loizou et al., 2019; Singh et al., 2019; Rajagopalan et al., 2023). While the GOF of mutated p53 in AML harboring *TP53* mut/mut is still debated, an alternative mechanism called separation of function seems to contribute to AML pathogenesis (Kennedy and Lowe, 2022). Table 1 summarizes the two main types of mutations that can affect the p53 protein, a critical tumor suppressor in the human body. Understanding these mutations leads to a fuller understanding of how cancers develop and progress.

1.2.2 p53 phosphorylation status and its role in AML

p53 activity is tightly regulated by posttranslational modifications, with phosphorylation being a crucial event (Ashcroft et al., 1999). Understanding p53 phosphorylation at multiple serine, threonine, and tyrosine residues by specific kinases [ataxia telangiectasia mutated (ATM), ataxia telangiectasia and Rad3-related (ATR), and checkpoint kinase 2 (CHK2)] in response to diverse cellular stresses (e.g., DNA damage, oxidative stress) and examining the multifaceted consequences of p53 phosphorylation, including enhanced protein stability, augmented transcriptional activity, and modulation of subcellular localization, may lead to the development of new therapeutic strategies (Sakaguchi et al., 1998; Ashcroft et al., 1999). These phosphorylation events orchestrate the activation of various target genes involved in cell-cycle arrest, DNA repair, and apoptosis, ultimately determining cellular fate following stress induction (Loughery and Meek, 2013). A significant percentage of AML cases have mutations in the *TP53* gene, and these mutations can disrupt the normal phosphorylation and regulation of p53, leading to its dysfunction (Ni et al., 2024). Mutant p53 proteins may have altered phosphorylation patterns or impaired interactions with kinases and other regulatory proteins, affecting their ability to properly respond to cellular stresses (Hales et al., 2014).

Several signaling pathways, such as the PI3K/AKT/mTOR pathway, MAPK pathway, and JAK/STAT pathway, can modulate p53 phosphorylation and activity in leukemias (Leu et al., 2020). Dysregulation of these pathways in AML can influence p53 phosphorylation and its downstream functions, potentially promoting leukemic cell survival or drug resistance (Motlagh et al., 2022).

2 The role of p53 in the hallmarks of leukemia

p53 is a master regulator of cancer-relevant pathways, governing genomic stability (DNA repair), cell fate (cell cycle arrest, senescence, apoptosis), and cellular processes (metabolism, autophagy, ferroptosis) (Figure 1) (Singh et al., 2019).

2.1 *TP53* and the regulation of energetics, metabolism, and metabolic reprogramming

The *TP53* gene plays a crucial role in regulating cellular energy and metabolism (Leu et al., 2020). As a transcription factor, *TP53* controls the expression of various genes involved in metabolic pathways (Motlagh et al., 2022; Luo et al., 2023). It influences the balance between glycolysis and oxidative phosphorylation (Motlagh et al., 2022; Luo et al., 2023). *TP53* also impacts glycolysis through reduction or downregulation of key glycolytic enzymes, or transporters for glucose, pyruvate or other essential for glycolysis nutrients, and through suppression of the AKT/mTOR and NF-κB signaling pathways. (Motlagh et al., 2022; Luo et al., 2023; McClure et al., 2023; Roche et al., 2023). Additionally, *TP53* controls glucose-regulating cellular energetics and metabolism by suppressing the glucose transporters (GLUT1 and GLUT4) that bring glucose into the cell. *TP53* can also induce *TP53*-induced glycolysis and apoptosis regulator, which diverts glucose away from glycolysis and towards the pentose-phosphate pathway, involved in nucleotide synthesis, lipids synthesis, and amino acids synthesis to meet the energy demands of the cell (Motlagh et al., 2022; Luo et al., 2023; McClure et al., 2023; Roche et al., 2023). *TP53* can induce the expression of genes involved in antioxidant defense, protecting cells from oxidative stress (Sakaguchi et al., 1998; Ashcroft et al., 1999; Loughery and Meek, 2013; Hales et al.,

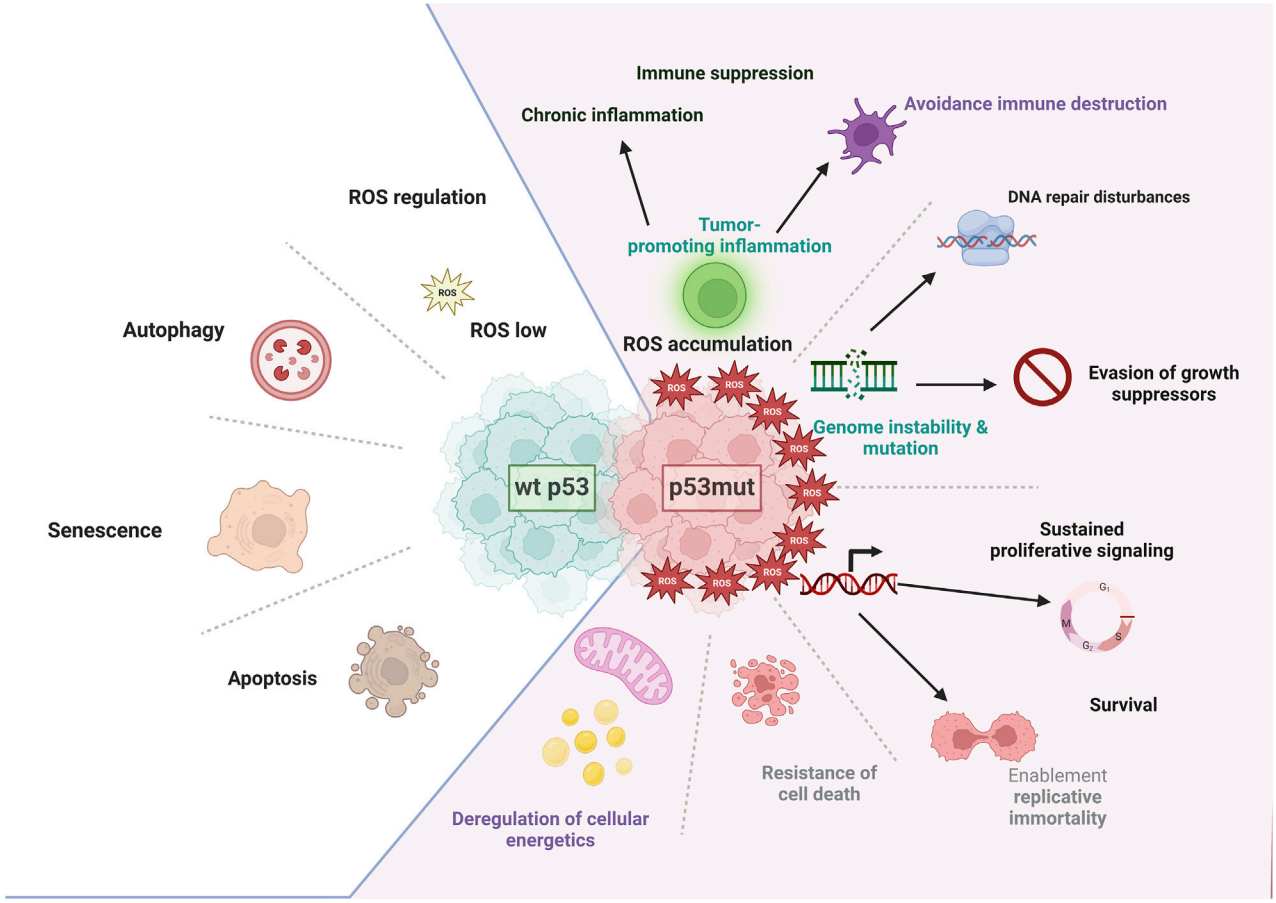

FIGURE 2
p53 and metabolism. A crucial protein in cellular regulation, p53 exerts control over several metabolic pathways involved in energy production and cellular homeostasis. It also plays a substantial role in regulating mitochondrial oxidative phosphorylation, glycolysis, glutaminolysis, fatty-acid oxidation, and nucleotide synthesis. To maintain mitochondrial integrity and promote oxidative phosphorylation, p53 transcriptionally induces the expression of SCO2, AIF1, and p53R2, while also physically interacting with mitochondrial DNA polymerase γ and MIAP (mitochondrial import associated protein). Additionally, p53 reduces glucose uptake by directly repressing the transcription of GLUT1 and GLUT4 and indirectly repressing the expression of GLUT3. Furthermore, p53 negatively regulates phosphoglycerate mutase, activates hexokinase and phosphofructokinase one at the protein level, and transcriptionally induces *TP53*-induced glycolysis and apoptosis regulator (TIGAR) and Parkin, which inhibit glycolysis. Parkin, in turn, positively regulates pyruvate dehydrogenase and the expression of monocarboxylate transporter 1. In contrast, p53 negatively regulates the expression of pyruvate dehydrogenase kinase isoform 2, which inhibits PDH activity. It also induces the expression of glutaminase 2 (GLS2), which catalyzes the hydrolysis of glutamine to glutamate. Glutamate is converted to α-ketoglutarate, which promotes the tricarboxylic acid (TCA) cycle and oxidative phosphorylation. p53 also interacts with glucose-6-phosphate dehydrogenase (G6PD) to negatively regulate its activity, leading to the downregulation of the pentose phosphate pathway, nucleotide synthesis, and nicotinamide adenine dinucleotide phosphate (NADPH) production. p53 induces the expression of GAMT and Lipin1, promoting fatty-acid oxidation and the production of acetyl-CoA. (Image created with BioRender.com).

2014; Ni et al., 2024). This shift towards oxidative phosphorylation increases ATP production and provides more efficient energy for cellular processes (Luo et al., 2023; McClure et al., 2023; Roche et al., 2023). *TP53* also inhibits the expression of genes involved in fatty-acid synthesis, promoting lipid breakdown and utilization (Luo et al., 2023; McClure et al., 2023; Roche et al., 2023). Furthermore, *TP53* can modulate the activity of enzymes involved in energy metabolism, such as AMP-activated protein kinase (AMPK) (Motlagh et al., 2022; Luo et al., 2023; McClure et al., 2023; Roche et al., 2023). In addition, it can influence mitochondrial function and biogenesis, affecting cellular energy production (Motlagh et al., 2022; Luo et al., 2023; McClure et al., 2023; Roche et al., 2023; Sanford et al., 2023; Li et al., 2024). Overall, *TP53* plays a multifaceted role in cellular energy and metabolism, maintaining the balance between energy production and utilization and the protection against cellular stress. Dysregulation of *TP53* can lead to metabolic reprogramming, which is often observed in cancer and other diseases (Leu et al., 2020; Motlagh et al., 2022; Luo et al., 2023; Roche et al., 2023) and can also lead to decreased mitochondrial activity, further compromising energy production and forcing cells to increasingly rely on glycolysis, which is inefficient (Figure 2) (Motlagh et al., 2022; Luo et al., 2023; Roche et al., 2023).

2.2 *TP53*, the immune response, immune evasion, immunosuppression, and tumor-promoting inflammation

TP53 mutations can lead to the downregulation of major histocompatibility complex (MHC) molecules, which present antigens to immune cells (Alos et al., 2020; Motlagh et al., 2022;

Hassin and Oren, 2023). By reducing MHC expression, cancer cells can evade recognition by cytotoxic T cells, which rely on MHC-antigen complexes to identify and eliminate abnormal cells (Alos et al., 2020; Wang et al., 2024). Compared to patients with TP53-WT, patients who have AML with *TP53* mutations have shown higher expression levels of *IFNG, FOXP3* in blast cells of primary BM samples, immune checkpoints, markers of immune senescence, and phosphatidylinositol 3-kinase-Akt and NF-κB signaling intermediates (Vadakekolathu et al., 2020). *TP53* mutations can also impair the activation of T cells, which are crucial for mounting an effective immune response against cancer cells (Desai et al., 2023; Wang et al., 2024). *TP53* regulates the expression of costimulatory molecules and cytokines involved in T-cell activation (Desai et al., 2023; Wang et al., 2024). Mutations in *TP53* can disrupt this regulation, leading to insufficient T-cell activation and compromised antitumor immune responses (Alos et al., 2020; Desai et al., 2023). *TP53* mutations can also negatively impact the effector functions of immune cells such as cytotoxic T cells and natural killer (NK) cells (Alos et al., 2020). These mutations can result in the downregulation of cytotoxic molecules such as perforin and granzyme B, which are responsible for killing cancer cells (Desai et al., 2023). As a result, cancer cells can evade immune-mediated cell death.

Programmed cell death protein one and its ligand, programmed cell death ligand 1 (PD-L1), play a role in immune tolerance and the suppression of antitumor immune responses, and *TP53* has been shown to regulate the expression of these immune checkpoint molecules (Alos et al., 2020). Dysregulation of *TP53* can lead to abnormal expression of PD-L1, which can inhibit T-cell function and promote immune evasion (Alos et al., 2020). *TP53* mutations induce immunosuppressive factors such as transforming growth factor beta and interleukin-10 (Daver et al., 2021). These factors can inhibit the activation and function of immune cells, creating an immunosuppressive microenvironment that favors tumor growth and immune evasion (Alos et al., 2020; Daver et al., 2021). *TP53* mutations also can disrupt the normal processes of tumor immune surveillance, which is the mechanism by which the immune system detects and eliminates cancer cells (Alos et al., 2020; Daver et al., 2021).

TP53 can activate immune cells such as macrophages, dendritic cells, and NK cells (Motlagh et al., 2022). It regulates the expression of cytokines such as interferons and interleukins, chemokines, and costimulatory molecules involved in immune-cell activation, immune signaling, immune cell function, and coordination (Motlagh et al., 2022). Proper T-cell activation is crucial for an effective immune response (Hassin and Oren, 2023; Wang et al., 2024). *TP53* controls the recruitment of immune cells to the site of infection or inflammation by regulating the expression of chemokines (Wang et al., 2024). This helps in mobilizing immune cells and directing them to the specific locations where they are needed (Wang et al., 2024). In addition, *TP53* influences the differentiation of immune cells such as macrophages and dendritic cells, which are responsible for phagocytosis, antigen presentation, and immune regulation, and ensures an effective immune response (Singh et al., 2019; Motlagh et al., 2022; Wang et al., 2024).

Tp53 participates in tumor immune surveillance and is involved in the resolution of inflammation by promoting the clearance of inflammatory cells and the restoration of tissue homeostasis. This helps in preventing chronic inflammation, which can have detrimental effects on the immune system (Alos et al., 2020). Tumor-promoting inflammation, also known as chronic inflammation, is caused by an overproduction of proinflammatory cytokines such as tumor necrosis factor-α, interleukin-1, and interleukin-6 (Shi and Jiang, 2021; Morganti et al., 2022; Miller et al., 2023; Muto et al., 2023; Qin et al., 2023). These cytokines can promote tumor growth by stimulating cell proliferation, angiogenesis, and tissue remodeling (Shi and Jiang, 2021; Morganti et al., 2022; Muto et al., 2023; Qin et al., 2023). Immune cells, including macrophages, neutrophils, and lymphocytes, release additional proinflammatory molecules, creating a positive feedback loop that sustains inflammation and promotes tumor growth (Herbrich et al., 2021; Muto et al., 2023; Qin et al., 2023). Inflammatory cells release reactive oxygen species and reactive nitrogen species, which can cause DNA damage and genomic instability (Shi and Jiang, 2021; Muto et al., 2023; Qin et al., 2023). Inflammatory mediators can suppress the function of immune cells such as T cells and NK cells (Vadakekolathu et al., 2020; Shi and Jiang, 2021; Muto et al., 2023; Qin et al., 2023). The main events impacted by p53 mutations or p53 loss are summarized in Figure 3.

2.3 TP53 and other hallmarks of AML

One of the hallmarks of cancer is uncontrolled cell proliferation; p53 controls cell division and prevents excessive proliferation (Mantovani et al., 2019). When DNA damage is detected, p53 halts the cell cycle to allow for repair, or it triggers apoptosis if the damage is too severe. Mutations in p53 render cells incapable of this checkpoint control, leading to uncontrolled proliferation (Mantovani et al., 2019; Capaci et al., 2020). In regard to the cancer hallmarks of stem-cell homeostasis and differentiation, p53 maintains a delicate balance between stem cell self-renewal and differentiation into mature cells (Shi and Jiang, 2021; Qin et al., 2023). It ensures the proper development of stem cells and prevents uncontrolled stem-cell expansion that could lead to tumors (Perez Montero et al., 2024; Scott et al., 2024).

Nutlin-3a, an MDM2 inhibitor and a selective activator of the p53 pathway, has been shown to exhibit dose-dependent antiproliferative and cytotoxic activity in OCI-AML-3 and MOLM-13 cells with wt p53 but to produce no response in HL-60 and NB4 cells expressing mutant p53 (Haaland et al., 2014; Borthakur et al., 2015; Trino et al., 2016; Fontana et al., 2021). The lack of response to Nutlin-3a indicated that the p53 pathway can be activated by Nutlin-3a only in cells with wt p53 (Kojima et al., 2005; Cheng et al., 2023; Zhou et al., 2023; Liu et al., 2024; Tomiyasu et al., 2024; Varineau and Calo, 2024).

In response to severe DNA damage or cellular stress, p53 triggers apoptosis, a process of controlled cell suicide. This eliminates potentially dangerous cells and prevents the spread of mutations (Cheng et al., 2023; Zhou et al., 2023; Liu et al., 2024; Tomiyasu et al., 2024; Varineau and Calo, 2024). Mutant p53 can malfunction in this pathway, allowing damaged cells to survive (Cheng et al., 2023; Zhou et al., 2023; Liu et al., 2024; Tomiyasu et al., 2024; Varineau and Calo, 2024). Furthermore, mutations that specifically keep the proliferation-promoting features or survival-preserving functions

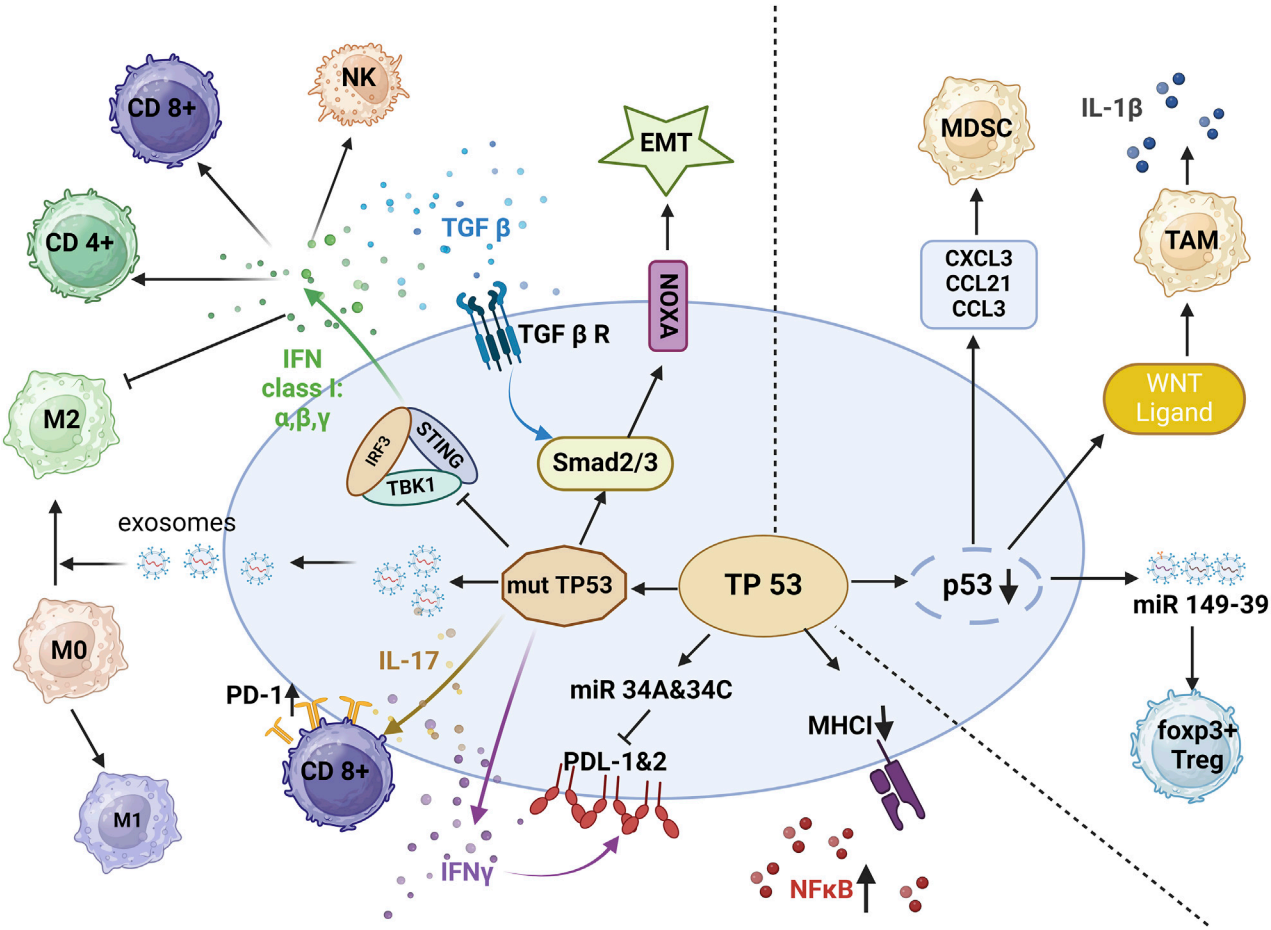

FIGURE 3
p53 and immune suppression. In the setting of mutant p53, decreased release of IFN-I reduces infiltration by $CD4^+$ T cells, $CD8^+$ T cells, and natural killer (NK) cells, and interferon gamma (IFNγ) increases the expression of programmed cell death ligand 1 (PD-L1) and programmed cell death ligand 2 (PD-L2). By activation of interleukin 17 (IL-17) signaling, mutant p53 leads to $CD8^+$T-cell exhaustion. In concert with transforming growth factor beta (TGF-β), mutant p53 promotes epithelial-to-mesenchymal transition EMT. With the release of exosomes, mutant p53 also promotes the polarization of M1 macrophages to M2 macrophages, protecting tumor cells from phagocytosis. In the setting of p53 deletion, tumor cells release WNT ligands, chemokine ligand 1 (CXCL1), chemokine ligand 3 (CCL3) and chemokine ligand 21 (CCL21), and miR-149–39 to enhance the differentiation of tumor-associated macrophages (TAMs) and regulatory T cells (Tregs) (Image created with BioRender.com).

of wild-type p53, such as adaptation to metabolic stress, while disrupting the canonical tumor suppressive activities (such as apoptosis and senescence), can result in phenotypes that resemble those associated with gain-of-function mutations (Pfister and Prives, 2017). Controlling genome stability by p53 is another hallmark of AML and plays a central role in maintaining genomic integrity. It helps repair DNA damage through various mechanisms and activates checkpoints to halt cell division if DNA repair is incomplete (Vaddavalli and Schumacher, 2022). Dysfunction of p53 leads to an accumulation of mutations, increasing the risk of cancer (Wiederschain et al., 2005; Meyer et al., 2009), and alterations such as microsatellite instability or p53 mutations were enriched substantially in patients with therapy-related AML (Wiederschain et al., 2005; Meyer et al., 2009). Normal cells have a limited lifespan and eventually stop dividing after reaching a certain number of cell divisions (replicative senescence), but p53 can induce this senescence state in damaged or stressed cells, preventing them from becoming cancerous (Wiederschain et al., 2005; Meyer et al., 2009). Mutations in *TP53* can bypass this safeguard, allowing abnormal cell proliferation and leading to uncontrolled cell growth (Gutu et al., 2023). Research suggests a potential link between p53 function and lifespan regulation, indicating that heightened p53 activity is associated with a shorter lifespan as shown in murine models. Conversely, experiments in flies suggest that reduced p53 activity appears to extend lifespan (Wiederschain et al., 2005). *TP53* is well known as a "gatekeeper" of the cell cycle; it is capable of blocking cells in the G1/S phase if activated by hypoxia, heat shock, or other extrinsic or intrinsic stress signals (Olivier et al., 2010; Wang H. et al., 2023). In healthy cells, in case of DNA damage, ATM or ATR kinases activate checkpoint kinases (CHK1 and CHK2), which activate p53 and p21 and initiate G1 arrest and senescence phenotype (Wang H. et al., 2023). p53 activates cyclin-dependent kinase inhibitor 1A and p14 alternate open reading frame, which are involved in senescence and growth arrest, and targets several genes involved in the apoptosis and necrosis pathway (Barnoud et al., 2021). Mutations in *TP53* have shown partial or complete alteration of the target gene set, depending on the position and the type of

mutation (Olivier et al., 2010; Barnoud et al., 2021; Kennedy and Lowe, 2022).

3 Current therapeutic strategies for *TP53* in AML

As previously mentioned, choosing and managing therapy for patients with AML who harbor *TP53* mutations or have complex karyotypes remains challenging (Abramowitz et al., 2017; Latif et al., 2021; Hassin and Oren, 2023). Moreover, the current therapeutic management of AML considers several risk factors that are included in prognostic models predicting therapy responses and outcomes, and these models classify patients with *TP53* mutations as poor responders (Haase et al., 2019). Here we will discuss the outcomes of patients with *TP53* mutations after treatment with selected therapy regimens (Olivier et al., 2010).

3.1 Intense chemotherapy

Intense chemotherapy is based on the combination of antimetabolic and antiproliferative agents like cytarabine and anthracyclines, and it is a backbone of AML therapy (DiNardo et al., 2019; Kadia et al., 2021). Intense chemotherapy based on high-dose cytarabine (AraC)/daunorubicin, known as the 7 + 3 regime, is still considered the gold standard of care (Kantarjian et al., 2021; Daver et al., 2022). Therapy modification by dose reduction of AraC or daunorubicine and the further introduction of fludarabine or cladribine has been shown to improve the response to therapy, patient outcomes, and therapy safety profile (Kadia et al., 2021). Intense chemotherapy is mainly followed by consolidation and/or maintenance therapy, and in some cases is followed by HSC transplantation (Guerra et al., 2019). A study has shown that drug-induced pancytopenia, which frequently occurs in patients treated with intense chemotherapy, became managable with protocol administration of granulocyte colony-stimulation factor (Kadia et al., 2021). Also, a new liposomal formulation of AraC/daunorubicin, known as CPX-351, has been shown to reduce the risk of cardiotoxicity in patients treated with that combination (Daver et al., 2020). However, none of these regimens specifically address the challenges of drug resistance linked to *TP53* (DiNardo et al., 2019; Daver et al., 2022). Mutations in the *TP53* gene render Acute Myeloid Leukemia (AML) resistant to traditional chemotherapies. Consequently, effective treatment strategies for *TP53*-mutated AML either bypass the need for wild-type p53 function altogether or aim to restore its normal activity (Daver et al., 2020). Most patients with *TP53*-mutated AML have a median overall survival of only a few months, despite receiving active anticancer treatment.

Counterintuitively, although chemotherapy and radiation (cytotoxic stress) aim to damage cancer cells, they do not directly cause *TP53* mutations (Yan et al., 2020). Individuals with *TP53* mutations in their blood stem cells (hematopoietic clones) face a significantly increased risk of developing Acute Myeloid Leukemia (AML). The median time to AML diagnosis after detecting a *TP53* mutation is approximately 4.9 years (Desai et al., 2019; Young et al., 2019; Saygin et al., 2023). While *TP53* mutations are rare in blood stem cells, these mutated cells have a survival advantage. This allows them to outcompete healthy cells under pressure from chemotherapy or stem cell transplant (Desai et al., 2019; Young et al., 2019; Saygin et al., 2023).

3.2 Hypomethylating agents

In the last decade, many hypomethylating agents (HMAs) have been developed for patients who cannot undergo intense chemotherapy, especially those over the age of 60 with high-risk features (Haase et al., 2019; Daver et al., 2023a; Wang H. et al., 2023). The most relevant approved drugs belonging to this category are azacytidine (AZA) and decitabine (DEC), which have gained considerable interest in the last decade due to the possibility of combining them with other types of therapies. (Daver et al., 2020; George et al., 2021; Kennedy and Lowe, 2022; Daver et al., 2023a; Wang H. et al., 2023). For instance, a 10-day decitabine regimen in patients with AML led to an excellent 100% ORR in patients with mutated *TP53* disease compared to 41% in those with wt *TP53* ($p < 0.001$), however was not sufficient for mutational clearance.

3.3 Allogenic stem cell transplantation

Allogenic stem cell transplantation (allo-SCT) is used in secondary AML following other therapies such as intense chemotherapy and HMA treatments. Allo-SCT can have a curative effect and can lower the probability of disease relapse in patients with a poor prognosis, but it requires early minimal residual disease (MRD) monitoring, and the incidence of complications is still high (Loke et al., 2022; Dekker et al., 2023; Gutman et al., 2023; Tettero et al., 2023). Genetic aberrations involving *TP53, FLT3, NPM1, RUNX1*, and *ASXL1*, together with factors such as age, sex, and cytogenetic characteristics, are the main risk factors affecting the outcome of patients undergoing allo-SCT (Yan et al., 2020; Loke et al., 2022; Malagola et al., 2023; Chattopadhyay et al., 2024; Park et al., 2024). *TP53* positive MRD status in patients with AML, for example, has been associated with a significantly worse survival (median overall survival, 6.4 months vs 21.7 months, $p = 0.042$) both in patients with *TP53*-mutated AML and myelodysplastic syndrome receiving HMA as frontline therapy (n = 24) prior allo-SCT (Olivier et al., 2010; Malagola et al., 2023; Song et al., 2023; Chattopadhyay et al., 2024; Park et al., 2024; Sahasrabudhe and Mims, 2024). Thus, the early detection of these mutations using complex MRD monitoring and testing for the loss of chimerism (LoC after allo-SCT is a serious concern as it can be an early indicator of relapse) after stem cell transplant are the key strategies for addressing the otherwise-poor survival of patients relapsing after allo-SCT (Sahasrabudhe and Mims, 2024).

3.4 Bcl-2 inhibitors

Bcl-2 family genes are composed of antiapoptotic and proapoptotic genes such as *Bcl-2* and *BAX/BAK*, respectively (DiNardo et al., 2019; Guerra et al., 2019). Bcl-2 inhibitor–based therapy relies on altering the equilibrium of Bcl-2 components by depleting the antiapoptotic members and allowing the p53-mediated activation of *BAX* and *BAK* following the permeabilization of the

outer mitochondrial membrane and caspase cascade (DiNardo et al., 2019; Guerra et al., 2019; Carter et al., 2023a). Venetoclax (VEN) has proven to be as effective as monotherapy, especially in AML harboring *IDH1/2* and *SRSF2/ZRSF2* mutations (Daver et al., 2020; George et al., 2021; Thijssen et al., 2021). Further synergistic activity was observed with AZA in the VIALE-A trial and with low-dose cytarabine in the VIALE-C trial (Thijssen et al., 2021; Carter et al., 2023a; Malagola et al., 2023; Song et al., 2023; Pratz et al., 2024; Sahasrabudhe and Mims, 2024). However, the best outcome was obtained when VEN was combined with MCL-1 inhibitor in therapies (Thijssen et al., 2021; Casado and Cutillas, 2023). A cohort analysis of patients harboring *TP53* mutations demonstrated a lack of improvement among patients on the VEN + AZA regimen compared with historical controls (Hong et al., 2016; DiNardo et al., 2019). However, given the limited number of patients, further studies in this specific patient cohort are warranted. Although therapy with VEN + AZA has a good safety profile in elderly patients, the short response duration in patients with *TP53* mutation and rapidly acquired resistance to VEN warrants further investigations on the mechanisms of resistance in these patients as well as further work on novel combinatorial strategies (DiNardo et al., 2019; Guerra et al., 2019; Kadia et al., 2021; Zhang et al., 2022; Gutman et al., 2023). However, due to the rewiring of other BH3-mimetic family members upon Bcl-2 pharmacological inhibition, other therapeutic strategies with molecules targeting Bcl-2, Bcl-XL, and Bcl-W were evaluated. Navitoclax (ABT-263) is an antagonist of the antiapoptotic members of the Bcl-2 family—Bcl-2, Bcl-XL, and Bcl-W—and prevents their binding to the apoptotic effectors proteins Bax and Bak, thereby triggering apoptotic processes in cells overexpressing these proteins (Gress et al., 2024). However, the application of navitoclax in patients is challenging because its induction of severe thrombocytopenia limits its utility. Besides navitoclax, several other molecules have been tested in phase I and Ib clinical trials, including the Mcl-1 inhibitors AZD5991, MIK665, AMG176, and AMG397, alone or in combination with VEN (Luedtke et al., 2017; Tron et al., 2018; Carter et al., 2022; Fang et al., 2022; Liu et al., 2022; Carter et al., 2023a; Wang Y. et al., 2023; Torka et al., 2023). Furthermore, several dual inhibitors targeting Bcl-2/-XL have been developed, including LP-118, AZD0466, and dual Bcl-2/-XL PROTAC degraders (Khan et al., 2022; Gress et al., 2024). Finally, VEN has been tested with several FLT3 inhibitors such as quizartinib or gliteritinib in patients with FLT3-mutated AML as well as in those with wt FLT. VEN improved survival in a cohort of patients with mutated *FLT3*, successfully impairing leukemia progression (Yilmaz et al., 2022). While the list of potential combinations of BCL2 and FLT3 co-inhibition in acute myeloid leukemia tested preclinically expands rapidly, none of these so far has shown improved efficacy in patients with *TP53* mutations (Perl, 2019; Brinton et al., 2020; Carter et al., 2021; Zhu et al., 2021; Carter et al., 2023b; Popescu et al., 2023).

4 Future directions in the treatment of AML

In recent years, increased knowledge regarding the features about AML—obtained through genome-wide association studies, single-cell RNA sequencing, and proteomic approaches—has enabled the consideration of several novel therapeutic approaches for the treatment of patients with AML. These approaches could pave the way for new generations of HMA and BCL-2 inhibitors; such inhibitors are currently being evaluated as monotherapies or in combination with approved therapies (Daver et al., 2020).

4.1 *TP53* pathway interference

The main inhibitors of p53, MDM2 and MDM4, are often upregulated in many malignancies harboring wt p53 (Wang H. et al., 2023). While several molecules such as HDM201, MK-8242, BI-907828, RG7388, and RG7112 have been developed to interfere with p53 activity, most remain in the preclinical testing phase (Wang H. et al., 2023). Idasanutlin (RG7388), an MDM2 antagonist with a pyrrolidine structure, has demonstrated better efficacy, selectivity, and availability for the treatment of AML compared with the other drugs of the nutlin family (Trino et al., 2016; Fontana et al., 2021), and in a phase III trial with cytarabine, it improved survival and recovery in patients with R/R AML (Italiano et al., 2021; Konopleva et al., 2022; Daver et al., 2023b; Smalley et al., 2024). Mutant p53 tends to aggregate with p73, p63, or other p53 molecules, inactivating or reducing their activity (Kennedy and Lowe, 2022). Interference with these interactions would restore the activity of p73 and residual wtp53 (Ramos et al., 2020; Klein et al., 2021; Cai et al., 2022). ReACp53, for example, is a small peptide that interferes with the aggregation of mutant p53 with p73 and p63, and it has been shown to restore the wt conformation and nuclear localization of p53, promoting apoptosis *in vitro* and tumor suppression *in vivo* (Spaety et al., 2019; Zhang et al., 2019; Ramos et al., 2020; Klein et al., 2021; Rozenberg et al., 2021; Cai et al., 2022; Wang H. et al., 2023; Hassin and Oren, 2023).

4.2 *TP53* reactivation

Another strategy to address the severe outcomes of mutant *TP53* and the consequent LOF is to reverse the altered mutant conformation to one resembling that of wt *TP53* (Prokocimer et al., 2017; Hassin and Oren, 2023). Eprenetapopt (APR-246), also known as PRIMA1-MET, is a small molecule that causes selective apoptosis in cancer cells with *TP53* mutations (Hassin and Oren, 2023). Eprenetapopt binds covalently to cysteine residues in the DBD and forces conformational changes in the wt conformation, leading to the depletion of antioxidants and d-nucleotides and the induction of ROS(Reactive Oxygen Species)-linked cell death through ferroptosis (Sallman, 2020; Birsen et al., 2022; Daver et al., 2022). Eprenetapopt was evaluated with AZA in phase III clinical trial, but it showed no significant benefits in patients with *TP53* mutations (Daver et al., 2022; Hassin and Oren, 2023). In contrast, in combination with AZA and VEN, this combination therapy demonstrated an acceptable safety profile and promising signs of effectiveness. These findings support further investigation of this approach as a first-line treatment for *TP53*-mutated AML (Garcia-Manero et al., 2023; Wang H. et al., 2023). Other trial have evaluated APR-246 as post-transplant maintenance therapy and focused on patients with *TP53*-mutated acute myeloid leukemia (AML) or myelodysplastic

syndromes (MDS) who had undergone allogeneic hematopoietic stem cell transplantation (allo-SCT) leading to encouraging RFS and OS outcomes in this high-risk population (Spaety et al., 2019). APR-246 was also evaluated with DEC, VEN, and low-dose cytarabine in patients with AML who were over 60 years old and ineligible for intense chemotherapy. The drug combination produced encouraging results and had an acceptable safety profile (Mishra et al., 2022).

In addition, APR-548, an orally available *TP53* reactivator, has undergone clinical evaluation in patients with solid tumors and hematological malignancies, indicating that p53 mutants differ in functionality and form from typical AML cases and subsequently display inconsistent responses to therapy with APR-548 at the cellular level (George et al., 2021).

Finally, ZMC1, ZMC2, and ZMC3, which belong to a new class of zinc metallochaperones, sequester zinc ions crucial for DNA recognition from mutated p53, promoting wt-like behavior, p53-dependent apoptosis *in vitro*, and tumor regression *in vivo* (Wang H. et al., 2023; Hassin and Oren, 2023). These zinc metallochaperones have been shown to reactivate mutant p53 using an on/off switch, and they have shown specificity for mutant p53 (Hassin and Oren, 2023).

4.3 Trisenox

Trisenox (ATO) (As_2O_3) is a small molecule that binds to allosteric sites on a wide subset of p53 mutants and induces p53 proteasome–mediated degradation via structural stabilization (Gummlich, 2021; Song et al., 2023). It has been observed that a few p53 mutants treated with ATO demonstrate restored wt p53 activity (Daver et al., 2022; Hassin and Oren, 2023). Trisenox is mainly used in certain subtypes of AML, including acute promyeloid leukemia, in which it has shown dose-dependent dual effects, including differentiation at low concentrations and apoptosis at high concentrations, on Leukemia Stem Cells (LSC) (Yilmaz et al., 2021). Clinical trials involving treatments with trisenox + HMA + all-trans retinoic acid are ongoing (Yilmaz et al., 2021).

4.4 Chimeric antigen receptor T cells

Development of adoptive T cell therapy for relapsed/refractory acute myeloid leukemia (R/R AML) has shown limited progress to date. Chimeric antigen receptors (CARs) implemented *in vitro* in T cells have proven to be effective for R/R B-cell lymphoid malignancies ($CD19^+$) and multiple myeloma (Caruso et al., 2022; Gurney and O'Dwyer, 2021; Mueller et al., 2024). Several proteins commonly overexpressed in AML, such as CD38, CD123, TIM3, CD7, CD19, and NKG2D, have been considered as targets for evaluation in AML treatments, with the aim of treatment being to eradicate the LSC-like population (Gurney and O'Dwyer, 2021; Valeri et al., 2022; Cao et al., 2022; Cui et al., 2021; El et al., 2021; Jetani et al., 2021; Mai et al., 2023). However, it has been difficult to find suitable tumor-associated antigens for CAR T-cell administration in patients with AML (Cui et al., 2021; El et al., 2021; Yilmaz et al., 2021; Sanford et al., 2023); thus, clinical responses to CAR T-cell therapy are seen in only one-fourth of treated subjects (Atilla and Benabdellah, 2023). Recent studies have tried to overcome *TP53* deficiency–linked resistance to CAR T cells by targeting the lipids metabolism aiming at blocking cholesterol metabolism or activity of carnitine o-octanoyltransferase and at improving CAR T-cell anti-leukemic properties. While the specific results of targeting these pathways are not provided here, further investigation might lead to more effective and personalized treatment options in the future. (Mueller et al., 2023; Roche et al., 2023; Sanford et al., 2023; Albinger et al., 2024). Although CAR T-cell therapy alone might not be sufficient to achieve a complete eradication of residual disease, some studies suggest that combined CAR T-cell therapy and pharmacological blockade with demethylating agents or venetoclax (VEN) might be a promising strategy. This approach could lead to more effective and better-tolerated cellular therapies for patients with *TP53*-mutated myeloid neoplasms (Leick et al., 2022; Mandeville et al., 2023; Mueller et al., 2023; Sanford et al., 2023).

4.5 CAR NK cells

NK cells are the first line of defense against tumor cells (Mandeville et al., 2023; Albinger et al., 2024). They induce cell death in two ways: by releasing tumor necrosis factor-α and IFN-γ, which activate the extrinsic apoptosis pathway, and by triggering cell death using the tumor necrosis factor–related apoptosis-inducing ligand or Fas ligand. Compared to the use of CAR T cells, the use of CAR NK cells has significantly fewer side effects (Gurney and O'Dwyer, 2021; Albinger et al., 2024; Albinger et al., 2022). Until now, CAR NK therapy has shown good efficacy in clinical trials against circulating AML cells, but it displays a low penetrative ability in bone marrow niches; thus, it is considered as a maintenance or consolidation therapy before or following an allo-SCT rather than as induction therapy (Gurney and O'Dwyer, 2021). After intensive therapy and allogenic hematopoietic cell transplantation, the outcomes of CAR NK cell therapy in AML patients with *TP53* mutations remains poor, those patients with lower *TP35* VAFs at diagnosis might still benefit from transplantation. combined with CAR NK therapy (Zhao et al., 2023). One possible mechanism of overcoming resistance to CAR NK therapy would be to select AML clones that resist or even suppress NK cell activity and mobilize them from Bone marrow, making them more susceptible to therapy (Gurney and O'Dwyer, 2021; Valeri et al., 2022; Albinger et al., 2024; Li et al., 2023). Persistent hypoxia and bone marrow remodeling with poor vascularization might also be obstacles to the efficacy of CAR NK therapy (Caruso et al., 2022). These and other factors contributing to therapy resistance need further investigation to improve the chances of disease eradication.

4.6 Immunotherapy

Since the approval of gemtuzumab ozogamicin (GO, a monoclonal antibody targeting CD33, conjugated with calicheamicin) (Laszlo et al., 2019; Bouvier et al., 2021; Casado and Cutillas, 2023), immunotherapy for AML has advanced substantially. New monoclonal antibodies, used along with other types of therapies in the induction phase or as a part of consolidation therapy after intense chemotherapy, have been added to the available treatment options (Hassin and Oren, 2023). For

TABLE 2 Examples of clinical trials in acute myeloid leukemia with the potential to target *TP53*.

Trial code	Phase	Approach type	Evaluated therapy
NCT05455294	Phase I	HMA + Bcl-2 inhibitors	DEC + VEN + navitoclax
NCT03745716	Phase III	HMA + mutTP53 alteration	AZA + APR-246
NCT03855371	Phase I	HMA + small molecule	DEC + ATO
NCT04638309	Phase I	HMA + mut*TP53* alteration	AZA + APR-548
NCT05297123	Phase I	Small-molecule combination	ATO + ATRA
NCT03766126	Phase I	Cell-mediated	CD123 CAR-T
NCT04678336	Phase I	Cell-mediated	CD123 CAR-T
NCT02944162	Phase I-II	Cell-mediated	CD33 CAR-NK cells
NCT04623944	Phase I	Cell-mediated	NKX101-CAR NK
NCT01217203	Phase I	Antibody	IPH2101 + lenalidomide (anti-KIR2D+)
NCT01687387	Phase II	Antibody	Lirilumab (anti-KIR2D)
NCT01714739	Phase I-II	Antibodies (PD-1, KIR2, CTLA-4)	Nivolumab + Lirilumab/ipilimumab
NCT02848248	Phase I	Antibody-drug conjugate	SGN-CD123A
NCT05396859	Recruiting	Cytidine deaminase inhibitors	Entrectinib + ASTX727
NCT02545283	Terminated	MDM2 antagonist	Idasanutlin + cytarabine

HMA, Hypomethylating agent; DEC, Decitabine (a specific HMA, drug); ATO, Arsenic trioxide (a small molecule drug); AZA, Azacitidine (another HMA, drug); APR-548, A small molecule drug targeting specific pathways; ATRA, All-trans retinoic acid (a small molecule drug); CD123 CAR-T, Chimeric antigen receptor T cells engineered to target the CD123 protein on leukemia cells; CD33 CAR-NK, cells, Chimeric antigen receptor Natural Killer cells engineered to target the CD33 protein on leukemia cells; NKX101- CAR NK, Specific brand name for CAR-NK, cells targeting a certain molecule; IPH2101, A specific antibody targeting the KIR2D + receptor; Lenalidomide, An immunomodulatory drug; Lirilumab, antibody targeting the KIR2D + receptor; Nivolumab, antibody targeting the PD-1, checkpoint protein; Lirilumab/Ipilimumab, Antibodies targeting KIR2D+ and CTLA-4, checkpoint protein, respectively; Antibody-drug conjugate (ADC): an antibody linked to a chemotherapy drug that delivers the drug directly to cancer cells; SGN-CD123A, A specific type of ADC, targeting the CD123 protein; Cytidine deaminase inhibitors, Drugs that block the enzyme cytidine deaminase; Entrectinib, A small molecule drug targeting specific mutations; ASTX727, Another small molecule drug targeting specific pathways; MDM2 antagonist, Drug that blocks the interaction between MDM2 and p53 protein; Idasanutlin, specific MDM2 antagonist; Cytarabine, chemotherapy drug.

example, sabatolimab (MBC453) is a humanized, high-affinity, IgG4, anti-TIM3 antibody that uses an autocrine signaling loop via galactin-9 and promotes LSC renewal; it is currently being combined with HMA in an ongoing clinical trial (Brunner et al., 2024; Zeidan et al., 2024). Its observed side effects have been minimal, and the parameters of recovery and patients' OS have been encouraging, especially in patients with AML harboring mutations such as *RUNX1* and *ASXL1* (Kantarjian et al., 2021; Daver et al., 2022). Another antibody, magrolimab, is a humanized antibody against CD47, a surface receptor expressed by myeloid malignancies that helps tumor cells evade phagocytosis (Bouvier et al., 2021; Zhao et al., 2023). Magrolimab has been evaluated in AML patients not eligible for intense chemotherapy who were in the early stages of treatments with AZA + VEN, and it demonstrated good tolerability, but it also caused frequent side effects such as anemia and fatigue (George et al., 2021; Zeidan et al., 2022; Daver et al., 2023c).

Bispecific and trispecific antibodies are a promising new area of immunotherapy for AML (Arvindam et al., 2021; Bouvier et al., 2021; Boyiadzis et al., 2023). These engineered molecules, which offer a targeted approach of attacking AML cells by harnessing the immune system, include flotetuzumab (targets CD33 on AML cells and CD16 on NK cells), AMG 330 (targets CD33 on AML cells and CD3 on T cells), and JNJ-63709178 (targets CD33; bispecific antibody) (Krupka et al., 2016; Jitschin et al., 2018; Laszlo et al., 2019; Vadakekolathu et al., 2020; Uy et al., 2021; Barwe et al., 2022; Boyiadzis et al., 2023; Marcinek et al., 2023; Rimando et al., 2023). Study investigating the CD123 × CD3 bispecific, dual-affinity, retargeting antibody flotetuzumab (CP-MGD006-01; NCT02152956) demonstrated complete remission in almost 50% of patients with *TP53*-mutated, R/R AML, and these patients had significantly higher tumor inflammation signature, FOXP3, CD8, inflammatory chemokine, and PD1 gene expression scores at baseline compared with nonresponders (Vadakekolathu et al., 2020). Examples of relevant clinical trials are given in Table 2.

5 Conclusion

For over four decades, high-dose cytotoxic chemotherapy remained the mainstay treatment for AML. However, recent scientific breakthroughs have revolutionized our understanding of this leukemia's molecular basis. This newfound knowledge has not only shed light on the underlying causes of AML but also led to the development of several targeted therapies. These novel agents offer greater efficacy and reduced toxicity compared to conventional chemotherapy. With novel compounds selectively targeting *TP53*, therapeutic approaches targeting the *TP53* pathway are progressing in early clinical testing and could soon be considered the standard of care for individuals with AML who are 60 and older and ineligible for intense therapy or who have been diagnosed with advanced disease. Moreover, many targeted approaches and combinations are currently being tested in clinical trials with the aims of reducing the rate of disease recurrence and minimizing drug toxicities, making

the prospects of new AML therapies promising. However, further investigation of the factors contributing to therapy resistance is warranted, and efforts to understand the metabolic and immune mechanisms contributing to therapy failure with the help of single-cell, high-throughput technology and spatial analysis are ongoing.

6 Simple summary

Acute myeloid leukemia (AML), an aggressive malignancy of hematopoietic stem cells, is associated with poor outcomes, especially in elderly patients, due to several genetic and chromosomal aberrations. Tumor protein p53 (*TP53*) is a key tumor-suppressor gene involved in a variety of cellular processes, including the regulation of apoptosis, metabolism, and the rewiring of the immune environment. Although *TP53* mutations are relatively rare in patients with *de novo* AML, these mutations has been identified as an important molecular subgroup, and patients with these mutations have the worst prognosis and shortest overall survival among patients with AML, even when treated with aggressive chemotherapy and allogeneic stem cell transplant for relapsed or therapy-related AML. Progress in AML genetics and biology has brought the novel therapies, however, the clinical benefit of these agents for patients whose disease is driven by *TP53* mutations remains largely unexplored. This review focuses on examining the role of *TP53* mutations on such hallmarks of leukemia like metabolic rewiring and immune evasion, the clinical significance of these changes, and the current progress in the therapeutic targeting of mutated p53 and its downstream effects.

Author contributions

MC: Writing–review and editing, Writing–original draft, Visualization, Methodology, Conceptualization. LG: Writing–original draft. SD: Writing–review and editing, Visualization, Methodology, Conceptualization. PF: Writing–review and editing, Visualization, Methodology, Conceptualization. BG: Writing–review and editing. VM: Writing–review and editing, Visualization, Methodology, Conceptualization. HA: Writing–review and editing. NB: Writing–review and editing, Writing–original draft, Visualization, Validation, Supervision, Project administration, Methodology, Funding acquisition, Conceptualization.

Funding

The author(s) declare that financial support was received for the research, authorship, and/or publication of this article. This research was funded by the National Science Centre, Poland (2021/43/B/NZ5/03345) (NB), and in part by the NIH/NCI Cancer Center Support Grant P30CA016672, as well as by NIH/NCI R01CA231364 (NB); HA was supported by the Physician Scientist Program and Cancer Prevention and Research Institute of Texas Funding.

Acknowledgments

All figures were created using BioRender software. We thank Laura L. Russell, scientific editor, Research Medical Library, The University of Texas MD Anderson Cancer Center for editing this manuscript.

Conflict of interest

The authors declare that the research was conducted in the absence of any commercial or financial relationships that could be construed as a potential conflict of interest.

Publisher's note

References

Abramowitz, J., Neuman, T., Perlman, R., and Ben-Yehuda, D. (2017). Gene and protein analysis reveals that p53 pathway is functionally inactivated in cytogenetically normal Acute Myeloid Leukemia and Acute Promyelocytic Leukemia. *BMC Med. Genomics* 10 (1), 18. doi:10.1186/s12920-017-0249-2

Albinger, N., Muller, S., Kostyra, J., Kuska, J., Mertlitz, S., Penack, O., et al. (2024). Manufacturing of primary CAR-NK cells in an automated system for the treatment of acute myeloid leukemia. *Bone Marrow Transpl.* 59 (4), 489–495. doi:10.1038/s41409-023-02180-4

Albinger, N., Pfeifer, R., Nitsche, M., Mertlitz, S., Campe, J., Stein, K., et al. (2022). Primary CD33-targeting CAR-NK cells for the treatment of acute myeloid leukemia. *Blood Cancer J.* 12 (4), 61. doi:10.1038/s41408-022-00660-2

Alos, L., Fuster, C., Castillo, P., Jares, P., Garcia-Herrera, A., Marginet, M., et al. (2020). *TP53* mutation and tumoral PD-L1 expression are associated with depth of invasion in desmoplastic melanomas. *Ann. Transl. Med.* 8 (19), 1218. doi:10.21037/atm-20-1846

Appelbaum, J. S., Wei, A. H., Mandrekar, S. J., Tiong, I. S., Chua, C. C., Teh, T. C., et al. (2024). Clinical evaluation of complete remission (CR) with partial hematologic recovery (CRh) in acute myeloid leukemia: a report of 7235 patients from seven cohorts. *Leukemia* 38 (2), 389–392. doi:10.1038/s41375-024-02143-8

Arvindam, U. S., van Hauten, P. M. M., Schirm, D., Schaap, N., Hobo, W., Blazar, B. R., et al. (2021). A trispecific killer engager molecule against CLEC12A effectively induces NK-cell mediated killing of AML cells. *Leukemia* 35 (6), 1586–1596. doi:10.1038/s41375-020-01065-5

Ashcroft, M., Kubbutat, M. H., and Vousden, K. H. (1999). Regulation of p53 function and stability by phosphorylation. *Mol. Cell Biol.* 19 (3), 1751–1758. PMID: 10022862; PMCID: PMC83968. doi:10.1128/MCB.19.3.1751

Atilla, E., and Benabdellah, K. (2023). The black hole: CAR T cell therapy in AML. *Cancers (Basel)* 15 (10), 2713. doi:10.3390/cancers15102713

Barnoud, T., Indeglia, A., and Murphy, M. E. (2021). Shifting the paradigms for tumor suppression: lessons from the p53 field. *Oncogene* 40 (25), 4281–4290. doi:10.1038/s41388-021-01852-z

Barwe, S. P., Kisielewski, A., Bonvini, E., Muth, J., Davidson-Moncada, J., Kolb, E. A., et al. (2022). Efficacy of flotetuzumab in combination with cytarabine in patient-derived xenograft models of pediatric acute myeloid leukemia. *J. Clin. Med.* 11 (5), 1333. doi:10.3390/jcm11051333

Birsen, R., Larrue, C., Decroocq, J., Johnson, N., Guiraud, N., Gotanegre, M., et al. (2022). APR-246 induces early cell death by ferroptosis in acute myeloid leukemia. *Haematologica* 107 (2), 403–416. doi:10.3324/haematol.2020.259531

Boettcher, S., Miller, P. G., Sharma, R., McConkey, M., Leventhal, M., Krivtsov, A. V., et al. (2019). A dominant-negative effect drives selection of TP53 missense mutations in myeloid malignancies. *Science* 365 (6453), 599–604. doi:10.1126/science.aax3649

Borthakur, G., Duvvuri, S., Ruvolo, V., Tripathi, D. N., Piya, S., Burks, J., et al. (2015). MDM2 inhibitor, nutlin 3a, induces p53 dependent autophagy in acute leukemia by AMP kinase activation. *PLoS One* 10 (10), e0139254. doi:10.1371/journal.pone.0139254

Bouvier, A., Hamel, J. F., Delaunay, J., Delabesse, E., Dumas, P. Y., Ledoux, M. P., et al. (2021). Molecular classification and prognosis in younger adults with acute myeloid leukemia and intermediate-risk cytogenetics treated or not by gemtuzumab ozogamycin: final results of the GOELAMS/FILO acute myeloid leukemia 2006-intermediate-risk trial. *Eur. J. Haematol.* 107 (1), 111–121. doi:10.1111/ejh.13626

Boyiadzis, M., Desai, P., Daskalakis, N., Donnellan, W., Ferrante, L., Goldberg, J. D., et al. (2023). First-in-human study of JNJ-63709178, a CD123/CD3 targeting antibody, in relapsed/refractory acute myeloid leukemia. *Clin. Transl. Sci.* 16 (3), 429–435. doi:10.1111/cts.13467

Brinton, L. T., Zhang, P., Williams, K., Canfield, D., Orwick, S., Sher, S., et al. (2020). Synergistic effect of BCL2 and FLT3 co-inhibition in acute myeloid leukemia. *J. Hematol. Oncol.* 13 (1), 139. doi:10.1186/s13045-020-00973-4

Brunner, A. M., Esteve, J., Porkka, K., Knapper, S., Traer, E., Scholl, S., et al. (2024). Phase Ib study of sabatolimab (MBG453), a novel immunotherapy targeting TIM-3 antibody, in combination with decitabine or azacitidine in high- or very high-risk myelodysplastic syndromes. *Am. J. Hematol.* 99 (2), E32–E36. doi:10.1002/ajh.27161

Cai, B. H., Hsu, Y. C., Yeh, F. Y., Lin, Y. R., Lu, R. Y., Yu, S. J., et al. (2022). P63 and P73 activation in cancers with p53 mutation. *Biomedicines* 10 (7), 1490. doi:10.3390/biomedicines10071490

Cao, X., Dai, H., Cui, Q., Li, Z., Shen, W., Pan, J., et al. (2022). CD7-directed CAR T-cell therapy: a potential immunotherapy strategy for relapsed/refractory acute myeloid leukemia. *Exp. Hematol. Oncol.* 11 (1), 67. doi:10.1186/s40164-022-00318-6

Capaci, V., Mantovani, F., and Sal, G. D. (2020). A mutant p53/Hif1α/miR-30d axis reprograms the secretory pathway promoting the release of a prometastatic secretome. *Cell Stress* 4 (11), 261–264. doi:10.15698/cst2020.11.235

Carter, B. Z., Mak, P. Y., Tao, W., Ayoub, E., Ostermann, L. B., Huang, X., et al. (2023a). Combined inhibition of BCL-2 and MCL-1 overcomes BAX deficiency-mediated resistance of TP53-mutant acute myeloid leukemia to individual BH3 mimetics. *Blood Cancer J.* 13 (1), 57. doi:10.1038/s41408-023-00830-w

Carter, B. Z., Mak, P. Y., Tao, W., Ostermann, L. B., Mak, D. H., Ke, B., et al. (2023b). Inhibition of menin, BCL-2, and FLT3 combined with a hypomethylating agent cures NPM1/FLT3-ITD/-TKD mutant acute myeloid leukemia in a patient-derived xenograft model. *Haematologica* 108 (9), 2513–2519. doi:10.3324/haematol.2022.281927

Carter, B. Z., Mak, P. Y., Tao, W., Warmoes, M., Lorenzi, P. L., Mak, D., et al. (2022). Targeting MCL-1 dysregulates cell metabolism and leukemia-stroma interactions and resensitizes acute myeloid leukemia to BCL-2 inhibition. *Haematologica* 107 (1), 58–76. doi:10.3324/haematol.2020.260331

Carter, B. Z., Tao, W., Mak, P. Y., Ostermann, L. B., Mak, D., McGeehan, G., et al. (2021). Menin inhibition decreases Bcl-2 and synergizes with venetoclax in NPM1/FLT3-mutated AML. *Blood* 138 (17), 1637–1641. doi:10.1182/blood.2021011917

Caruso, S., De Angelis, B., Del Bufalo, F., Ciccone, R., Donsante, S., Volpe, G., et al. (2022). Safe and effective off-the-shelf immunotherapy based on CAR.CD123-NK cells for the treatment of acute myeloid leukaemia. *J. Hematol. Oncol.* 15 (1), 163. doi:10.1186/s13045-022-01376-3

Casado, P., and Cutillas, P. R. (2023). Proteomic characterization of acute myeloid leukemia for precision medicine. *Mol. Cell Proteomics* 22 (4), 100517. doi:10.1016/j.mcpro.2023.100517

Chattopadhyay, S., Lionel, S., Selvarajan, S., Devasia, A. J., Korula, A., Kulkarni, U., et al. (2024). Relapse and transformation to myelodysplastic syndrome and acute myeloid leukemia following immunosuppressive therapy for aplastic anemia is more common as compared to allogeneic stem cell transplantation with a negative impact on survival. *Ann. Hematol.* 103 (3), 749–758. doi:10.1007/s00277-024-05621-2

Chen, X., Zhang, T., Su, W., Dou, Z., Zhao, D., Jin, X., et al. (2022). Mutant p53 in cancer: from molecular mechanism to therapeutic modulation. *Cell Death Dis.* 13 (11), 974. doi:10.1038/s41419-022-05408-1

Cheng, J., Yan, Z., Jiang, K., Liu, C., Xu, D., Lyu, X., et al. (2023). Discovery of JN122, a spiroindoline-containing molecule that inhibits MDM2/p53 protein-protein interaction and exerts robust *in vivo* antitumor efficacy. *J. Med. Chem.* 66 (24), 16991–17025. doi:10.1021/acs.jmedchem.3c01815

Cui, Q., Qian, C., Xu, N., Kang, L., Dai, H., Cui, W., et al. (2021). CD38-directed CAR-T cell therapy: a novel immunotherapy strategy for relapsed acute myeloid leukemia after allogeneic hematopoietic stem cell transplantation. *J. Hematol. Oncol.* 14 (1), 82. doi:10.1186/s13045-021-01092-4

Daver, N., Alotaibi, A. S., Bucklein, V., and Subklewe, M. (2021). T-cell-based immunotherapy of acute myeloid leukemia: current concepts and future developments. *Leukemia* 35 (7), 1843–1863. doi:10.1038/s41375-021-01253-x

Daver, N., Wei, A. H., Pollyea, D. A., Fathi, A. T., Vyas, P., and DiNardo, C. D. (2020). New directions for emerging therapies in acute myeloid leukemia: the next chapter. *Blood Cancer J.* 10 (10), 107. doi:10.1038/s41408-020-00376-1

Daver, N. G., Dail, M., Garcia, J. S., Jonas, B. A., Yee, K. W. L., Kelly, K. R., et al. (2023b). Venetoclax and idasanutlin in relapsed/refractory AML: a nonrandomized, open-label phase 1b trial. *Blood* 141 (11), 1265–1276. doi:10.1182/blood.2022016362

Daver, N. G., Iqbal, S., Renard, C., Chan, R. J., Hasegawa, K., Hu, H., et al. (2023a). Treatment outcomes for newly diagnosed, treatment-naive *TP53*-mutated acute myeloid leukemia: a systematic review and meta-analysis. *J. Hematol. Oncol.* 16 (1), 19. doi:10.1186/s13045-023-01417-5

Daver, N. G., Maiti, A., Kadia, T. M., Vyas, P., Majeti, R., Wei, A. H., et al. (2022). TP53-Mutated myelodysplastic syndrome and acute myeloid leukemia: biology, current therapy, and future directions. *Cancer Discov.* 12 (11), 2516–2529. doi:10.1158/2159-8290.CD-22-0332

Daver, N. G., Vyas, P., Kambhampati, S., Al Malki, M. M., Larson, R. A., Asch, A. S., et al. (2023c). Tolerability and efficacy of the anticluster of differentiation 47 antibody magrolimab combined with azacitidine in patients with previously untreated AML: phase Ib results. *J. Clin. Oncol.* 41 (31), 4893–4904. doi:10.1200/JCO.22.02604

Dekker, S. E., Rea, D., Cayuela, J. M., Arnhardt, I., Leonard, J., and Heuser, M. (2023). Using measurable residual disease to optimize management of AML, ALL, and chronic myeloid leukemia. *Am. Soc. Clin. Oncol. Educ. Book* 43, e390010. doi:10.1200/EDBK_390010

Deng, J., Wu, X., Ling, Y., Liu, X., Zheng, X., Ye, W., et al. (2020). The prognostic impact of variant allele frequency (VAF) in TP53 mutant patients with MDS: a systematic review and meta-analysis. *Eur. J. Haematol.* 105 (5), 524–539. doi:10.1111/ejh.13483

Desai, P., Hassane, D., and Roboz, G. J. (2019). Clonal hematopoiesis and risk of acute myeloid leukemia. *Best. Pract. Res. Clin. Haematol.* 32 (2), 177–185. doi:10.1016/j.beha.2019.05.007

Desai, P. N., Wang, B., Fonseca, A., Borges, P., Jelloul, F. Z., Reville, P. K., et al. (2023). Single-cell profiling of CD8+ T cells in acute myeloid leukemia reveals a continuous spectrum of differentiation and clonal hyperexpansion. *Cancer Immunol. Res.* 11, 1011–1028. doi:10.1158/2326-6066.CIR-22-0961

DiNardo, C. D., Pratz, K., Pullarkat, V., Jonas, B. A., Arellano, M., Becker, P. S., et al. (2019). Venetoclax combined with decitabine or azacitidine in treatment-naive, elderly patients with acute myeloid leukemia. *Blood* 133 (1), 7–17. doi:10.1182/blood-2018-08-868752

Donehower, L. A., Soussi, T., Korkut, A., Liu, Y., Schultz, A., Cardenas, M., et al. (2019). Integrated analysis of TP53 gene and pathway alterations in the cancer genome atlas. *Cell Rep.* 28 (11), 1370–1384. doi:10.1016/j.celrep.2019.07.001

El, K. N., Hughes, A., Yu, W., Myburgh, R., Matschulla, T., Taromi, S., et al. (2021). Demethylating therapy increases anti-CD123 CAR T cell cytotoxicity against acute myeloid leukemia. *Nat. Commun.* 12 (1), 6436. doi:10.1038/s41467-021-26683-0

Fang, D. D., Zhu, H., Tang, Q., Wang, G., Min, P., Wang, Q., et al. (2022). FLT3 inhibition by olverembatinib (HQP1351) downregulates MCL-1 and synergizes with BCL-2 inhibitor lisaftoclax (APG-2575) in preclinical models of FLT3-ITD mutant acute myeloid leukemia. *Transl. Oncol.* 15 (1), 101244. doi:10.1016/j.tranon.2021.101244

Fleming, S., Tsai, X. C., Morris, R., Hou, H. A., and Wei, A. H. (2023). TP53 status and impact on AML prognosis within the ELN 2022 risk classification. *Blood* 142 (23), 2029–2033. doi:10.1182/blood.2023020855

Fontana, M. C., Nanni, J., Ghelli Luserna di Rora, A., Petracci, E., Padella, A., Ghetti, M., et al. (2021). Pharmacological inhibition of WIP1 sensitizes acute myeloid leukemia cells to the MDM2 inhibitor nutlin-3a. *Biomedicines* 9 (4), 388. doi:10.3390/biomedicines9040388

Garcia-Manero, G., Goldberg, A. D., Winer, E. S., Altman, J. K., Fathi, A. T., Odenike, O., et al. (2023). Eprenetapopt combined with venetoclax and azacitidine in TP53-mutated acute myeloid leukaemia: a phase 1, dose-finding and expansion study. *Lancet Haematol.* 10 (4), e272–e283. doi:10.1016/S2352-3026(22)00403-3

George, B., Kantarjian, H., Baran, N., Krocker, J. D., and Rios, A. (2021). TP53 in acute myeloid leukemia: molecular aspects and patterns of mutation. *Int. J. Mol. Sci.* 22 (19), 10782. doi:10.3390/ijms221910782

Gress, V., Roussy, M., Boulianne, L., Bilodeau, M., Cardin, S., El-Hachem, N., et al. (2024). CBFA2T3::GLIS2 pediatric acute megakaryoblastic leukemia is sensitive to BCL-XL inhibition by navitoclax and DT2216. *Blood Adv.* 8 (1), 112–129. doi:10.1182/bloodadvances.2022008899

Guerra, V. A., DiNardo, C., and Konopleva, M. (2019). Venetoclax-based therapies for acute myeloid leukemia. *Best. Pract. Res. Clin. Haematol.* 32 (2), 145–153. doi:10.1016/j.beha.2019.05.008

Gummlich, L. (2021). ATO stabilizes structural p53 mutants. *Nat. Rev. Cancer* 21 (3), 141. doi:10.1038/s41568-021-00337-1

Gurney, M., and O'Dwyer, M. (2021). Realizing innate potential: CAR-NK cell therapies for acute myeloid leukemia. *Cancers (Basel)* 13 (7), 1568. doi:10.3390/cancers13071568

Gutman, J. A., Winters, A., Kent, A., Amaya, M., McMahon, C., Smith, C., et al. (2023). Higher-dose venetoclax with measurable residual disease-guided azacitidine discontinuation in newly diagnosed acute myeloid leukemia. *Haematologica* 108 (10), 2616–2625. doi:10.3324/haematol.2023.282681

Gutu, N., Binish, N., Keilholz, U., Herzel, H., and Granada, A. E. (2023). p53 and p21 dynamics encode single-cell DNA damage levels, fine-tuning proliferation and shaping population heterogeneity. *Commun. Biol.* 6 (1), 1196. doi:10.1038/s42003-023-05585-5

Haaland, I., Hjelle, S. M., Reikvam, H., Sulen, A., Ryningen, A., McCormack, E., et al. (2021). p53 protein isoform profiles in AML: correlation with distinct differentiation stages and response to epigenetic differentiation therapy. *Cells* 10 (4), 833. doi:10.3390/cells10040833

Haaland, I., Opsahl, J. A., Berven, F. S., Reikvam, H., Fredly, H. K., Haugse, R., et al. (2014). Molecular mechanisms of nutlin-3 involve acetylation of p53, histones and heat shock proteins in acute myeloid leukemia. *Mol. Cancer* 13, 116. doi:10.1186/1476-4598-13-116

Haase, D., Stevenson, K. E., Neuberg, D., Maciejewski, J. P., Nazha, A., Sekeres, M. A., et al. (2019). TP53 mutation status divides myelodysplastic syndromes with complex karyotypes into distinct prognostic subgroups. *Leukemia* 33 (7), 1747–1758. doi:10.1038/s41375-018-0351-2

Hales, E. C., Taub, J. W., and Matherly, L. H. (2014). New insights into Notch1 regulation of the PI3K-AKT-mTOR1 signaling axis: targeted therapy of γ-secretase inhibitor resistant T-cell acute lymphoblastic leukemia. *Cell Signal* 26 (1), 149–161. Epub 2013 Oct 16. PMID: 24140475. doi:10.1016/j.cellsig.2013.09.021

Hassin, O., and Oren, M. (2023). Drugging p53 in cancer: one protein, many targets. *Nat. Rev. Drug Discov.* 22 (2), 127–144. doi:10.1038/s41573-022-00571-8

Herbrich, S., Baran, N., Cai, T., Weng, C., Aitken, M. J. L., Post, S. M., et al. (2021). Overexpression of CD200 is a stem cell-specific mechanism of immune evasion in AML. *J. Immunother. Cancer* 9 (7), e002968. doi:10.1136/jitc-2021-002968

Hong, M., Hao, S., Patel, K. P., Kantarjian, H. M., Garcia-Manero, G., Yin, C. C., et al. (2016). Whole-arm translocation of der(5;17)(p10;q10) with concurrent *TP53* mutations in acute myeloid leukemia (AML) and myelodysplastic syndrome (MDS): A unique molecular-cytogenetic subgroup. *Cancer Genet.* 209 (5), 205–214. doi:10.1016/j.cancergen.2016.04.001

Italiano, A., Miller, W. H., Jr., Blay, J. Y., Gietema, J. A., Bang, Y. J., Mileshkin, L. R., et al. (2021). Phase I study of daily and weekly regimens of the orally administered MDM2 antagonist idasanutlin in patients with advanced tumors. *Invest. New Drugs* 39 (6), 1587–1597. doi:10.1007/s10637-021-01141-2

Jetani, H., Navarro-Bailon, A., Maucher, M., Frenz, S., Verbruggen, C., Yeguas, A., et al. (2021). Siglec-6 is a novel target for CAR T-cell therapy in acute myeloid leukemia. *Blood* 138 (19), 1830–1842. doi:10.1182/blood.2020009192

Jitschin, R., Saul, D., Braun, M., Tohumeken, S., Volkl, S., Kischel, R., et al. (2018). CD33/CD3-bispecific T-cell engaging (BiTE®) antibody construct targets monocytic AML myeloid-derived suppressor cells. *J. Immunother. Cancer* 6 (1), 116. doi:10.1186/s40425-018-0432-9

Kadia, T. M., Reville, P. K., Borthakur, G., Yilmaz, M., Kornblau, S., Alvarado, Y., et al. (2021). Venetoclax plus intensive chemotherapy with cladribine, idarubicin, and cytarabine in patients with newly diagnosed acute myeloid leukaemia or high-risk myelodysplastic syndrome: a cohort from a single-centre, single-arm, phase 2 trial. *Lancet Haematol.* 8 (8), e552–e561. doi:10.1016/S2352-3026(21)00192-7

Kantarjian, H. M., Kadia, T. M., DiNardo, C. D., Welch, M. A., and Ravandi, F. (2021). Acute myeloid leukemia: treatment and research outlook for 2021 and the MD Anderson approach. *Cancer* 127 (8), 1186–1207. doi:10.1002/cncr.33477

Kennedy, M. C., and Lowe, S. W. (2022). Mutant p53: it's not all one and the same. *Cell Death Differ.* 29 (5), 983–987. doi:10.1038/s41418-022-00989-y

Khan, S., Wiegand, J., Zhang, P., Hu, W., Thummuri, D., Budamagunta, V., et al. (2022). BCL-X(L) PROTAC degrader DT2216 synergizes with sotorasib in preclinical models of KRAS(G12C)-mutated cancers. *J. Hematol. Oncol.* 15 (1), 23. doi:10.1186/s13045-022-01241-3

Klein, A. M., Biderman, L., Tong, D., Alaghebandan, B., Plumber, S. A., Mueller, H. S., et al. (2021). MDM2, MDMX, and p73 regulate cell-cycle progression in the absence of wild-type p53. *Proc. Natl. Acad. Sci. U. S. A.* 118 (44), e2102420118. doi:10.1073/pnas.2102420118

Kojima, K., Konopleva, M., Samudio, I. J., Shikami, M., Cabreira-Hansen, M., McQueen, T., et al. (2005). MDM2 antagonists induce p53-dependent apoptosis in AML: implications for leukemia therapy. *Blood* 106 (9), 3150–3159. doi:10.1182/blood-2005-02-0553

Konopleva, M. Y., Rollig, C., Cavenagh, J., Deeren, D., Girshova, L., Krauter, J., et al. (2022). Idasanutlin plus cytarabine in relapsed or refractory acute myeloid leukemia: results of the MIRROS trial. *Blood Adv.* 6 (14), 4147–4156. doi:10.1182/bloodadvances.2021006303

Krupka, C., Kufer, P., Kischel, R., Zugmaier, G., Lichtenegger, F. S., Kohnke, T., et al. (2016). Blockade of the PD-1/PD-L1 axis augments lysis of AML cells by the CD33/CD3 BiTE antibody construct AMG 330: reversing a T-cell-induced immune escape mechanism. *Leukemia* 30 (2), 484–491. doi:10.1038/leu.2015.214

Laszlo, G. S., Beddoe, M. E., Godwin, C. D., Bates, O. M., Gudgeon, C. J., Harrington, K. H., et al. (2019). Relationship between CD33 expression, splicing polymorphism, and *in vitro* cytotoxicity of gemtuzumab ozogamicin and the CD33/CD3 BiTE® AMG 330. *Haematologica* 104 (2), e59–e62. doi:10.3324/haematol.2018.202069

Latif, A. L., Newcombe, A., Li, S., Gilroy, K., Robertson, N. A., Lei, X., et al. (2021). BRD4-mediated repression of p53 is a target for combination therapy in AML. *Nat. Commun.* 12 (1), 241. doi:10.1038/s41467-020-20378-8

Leick, M. B., Silva, H., Scarfo, I., Larson, R., Choi, B. D., Bouffard, A. A., et al. (2022). Non-cleavable hinge enhances avidity and expansion of CAR-T cells for acute myeloid leukemia. *Cancer Cell* 40 (5), 494–508 e5. doi:10.1016/j.ccell.2022.04.001

Leu, J. I., Murphy, M. E., and George, D. L. (2020). Functional interplay among thiol-based redox signaling, metabolism, and ferroptosis unveiled by a genetic variant of TP53. *Proc. Natl. Acad. Sci. U. S. A.* 117 (43), 26804–26811. doi:10.1073/pnas.2009943117

Li, F., Zhang, F., Wang, T., Xie, Z., Luo, H., Dong, W., et al. (2024). A self-amplifying loop of TP53INP1 and P53 drives oxidative stress-induced apoptosis of bone marrow mesenchymal stem cells. *Apoptosis* 29, 882–897. doi:10.1007/s10495-023-01934-1

Li, L., Mohanty, V., Dou, J., Huang, Y., Banerjee, P. P., Miao, Q., et al. (2023). Loss of metabolic fitness drives tumor resistance after CAR-NK cell therapy and can be overcome by cytokine engineering. *Sci. Adv.* 9 (30), eadd6997. doi:10.1126/sciadv.add6997

Liu, S., Qiao, X., Wu, S., Gai, Y., Su, Y., Edwards, H., et al. (2022). c-Myc plays a critical role in the antileukemic activity of the Mcl-1-selective inhibitor AZD5991 in acute myeloid leukemia. *Apoptosis* 27 (11-12), 913–928. doi:10.1007/s10495-022-01756-7

Liu, Z., Yang, Y., Sun, X., Ma, R., Zhang, W., Wang, W., et al. (2024). Discovery of novel antitumor small-molecule agent with dual action of CDK2/p-RB and MDM2/p53. *Molecules* 29 (3), 725. doi:10.3390/molecules29030725

Loizou, E., Banito, A., Livshits, G., Ho, Y. J., Koche, R. P., Sanchez-Rivera, F. J., et al. (2019). A gain-of-function p53-mutant oncogene promotes cell fate plasticity and myeloid leukemia through the pluripotency factor FOXH1. *Cancer Discov.* 9 (7), 962–979. doi:10.1158/2159-8290.CD-18-1391

Loke, J., Labopin, M., Craddock, C., Cornelissen, J. J., Labussiere-Wallet, H., Wagner-Drouet, E. M., et al. (2022). Additional cytogenetic features determine outcome in patients allografted for TP53 mutant acute myeloid leukemia. *Cancer* 128 (15), 2922–2931. doi:10.1002/cncr.34268

Loughery, J. E. P., and Meek, D. W. (2013). Switching on p53: an essential role for protein phosphorylation? *Biodiscovery*. doi:10.7750/biodiscovery.2013.8.1

Luedtke, D. A., Niu, X., Pan, Y., Zhao, J., Liu, S., Edwards, H., et al. (2017). Inhibition of Mcl-1 enhances cell death induced by the Bcl-2-selective inhibitor ABT-199 in acute myeloid leukemia cells. *Signal Transduct. Target Ther.* 2, 17012. doi:10.1038/sigtrans.2017.12

Luo, K., Qian, Z., Jiang, Y., Lv, D., Zhu, K., Shao, J., et al. (2023). Characterization of the metabolic alteration-modulated tumor microenvironment mediated by TP53 mutation and hypoxia. *Comput. Biol. Med.* 163, 107078. doi:10.1016/j.compbiomed.2023.107078

Mai, S., Hodges, A., Chen, H. M., Zhang, J., Wang, Y. L., Liu, Y., et al. (2023). LILRB3 modulates acute myeloid leukemia progression and acts as an effective target for CAR T-cell therapy. *Cancer Res.* 83 (24), 4047–4062. doi:10.1158/0008-5472.CAN-22-2483

Malagola, M., Polverelli, N., Beghin, A., Bolda, F., Comini, M., Farina, M., et al. (2023). Bone marrow CD34+ molecular chimerism as an early predictor of relapse after allogeneic stem cell transplantation in patients with acute myeloid leukemia. *Front. Oncol.* 13, 1133418. doi:10.3389/fonc.2023.1133418

Mandeville, T. K., Mavis, C., Gu, J., Bowman, K., Olejniczak, S., Dey, P., et al. (2023). Mitochondrial reprogramming by bcl-2 inhibitor venetoclax enhances αCD19 CAR-T cell fitness and anti-tumor efficacy. *Blood* 142, 6845. doi:10.1182/blood-2023-191051

Mantovani, F., Collavin, L., and Del Sal, G. (2019). Mutant p53 as a guardian of the cancer cell. *Cell Death Differ.* 26 (2), 199–212. doi:10.1038/s41418-018-0246-9

Marcinek, A., Brauchle, B., Rohrbacher, L., Hanel, G., Philipp, N., Markl, F., et al. (2023). CD33 BiTE® molecule-mediated immune synapse formation and subsequent T-cell activation is determined by the expression profile of activating and inhibitory checkpoint molecules on AML cells. *Cancer Immunol. Immunother.* 72 (7), 2499–2512. doi:10.1007/s00262-023-03439-x

McClure, M. B., Kogure, Y., Ansari-Pour, N., Saito, Y., Chao, H. H., Shepherd, J., et al. (2023). Landscape of genetic alterations underlying hallmark signature changes in cancer reveals TP53 aneuploidy-driven metabolic reprogramming. *Cancer Res. Commun.* 3 (2), 281–296. doi:10.1158/2767-9764.CRC-22-0073

Meyer, M., Rubsamen, D., Slany, R., Illmer, T., Stabla, K., Roth, P., et al. (2009). Oncogenic RAS enables DNA damage- and p53-dependent differentiation of acute myeloid leukemia cells in response to chemotherapy. *PLoS One* 4 (11), e7768. doi:10.1371/journal.pone.0007768

Miller, K. N., Li, B., Pierce-Hoffman, H. R., Lei, X., Havas, A. P., Patel, S., et al. (2023). *A mitochondria-regulated p53-CCF circuit integrates genome integrity with inflammation*. bioRxiv, 2023.11.20.567963. Nov 21:2023.11.20.567963. doi:10.1101/2023.11.20.567963

Mishra, A., Tamari, R., DeZern, A. E., Byrne, M. T., Gooptu, M., Chen, Y. B., et al. (2022). Eprenetapopt plus azacitidine after allogeneic hematopoietic stem-cell transplantation for TP53-mutant acute myeloid leukemia and myelodysplastic syndromes. *J. Clin. Oncol.* 40 (34), 3985–3993. doi:10.1200/JCO.22.00181

Morganti, C., Ito, K., Yanase, C., Verma, A., Teruya-Feldstein, J., and Ito, K. (2022). NPM1 ablation induces HSC aging and inflammation to develop myelodysplastic syndrome exacerbated by p53 loss. *EMBO Rep.* 23 (5), e54262. doi:10.15252/embr.202154262

Motlagh, A. V., Mahdevar, M., Mirzaei, S., Entezari, M., Hashemi, M., Hushmandi, K., et al. (2022). Introduction of mutant TP53 related genes in metabolic pathways and evaluation their correlation with immune cells, drug resistance and sensitivity. *Life Sci.* 303, 120650. doi:10.1016/j.lfs.2022.120650

Mueller, J., Schimmer, R., Schneiter, F., Fulin, J., Lysenko, V., Myburgh, R., et al. (2023). Deficiency in human aml confers resistance to car T-cells that can Be overcome by synergistical pharmacological interventions targeting the cholesterol or wnt pathway. *Ann. Hematol.* 102 (Suppl. 1), S63–S. doi:10.1038/s44321-024-00024-2

Mueller, J., Schimmer, R. R., Koch, C., Schneiter, F., Fullin, J., Lysenko, V., et al. (2024). Targeting the mevalonate or Wnt pathways to overcome CAR T-cell resistance in TP53-mutant AML cells. *EMBO Mol. Med.* 16 (3), 445–474. doi:10.1038/s44321-024-00024-2

Muto, T., Walker, C. S., Agarwal, P., Vick, E., Sampson, A., Choi, K., et al. (2023). Inactivation of p53 provides a competitive advantage to del(5q) myelodysplastic syndrome hematopoietic stem cells during inflammation. *Haematologica* 108 (10), 2715–2729. doi:10.3324/haematol.2022.282349

Ni, X., Lu, C. P., Xu, G. Q., and Ma, J. J. (2024). Transcriptional regulation and post-translational modifications in the glycolytic pathway for targeted cancer therapy. *Acta Pharmacol. Sin.* Epub ahead of print. PMID: 38622288. doi:10.1038/s41401-024-01264-1

Olivier, M., Hollstein, M., and Hainaut, P. (2010). TP53 mutations in human cancers: origins, consequences, and clinical use. *Cold Spring Harb. Perspect. Biol.* 2 (1), a001008. doi:10.1101/cshperspect.a001008

Park, S., Bang, S. Y., Kwag, D., Lee, J. H., Kim, T. Y., Lee, J., et al. (2024). Reduced toxicity (FluBu3) versus myeloablative (BuCy) conditioning in acute myeloid leukemia patients who received first allogeneic hematopoietic stem cell transplantation in measurable residual disease-negative CR1. *Bone Marrow Transpl.* 59 (6), 813–823. doi:10.1038/s41409-024-02255-w

Perez Montero, S., Paul, P. K., di Gregorio, A., Bowling, S., Shepherd, S., Fernandes, N. J., et al. (2024). Mutation of p53 increases the competitive ability of pluripotent stem cells. *Development* 151 (2), dev202503. doi:10.1242/dev.202503

Perl, A. E. (2019). Improving response to FLT3 inhibitors-BCL2 the rescue? *Clin. Cancer Res.* 25 (22), 6567–6569. doi:10.1158/1078-0432.CCR-19-2339

Pfister, N. T., and Prives, C. (2017). Transcriptional regulation by wild-type and cancer-related mutant forms of p53. *Cold Spring Harb. Perspect. Med.* 7 (2), a026054. doi:10.1101/cshperspect.a026054

Popescu, B., Stahlhut, C., Tarver, T. C., Wishner, S., Lee, B. J., Peretz, C. A. C., et al. (2023). Allosteric SHP2 inhibition increases apoptotic dependency on BCL2 and synergizes with venetoclax in FLT3-and KIT-mutant AML. *Cell Rep. Med.* 4 (11), 101290. doi:10.1016/j.xcrm.2023.101290

Pratz, K. W., Jonas, B. A., Pullarkat, V., Thirman, M. J., Garcia, J. S., Dohner, H., et al. (2024). Long-term follow-up of VIALE-A: venetoclax and azacitidine in chemotherapy-ineligible untreated acute myeloid leukemia. *Am. J. Hematol.* 99 (4), 615–624. doi:10.1002/ajh.27246

Prokocimer, M., Molchadsky, A., and Rotter, V. (2017). Dysfunctional diversity of p53 proteins in adult acute myeloid leukemia: projections on diagnostic workup and therapy. *Blood* 130 (6), 699–712. doi:10.1182/blood-2017-02-763086

Qin, Z., Liu, H., Sheng, Q., Dan, J., Wu, X., Li, H., et al. (2023). Mutant p53 leads to low-grade IFN-I-induced inflammation and impairs cGAS-STING signalling in mice. *Eur. J. Immunol.* 53 (9), e2250211. doi:10.1002/eji.202250211

Rajagopalan, A., Feng, Y., Gayatri, M. B., Ranheim, E. A., Klungness, T., Matson, D. R., et al. (2023). A gain-of-function p53 mutant synergizes with oncogenic NRAS to promote acute myeloid leukemia in mice. *J. Clin. Invest.* 133 (24), e173116. doi:10.1172/JCI173116

Ramos, H., Raimundo, L., and Saraiva, L. (2020). p73: from the p53 shadow to a major pharmacological target in anticancer therapy. *Pharmacol. Res.* 162, 105245. doi:10.1016/j.phrs.2020.105245

Rimando, J. C., Chendamarai, E., Rettig, M. P., Jayasinghe, R., Christopher, M. J., Ritchey, J. K., et al. (2023). Flotetuzumab and other T-cell immunotherapies upregulate MHC class II expression on acute myeloid leukemia cells. *Blood* 141 (14), 1718–1723. doi:10.1182/blood.2022017795

Roche, M. E., Ko, Y. H., Domingo-Vidal, M., Lin, Z., Whitaker-Menezes, D., Birbe, R. C., et al. (2023). TP53 Induced Glycolysis and Apoptosis Regulator and Monocarboxylate Transporter 4 drive metabolic reprogramming with c-MYC and NFkB activation in breast cancer. *Int. J. Cancer* 153 (9), 1671–1683. doi:10.1002/ijc.34660

Rozenberg, J. M., Zvereva, S., Dalina, A., Blatov, I., Zubarev, I., Luppov, D., et al. (2021). The p53 family member p73 in the regulation of cell stress response. *Biol. Direct* 16 (1), 23. doi:10.1186/s13062-021-00307-5

Sahasrabudhe, K. D., and Mims, A. S. (2024). MRD in AML: who, what, when, where, and how? *Blood* 143 (4), 296–298. doi:10.1182/blood.2023022226

Sakaguchi, K., Herrera, J. E., Saito, S., Miki, T., Bustin, M., Vassilev, A., et al. (1998). DNA damage activates p53 through a phosphorylation-acetylation cascade. *Genes Dev.* 12 (18), 2831–2841. PMID: 9744860; PMCID: PMC317174. doi:10.1101/gad.12.18.2831

Sallman, D. A. (2020). To target the untargetable: elucidation of synergy of APR-246 and azacitidine in TP53 mutant myelodysplastic syndromes and acute myeloid leukemia. *Haematologica* 105 (6), 1470–1472. doi:10.3324/haematol.2020.249060

Sanford, J. D., Franklin, D., Grois, G. A., Jin, A., and Zhang, Y. (2023). Carnitine o-octanoyltransferase is a p53 target that promotes oxidative metabolism and cell survival following nutrient starvation. *J. Biol. Chem.* 299 (7), 104908. doi:10.1016/j.jbc.2023.104908

Saygin, C., Zhang, P., Stauber, J., Aldoss, I., Sperling, A. S., Weeks, L. D., et al. (2023). Acute lymphoblastic leukemia with myeloid mutations is a high-risk disease associated with clonal hematopoiesis. *Blood Cancer Discov.* 5 (3), 164–179. doi:10.1158/2643-3230.BCD-23-0106

Scott, M. T., Liu, W., Mitchell, R., Clarke, C. J., Kinstrie, R., Warren, F., et al. (2024). Activating p53 abolishes self-renewal of quiescent leukaemic stem cells in residual CML disease. *Nat. Commun.* 15 (1), 651. doi:10.1038/s41467-024-44771-9

Shah, M. V., Tran, E. N. H., Shah, S., Chhetri, R., Baranwal, A., Ladon, D., et al. (2023). TP53 mutation variant allele frequency of ≥10% is associated with poor prognosis in therapy-related myeloid neoplasms. *Blood Cancer J.* 13 (1), 51. doi:10.1038/s41408-023-00821-x

Shi, D., and Jiang, P. (2021). A different facet of p53 function: regulation of immunity and inflammation during tumor development. *Front. Cell Dev. Biol.* 9, 762651. doi:10.3389/fcell.2021.762651

Singh, S., Kumar, M., Kumar, S., Sen, S., Upadhyay, P., Bhattacharjee, S., et al. (2019). The cancer-associated, gain-of-function TP53 variant P152Lp53 activates multiple signaling pathways implicated in tumorigenesis. *J. Biol. Chem.* 294 (38), 14081–14095. doi:10.1074/jbc.RA118.007265

Smalley, J. P., Cowley, S. M., and Hodgkinson, J. T. (2024). MDM2 antagonist idasanutlin reduces HDAC1/2 abundance and corepressor Partners but not HDAC3. *ACS Med. Chem. Lett.* 15 (1), 93–98. doi:10.1021/acsmedchemlett.3c00449

Song, H., Wu, J., Tang, Y., Dai, Y., Xiang, X., Li, Y., et al. (2023). Diverse rescue potencies of p53 mutations to ATO are predetermined by intrinsic mutational properties. *Sci. Transl. Med.* 15 (690), eabn9155. doi:10.1126/scitranslmed.abn9155

Spaety, M. E., Gries, A., Badie, A., Venkatasamy, A., Romain, B., Orvain, C., et al. (2019). HDAC4 levels control sensibility toward cisplatin in gastric cancer via the p53-p73/BIK pathway. *Cancers (Basel)* 11 (11), 1747. doi:10.3390/cancers11111747

Tashakori, M., Kadia, T., Loghavi, S., Daver, N., Kanagal-Shamanna, R., Pierce, S., et al. (2022). TP53 copy number and protein expression inform mutation status across risk categories in acute myeloid leukemia. *Blood* 140 (1), 58–72. doi:10.1182/blood.2021013983

Tettero, J. M., Ngai, L. L., Bachas, C., Breems, D. A., Fischer, T., Gjertsen, B. T., et al. (2023). Measurable residual disease-guided therapy in intermediate-risk acute myeloid leukemia patients is a valuable strategy in reducing allogeneic transplantation without negatively affecting survival. *Haematologica* 108 (10), 2794–2798. doi:10.3324/haematol.2022.282639

Thijssen, R., Diepstraten, S. T., Moujalled, D., Chew, E., Flensburg, C., Shi, M. X., et al. (2021). Intact TP-53 function is essential for sustaining durable responses to BH3-mimetic drugs in leukemias. *Blood* 137 (20), 2721–2735. doi:10.1182/blood.2020010167

Tomiyasu, H., Habara, M., Hanaki, S., Sato, Y., Miki, Y., and Shimada, M. (2024). FOXO1 promotes cancer cell growth through MDM2-mediated p53 degradation. *J. Biol. Chem.* 300 (4), 107209. doi:10.1016/j.jbc.2024.107209

Torka, P., Russell, T., Mavis, C., Gu, J., Ghione, P., Barth, M., et al. (2023). AMG176, an MCL-1 inhibitor, is active in pre-clinical models of aggressive B-cell lymphomas. *Leuk. Lymphoma* 64 (6), 1175–1185. doi:10.1080/10428194.2023.2200876

Trino, S., Iacobucci, I., Erriquez, D., Laurenzana, I., De Luca, L., Ferrari, A., et al. (2016). Targeting the p53-MDM2 interaction by the small-molecule MDM2 antagonist Nutlin-3a: a new challenged target therapy in adult Philadelphia positive acute lymphoblastic leukemia patients. *Oncotarget* 7 (11), 12951–12961. doi:10.18632/oncotarget.7339

Tron, A. E., Belmonte, M. A., Adam, A., Aquila, B. M., Boise, L. H., Chiarparin, E., et al. (2018). Discovery of Mcl-1-specific inhibitor AZD5991 and preclinical activity in multiple myeloma and acute myeloid leukemia. *Nat. Commun.* 9 (1), 5341. doi:10.1038/s41467-018-07551-w

Uy, G. L., Aldoss, I., Foster, M. C., Sayre, P. H., Wieduwilt, M. J., Advani, A. S., et al. (2021). Flotetuzumab as salvage immunotherapy for refractory acute myeloid leukemia. *Blood* 137 (6), 751–762. doi:10.1182/blood.2020007732

Vadakekolathu, J., Lai, C., Reeder, S., Church, S. E., Hood, T., Lourdusamy, A., et al. (2020). TP53 abnormalities correlate with immune infiltration and associate with response to flotetuzumab immunotherapy in AML. *Blood Adv.* 4 (20), 5011–5024. doi:10.1182/bloodadvances.2020002512

Vaddavalli, P. L., and Schumacher, B. (2022). The p53 network: cellular and systemic DNA damage responses in cancer and aging. *Trends Genet.* 38 (6), 598–612. doi:10.1016/j.tig.2022.02.010

Valeri, A., Garcia-Ortiz, A., Castellano, E., Cordoba, L., Maroto-Martin, E., Encinas, J., et al. (2022). Overcoming tumor resistance mechanisms in CAR-NK cell therapy. *Front. Immunol.* 13, 953849. doi:10.3389/fimmu.2022.953849

Varineau, J. E., and Calo, E. (2024). A common cellular response to broad splicing perturbations is characterized by metabolic transcript downregulation driven by the Mdm2-p53 axis. *Dis. Model Mech.* 17 (2), dmm050356. doi:10.1242/dmm.050356

Villatoro, A., Konieczny, J., Cuminetti, V., and Arranz, L. (2020). Leukemia stem cell release from the stem cell niche to treat acute myeloid leukemia. *Front. Cell Dev. Biol.* 8, 607. doi:10.3389/fcell.2020.00607

Wang, B., Reville, P. K., Yassouf, M. Y., Jelloul, F. Z., Ly, C., Desai, P. N., et al. (2024). Comprehensive characterization of IFNγ signaling in acute myeloid leukemia reveals prognostic and therapeutic strategies. *Nat. Commun.* 15 (1), 1821. doi:10.1038/s41467-024-45916-6

Wang, H., Guo, M., Wei, H., and Chen, Y. (2023a). Targeting p53 pathways: mechanisms, structures, and advances in therapy. *Signal Transduct. Target Ther.* 8 (1), 92. doi:10.1038/s41392-023-01347-1

Wang, Y., Wang, D., Wang, Y., Yang, H., Wang, G., and Wu, S. (2023b). Synergistic activity and mechanism of cytarabine and MCL-1 inhibitor AZD5991 against acute myeloid leukemia. *Neoplasma* 70 (2), 287–293. doi:10.4149/neo_2023_221217N1185

Wiederschain, D., Kawai, H., Shilatifard, A., and Yuan, Z. M. (2005). Multiple mixed lineage leukemia (MLL) fusion proteins suppress p53-mediated response to DNA damage. *J. Biol. Chem.* 280 (26), 24315–24321. doi:10.1074/jbc.M412237200

Yan, B., Claxton, D., Huang, S., and Qiu, Y. (2020). AML chemoresistance: the role of mutant TP53 subclonal expansion and therapy strategy. *Exp. Hematol.* 87, 13–19. doi:10.1016/j.exphem.2020.06.003

Yang, M., Pan, Z., Huang, K., Busche, G., Liu, H., Gohring, G., et al. (2022). A unique role of p53 haploinsufficiency or loss in the development of acute myeloid leukemia with FLT3-ITD mutation. *Leukemia* 36 (3), 675–686. doi:10.1038/s41375-021-01452-6

Yilmaz, M., Kantarjian, H., and Ravandi, F. (2021). Acute promyelocytic leukemia current treatment algorithms. *Blood Cancer J.* 11 (6), 123. doi:10.1038/s41408-021-00514-3

Yilmaz, M., Kantarjian, H., Short, N. J., Reville, P., Konopleva, M., Kadia, T., et al. (2022). Hypomethylating agent and venetoclax with FLT3 inhibitor "triplet" therapy in older/unfit patients with FLT3 mutated AML. *Blood Cancer J.* 12 (5), 77. doi:10.1038/s41408-022-00670-0

Young, A. L., Tong, R. S., Birmann, B. M., and Druley, T. E. (2019). Clonal hematopoiesis and risk of acute myeloid leukemia. *Haematologica* 104 (12), 2410–2417. doi:10.3324/haematol.2018.215269

Zeidan, A. M., Ando, K., Rauzy, O., Turgut, M., Wang, M. C., Cairoli, R., et al. (2024). Sabatolimab plus hypomethylating agents in previously untreated patients with higher-risk myelodysplastic syndromes (STIMULUS-MDS1): a randomised, double-blind, placebo-controlled, phase 2 trial. *Lancet Haematol.* 11 (1), e38–e50. doi:10.1016/S2352-3026(23)00333-2

Zeidan, A. M., DeAngelo, D. J., Palmer, J., Seet, C. S., Tallman, M. S., Wei, X., et al. (2022). Phase 1 study of anti-CD47 monoclonal antibody CC-90002 in patients with relapsed/refractory acute myeloid leukemia and high-risk myelodysplastic syndromes. *Ann. Hematol.* 101 (3), 557–569. doi:10.1007/s00277-021-04734-2

Zhang, J., Sun, W., Kong, X., Zhang, Y., Yang, H. J., Ren, C., et al. (2019). Mutant p53 antagonizes p63/p73-mediated tumor suppression via Notch1. *Proc. Natl. Acad. Sci. U. S. A.* 116 (48), 24259–24267. doi:10.1073/pnas.1913919116

Zhang, Q., Riley-Gillis, B., Han, L., Jia, Y., Lodi, A., Zhang, H., et al. (2022). Activation of RAS/MAPK pathway confers MCL-1 mediated acquired resistance to BCL-2 inhibitor venetoclax in acute myeloid leukemia. *Signal Transduct. Target Ther.* 7 (1), 51. doi:10.1038/s41392-021-00870-3

Zhao, D., Zarif, M., Zhou, Q., Capo-Chichi, J. M., Schuh, A., Minden, M. D., et al. (2023). TP53 mutations in AML patients are associated with dismal clinical outcome irrespective of frontline induction regimen and allogeneic hematopoietic cell transplantation. *Cancers (Basel)* 15 (12), 3210. doi:10.3390/cancers15123210

Zhou, T., Ke, Z., Ma, Q., Xiang, J., Gao, M., Huang, Y., et al. (2023). Molecular mechanism of CCDC106 regulating the p53-Mdm2/MdmX signaling axis. *Sci. Rep.* 13 (1), 21892. doi:10.1038/s41598-023-47808-z

Zhou, Y., Takacs, G. P., Lamba, J. K., Vulpe, C., and Cogle, C. R. (2020). Functional dependency analysis identifies potential druggable targets in acute myeloid leukemia. *Cancers (Basel)* 12 (12), 3710. doi:10.3390/cancers12123710

Zhu, R., Li, L., Nguyen, B., Seo, J., Wu, M., Seale, T., et al. (2021). FLT3 tyrosine kinase inhibitors synergize with BCL-2 inhibition to eliminate FLT3/ITD acute leukemia cells through BIM activation. *Signal Transduct. Target Ther.* 6 (1), 186. doi:10.1038/s41392-021-00578-4

frontiers | Frontiers in Pharmacology

TYPE Original Research
PUBLISHED 02 September 2024
DOI 10.3389/fphar.2024.1440985

OPEN ACCESS

EDITED BY
Gregory Wiedman,
Seton Hall University, United States

REVIEWED BY
Romain Désert,
Institut National de la Santé et de la Recherche Médicale (INSERM), France
Vlad Toma,
Babeş-Bolyai University, Romania

*CORRESPONDENCE
Maria Iacobescu,
maria.iacobescu@medfuture.ro

†These authors have contributed equally to this work and share first authorship

‡These authors have contributed equally to this work and share last authorship

RECEIVED 30 May 2024
ACCEPTED 19 August 2024
PUBLISHED 02 September 2024

CITATION
Mocan LP, Grapa C, Crăciun R, Pralea IE, Uifălean A, Soporan AM, Mureșan XM, Iacobescu M, Al Hajjar N, Mihu CM, Spârchez Z, Mocan T and Iuga CA (2024) Unveiling novel serum biomarkers in intrahepatic cholangiocarcinoma: a pilot proteomic exploration.
Front. Pharmacol. 15:1440985.
doi: 10.3389/fphar.2024.1440985

Unveiling novel serum biomarkers in intrahepatic cholangiocarcinoma: a pilot proteomic exploration

Lavinia Patricia Mocan[1†], Cristiana Grapa[2,3†], Rareș Crăciun[2,3], Ioana Ecaterina Pralea[4], Alina Uifălean[5], Andreea Maria Soporan[4,5], Ximena Maria Mureșan[6], Maria Iacobescu[4*], Nadim Al Hajjar[2,7], Carmen Mihaela Mihu[1], Zeno Spârchez[2,3], Tudor Mocan[2,8‡] and Cristina Adela Iuga[4,5‡]

[1]Department of Histology, "Iuliu Haţieganu" University of Medicine and Pharmacy, Cluj-Napoca, Romania, [2]Department of Gastroenterology, "Prof. Dr. Octavian Fodor" Regional Institute of Gastroenterology and Hepatology, Cluj-Napoca, Romania, [3]Department of Gastroenterology and Hepatology, "Iuliu Haţieganu" University of Medicine and Pharmacy, Cluj-Napoca, Romania, [4]Department of Proteomics and Metabolomics, Institute of Medical Research and Life Sciences – Medfuture, "Iuliu Haţieganu" University of Medicine and Pharmacy, Cluj-Napoca, Romania, [5]Department of Pharmaceutical Analysis, Faculty of Pharmacy, "Iuliu Haţieganu" University of Medicine and Pharmacy, Cluj-Napoca, Romania, [6]Department of Translational Medicine, Institute of Medical Research and Life Sciences – Medfuture, "Iuliu Haţieganu" University of Medicine and Pharmacy, Cluj-Napoca, Romania, [7]Department of Surgery, "Iuliu Haţieganu" University of Medicine and Pharmacy, Cluj-Napoca, Romania, [8]UBBMed Department, Babeş-Bolyai University, Cluj-Napoca, Romania

Recent advancements in proteomics have shown promise in identifying biomarkers for various cancers. Our study is the first to compare the serum proteomes of intrahepatic cholangiocarcinoma (iCCA) with cirrhosis (CIR), primary sclerosing cholangitis (PSC), and hepatocellular carcinoma (HCC), aiming to identify a proteomic signature that can effectively distinguish among these conditions. Utilizing high-throughput mass spectrometry on serum samples, we identified 845 proteins, of which 646 were suitable for further analysis. Unique clustering patterns were observed among the five groups, with significant proteomic differences. Our key findings include: S100 calcium-binding protein A9 (S100A9) and haptoglobin (HP) were more abundant in iCCA, while intercellular adhesion molecule 2 (ICAM2) was higher in HCC. Serum amyloid A1 (SAA1) and A4 (SAA4) emerged as potential biomarkers, with SAA1 significantly different in the iCCA vs healthy controls (HC) comparison, and SAA4 in the HCC vs HC comparison. Elevated levels of vascular cell adhesion molecule 1 (VCAM-1) in HCC suggested its potential as a differentiation and diagnostic marker. Angiopoietin-1 receptor (TEK) also showed discriminatory and diagnostic potential in HCC. ELISA validation corroborated mass spectrometry findings. Our study underscores the potential of proteomic profiling in distinguishing iCCA from other liver conditions and highlights the need for further validation to establish robust diagnostic biomarkers.

KEYWORDS

biomarker, intrahepatic cholangiocarcinoma, hepatocellular carcinoma, liver cirrhosis, primary sclerosing cholangitis, proteomics

1 Introduction

Cholangiocarcinoma (CCA), originating from cholangiocytes in the biliary duct system, is the second most common primary liver cancer, following hepatocellular carcinoma (HCC). Known for its aggressive behavior among biliary tract malignancies, global projections forecast a surge in its incidence (Rumgay et al., 2022). CCA is typically categorized as either intrahepatic (iCCA) or extrahepatic and predominantly affects individuals in their seventies, with a slight male predominance (Shaib et al., 2005). Contributing risk factors include viral hepatitis infections, inflammatory conditions such as obesity and diabetes mellitus, and congenital hepatic fibrosis (Shaib Hashem and Yasser, 2004). Notably, primary sclerosing cholangitis (PSC) significantly predisposes individuals to CCA, with about 40% of PSC patients at risk. The carcinogenesis mechanisms in this context involve chronic inflammation, epithelial proliferation, bile mutagens, and biliary stasis (Claessen et al., 2009; Izquierdo-Sanchez et al., 2022).

Despite advancements in diagnostic techniques such as computed tomography (CT) and ultrasound (US), their sensitivity remains limited, particularly for detecting small liver lesions (Patel et al., 2000). Additionally, distinguishing between HCC, PSC and liver cirrhosis (CIR) poses significant challenges. Commonly used biomarkers like carcinoembryonic antigen (CEA) and carbohydrate antigen 19-9 (CA19-9) do not possess the necessary sensitivity or specificity for effective CCA detection (Shi et al., 2013). Furthermore, the diagnostic reliability of CA 19-9 and alpha-fetoprotein (AFP) is compromised due to their variable elevation in different liver diseases (Best et al., 2020; Zhou et al., 2011; Izquierdo-Sanchez et al., 2022).

The need for improved medical approaches highlights the critical importance of developing innovative strategies for the early detection and management of CCA (Mocan et al., 2022). Omics sciences offer promising pathways, as evidenced by their success in various other cancer types. However, the rarity of CCA cases has hindered our molecular understanding, resulting in limited comprehensive omics studies. While genomic and transcriptomic research has illuminated key genes and molecular subtypes associated with iCCA development (Voigtländer et al., 2020; Job et al., 2020; Martin-Serrano et al., 2023), the proteomic landscape of iCCA remains relatively unexplored. Current studies have primarily focused on specific histotypes or ethnic backgrounds, often linked to relevant risk factors. For instance, Lapitz et al. focused on CCA with an emphasis on PSC-CCA patients, employing proteome profiling of serum extracellular vesicles (EVs). This study identified diagnostic biomarkers such as C-reactive protein (CRP), Fibrinogen, and von Willebrand factor (VWF) for early diagnosis and prognosis (Lapitz et al., 2023). Christensen et al. targeted biliary tract cancer (BTC) broadly, using proximity extension assays and statistical modeling to generate multiprotein signatures, including CA19-9 and chemokine C-C motif ligand 20, for differentiating BTC from non-cancer controls (Christensen et al., 2023).

Recently, an integrated proteogenomic profile delineating iCCA subtypes was introduced, laying the groundwork for future research (Dong et al., 2022). Proteomics, as a leading technology, holds significant promise for identifying disease-specific biomarkers essential for diagnosis, prognosis, and treatment response assessment (B. B. Sun, Suhre, and Gibson, 2024). Despite extensive knowledge of CCA's transcriptomic and mutational landscapes, its proteomic landscape remains largely uncharted.

Consequently, there is an urgent need for proteomics-driven research to discover new biomarkers, which are vital for improving our understanding and management of CCA across various populations and subtypes.

From a clinical perspective, there is a pressing need for biomarkers to differentiate between iCCA and HCC, as well as between iCCA and PSC. Imagine the ideal scenario where we could screen for HCC in cirrhotic patients, detect a nodule, and inform the patient whether it is HCC or iCCA, all based on just two drops of blood. Wouldn't it be incredible to have the capability to distinguish early between PSC and iCCA based on non-invasive biomarkers?

Hence, our study aims to explore the potential of proteomics in uncovering valuable serum biomarkers capable of distinguishing between iCCA and HCC, PSC, CIR and healthy controls (HC). By leveraging proteomic analysis, we seek to identify novel biomarkers with enhanced diagnostic accuracy and clinical relevance. Through comparative analysis of the serum proteome profiles, our research endeavors to unveil unique protein signatures associated with distinct liver pathologies, thereby facilitating early detection and the development of personalized treatment strategies.

2 Results

2.1 Baseline characteristics of the study participants

A detailed overview of the study participants baseline characteristics can be found in Supplementary Table S1. The table provides a detailed comparison of demographics, environmental factors, and laboratory values for both discovery and validation cohorts. The mean age of the patients varies across cohorts, with iCCA, HCC, CIR patients averaging around 60 years, PSC patients around 50 years, and HC at around 30 years. Gender distribution shows a predominance of males in the iCCA and CIR cohorts and a higher proportion of females in the PSC cohort. Environmental exposure indicates that most iCCA and PSC patients are from urban areas, while the HCC cohort shows a more balanced distribution. Laboratory findings highlight variations in albumin levels, AFP, CA 19-9, and other liver function tests across cohorts, reflecting the different disease states. This comprehensive data underscores the clinical profiles and underlying health conditions of the patients and is in line with the characteristics of the liver diseases.

2.2 Serum proteome characterization

845 proteins with at least one unique peptide were identified. After applying the criterion for inclusion in the analysis (please see Section 4.3.3 Statistical Analysis), a total number of 646 proteins were further subjected to the biomarker analysis. The complete list of the proteins considered for the analysis is shown in Supplementary Table S2. A complete overview of the statistical

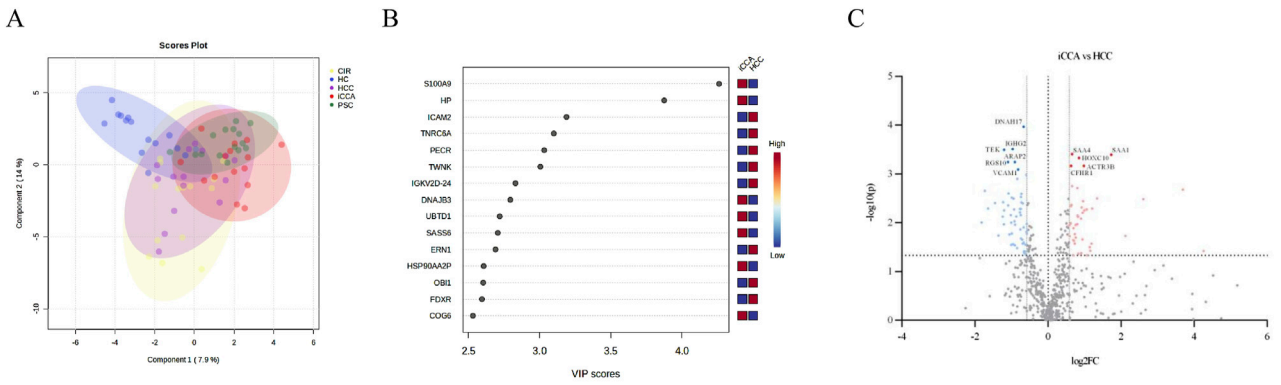

FIGURE 1
(A). Sampling group clustering by the serum proteome of the groups studied (CIR = liver cirrhosis; HC = healthy controls; HCC = hepatocellular carcinoma; iCCA = intrahepatic cholangiocarcinoma; PSC = primary sclerosing cholangitis). **(B)**. Top discriminatory serum proteins among the iCCA and HCC patient's groups. **(C)**. Volcano plot showing all significantly different serum proteins ($p < 0.05$, |FC| >1.5, proteins with FDR<0.05 are labeled) among the iCCA and the HCC patients' groups.

TABLE 1 Serum proteins that could aid iCCA vs. HCC discrimination.

No.	Protein name	Gene	iCCA vs. HCC				iCCA vs. HC	HCC vs. HC
			FC	AUC	SEN	SPE	FC	FC
1	Serum amyloid A-1 protein*	SAA1	3.3	0.86	0.7	0.9	3.2	ns
2	Actin-related protein 3B*	ACTR3B	2.0	0.88	0.8	0.9	2.6	ns
3	Homeobox protein Hox-C10*	HOXC10	1.8	0.87	0.8	0.8	2.3	ns
4	Serum amyloid A-4 protein	SAA4	1.6	0.87	0.7	0.9	ns	−1.5
5	Complement factor H-related protein 1	CFHR1	1.5	0.86	0.8	0.7	ns	−1.7
6	Dynein axonemal heavy chain 17*	DNAH17	−1.6	0.87	0.7	0.8	−1.3	ns
7	Vascular cell adhesion protein 1**	VCAM1	−1.8	0.87	0.8	0.8	2.36	4.2
8	Arf-GAP with Rho-GAP domain ANK repeat and PH domain-containing protein 2*	ARAP2	−1.9	0.85	0.9	0.7	ns	2.3
9	Immunoglobulin heavy constant gamma 2**	IGHG2	−2.0	0.89	0.8	0.8	1.9	3.7
10	Regulator of G-protein signaling 10**	RGS10	−2.1	0.84	0.7	0.9	1.9	4.0
11	Angiopoietin-1 receptor**	TEK	−2.3	0.90	0.9	0.9	2.2	5.0

iCCA, intrahepatic cholangiocarcinoma; HCC, hepatocellular carcinoma; HC, healthy controls; FC , fold change (calculated as the ratio of the two group means, AUC, area under the receiver operating characteristic (ROC) curve; SEN, sensitivity; SPE, specificity; ns = no significance for t-test, therefore also no FC, reported; *significant for iCCA, vs. HCC, and either iCCA, vs. HC, or HCC, vs. HC; **significant for all three comparisons.

analysis results is shown in Supplementary Table S3 where only the significant proteins among all comparisons are shown.

2.3 Serum proteome pattern exploration

As an initial demonstration of the study's viability, we conducted a group clustering analysis. The serum patterns identified exhibited a noteworthy clustering pattern among the studied groups as shown through the utilization of partial least squares discriminant analysis (PLS-DA), demonstrating discernible separation according to the first two components (Figure 1A).

2.4 Serum proteome alterations in liver cancer

By elucidating the discriminatory protein profile through PLS-DA (Figure 1A) and visualizing them in the variable importance in projection (VIP) score plot, top discriminatory proteins among the iCCA and the HCC patient groups were highlighted. The most significant three proteins were: S100 calcium-binding protein A9 (S100A9), Haptoglobin (HP), and Intercellular Adhesion Molecule 2 (ICAM2) (Figure 1B). For scouting potential biomarkers, t-test was applied. A total of 154 proteins exhibited significant differences ($p <$ 0.05, no false discovery rate (FDR) cut-off) in the comparison between

10.3389/fphar.2024.1440985

TABLE 2 Serum proteome alterations in the iCCA group compared to the risk factor group CIR.

No.	Protein name	Gene	FC	AUC	SEN	SPE	iCCA vs. HC	CIR vs. HC
1	Haptoglobin*	HP	3.2	0.73	0.9	0.6	12.9	ns
2	cAMP-dependent protein kinase catalytic subunit beta*	PRKACB	2.5	0.79	0.7	0.7	ns	−2.7
3	Heat shock protein HSP 90-alpha A2	HSP90AA2P	2.3	0.78	0.8	0.8	ns	ns
4	Chromatin assembly factor 1 subunit A*	CHAF1A	2.0	0.79	0.8	0.7	3.0	ns
5	Trinucleotide repeat-containing gene 18 protein	TNRC18	2.0	0.79	0.7	0.7	ns	ns
6	Protein CIP2A*	CIP2A	1.5	0.73	0.7	0.8	ns	−1.7
7	Voltage-dependent calcium channel subunit alpha-2/delta-3	CACNA2D3	1.5	0.83	0.9	0.7	ns	−1.4
8	M-phase inducer phosphatase 1*	CDC25A	−1.5	0.79	0.8	0.7	−2.0	ns
9	Unconventional myosin-XV*	MYO15A	−1.5	0.78	0.9	0.7	−1.8	ns
10	Zygote arrest protein 1**	ZAR1	−1.5	0.76	0.7	0.7	−2.5	−1.6
11	Huntingtin-interacting protein 1*	HIP1	−1.5	0.84	0.7	0.9	−1.9	ns
12	Villin-like protein*	VILL	−1.5	0.80	0.7	0.8	−1.9	ns
13	Transcription factor ETV7*	ETV7	−1.6	0.77	0.7	0.7	−2.2	ns
14	ELKS/Rab6-interacting/CAST family member 1*	ERC1	−1.7	0.80	0.7	0.7	−2.3	ns
15	Proline/serine-rich coiled-coil protein 1*	PSRC1	−1.7	0.85	0.7	0.9	−1.9	ns
16	Neurofibromin*	NF1	−1.7	0.72	0.7	0.6	ns	1.8
17	Prefoldin subunit 1*	PFDN1	−1.8	0.83	0.8	0.8	ns	2.2
18	Regulator of G-protein signaling 10**	RGS10	−1.9	0.83	0.7	0.8	1.9	3.6
19	Microtubule-associated protein 1A*	MAP1A	−1.9	0.83	0.8	0.8	ns	2.0
20	Annexin A9*	ANXA9	−1.9	0.90	0.9	0.9	−2.1	ns
21	Complexin-4*	CPLX4	−2.1	0.91	0.8	0.9	−1.9	ns
22	Caveolin-3**	CAV3	−2.1	0.74	0.5	0.9	2.1	4.5
23	Adaptin ear-binding coat-associated protein 2*	NECAP2	−2.2	0.80	0.9	0.7	ns	5.6
24	Calcium-binding mitochondrial carrier protein SCaMC-2*	SLC25A25	−2.2	0.80	0.7	0.8	ns	3.0
25	Paired box protein Pax-9*	PAX9	−2.2	0.79	0.6	0.9	ns	2.8
26	Peroxisomal trans-2-enoyl-CoA reductase*	PECR	−2.3	0.78	0.7	0.7	−2.6	ns
27	Alkaline phosphatase_ tissue-nonspecific isozyme*	ALPL	−3.1	0.83	0.7	1.0	ns	4.2
28	ORC ubiquitin ligase 1*	OBI1	−4.6	0.86	0.9	0.8	ns	3.4

iCCA, intrahepatic cholangiocarcinoma; CIR, liver cirrhosis; HC, healthy controls; FC , fold change (calculated as the ratio of the two group means, AUC, area under the receiver operating characteristic (ROC) curve; SEN, sensitivity; SPE, specificity; ns = no significance for t-test, therefore also no FC is reported; *significant for both iCCA, vs. PSC, and iCCA, vs. HC.

iCCA and HCC, out of which 65 had also a minimum of 1.5-fold change (FC) (log2FC > 0.58). Also considering the FDR criterion of <0.05, 11 proteins were highlighted and the findings are shown in a volcano-plot (Figure 1C). For the 11 proteins, a receiver operating characteristic analysis (ROC) was applied and the area under the ROC curve (AUC) was calculated showing values greater than 0.80. Table 1 presents a comprehensive overview which includes the iCCA vs. HCC analysis: the 11 statistically significant proteins, the FC, AUC, sensitivity (SEN), specificity (SPE). To gain a more in-depth understanding, we additionally assessed the significance of the proteins between the iCCA and the HC serum samples, as well as between the HCC and the HC serum samples, and provided only the FC for the significant proteins (Table 1).

2.5 Serum proteome alterations towards anticipating the upcoming malignancy in the risk factor groups

One-way analysis of variance (ANOVA) identified 47 proteins with statistically significant differences ($p < 0.05$) in abundance across the groups. This analysis considered potential iCCA risk

10.3389/fphar.2024.1440985

TABLE 3 Serum proteome alterations in the iCCA group compared to the risk factor group PSC.

No.	Protein name	Gene	iCCA vs. PSC				iCCA vs. HC
			FC	AUC	SEN	SPE	FC
1	Aminopeptidase Q*	LVRN	14.0	0.83	0.90	0.70	15.7
2	Leucine-rich alpha-2-glycoprotein*	LRG1	1.9	0.77	0.60	0.90	2.2
3	Melanophilin	MLPH	1.9	0.82	0.90	0.90	ns
4	Probable asparagine--tRNA ligase_ mitochondrial	NARS2	1.9	0.68	0.80	0.50	ns
5	Alpha-1-antichymotrypsin	SERPINA3	1.8	0.80	0.80	0.80	ns
6	Immunoglobulin lambda constant 7*	IGLC7	1.7	0.80	0.80	0.80	1.9
7	NACHT_ LRR and PYD domains-containing protein 14*	NLRP14	1.6	0.83	0.70	0.80	1.6
8	Huntingtin-interacting protein 1*	HIP1	−1.5	0.87	0.90	0.80	−1.9
9	Nicotinamide N-methyltransferase*	NNMT	−1.5	0.76	0.70	0.80	−2.2
10	Annexin A9*	ANXA9	−1.5	0.78	0.90	0.60	−2.1
11	Phosphatidylcholine-sterol acyltransferase*	LCAT	−1.5	0.76	0.80	0.70	−1.9
12	Unconventional myosin-XV*	MYO15A	−1.5	0.74	0.70	0.80	−1.8
13	M-phase inducer phosphatase 1*	CDC25A	−1.5	0.76	0.70	0.80	−2.0
14	EF-hand calcium-binding domain-containing protein 3*	EFCAB3	−1.5	0.75	0.90	0.50	−2.0
15	Villin-like protein*	VILL	−1.6	0.76	0.70	0.80	−1.9
16	ELKS/Rab6-interacting/CAST family member 1*	ERC1	−1.6	0.79	0.70	0.70	−2.3
17	Transcription factor ETV7*	ETV7	−1.7	0.77	0.70	0.80	−2.2
18	Sialic acid-binding Ig-like lectin 9*	SIGLEC9	−1.7	0.74	0.70	0.80	−2.3
19	Probable rRNA-processing protein EBP2*	EBNA1BP2	−1.7	0.77	0.60	0.90	−1.6
20	Complexin-4*	CPLX4	−1.7	0.80	0.80	0.80	−1.9
21	Glucose-6-phosphate 1-dehydrogenase	G6PD	−1.9	0.80	0.90	0.70	ns
22	Insulin-like growth factor-binding protein 3*	IGFBP3	−1.9	0.80	0.70	0.90	−3.0
23	Cilia- and flagella-associated protein 36*	CFAP36	−2.1	0.84	0.70	0.90	−3.0
24	Serine/threonine-protein kinase MRCK beta	CDC42BPB	−2.1	0.85	0.90	0.70	ns
25	Zinc finger protein 532*	ZNF532	−2.2	0.80	0.80	0.80	−4.1
26	Melanoma-associated antigen 2*	MAGEA2	−2.5	0.83	0.90	0.70	−2.3
27	DNA repair protein XRCC2*	XRCC2	−4.2	0.76	0.80	0.70	−10.4

iCCA, intrahepatic cholangiocarcinoma; PSC, primary sclerosing cholangitis; HC, healthy controls; FC , fold change (calculated as the ratio of the two group means, AUC, area under the receiver operating characteristic (ROC) curve; SEN, sensitivity; SPE, specificity; ns = no significance for t-test, therefore also no FC is reported; *significant for both iCCA, vs. PSC, and iCCA, vs. HC.

factors like PSC and CIR. Additionally, these proteins exhibited a fold change (FC) greater than 1.5, further supporting their statistical significance and potential relevance to iCCA. Furthermore, to delve deeper into the analysis, we evaluated the significance of proteins between iCCA, CIR, PSC and HC.

For the iCCA vs. CIR comparison, 28 proteins emerged as potential discriminators. Table 2 provides a detailed breakdown, including FC values and ROC analysis parameters specific to the iCCA vs CIR comparison. Additionally, the table presents FC values for proteins showing significant differences when comparing both iCCA and CIR to HC.

For the iCCA vs. PSC comparison, Table 3 presents a comprehensive overview on the data, which includes 27 statistically significant proteins, the FC, AUC, SEN, SPE. We then reported the FC only for those proteins with significant differences between iCCA and HC patients. No proteins met the same stringent criteria for showing significance between PSC and HC patients.

2.6 Biomarker panel scounting

For each of the targeted comparisons, proteins from the significant ones were tested by ROC analysis using the PLS-DA algorithm for inclusion into biomarker panels. The selection was based on their significance level both between the liver diseases groups and the HC, as well as their implication in the liver disease, as

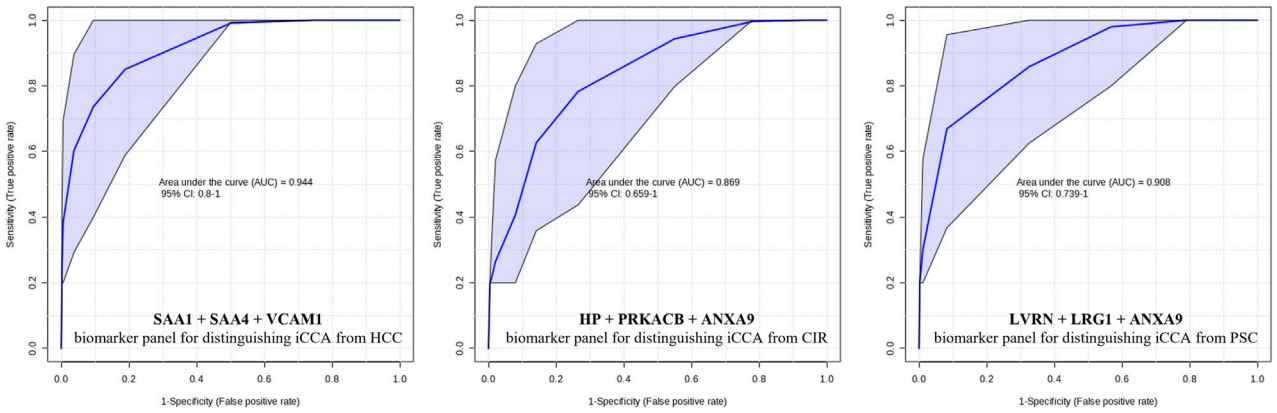

FIGURE 2
Proposed biomarker panels for distinguishing the different liver diseases. AUC = area under the receiver operating characteristic (ROC) curve; CI = confidence interval; iCCA = intrahepatic cholangiocarcinoma; HCC = hepatocellular carcinoma; CIR = liver cirrhosis; PSC = primary sclerosing cholangitis; SAA1 = Serum amyloid-1; SAA4 = Serum amyloid-4; VCAM1 = Vascular cell adhesion protein 1; LRG1 = HP = Haptoglobin, PRKACB = cAMP-dependent protein kinase catalytic subunit beta; ANXA9 = Annexin A9; LVRN = Leucine-rich alpha-2-glycoprotein.

TABLE 4 Serum levels of SAA1, SAA4, VCAM1, and LRG1 by ELISA.

ng/mL ± SD	HC	iCCA	HCC	PSC
SAA1	1,351.08 ± 759.56	13417.21 ± 10106.14	5,766.75 ± 4667.69	
SAA4	42550.59 ± 2501.47	37907.35 ± 14592.45	31350.66 ± 11565.65	
VCAM1	879.79 ± 299.49	4901.46 ± 1815.49	7099.19 ± 2540.60	
LRG1	4510.32 ± 716.18	23974.41 ± 3411.92		10205.67 ± 6838.53

SD, standard deviation; HC, healthy controls; iCCA, intrahepatic cholangiocarcinoma; HCC, hepatocellular carcinoma; PSC, primary sclerosing cholangitis; SAA1 = Serum amyloid-1; SAA4 = Serum amyloid-4; VCAM1 = Vascular cell adhesion protein 1; LRG1 = Leucine-rich alpha-2-glycoprotein.

reported in the literature. The most promising panels showing an AUC 0.9 are presented in Figure 2.

2.7 Quantitation of serum biomarkers SAA1, SAA4, VCAM1, and LRG1 by ELISA

Four proteins were selected to be analyzed on an independent patient validation cohort by a complementary method, namely, an enzyme-linked immunosorbent assay (ELISA). SAA1, SAA4, VCAM1, and LRG1 were chosen for quantification from the identified proteins in undepleted serum samples from the iCCA, HCC, and PSC groups. Selection criteria for these proteins included their abundance patterns across the groups, potential links to liver pathophysiology, and the significance of their differences between the groups. The serum levels of these markers are presented in Table 4 as mean (ng/mL) ± standard deviation (SD). The significance among the groups was tested by t-test and SAA1, SAA4, VCAM1, and LRG1 showed the same significance as the MS data. Figure 3 shows the results.

3 Discussion

Recently, there has been growing interest and investment in proteomics to identify biomarkers for various diseases, including different cancers. Our study is the first to compare the serum proteomes of iCCA with those of CIR, PSC, and HCC, aiming to identify a proteomic signature that can effectively distinguish among them. The findings highlight the urgent need for a proteomics-driven research to discover new biomarkers essential for improving our understanding and management of iCCA, especially given the largely unexplored proteomic landscape of this malignancy. Differentiating between iCCA and HCC is crucial in clinical practice, but it remains challenging, often requiring a liver biopsy for a definitive diagnosis (Mocan et al., 2023). Liver biopsy is an invasive procedure with potential risks such as bleeding and tumor seeding. Currently, there are no biomarkers available to differentiate between iCCA and HCC, or between iCCA and CIR or PSC, known as risk factors.

Our findings stem from a thorough proteomic approach, utilizing high-throughput mass spectrometry techniques on serum samples depleted of six highly abundant proteins through immunoaffinity. Following our methodology, we successfully identified 845 proteins that met the identification criteria outlined in Section 4.4. Of these, 646 proteins were considered suitable for subsequent analysis, consistent with similar studies (Lucaciu et al., 2023). Notably, our approach was the first to include the four patient groups alongside healthy controls. As proof of concept, we successfully identified unique clustering patterns among the five groups using PLS-DA analysis (Figure 1A). Interestingly, the serum proteome clusters of the four liver diseases were noticeably different compared to HC, with partial

10.3389/fphar.2024.1440985

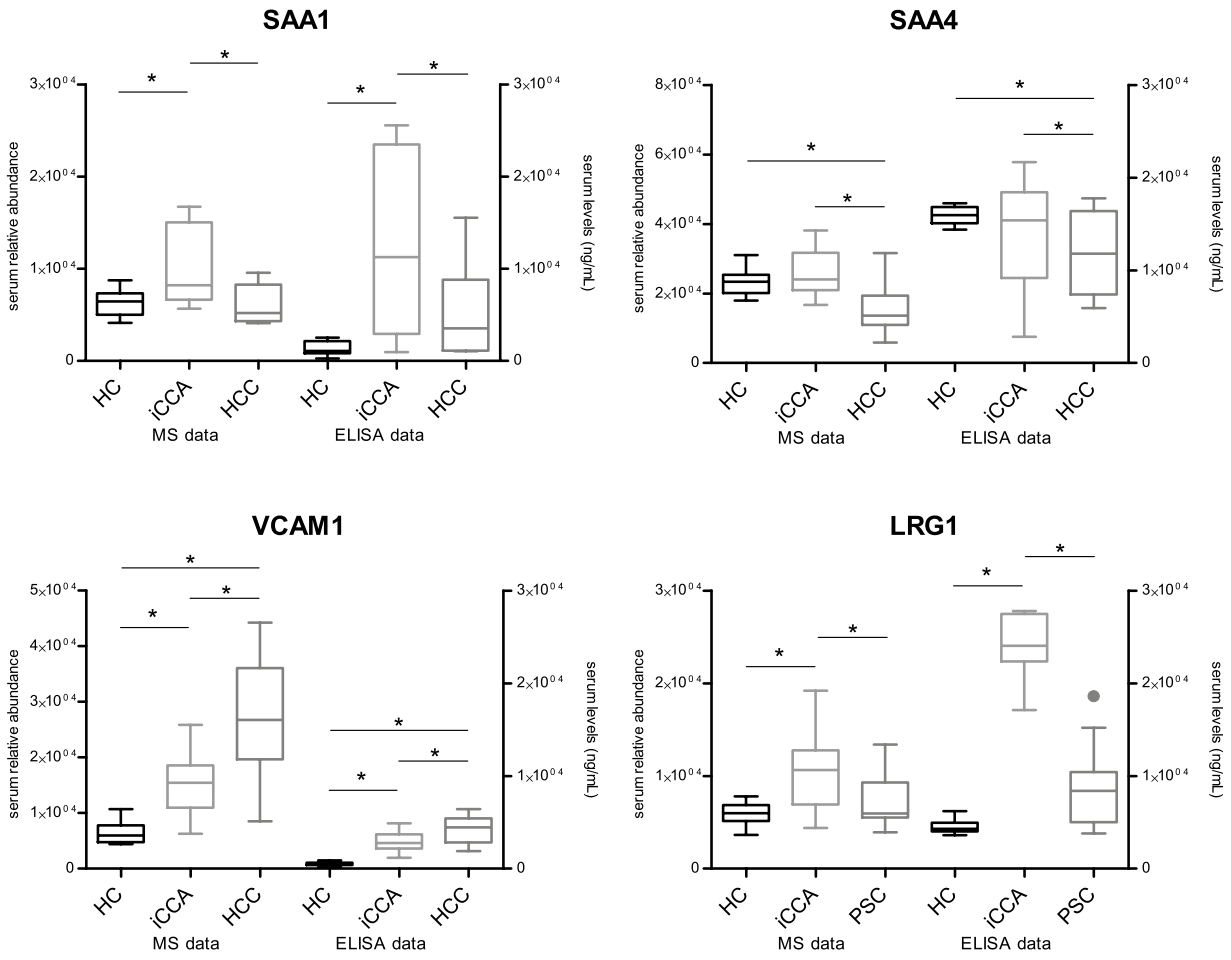

FIGURE 3
Validation of mass spectrometry-based results by ELISA HC = healthy controls; iCCA = intrahepatic cholangiocarcinoma; HCC = hepatocellular carcinoma; PSC = primary sclerosing cholangitis; SAA1 = Serum amyloid-1; SAA4 = Serum amyloid-4; VCAM1 = Vascular cell adhesion protein 1; LRG1 = Leucine-rich alpha-2-glycoprotein; * = statistically significant ($p < 0.05$); MS = mass spectrometry; ELISA = enzyme-linked immunosorbent assay.

overlap among them, highlighting a shared protein profile corresponding to similarities in liver disease. Particularly, the clustering clearly illustrated the relationship between iCCA and HCC, as well as the associations with their risk factor groups. The initial investigation into serum proteome alterations commenced with a wide-ranging comparative analysis between the iCCA and HCC groups. Discriminatory proteins were identified initially using the VIP score plot generated from the PLS-DA. The top three discriminatory proteins between the iCCA and HCC groups were S100 calcium-binding protein A9 (S100A9) and haptoglobin (HP), which were more abundant in iCCA, and Intercellular adhesion molecule 2 (ICAM2), which was higher in HCC (Figure 1B).

Additionally, we employed supplementary statistical analyses, along with stringent criteria, to further confirm the identification of potential biomarkers. Consequently, our comparison revealed distinct protein profiles, with five serum proteins exhibiting increased abundance in the iCCA group and six proteins in the HCC group. Additionally, their significance for the comparison to HC was also interrogated. Remarkably, the ROC analysis for both individual markers demonstrated robust discriminatory power as shown in Table 2. Among the proteins showing increased abundance in iCCA compared to HCC, serum amyloid A1 and A4 were identified. Even more, SAA1 was found to be significantly different in the iCCA vs. HC comparison, and SAA4 in the HCC vs. HC comparison. Serum amyloid A (SAA) proteins, consisting of SAA one to 4, are small molecules (104 amino acids) intricately linked to the acute phase response. Although their precise physiological roles remain elusive (Sack, 2018), recent studies suggest their potential as biomarkers for various cancers, including gastric, colon, and breast cancer, and their correlation with tumor staging (Ignacio et al., 2019; Liang et al., 2016; Wu et al., 2017). A decreased abundance of SAA1 in HCC, correlated with reduced survival rates and involvement in anti-tumor immune pathways, was observed (Zhang Hongying et al., 2020). Moreover, through scRNA-seq analysis, a correlation between SSA1 expression and the regulation of inflammatory responses and activation of the complement system, indicating a potential role in iCCA pathogenesis, was highlighted (Zhang Min et al., 2020). Thus, our study supports the utility of SAA proteins as biomarkers for distinguishing between iCCA and HCC. In light of these findings, SAA1 and SAA4 emerged as candidates for further validation.

Elevated levels of Vascular cell adhesion molecule 1 (VCAM-1) were observed in the HCC group, indicating its potential as a differentiation marker. Furthermore, significant differences in VCAM-1 levels were also noted in comparisons between both iCCA and HCC vs. HC, highlighting its utility as a discriminatory marker between iCCA and HCC, as well as a diagnostic marker for both iCCA and HCC. Based on these findings, VCAM-1 was also selected for further validation. VCAM-1 plays a crucial role in angiogenesis, leukocyte adhesion at inflamed tissues, and tumor sites, indicating its involvement in facilitating metastasis (Fox et al., 1995; Ho et al., 2004). Consistently elevated expression of VCAM-1 in chronic liver diseases imply its association with conditions such as chronic hepatitis or CIR (Kaplanski et al., 1997; Yamaguchi et al., 1999). However, despite this, the clinical significance of increased serum VCAM-1 in HCC patients remains largely unexplored, even though the majority of HCC cases are associated with underlying chronic hepatitis or CIR. Therefore, further investigation into serum VCAM-1 levels in HCC patients is warranted (Pirisi et al., 1996). Another protein exhibiting increased abundance in the HCC group was angiopoietin-1 receptor (TEK). Like VCAM1, TEK also showed both discriminatory and diagnostic potential. Angiopoietin-1, among factors implicated in tumor angiogenesis, has been linked to HCC progression and has shown superior performance to AFP in predicting overall survival (Choi et al., 2021). Given the pivotal role of angiogenesis inhibitors in the treatment of solid cancers, investigating angiogenic cytokines such as angiopoietin-1 can yield valuable insights into the progression of HCC (Torimura et al., 2004). Our findings underscore the promising clinical significance of these proteins, reaffirming their potential utility as biomarkers for distinguishing between iCCA and HCC. Moreover, a biomarker panel was built and tested by ROC analysis using the PLS-DA algorithm. This was comprised of SAA1, SAA4 and VCAM1 and showed a promising discrimination power.

In clinical practice iCCA is often diagnosed on a background of advanced liver disease, such as CIR, or in patients with a known history of PSC. These diagnoses invariably depend on invasive procedures, such as liver biopsy. Due to the absence of reliable biomarkers, iCCA is often detected at an advanced stage, at which point curative treatment options are no longer viable. Our study is the first one to reveal 64 proteins that displayed notable differences among the iCCA, CIR and PSC groups.

In the iCCA vs. CIR comparison, seven proteins showed higher abundance in the iCCA patient group, among which haptoglobin (HP), cAMP-dependent protein kinase catalytic subunit beta (PRKACB), heat shock protein (HSP) 90-alpha A2 (HSP90AA2P) were previously reported with respect to liver cancer. Haptoglobin (HP), a plasma glycoprotein, scavenges free hemoglobin, preventing release of toxic heme and protecting tissues from oxidative damage. Its dynamic response in pathology makes HP a valuable clinical tool. Moreover, HP was shown to be elevated in liver cancer and decreased in cirrhosis (Naryzny and Legina, 2021). Our results revealed also a significant difference of HP in the iCCA vs. HC groups, confirming the above mentioned findings.

PRKACB, a vital member of the protein kinase A (PKA) family, regulates various cellular processes through the phosphorylation of target proteins. Dysregulated PKA signaling has been implicated in the progression of liver cancer, affecting tumor growth, invasion, and metastasis, as well as hepatic fibrosis in CIR (Zhang Wei et al., 2020). However, direct studies linking PRKACB to iCCA and CIR are limited. HSPs act as molecular chaperones essential for protein folding, stabilization, and degradation, thus maintaining cellular homeostasis and responding to stress. Specifically, HSP90AA2P, a member of the HSP90 family, modulates various cellular processes, including cell proliferation, survival, and apoptosis. In liver cancer, upregulated HSP90AA2P promotes cancer cell survival, proliferation, and stabilizes oncoproteins and signaling pathways associated with tumor progression. In the context of CIR, HSP90AA2P likely contributes to the cellular stress response induced by chronic liver injury and inflammation, potentially affecting fibrosis progression (Whitesell and Lindquist, 2005). Notably, HSP90 was recently identified as a prognostic marker for CCA using an immunohistochemistry approach (Shirota et al., 2015).

Among the proteins exhibiting significantly higher abundance in the CIR group compared to iCCA, Annexin A9 (ANXA9) stood out, being also significantly different in the iCCA vs. HC comparison.

Annexins, a superfamily of calcium-dependent phospholipid-binding proteins, play various roles in biological processes. Despite comprising 13 human members and frequently being dysregulated in cancer, their expression patterns and prognostic values in liver cancer remain largely unexplored. The potential of ANXAs 1-5 and 10 as therapeutic targets was described, while ANXAs 2, 5, 7, and 10 could serve as prognostic markers in liver cancer (Zhuang et al., 2019). Additionally, ANXAs 10 and 13 have shown promise as differential diagnostic biomarkers between iCCA and pancreatic cancer (Geramizadeh et al., 2021; Serag and Elsayed, 2021).

In the comparison between iCCA and PSC, some of the proteins displaying higher serum abundance in the iCCA group have been previously reported, such as alpha-1-antichymotrypsin (SERPINA3), Chromatin assembly factor 1 subunit A (CHAF1A), and Leucine-rich alpha-2-glycoprotein (LRG1). SERPINA3, predominantly secreted by the liver, has been found to have a decreased abundance in HCC, a phenomenon correlated with enhanced cell proliferation (Santamaria et al., 2013; Sun et al., 2023; Soman and Nair, 2022) with elevated expression serving as a diagnostic and poor prognosis biomarker, indicating resistance to endocrine therapy and chemotherapy, and potentially predicting immunotherapy sensitivity. LRG1, an inflammatory protein, is known to play a critical role in tumorigenesis, development, and metastasis in various tumors (Lin et al., 2022; Zou et al., 2022). Its elevated abundance was reported to serve as an independent prognostic factor in patients with postoperative iCCA (Jin et al., 2020). In our study, LRG1 showed discriminatory power between iCCA and PSC and a diagnostic potential for iCCA, because of the significant difference observed in the iCCA vs. HC comparison. Having a dual role, LRG1 was selected for further validation by ELISA.

To delve deeper into our approach towards biomarker discovery for liver diseases, particularly in discriminating iCCA from HCC, and the associated risk factors CIR and PSC, we focused on identifying biomarker panels comprising combinations of the most relevant proteins. Biomarker panels are more powerful than single biomarkers because they provide a comprehensive view of the biological processes underlying a condition. A single biomarker may

offer limited insight and be influenced by various factors, whereas a panel combines multiple biomarkers, enhancing diagnostic accuracy and reliability. This comprehensive approach improves the detection of complex diseases, tracks progression, and tailors personalized treatments by capturing a broader spectrum of biological activities and interactions. Such an approach was done by Kim et al. (Kim et al., 2022) for HCC. Consequently, we proposed three panels for the powerful discrimination of iCCA *versus* HCC, CIR, and PSC. All our panels, as shown in Figure 2, demonstrated higher AUC values compared to their single biomarker counterparts, thus confirming the validity of our approach.

As mentioned above, four proteins from our MS findings emerged for further validation. For this purpose, we employed ELISA and measured serum levels of SAA1, SAA4, VCAM1, and LRG1 in independent cohorts of patients. Obtained results showed the same trends of expression of all assayed markers in the serum across the iCCA, HCC, and PSC groups, as detected by MS. This underlines that our MS approach is valid and the protein levels are disease-dependent, strengthening the biomarker utility of the proposed proteins.

While our study has several strengths, such as providing a comprehensive comparison of the serum proteomes among iCCA, HCC, CIR, and PSC, it is important to acknowledge also its limitations. The small sample size may have impacted our findings. Despite these limitation, our study fills a crucial gap in the literature by offering insights into the serum proteome alterations associated with these liver pathologies. Additionally, our preliminary analysis serves as a valuable foundation for future research in this area. The statistical tests employed in our study, combined with stringent criteria, identified proteins with at least a 1.5-fold change, signifying significant differences between the compared groups. These findings underscore the reliability of initial proteomic analysis in identifying promising novel biomarker candidates for iCCA. Moving forward, it is imperative to validate these findings in larger-scale studies to further elucidate the clinical significance and utility of the identified biomarkers.

4 Conclusion

Our study provides a pioneering comparative analysis of the serum proteomes of iCCA and other liver conditions, including CIR, PSC, and HCC. By employing high-throughput mass spectrometry techniques, we successfully identified a distinct proteomic signature capable of differentiating these liver diseases. Notably, the identification and validation of specific proteins such as SAA1, SAA4, VCAM1, and LRG1 underscores their potential as biomarkers for distinguishing iCCA from HCC, as well as from PSC.

The findings from our study emphasize the need for continued proteomics-driven research to discover novel biomarkers that can improve the diagnosis and management of iCCA. The observed differential expression of proteins like S100A9, haptoglobin, and ICAM2 between iCCA and HCC further highlights the utility of proteomic profiling in refining diagnostic accuracy. Furthermore, the elevated levels of VCAM1 and TEK in HCC patients suggest their role in tumor progression and potential as diagnostic markers.

While our study demonstrates the feasibility and promise of serum proteomics in distinguishing between complex liver diseases, it is essential to validate these findings in larger cohorts. The integration of proteomic data with clinical practice could potentially reduce the reliance on invasive procedures like liver biopsies, thus minimizing associated risks and improving patient outcomes. Moving forward, extensive validation and functional studies are warranted to fully elucidate the clinical relevance of these biomarkers and to establish robust diagnostic tools for early and accurate detection of iCCA and other liver pathologies.

5 Materials and methods

5.1 Study participants and sampling

This was a cross-sectional, observational, analytical case–control study. Adult subjects with an established diagnosis iCCA, HCC, CIR, PSC (n = 15 each, both for discovery and validation cohorts), undergoing regular clinic follow up or hospitalization at a tertiary care center, namely, the "Prof. Dr. Octavian Fodor" Regional Institute of Gastroenterology and Hepatology Cluj-Napoca, Romania, were prospectively recruited between 2018 and 2023, according to classical diagnosis criteria. Clinical management and decisions on diagnostic tests and medication were at the discretion of the treating physician. The HC group (both discovery and validation cohorts) consisted of 15 subjects referred to our center. Blood samples for the clinical routine analysis and the proteomics analysis were collected during admission as part of hospital protocol. Serum samples for the proteome analysis were aliquoted and stored at −80°C. The study was conducted according to the guidelines of the WMA Declaration of Helsinki and approved by the Ethics Committee of the study center (decision number 18/2021). Written informed consent was sought from all participants prior to inclusion and sample collection.

5.2 Sample preparation for proteomics analysis

Blood samples were drawn into tubes with serum separator gel (BD Vacutainer, Franklin Lakes, NJ, USA) and processed following the manufacturer's guidelines. Serum aliquots were immediately stored at −80°C until analysis.

5.3 Depletion of six highly abundant serum proteins

Serum albumin, immunoglobulin gamma, immunoglobulin alpha, serotransferrin, haptoglobin, and alpha-1-antitrypsin were removed using multi-affinity chromatography (MARS6-human) from Agilent Technologies, Waldbronn, Germany, following the manufacturer's instructions. Post-depletion, samples underwent concentration via trichloroacetic acid precipitation, reaching a final concentration of 15% for the remaining protein fraction. The resulting pellet was then resuspended in a urea/thiourea buffer (8/2 M VWR, Radnor, PA, USA), in accordance with previously established procedures (Ilies et al., 2018; Lucaciu et al., 2023). Subsequently, samples were stored at −80°C until use.

5.4 Proteolytic digestion by trypsin

Proteolytic digestion by trypsin followed standard protocol of our proteomics team (Ilies et al., 2018; Lucaciu et al., 2023). Briefly, the protein concentration in the samples was assessed using the microplate Bradford Assay (Invitrogen, Waltham, MA, USA) with bovine serum albumin as the standard protein. For each protein sample, a total of 11 µg was subjected to a series of steps: reduction with dithiothreitol (2.5 mM, 30 min at 37°C), alkylation with iodoacetamide (10 mM, 15 min at 37°C), and proteolytic digestion by trypsin (Merck KGaA, Darmstadt, Germany) at a 1:25 protease-to-protein ratio (overnight at 37°C). The digestion process was halted using 1% acetic acid, and peptide desalting was carried out using an Oasis HLB 96-well µElution plate (Waters Corporation, Milford, MA, USA) in accordance with the manufacturer's guidelines. The lyophilized peptides were reconstituted in 0.1% formic acid to achieve a final concentration of 0.1 µg/µL before injection.

5.5 Proteome profiling by mass spectrometry

Nano-LC-HDMS^E analysis also followed standard protocol of our mass spectrometry lab (Lucaciu et al., 2023). In short, peptides (300 ng) were chromatographically separated on an ACQUITY UPLC® M-Class HSS T3 column (Waters Corporation, Milford, MA, USA) over a 120-min period, employing a non-linear gradient ranging from 5% to 85% acetonitrile and 0.1% formic acid at a flow rate of 300 nL/min. Detection of eluted peptides was accomplished using an online-coupled traveling wave ion-mobility-enabled hybrid quadrupole orthogonal acceleration time-of-flight mass spectrometer (SYNAPT G2-Si HDMS, Waters Corporation, Milford, MA, USA). The data acquisition utilized the independent acquisition mode, a feature programmed for parent and product ion measurement by switching between low energy (MS) and elevated energy (MS^E), with collision voltage ramping set as a default. Two technical replicates were performed for each sample, and raw data were acquired through MassLynx™ Software Version 1.74.2662 (Waters Corporation, Milford, MA, USA). Detailed settings can be found in the Supplementary Methods.

5.6 Human proteome database search

LC–HDMS^E data underwent processing following established protocols (Lucaciu et al., 2023). In essence, Progenesis QI (v2.0, Waters Corporation, Milford, MA, USA) was employed for automated peak picking and chromatogram alignment. The built-in search engine of the software conducted a spectra search using a Uniprot/Swissprot database (2022) limited to human entries (20,361). The specified parameters included enzyme specificity (trypsin with a maximum of one missed cleavage allowed), fixed modification for carbamidomethylation of cysteine, and variable modification for oxidation of methionine. The search tolerance parameters encompassed a false discovery rate of <4%. Further analysis considered proteins only if they met ion matching requirements of fragments/peptide ≥2, fragments/protein ≥5, and peptides/protein ≥1. Peptide identifications adhered to restrictions of absolute mass error <10 ppm, sequence length >5, and a score >5. Protein relative quantification was conducted based on the summed peptide abundance, utilizing only peptides with no conflicting protein identification.

5.7 Statistical analysis

For the dataset capturing study participants' characteristics at study entry (Table 1): The normality of the dataset was evaluated through the Shapiro–Wilk Test, revealing non-normality ($p > 0.05$). Consequently, non-parametric tests, without normalization, were employed. To assess distinctions between the two groups (iCCA and HCC), the Mann–Whitney test was utilized. Fisher's exact test was applied to examine differences in qualitative data.

For the dataset encompassing global proteome profiling: Initial proteome data, inherently conforming to a normal distribution, were extracted from ProgenesisQI for proteomics following the software's default normalization process at the protein level. Subsequently, a minimum of 70% valid values filter was applied to each patient group, and an abundance average was computed between the two technical replicates. The resulting matrix was then imported into MetaboAnalyst 6.0 (https://www.metaboanalyst.ca). To address identified missing values, estimation was performed using the k-nearest neighbors (KNN) algorithm on a feature-wise basis. Finally, a log10 transformation was implemented before embarking on the statistical analysis. Clustering of sampling groups was assessed using partial least squares discriminant analysis (PLS-DA), and proteins with discriminatory potential were identified through PLS-DA variable importance projection (VIP) scores.

Given the normal distribution of the proteomic data, parametric tests were employed. Statistical significance was assessed using the t-test and ANOVA with Tukey's Honest Significant Difference (HSD) test, with the significance cut-off set at $p < 0.05$. The fold change, calculated as the ratio of two group means, was considered significant at a cut-off level of fold change = 1.5 (log2FC = 0.58).

Biomarker performance was evaluated by Receiver Operating Characteristic (ROC) analysis along with the corresponding Area Under the Curve (AUC) analysis and AUC PLS-DA algorithm. Thecut-off value was set to AUC = 0.7. All statistical analyses were performed using default settings of the MetaboAnalyst 6.0 online omics data analysis platform.

6 ELISA

The levels of serum Amyloid A1 (SAA1), Serum Amyloid A4 (SAA4), Vascular cell adhesion protein 1 (VCAM1) and Leucine-rich alpha-2-glycoprotein 1 (LRG1) were determined using sandwich enzyme-linked immunosorbent assays (ELISA) kits. These measurements were made from individual samples of the validation cohort and were performed in duplicate, following the instructions provided with the kits. (SAA1: ABclonal, WoburnMA, USA, catalogue number RK04228, detection range = 0.156–10 ng/mL sensitivity = 0.071 ng/mL, intra-assay precision coefficient of variation (CV) < 10%, inter-assay precision CV < 15%; SAA4: Elabscience Wuhan, China, catalogue number E-EL-H5638, detection range = 78.13–5,000 pg/mL sensitivity = 46.88 pg/mL, intra-assay precision coefficient of variation

(CV) < 5%, inter-assay precision CV < 5%; VCAM1: ABclonal, WoburnMA, USA, catalogue number RK00026, detection range = 15.6–1,000 pg/mL sensitivity = 3.85 pg/mL, intra-assay precision coefficient of variation (CV) ≤10%, inter-assay precision CV ≤ 15%; LRG1: ABclonal, WoburnMA, USA, catalogue number RK01800, detection range = 31.2–2000 pg/mL, sensitivity = 15.6 pg/mL, intra-assay precision coefficient of variation (CV) ≤10%, inter-assay precision CV ≤ 15%). For each parameter, a calibration curve was constructed using the protein standard supplied. Absorbance readings were taken with a microplate reader (ClarioStar, BMGLabtech, Ortenberg, Germany), and data acquisition and analysis were performed using the built-in MARS software. A 4-parameter logistic regression model was employed to generate the calibration curve for quantification, and the final concentration was determined by averaging the two measurements. Outliers were tested using Grubb's test, when significance level was set to alpha = 0.05. Significant outliers were excluded from the dataset and data are presented as mean ± standard deviation (SD).

Data availability statement

The original contributions presented in the study are included in the article/Supplementary Material, further inquiries can be directed to the corresponding author.

Ethics statement

The studies involving humans were approved by "Iuliu Haţieganu" University of Medicine and Pharmacy, Cluj-Napoca, Romania. The studies were conducted in accordance with the local legislation and institutional requirements. The participants provided their written informed consent to participate in this study.

Author contributions

LM: Writing–original draft, Software, Investigation, Formal Analysis, Data curation. CG: Writing–original draft, Investigation, Formal Analysis, Data curation. RC: Writing–original draft, Investigation, Formal Analysis, Data curation. IP: Writing–original draft, Software, Formal Analysis, Data curation. AU: Writing–original draft, Formal Analysis, Data curation. AS: Writing–original draft, Formal Analysis, Data curation. XM: Writing–review and editing, Investigation, Data curation. MI: Writing–review and editing, Writing–original draft, Supervision, Software, Project administration, Methodology, Investigation, Funding acquisition, Formal Analysis, Data curation, Conceptualization. NA: Writing–review and editing, Supervision, Methodology, Investigation. CM: Writing–review and editing, Supervision, Methodology. ZS: Writing–review and editing, Supervision, Methodology. TM: Writing–review and editing, Supervision, Methodology, Investigation, Funding acquisition, Conceptualization. CI: Writing–review and editing, Supervision, Funding acquisition, Conceptualization.

Funding

The author(s) declare that financial support was received for the research, authorship, and/or publication of this article. The Romanian National Ministry of Research, Innovation and Digitalization, CNCS-UEFISCDI: Postdoctoral Research Project PN-III-P1-1.1-PD-2019-0852/PD113 within PNCDI III, awarded to Maria Iacobescu (former Ilies).

Acknowledgments

The authors would like to thank the research assistant Andrada Maria Uhl for the contribution to the data analysis as part of her MEDFUTURE volunteering program. The authors acknowledge the use of generative AI technology, specifically OpenAI's ChatGPT (version: GPT-4, model: GPT-4, source: OpenAI). The AI tool was employed to assist in refining language and ensuring clarity in the presentation of ideas. The final content was reviewed and approved by the authors to ensure accuracy and adherence to the research's academic standards.

Conflict of interest

The authors declare that the research was conducted in the absence of any commercial or financial relationships that could be construed as a potential conflict of interest.

The author(s) declared that they were an editorial board member of Frontiers, at the time of submission. This had no impact on the peer review process and the final decision.

Publisher's note

Supplementary material

The Supplementary Material for this article can be found online at: https://www.frontiersin.org/articles/10.3389/fphar.2024.1440985/full#supplementary-material

References

Best, J., Bechmann, L. P., Sowa, J.-P., Sydor, S., Dechêne, A., Pflanz, K., et al. (2020). GALAD score detects early hepatocellular carcinoma in an international cohort of patients with nonalcoholic steatohepatitis. *Clin. Gastroenterology Hepatology Official Clin. Pract. J. Am. Gastroenterological Assoc.* 18 (3), 728–735. doi:10.1016/j.cgh.2019.11.012

Choi, G. H., Jang, E. S., Kim, J.-W., and Jeong, S.-H. (2021). Prognostic role of plasma level of angiopoietin-1, angiopoietin-2, and vascular endothelial growth factor in hepatocellular carcinoma. *World J. Gastroenterology* 27 (27), 4453–4467. doi:10.3748/wjg.v27.i27.4453

Christensen, T. D., Jensen, C., Larsen, O., Leerhøy, B., Hansen, C. P., Madsen, K., et al. (2023). Blood-based tumor fibrosis markers as diagnostic and prognostic biomarkers in patients with biliary tract cancer. *Int. J. Cancer* 152 (5), 1036–1049. doi:10.1002/ijc.34356

Claessen, M. M. H., Frank, P. V., Tytgat, K. M. A. J., Siersema, P. D., and Buuren, H. R. van (2009). High lifetime risk of cancer in primary sclerosing cholangitis. *J. Hepatology* 50 (1), 158–164. doi:10.1016/j.jhep.2008.08.013

Dong, L., Lu, D., Chen, R., Lin, Y., Zhu, H., Zhang, Z., et al. (2022). Proteogenomic characterization identifies clinically relevant subgroups of intrahepatic cholangiocarcinoma. *Cancer Cell* 40 (1), 70–87.e15. doi:10.1016/j.ccell.2021.12.006

Fox, S. B., Turner, G. D., Gatter, K. C., and Harris, A. L. (1995). The increased expression of adhesion molecules ICAM-3, E- and P-selectins on breast cancer endothelium. *J. Pathology* 177 (4), 369–376. doi:10.1002/path.1711770407

Geramizadeh, B., Sehat, M., Mehrmozayan, A., and Reza, A. R. A. (2021). Annexin expression in cholangiocarcinoma, and metastatic pancreatic ductal adenocarcinoma 'is it Be helpful for differential diagnosis of these tumors in the liver? *Iran. J. Pathology* 16 (4), 433–438. doi:10.30699/IJP.20201.138489.2512

Ho, J.-W., Poon, R.-T., Tong, C.-S., and Fan, S.-T. (2004). Clinical significance of serum vascular cell adhesion molecule-1 levels in patients with hepatocellular carcinoma. *World J. Gastroenterology* 10 (14), 2014–2018. doi:10.3748/wjg.v10.i14.2014

Ignacio, R. M. C., Gibbs, C. R., Kim, S., Lee, E.-S., Adunyah, S. E., and Son, D.-S. (2019). Serum amyloid A predisposes inflammatory tumor microenvironment in triple negative breast cancer. *Oncotarget* 10 (4), 511–526. doi:10.18632/oncotarget.26566

Ilies, M., Kumar Sappa, P., Iuga, C. A., Loghin, F., Salazar, M. G., Weiss, F. U., et al. (2018). Plasma protein profiling of patients with intraductal papillary mucinous neoplasm of the pancreas as potential precursor lesions of pancreatic cancer. *Clin. Chim. Acta* 477, 127–134. doi:10.1016/j.cca.2017.12.008

Izquierdo-Sanchez, L., Lamarca, A., Casta, A.La, Buettner, S., Utpatel, K., Klümpen, H.-J., et al. (2022). Cholangiocarcinoma landscape in europe: diagnostic, prognostic and therapeutic insights from the ENSCCA registry. *J. Hepatology* 76 (5), 1109–1121. doi:10.1016/j.jhep.2021.12.010

Jin, Z., Kobayashi, S., Gotoh, K., Takahashi, T., Eguchi, H., Naka, T., et al. 2020. The prognostic impact of leucine-rich α-2-glycoprotein-1 in cholangiocarcinoma and its association with the IL-6/TGF-β1 Axis. *J. Surg. Res.* 252 147–155. doi:10.1016/j.jss.2020.03.018

Job, S., Rapoud, D., Dos Santos, A., Gonzalez, P., Desterke, C., Pascal, G., et al. (2020). Identification of four immune subtypes characterized by distinct composition and functions of tumor microenvironment in intrahepatic cholangiocarcinoma. *Hepatol. Baltim. Md* 72 (3), 965–981. doi:10.1002/hep.31092

Kaplanski, G., Farnarier, C., Payan, M. J., Bongrand, P., and Durand, J. M. (1997). Increased levels of soluble adhesion molecules in the serum of patients with hepatitis C. Correlation with cytokine concentrations and liver inflammation and fibrosis. *Dig. Dis. Sci.* 42 (11), 2277–2284. doi:10.1023/a:1018818801824

Kim, Ju Y., Kim, J., Lim, Y.-S., Gwak, G.-Y., Yeo, I., Kim, Y., et al. (2022). Proteome multimarker panel for the early detection of hepatocellular carcinoma: multicenter derivation, validation, and comparison. *ACS Omega* 7 (34), 29934–29943. doi:10.1021/acsomega.2c02926

Lapitz, A., Azkargorta, M., Milkiewicz, P., Olaizola, P., Zhuravleva, E., Grimsrud, M. M., et al. (2023). Liquid biopsy-based protein biomarkers for risk prediction, early diagnosis, and prognostication of cholangiocarcinoma. *J. Hepatology* 79 (1), 93–108. doi:10.1016/j.jhep.2023.02.027

Liang, B., Li, C., and Zhao, J. (2016). Identification of key pathways and genes in colorectal cancer using bioinformatics analysis. *Med. Oncol. N. Lond. Engl.* 33 (10), 111. doi:10.1007/s12032-016-0829-6

Lin, M., Liu, J., Zhang, F., Qi, G., Tao, S., Fan, W., et al. (2022). The role of leucine-rich alpha-2-glycoprotein-1 in proliferation, migration, and invasion of tumors. *J. Cancer Res. Clin. Oncol.* 148 (2), 283–291. doi:10.1007/s00432-021-03876-0

Lucaciu, L. A., Seicean, R., Uifalean, A., Iacobescu, M., Iuga, C. A., and Seicean, A. (2023). Unveiling distinct proteomic signatures in complicated crohn's disease that could predict the disease course. *Int. J. Mol. Sci.* 24 (23), 16966. doi:10.3390/ijms242316966

Martin-Serrano, M. A., Kepecs, B., Torres-Martin, M., Bramel, E. R., Haber, P. K., Merritt, E., et al. (2023). Novel microenvironment-based classification of intrahepatic cholangiocarcinoma with therapeutic implications. *Gut* 72 (4), 736–748. doi:10.1136/gutjnl-2021-326514

Mocan, L. P., Ilieş, M., Stanca Melincovici, C., Spârchez, M., Crăciun, R., Nenu, I., et al. (2022). Novel approaches in search for biomarkers of cholangiocarcinoma. *World J. Gastroenterol.* 28 (15), 1508–1525. doi:10.3748/WJG.V28.I15.1508

Mocan, L. P., Rusu, I., Melincovici, C. S., Boşca, B. A., Mocan, T., Crăciun, R., Mihu, C. M., et al. (2023). The role of immunohistochemistry in the differential diagnosis between intrahepatic cholangiocarcinoma, hepatocellular carcinoma and liver metastasis, as well as its prognostic value. *Diagnostics*, 13 (9), 1542. doi:10.3390/diagnostics13091542

Naryzny, S. N., and Legina, O. K. (2021). Haptoglobin as a biomarker. *Biochem. Mosc. Suppl. Ser. B Biomed. Chem.* 15 (3), 184–198. doi:10.1134/S1990750821030069

Patel, A. H., Harnois, D. M., Klee, G. G., LaRusso, N. F., and Gores, G. J. (2000). The utility of CA 19-9 in the diagnoses of cholangiocarcinoma in patients without primary sclerosing cholangitis. *Am. J. Gastroenterology* 95 (1), 204–207. doi:10.1111/j.1572-0241.2000.01685.x

Pirisi, M., Fabris, C., Falleti, E., Soardo, G., Toniutto, P., Vitulli, D., et al. (1996). Serum soluble vascular-cell adhesion molecule-1 (VCAM-1) in patients with acute and chronic liver diseases. *Dis. Markers* 13 (1), 11–17. doi:10.1155/1996/129325

Rumgay, H., Arnold, M., Ferlay, J., Lesi, O., Cabasag, C. J., Vignat, J., et al. (2022). Global burden of primary liver cancer in 2020 and predictions to 2040. *J. Hepatology* 77 (6), 1598–1606. doi:10.1016/j.jhep.2022.08.021

Sack, G. H. Jr (2018). Serum amyloid A–a review. *Mol. Med. Camb. Mass.)* 24 (1), 46. doi:10.1186/s10020-018-0047-0

Santamaria, M., Pardo-Saganta, A., Alvarez-Asiain, L., Di Scala, M., Qian, C., Prieto, J., et al. (2013). Nuclear α1-antichymotrypsin promotes Chromatin condensation and inhibits proliferation of human hepatocellular carcinoma cells. *Gastroenterology* 144 (4), 818–828.e4. doi:10.1053/j.gastro.2012.12.029

Serag, W. M., and Elsayed, B. E. (2021). Annexin A5 as a marker for hepatocellular carcinoma in cirrhotic hepatitis C virus patients. *Egypt. Liver J.* 11 (1), 32. doi:10.1186/s43066-021-00101-y

Shaib, Y. H., El-Serag, H. B., Davila, J. A., Morgan, R., and McGlynn, K. A. (2005). Risk factors of intrahepatic cholangiocarcinoma in the United States: a case-control study. *Gastroenterology* 128 (3): 620–626. doi:10.1053/j.gastro.2004.12.048

Shaib Hashem, B., and Yasser, E.-S. (2004). The epidemiology of cholangiocarcinoma. *Semin. Liver Dis.* 24 (02), 115–125. doi:10.1055/s-2004-828889

Shi, Y., Deng, X., Zhan, Q., Shen, B., Jin, X., Zhu, Z., et al. (2013). A prospective proteomic-based study for identifying potential biomarkers for the diagnosis of cholangiocarcinoma. *J. Gastrointest. Surg.* 17 (9), 1584–1591. doi:10.1007/s11605-013-2182-9

Shirota, T., Ojima, H., Hiraoka, N., Shimada, K., Rokutan, H., Arai, Y., et al. (2015). Heat shock protein 90 is a potential therapeutic target in cholangiocarcinoma. *Mol. Cancer Ther.* 14 (9), 1985–1993. doi:10.1158/1535-7163.MCT-15-0069

Soman, A., and Nair, S. A. (2022). Unfolding the cascade of SERPINA3: inflammation to cancer. *Biochimica Biophysica Acta (BBA) - Rev. Cancer* 1877 (5), 188760. doi:10.1016/j.bbcan.2022.188760

Sun, B. B., Suhre, K., and Gibson, B. W. (2024). Promises and challenges of populational proteomics in health and disease. *Mol. and Cell. Proteomics* 100786, 100786. doi:10.1016/j.mcpro.2024.100786

Sun, X., Ma, Q., Cheng, Y., Huang, H., Qin, J., Zhang, M., et al. (2023). Overexpression of CHAF1A is associated with poor prognosis, tumor immunosuppressive microenvironment and treatment resistance. *Front. Genet.* 14, 1108004. doi:10.3389/fgene.2023.1108004

Torimura, T., Ueno, T., Kin, M., Harada, R., Taniguchi, E., Nakamura, T., et al. (2004). Overexpression of angiopoietin-1 and angiopoietin-2 in hepatocellular carcinoma. *J. Hepatology* 40 (5), 799–807. doi:10.1016/j.jhep.2004.01.027

Voigtländer, T., Metzger, J., Husi, H., Kirstein, M. M., Pejchinovski, M., Latosinska, A., et al. (2020). Bile and urine peptide marker profiles: access keys to molecular pathways and biological processes in cholangiocarcinoma. *J. Biomed. Sci.* 27 (1), 13. doi:10.1186/s12929-019-0599-5

Whitesell, L., and Lindquist, S. L. (2005). HSP90 and the chaperoning of cancer. *Nat. Rev. Cancer* 5 (10), 761–772. doi:10.1038/nrc1716

Wu, D.-C., Wang, K.-Yi, Wang, S. S. W., Huang, C.-M., Lee, Y.-W., Chen, M. I., et al. (2017). Exploring the expression bar code of SAA variants for gastric cancer detection. *Proteomics* 17 (11). doi:10.1002/pmic.201600356

Yamaguchi, N., Tokushige, K., Haruta, I., Yamauchi, K., and Hayashi, N. (1999). Analysis of adhesion molecules in patients with idiopathic portal hypertension. *J. Gastroenterology Hepatology* 14 (4), 364–369. doi:10.1046/j.1440-1746.1999.01857.x

Zhang, H., Kong, Q., Wang, J., Jiang, Y., and Hua, H. (2020a). Complex roles of CAMP-PKA-CREB signaling in cancer. *Exp. Hematol. and Oncol.* 9 (1), 32. doi:10.1186/s40164-020-00191-1

Zhang, M., Yang, H., Wan, L., Wang, Z., Wang, H., Ge, C., et al. (2020b). Single-cell transcriptomic architecture and intercellular crosstalk of human intrahepatic cholangiocarcinoma. *J. Hepatology* 73 (5), 1118–1130. doi:10.1016/j.jhep.2020.05.039

Zhang, W., Kong, H.-F., Gao, X.-D., Dong, Z., Lu, Y., Huang, J.-G., et al. (2020c). Immune infiltration-associated serum amyloid A1 predicts favorable prognosis for hepatocellular carcinoma. *World J. Gastroenterology* 26 (35), 5287–5301. doi:10.3748/wjg.v26.i35.5287

Zhou, J., Lei, Yu, Gao, X., Hu, J., Wang, J., Dai, Z., et al. (2011). Plasma MicroRNA panel to diagnose hepatitis B virus-related hepatocellular carcinoma. *J. Clin. Oncol. Official J. Am. Soc. Clin. Oncol.* 29 (36), 4781–4788. doi:10.1200/JCO.2011.38.2697

Zhuang, C., Wang, P., Sun, T., Zheng, L., and Ming, L. (2019). Expression levels and prognostic values of annexins in liver cancer. *Oncol. Lett.* 18 (6), 6657–6669. doi:10.3892/ol.2019.11025

Zou, Y., Xu, Yi, Chen, X., Wu, Y., Fu, L., and Lv, Y. (2022). Research progress on leucine-rich alpha-2 glycoprotein 1: a review. *Front. Pharmacol.* 12, 809225. doi:10.3389/fphar.2021.809225

Frontiers in Pharmacology

Explores the interactions between chemicals and living beings

The most cited journal in its field, which advances access to pharmacological discoveries to prevent and treat human disease.

Discover the latest Research Topics

See more →

Frontiers

Avenue du Tribunal-Fédéral 34
1005 Lausanne, Switzerland
frontiersin.org

Contact us

+41 (0)21 510 17 00
frontiersin.org/about/contact